DISSERTATION

OBSERVATIONS FROM A SERIES OF FLUME EXPERIMENTS ON CONTRACTION SCOUR ALONG A RECTANGULAR CHANNEL

Submitted by

Alireza Nowroozpour

Department of Civil and Environmental Engineering

In partial fulfillment of the requirements

For the Degree of Doctor of Philosophy

Colorado State University

Fort Collins, Colorado

Fall 2020

Doctoral Committee:

Advisor: Robert Ettema

Pierre Julien
Peter Nelson
Lyle Zevenbergen
Sean Gallen

ABSTRACT

OBSERVATIONS FROM A SERIES OF FLUME EXPERIMENTS ON CONTRACTION SCOUR ALONG A RECTANGULAR CHANNEL

This dissertation presents observations from extensive laboratory flume experiments on contraction scour along a straight rectangular channel. The objectives for the experiments included acquiring insights as to how contraction scour developed, then determining whether and (if so) in what manner the leading equations for estimating the depth of contraction should be adjusted. The approach taken in interpreting the observations entailed considering the hydraulics of flow along the rectangular channel of uniform width in which a contraction was subsequently formed.

The flume setup represented simplified waterways at bridge crossings of rivers. The approach channel and the contraction were rectangular in cross-section and had non-erodible sidewalls lining a bed of uniform fine sand. Three contraction ratios (contraction width/approach–channel width) were used: tight, medium and mild. Each ratio included a 45° narrowing transition linking the contraction to the approach channel. Clear-water and live-bed scour conditions were replicated. Approach flows were subcritical and were chosen so as not to choke at the exit or the entrance of the contractions. Choking produces supercritical flow, which would alter the flow field (including turbulence structures) at the contraction entrance or exit.

The observations comprised measurements of bed-surface profiles (LiDAR scanned), water-surface profiles, flow velocities and bedforms. These data and were augmented with photographs of the flow and the bed bathymetry before and after the experiments.

The flow-field considerations indicated that contraction scour associated with sub-critical approach flows should be grouped in terms of three contraction-length categories. Short contractions (typical of bridge waterways) are shorter than one to two times the width of the approach channel and are marked by the connection of the flow-separation region formed at the start of the contraction with the flow separation region at the end of the contraction. Intermediate-length contractions (typical of contractions formed by channel control structures) occur when the flow-separation region formed at the start of the contraction does not connect with the flow separation region at the end of the contraction. For intermediate-length contractions, the water-surface profile to and through the contraction is influenced by the length of the contracted channel, and therefore so is depth of contraction scour. Flow depth at the contraction exit is the flow control for short and intermediate-length contractions. Long contractions occur when the downstream control is depth of uniform flow along the contraction.

Of focal interest for this study was scour in intermediate-length contractions, as they were considered the more general form of contraction, producing non-uniform and unsteady loose-bed flow. The flume experiments revealed how the bed of a contraction deformed and how bed roughness varied spatially along the contraction. The flume experiments consistently showed that the deepest contraction scour occurred along the vena contracta formed by a flow contraction, but the non-uniform flow along the contraction could also produce a second deeper region at the exit of a contraction. A companion study to the present study provided values of the contraction coefficient for the study's experiments.

In addition to scour along the vena-contracta region, scour developed at the entrance corners of the contracted channel. The entrance corners usually were the locations of overall deepest scour, because of the turbulence structures generated by flow separation at the corners. For one flow condition involving the tight contraction, scour of the vena contracta merged with the corner scour to form practically a step scour similar in form to an arrested head-cut scour. The data from the flume experiments, when merged via regression analysis, form a single empirical equation relating vena-contracta scour depth to the shear-stress ratio and the contraction ratio for the given entrance transition to the contraction.

Also, the flume experiments showed that the leading and widely used method for estimating depth of contraction scour required several adjustments (the method described in the U.S. Federal Highway Administration's monograph HEC-18, *Evaluating Scour at Bridges*). One adjustment suggests that the HEC-18 equations apply to the narrowed vena contracta region formed within the entrance of a contraction. This adjustment entails including a vena-contracta coefficient (a width -narrowing coefficient) in the equations to account for the narrowing of flow as it enters the contracted channel. A second adjustment (or more aptly a clarification) involved affirming that theoretical approach-flow depth used when estimating contraction-scour depth should be the normal depth of approach flow to the contraction. In contraction-scour-depth estimation for bridges over actual river channels, the practice is to use the flow depth at the start of a bridge waterway to estimate depth of contraction scour; that flow depth, however, depends on the energy loss incurred with flow along the contraction. The practice is acceptable when this flow depth approximates the normal depth of flow, or if the resulting scour-depth estimate is judged adequately conservative for design purposes. However, designers must realize that the practice used together with the vena-contracta coefficient may over-estimate the depth of contraction scour.

Many complexities associated with contraction scour remain to be investigated (e.g., the effects of sediment characteristics, how turbulence structures influence scour depth and contraction morphology, and the extent to which pier presence affects flow and scour in a vena contracta).

This dissertation briefly discusses these complexities, which then are left as topics for further research.

ACKNOWLEDGMENTS

I would like to thank Dr. Robert Ettema for his tireless guidance and my family for their unlimited support.

This study was conducted as part of NCHRP Project 24-47, "*Revised Clear-Water and Live-Bed Contraction Scour Analysis*".

TABLE OF CONTENTS

LIST OF TABLES

LIST OF FIGURES

LIST OF SYMBOLS

B_1	width of the approach channel
B_2	width of the contracted channel
α	angle of the transition at the contraction entrance
Y_{n1}	normal flow depth in the approach channel
S_1	bed slope of the approach channel
d_{50}	median diameter of bed sediment
σ_g	geometric standard deviation of bed sediment diameter
ρ_s	sediment density
τ_c	critical bed shear stress for entrainment
τ_b	flow shear stress exerted on bed
ρ	density of water
ν	kinematic viscosity of water
g	gravity acceleration
t	time
E	specific energy
Y	flow depth
V	flow Velocity
V_c	critical velocity at incipient motion of bed sediment
S_f	friction slope
Y_{n2}	normal depth at the contracted section

q_1	unit discharge at the uncontracted section
q_2	unit discharge at the contracted section
D_s	scour depth
L	contraction length
H	dune or ripple height
λ	dune or ripple wavelength
τ_1	bed shear stress in the uncontracted approach section
τ_2	bed shear stress in the contracted section
Y_2	water depth in the contracted section
F_1	approach flow Froude number
D_a	mean diameter of armor particles
G_s	specific gravity
ρ_s	sediment density
ϕ	angle of repose
d_*	dimensionless particle diameter
τ_{*_c}	critical shields parameter
u_{*_c}	critical shear velocity
κ	von Karman constant
R	hydraulic radius
h_f	local headloss
K_v	vena-contracta coefficient
Y_1	backwater depth

1. Introduction

1.1. Introduction

Bridge waterways commonly contract river channels. The intrusion of a bridge's abutments and sometimes their approach embankments into a river narrows the river's flow and increase its discharge per unit width of channel. Additionally, the shape of a contraction entrance influences the flow along a contraction. The increase in unit discharge may cause the contracted scour to scour. The resulting scour is usually called "contraction scour" (e.g., Straub 1935, Laursen 1960&1963, Arneson et al. 2012). The present study shows that contraction scour is more complicated and varied in character than prior publications portray.

In particular, the contraction of a loose-boundary river channel produces a non-uniform and possibly unsteady open-channel flow difficult to quantify accurately. This difficulty is compounded for natural channels, as they usually are not straight or prismatic, and may comprise a main channel flanked with floodplains of irregular width. Moreover, the boundaries of such channels commonly comprise variable materials (sands, gravels, clays), and geotechnical considerations may affect the stability of a channel's banks. Therefore, accurate estimation of contraction-scour depth is burdened with uncertainties. For example, the approach flow assumes a non-uniform (an M1 or backwater) profile extending upstream from a contraction, as the flow to and through the contraction backs up the approach flow. Additionally, the channel's loose boundary may cause the flow to be unsteady as bed sediment deposits or scours, and as bedforms of spatially variable size form to and through the contraction.

The channel configuration used for the flume experiments comprised a straight channel of rectangular in cross-section, and with sides resistant to lateral erosion and geotechnical instability, and with bed formed of uniform sand. The middle of the channel was contracted to form a long, narrower channel of rectangular cross-section. The assumption of a straight, rectangular, alluvial channel is reasonable, and is commonly made, for relatively wide channels of slight local curvature at a bridge site and erosion-resistant banks. The experiments, nonetheless, were designed to yield insightful observations regarding contraction scour without some of the complexities mentioned above.

Among the several significant variables influencing contraction scour is the length of the contraction. The hydraulics of water flow through a contraction is influenced by contraction length and by the contraction's erodible bed. The hydraulics involves non-uniform flow, because the flows contain regions of gradually varied and rapidly varied flow. The development of scour and changes in bed roughness cause the hydraulics to be unsteady over time. Contraction scour at bridges, therefore, often involves complicated sets of processes that introduce uncertainties in estimates of depth of contraction scour.

During design flows, channel contractions may produce live-bed or clear-water conditions of scour. The former scour condition commonly occurs in the main channel of an alluvial river, whereas the latter condition more often occurs at a floodplain contraction or a relief bridge located on the floodplain. For clear-water scour, the governing principle is that the equilibrium depth of scour in the contracted section corresponds to the occurrence of critical bed shear stress or mean flow velocity for which the scour approaches its equilibrium state. For live-bed contraction scour, equilibrium depth of scour results from the continuity of bed-sediment transport between the approach-flow section and the contracted section. These equilibrium conditions appear to be straightforward. However, they are complicated by the effects of the complexities listed subsequently. One uncertainty to mention early is that sediment transport varies in composition between bedload (assumed in live-bed equilibrium) and suspended bed-sediment load as the rate of sediment transport increases. The suspended-load portion is unlikely to affect scour-depth equilibrium, because suspended sediment overshoots the region of deepest scour.

The current guidance given by the widely used Hydraulic Engineering Circular No. 18 (HEC-18), "Evaluating Scour at Bridges," (Arneson et al. 2012) gives equations for estimating contraction scour. However, as the present study shows, the HEC-18 equations are not entirely well-founded and are based on approximations that reflect the many uncertainties associated with contraction flow and loose-boundary hydraulics. The equations in HEC-18 stem back to (Laursen 1960) for live-bed contraction scour and Laursen (1963) on clear-water contraction scour. In both contraction-scour conditions, Laursen's formulations assume that contraction scour is due solely to flow-streamline contraction and that the contraction is hydraulically "long", a term coined by Straub (1934). The present study suggests that hydraulically long-contraction scour does not exist at bridge waterways.

Field data reflect the complexities of contraction scour. Analysis of existing field and laboratory data sets conducted under NCHRP[1] Project 24-34, *Risk and Reliability-Based Approaches for Bridge Scour Prediction* (Lagasse et al. 2013), for instance, indicates that the clear-water contraction scour equation does not envelope the reported field data on contraction-scour depth, especially in the region close to the entrance of channel contractions. Rather, the equation is a predictive equation that frequently seems to under-predict observed scour depths. In contrast,

[1] National Cooperative Highway Research Program, administered by the U.S. Transportation Research Board, a unit of the U.S. National Academy of Sciences

scour-depth estimations for bridge piers and abutments more typically agree better with field-observed scour depths.

Furthermore, although there are data from laboratory studies of live-bed scour at piers and abutments, no such data exist for live-bed contraction scour; for example, the NCHRP study mentioned above did not find any such data. Therefore, the accuracy of Laursen's live-bed contraction scour equation could not be assessed against observed data. However, there are contraction scour data embedded in data on live-bed scour at bridge abutments (e.g., Ettema et al. 2010) that can be gainfully evaluated in the light of an improved contraction-scour formulation. This point regarding the need for improved contraction scour estimates also is mentioned in NCHRP Study 24-14, *Scour at Contracted Bridges* (Wagner et al. 2006).

Although most bridge waterways form relatively short flow contractions, longer contractions of a river channel can occur when a bridge waterway comprises several bridges. Analogous situations arise too when a river channel is narrowed by other engineered structures (such as a series of wing dams) or by natural causes (such as rock outcrops). The results of the present study are of use for contractions of open channels generally.

The present study though does not evaluate the consequences of several real-world complexities that may limit the depth of vertical scour at actual bridge waterways. Vertical erosion of a waterway's bed may trigger geotechnical instabilities of a waterway's banks, and thereby also cause lateral erosion of a waterway. Lateral erosion may become pronounced at bridge sites where the channel bed (notably rock) is more resistant to erosion than channel banks and earthfill abutments. Also, the overall shape of a compound channel or a channel's curved alignment may introduce geometric complexities this study does not consider. The presence of piers and abutments, as well as the interface between main channel and floodplains, can introduce large-scale turbulence structures that may substantially affect the entrainment, transport and deposition of bed material in the contraction zone. These complexities too are not investigated in the present study, though they raise interesting questions warranting research beyond the scope of this study.

1.2. Objectives

This study's objectives align with the overall goals of the NCHRP project, and focused on straight rectangular channels, and were as follow:

1. Delineate the open-channel flow conditions associated with water flow along contracted waterways, and show how a loose boundary further complicates the conditions;
2. Obtain and interpret observation from a series of flume experiments on clear-water and live-bed contraction scour to confirm theoretical insights regarding contraction hydraulics and scour and to obtain further insights into these aspects. This objective involved getting CSU's 2.44m-wide flume (the "8ft flume") operational, as the flume had not been used for about a decade. To facilitate clarity of insight, the experiments must involve channels of rectangular cross-section and substantial length; and,
3. Improve existing, widely used equations for estimating depth of contraction scour. This objective entailed analyzing the results of the flume experiments to identify and support the improvements. Because the existing equations in HEC-18 (Arneson et al. 2012) are widely used (and generally accepted) by bridge engineers, the improvements aimed at modifying these equations rather than formulating an entirely new set of

equations. This objective said, however, the present study also sought to use the flume data to develop an improved estimation equation applicable for conditions like those of the flume experiments.

These objectives were mindful of the complexities listed above and adopted further simplifications:

- The contracted channel had a bed of uniform fine sand.
- The channel's banks were resistant to erosion (hydraulic or geotechnical). Therefore, no lateral erosion of the channel could occur.
- Clear-water scour meant that the sediment forming the bed of the approach channel was immobile.
- Live-bed scour meant that the sediment forming the bed of the approach channel was mobile.

These simplifications were judged to be necessary for determining the essential processes associated with the development of contraction scour in a bridge waterway. Other factors, such as non-uniformity of bed sediment, may introduce complications but were assessed as not altering the essential processes this study sought to illuminate.

Also, the study was mindful of the practical aspects of contraction-scour estimation as conducted by engineers designing or monitoring bridge waterways. In this regard, the study expends considerable effort describing the theoretical and interpretive importance of considering the normal flow conditions upstream and downstream of a contraction in a loose-bed channel. This effort is balanced somewhat by appreciating the appealing utility of basing scour-depth estimates on the flow depth at the upstream end of a contraction, even though the theoretical justification for using that depth is narrow. Given the need to accommodate the uncertainties in estimating contraction-scour depth, using Y_1 can be acceptable for bridge-design purpose.

1.3. Approach

The approach comprised a sequence of steps addressing the objectives stated above (while being mindful of the complexities and limitations mentioned above) and concentrating on common situations of flow contraction at bridge waterways. Additionally, the approach assessed how various factors could contribute uncertainty regarding the estimation of contraction-scour depth at bridges.

The sequence involved the ensuing steps:

1. Define and describe open-channel contraction hydraulics and contraction scour;
2. Review prior published studies and evaluate the data and observations they present;
3. Conduct laboratory flume experiments on clear-water and live-bed contraction scour;
4. Develop improved equations for estimating equilibrium depths of clear-water and live-bed contraction scour; and,
5. Explain, illustrate and document findings from the present study.

2. Hydraulics of Contracted Open Channels

2.1. Introduction

The hydraulics of flow at contractions in open-channels, especially rectangular channels with a loose-bed, frames this study's interpretation of observations from the series of contraction scour experiments this study involved. Many hydraulics books on flow in open channels (e.g., Chow 1959, Henderson 1964, Sturm 2001, and Chanson 2004) briefly cover the hydraulics of flow at contractions, but an extensive coverage flow contractions loose-bed open-channels is largely absent from such books. Therefore, the present description of the hydraulics of contracted, loose-bed open channels is largely new and had to be developed to aid design of the experiments and interpretation of the observations stemming from them.

The description of flow to, through and exiting open-channel contractions is given here in terms of the following factors:

- Approach flow channel
    1. Froude number associated with the normal depth of the approach flow in a rectangular channel (i.e., subcritical or supercritical flow)
    2. Choking (or not) at the entrance to the contraction
    3. Bed-sediment transport
- Contracted channel
    1. Width of contraction relative to the width of the rectangular approach channel
    2. Length of the contraction

3. Shape of the entrance to the contraction
4. Shape of the exit of the contraction
5. Flow condition in the channel immediately downstream of the contraction's exit (i.e., width, depth and slope of the channel at the exit of the contraction)

Table 2.1 arranges these factors for conditions typical of bridge waterways. For example, approach flows usually are sub-critical and occur along a river channel of more-or-less constant width. On entering the bridge waterway, the approach flow along a river channel contracts to the narrowed channel of the waterway, also taken here to be of constant width (essentialy like a typical bridge waterway), then the flow in the contracted channel returns to the river channel.

Table 2.1. Conditions associated with contraction scour in an open channel with a sub-critical approach flow. (Supercritical flow is not considered in this study)

Contraction Scour				
Approach flow				
Flow condition	Unchoked and subcritical flow		*Choked and/or supercritical flow*	
Bed-sediment transport	Clear-water	Live-bed	*Clear-water*	*Live-bed*
Contracted flow				
Length of contraction	short	short	*short*	*short*
	Intermediate	Intermediate	*intermediate*	*intermediate*
	long	long	*long*	*long*
			(Not considered here)	

An increase in flow velocity and turbulence due to narrowing of a loose-bed channel's cross-section (or the presence of a wide obstruction, such as a bridge pier, that initially reduces the channel's effective width) may cause contraction scour; i.e., a lowering of the bed in the contracted channel. The narrowing may occur due to a natural reduction in the width of the main channel for a bank-line abutment, or due to a concentration of floodplain flow into the contraction as a result of flow blockage by the bridge approach embankment for a setback abutment. Although contraction scour may vary across the cross-section in the field due to non-rectangular geometry and non-uniform velocity distribution, contraction scour usually is formulated to occur as a uniform decrease in bed elevation across the bridge waterway (e.g., HEC-18).

Flow contraction through a compound channel can be complicated and require the use of a numerical model to determine the flow field at the scour location (e.g., Morales and Ettema 2013). Difficulties, for example, include determining the discharge distribution between the floodplain and the main channel at the bridge section. As mentioned above, the present study focuses on scour in a laterally contracted, loose-bed rectangular channel. The assumption of a rectangular channel conveying the approach flow is reasonable for natural channels of typical aspect ratio (flow width/flow depth) during bank-full flow conditions.

2.2. Approach flow

Most bridge waterways are designed to convey subcritical approach flows, for which the flow-control is at the downstream end of the flow. All published studies of flow contraction at bridge waterways assume subcritical approach flows, except for bridges over channels in relatively steep river-channels that develop super-cirtical flow. Table 2.1 summarizes the main features of subcritical flows, and Figure 2.1 illustrates uniform flow along a rectangular channel of constant width. The use of uniform flow as the initial (or pre-bridge) condition enables calculation of flow conditions at channel contracted with a bridge waterway.

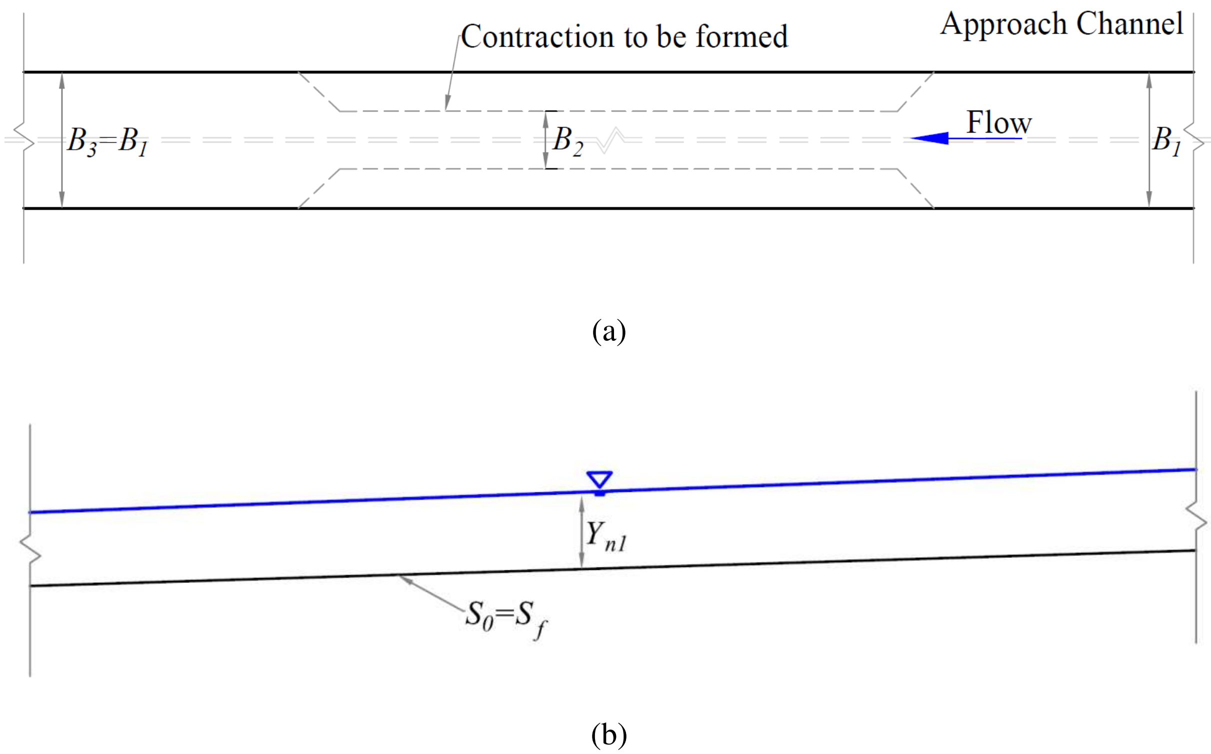

Figure 2.1. Uniform flow along a straight channel before bridge-waterway construction (channel width = $B_1 = B_2 = B_3$ and uniform flow depth $Y_{n1} = Y_{n2} = Y_{n3}$). For uniform flow, bed slope, S_0 = energy slope, S_f.

Though the assumption of subcritical approach flow is sound for most bridge waterways, two additional approach-flow features need to be considered:

1. Contraction severity causing choking of flow at the entrance or the exit of the contraction channel; and,
2. Rate of the sediment transport along the approach-flow channel.

The present study avoided situations where approach-flow choking could occur, because choking leads to super-critical flow at the exit or entrance of a bridge waterway. However, the study involved the two conditions of sediment transport: no sediment transport (clear-water flow) or active sediment transport (live-bed flow) by the approach channel. Because, many prior studies (e.g., Dey and Raikar 2005) inadvertently mix no-choking and choking conditions, the ensuing sub-section offers a short explanation of choking

2.2.1. Flow choking

Flow choking should be addressed early in a study of flow through an open-channel contraction, because choking produces supercritical flow. Choking can occur at the exit or the entrance of a contraction. Choking at the exit occurs when the flow must overcome the headlosses associated with the both the contraction entrance and the contraction exit. Choking at the contraction entrance occurs when the approach flow lacks the energy to overcome the headloss associated with entering the contraction. To determine whether an approach-flow will lead to choking at the exit and the entrance of a contraction, it is necessary to know the uniform (normal) condition of the approach flow.

If flow choking at the contraction entrance were to happen, the flow control would move from downstream end of the contraction to the upstream end of the contraction (for super-critical flow along the contraction). Also, if choking were to occur, a portion of the contraction entrance or exit would experience supercritical flow (e.g., as found by Solan et al. 2020; Grant 1997; Trieste 1992). Bridge-waterway scour associated with flow choking should be studied separately from non-choking cases because choking produces supercritical flow, which substantially alters the flow field in a contraction.

Blockage of bridge openings by accumulated woody debris or ice rubble may cause flow choking, often to a severe extent such that woody debris and ice rubble arch cross the waterway opening. Additionally, short-span bridges may choke when the channel they span conveys much larger flows than these bridges were designed to handle. This situation is common for short-span masonry arch bridges. Though choking is discussed further in Section 2.4, considerations regarding supercritical flow and choking require further investigation beyond the present study.

2.2.2. Bed-sediment transport

The literature on contraction scour at bridge waterways (e.g. Straub 1934, Laursen 1960, Komura 1966, Gill 1981, and Webby 1984) indicates that contraction-scour development and equilibrium depth is influenced by bed-sediment transport in the flow approach to the waterway. As mentioned above, the two conditions of bed sediment transport have somewhat different equilibrium conditions and have been treated separately:

1. Clear-water scour attains equilibrium when the bed erodes to a condition whereby the flow no longer entrains bed sediment in the scour region; and,
2. Live-bed scour attains equilibrium when the rate of erosion of sediment from the bed essentially equals the rate of sediment inflow to the scour region.

In other words, clear-water scour is a condition that flow shear stress exerted on the bed is lower than the critical shear stress of the bed materials; $\tau_{n1} < \tau_c$, with τ_{n1} = bed shear stress associated with uniform (or normal) flow along the approach channel, and τ_c = the critical value of bed shear stress related to the incipient motion of channel-bed particles of a certain diameter. Live-bed scour is a condition that flow shear stress exerted on the bed is greater than the critical shear stress of the bed materials; i.e., $\tau_{n1} > \tau_c$. Live-bed scour condition commonly occurs in the main channel of an alluvial river, while the latter is more likely to be found on a floodplain contraction or a so-called relief bridge located on the floodplain.

2.3. Contraction hydraulics

As mentioned above, the hydraulics of open-channel contractions involves non-uniform flow and unsteady flow (if scour occurs and changes the channel's shape). For the moment, it is expedient to begin by setting aside the unsteady aspect of contraction flow over a loose bed and consider contraction flow through a contraction of fixed width relative to the original river channel and having a bed fixed in continuous alignment with the bed of the original channel (and the approach and downstream reaches adjoining the contraction). It is useful to consider scour and the unsteady aspect of contraction flow in terms of "pre-scour" and "post-scour" hydraulics.

Pre-scour hydraulics implies that the bed of the contraction is in continuous alignment with the open-channel upstream and downstream, and fully turbulent flow occurs along the entire channel. Post-scour hydraulics occurs once scour has caused the channel's bed to have eroded to an equilibrium-profile condition along the contraction and attained an equilibrium (likely depositional for live-bed scour) upstream of the contraction.

To understand how contraction scour develops, it is necessary to describe how flow depth, velocity and bed-shear stress, and turbulent kinetic energy generally vary along open-channel contractions. Because the hydraulics of a flow contraction involves non-uniform open-channel flow, it is expedient to describe contraction hydraulics and scour with the aid of the specific energy diagram, a flow-resistance equation (e.g., Manning's equation), and the processes associated with loose-bed hydraulics.

2.3.1. Contraction Categories

A contraction formed in a subcritical flow along a rectangular channel (Figure 2.1) can be divided into three length categories, based on contraction length, as Figure 2.2 shows:

1. Short-length contraction (Figure 2.2a);
2. Intermediate-length contraction (Figure 2.2b); and,
3. Long-length contraction (Figure 2.2c).

These three categories express length-related changes in the flow field along a contraction. Each category involves a downstream location for flow control, as required for subcritical flows through bridge waterways. The control for short- and intermediate-length contractions is the flow depth at the exit cross-section of the contracted channel. However, the control for a long-length contraction is the uniform (or normal) depth of flow along the contracted channel. The first and third categories are mentioned frequently in contraction-scour publications (e.g., Arneson et al. 2012). The term intermediate-length scour is used here as a general contraction condition, because the water-surface profile of flow to and along the contracted channel varies with the length of the contraction.

Figure 2.3 is a general plan and longitudinal elevation view of flow along a channel of constant width (Figure 2.1) but now containing a contraction that may be termed short, intermediate or long. The description of flow along each category of the contraction is simplified, as it assumes the contracted sub-reach to be straight, having a constant width, and takes the approach and exit channels to be reaches of the same original, uncontracted channel (Figure 2.1). The cut or break line along the streamwise access of each figure indicates the variable width of the river. A term not included in Figure 2.2 is the difference between B_1 and B_2 or, in other words, the contraction ratio.

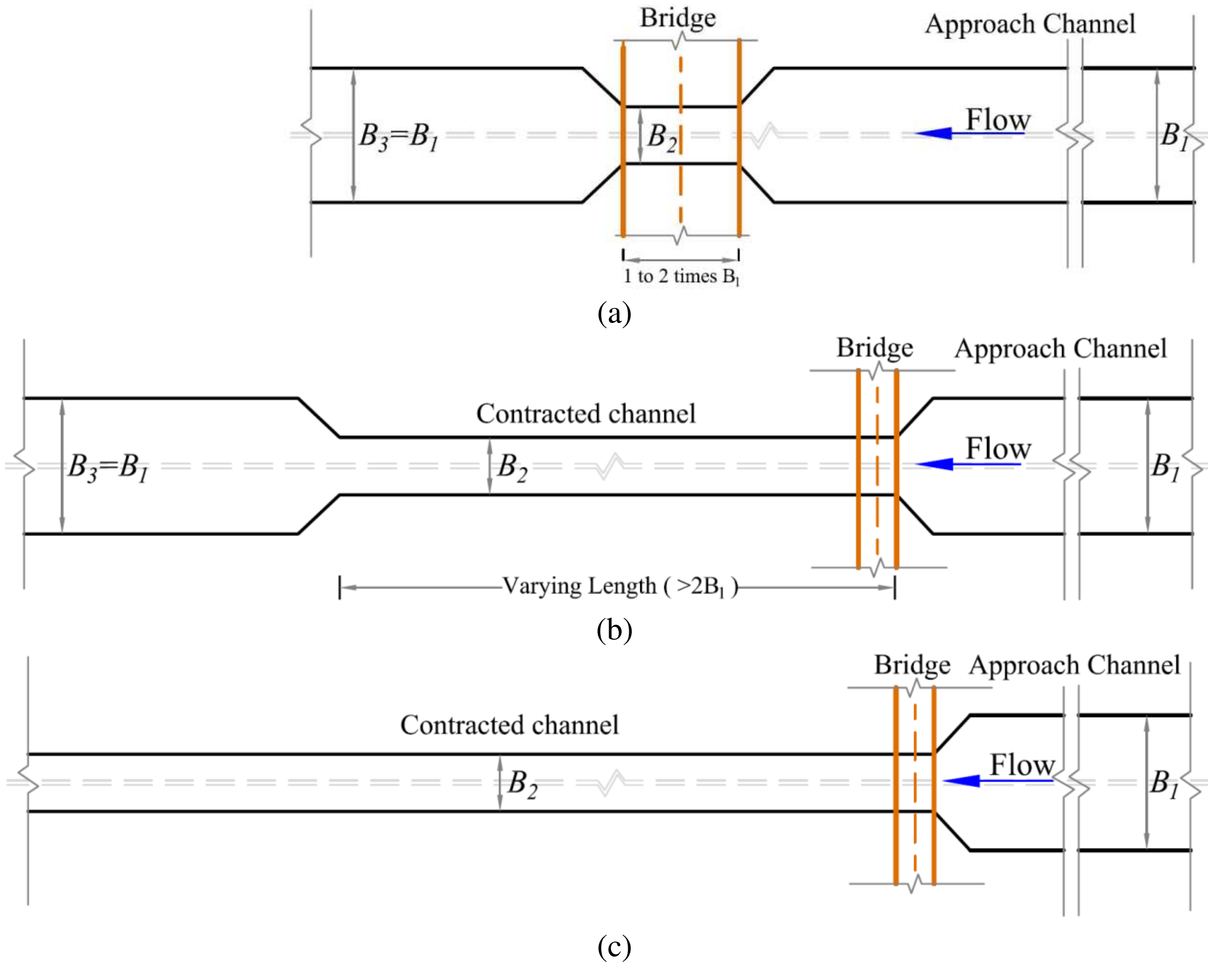

Figure 2.2. Schematic view of different types of contracted channel: (a) short-length contraction; (b) intermediate-length contraction; and, (c) long-length contraction. For sub-critical flow along a contracted channel, the flow control is the downstream section of the contracted channel.

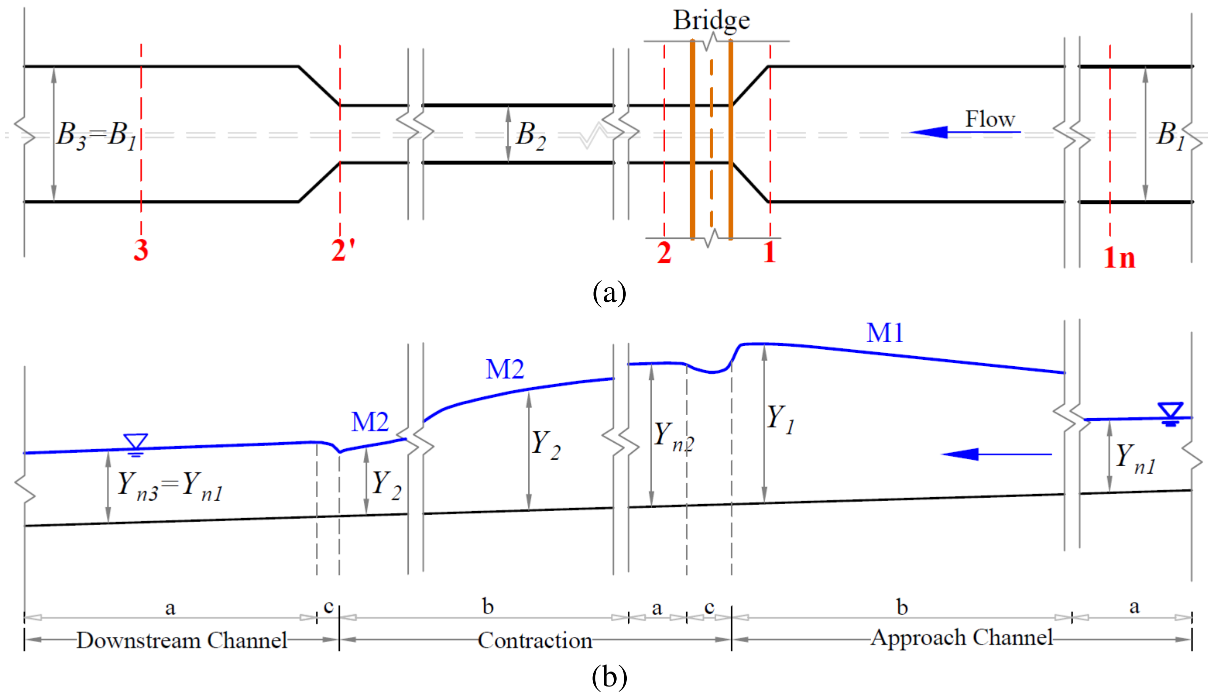

Figure 2.3. Pre-scour flow profile zoning: (a) plan view; and, (b) centerline cross-section. In this figure the sub-reaches have the following meaning:" a" signifies uniform flow (UF)," b" signifies gradually varied flow (GVF), and" c" signifies rapidly varied flow (RVF).

The general views of the contracted channel shown in Figure 2.2 comprise three zones:

1. The uncontracted approach channel;
2. The contraction; and,
3. The uncontracted downstream channel (same width as the upstream channel).

Within each of these three zones of channel, three sub-zones occur (based on the flow profile along the contraction):

- Uniform flow (UF) sub-zones, labelled "a." In these sub-zones, the flow is uniform and of normal depth.
- Gradually varied flow sub-zones (GVF) labelled "b". The GVF flow includes an M1 (backwater) water-surface profile in the approach channel leading up to the contraction.

Additionally, the GVF flow includes an M2 (drawdown) water-surface profile along the contraction.

- Rapidly varied flow (RVF) sub-zones, labelled "c". These sub-zones form because of the relatively rapid changes in channel geometry at the contraction entrance and possibly the switch from subcritical to supercritical flow.

Figure 2.3 illustrates how the contraction categories mentioned above can be defined quantitatively, relative to each other. In each category, it is assumed that the contraction forms an M1 water-surface profile (or backwater profile) upstream of the contraction.

When the length of a bridge contraction is less than about 1 to 2 times the width of the approach channel (to give a sense of magnitude) and encompasses only sub-zones "b" and "c" at the contraction's upstream end, the contraction is called a *short-length contraction* (or more simply, a *short contraction*), Figure 2.4 illustrates. This category is typical of bridge waterways for single bridges and is marked by the streamwise extent of the upstream flow-separation region extending the full length of the contraction. In the absence of flow choking (at the contraction's downstream or upstream ends), sub-zone "c" occurs only at the contraction entrance, and sub-zone "b" merges with the depth of uniform flow downstream of the contraction.

When the length of a contracted, bridge waterway exceeds the length of the contraction's region of upstream flow separation, the contraction here is called an *intermediate-length contraction*, as Figure 2.5 illustrates. The contraction length is not long enough for flow depth along the contraction to attain the normal depth, Y_{n2}, for flow along the contraction, but the contraction's length influences flow through the contraction, as mentioned above. In approximate terms (to give a sense of magnitude), the length of an intermediate contraction can range from about 2 to (say) about 300 times the width of the uncontracted approach channel. This category is typical of bridge waterways accommodating multiple bridges (e.g., a freeway road system with separate bridges for the different directions of traffic, and possibly flanked by one or more smaller bridges for local traffic). Further, this category was the focus of the present study, because this category includes a substantial length of sub-zone "b."

When the length of a contracted, bridge waterway is sufficiently long (say, to give a sense of magnitude, exceeding about 300 times the width of the approach channel) flow along the contraction attains the normal depth for a flow along the contraction. The normal depth becomes the flow control for the contracted channel, and the contraction is called a *long -contraction*. Figure 2.6 illustrates this category, for which typically does not occur at a bridge waterway. However, an example of long-contraction would be the engineered, long contractions sometimes built when a river channel is flanked and narrowed by flood-control levees or by a series of instream, channel-control structures (e.g., bendway weirs or rock vanes).

2.3.2. Hydraulics

The water surface profile along a contraction conveying a subcritical flow varies with the shape of the contraction entrance and with the length of the contraction. The ensuing sections describe how flow varies along the three categories of contraction.

2.3.2.1. Hydraulics of Short Contractions

When the length of the contracted section is less than about twice the width of the approach channel, the contraction is a short-contraction, because the flow field in the contraction is occupied largely by the formation of a vena contracta of flow entering the contraction. The turbulence structures generated by flow separation at the contraction's entrance and the exit connect and interact. The length of the contraction that these flow features occupy varies with the shape of the contraction entrance and characteristics of the approach channel (notably flow velocity and flow aspect ratio).

When describing contraction hydraulics, it is useful to use the variation of flow specific energy as flow enters the contraction. Figure 2.4 indicates the flow profile through a typical short contraction and shows how changes in flow specific energy occur as flow passes through a contraction. This figure, which has an amplified vertical scale to illustrate the flow profiles, does not show the likely interaction of the turbulence structures formed by flow separation at the entrance and the exit of the contraction. Those interactions would amplify scour at the walls of the contraction, doing so by exerting additional hydrodynamic forces on the bed in those areas.

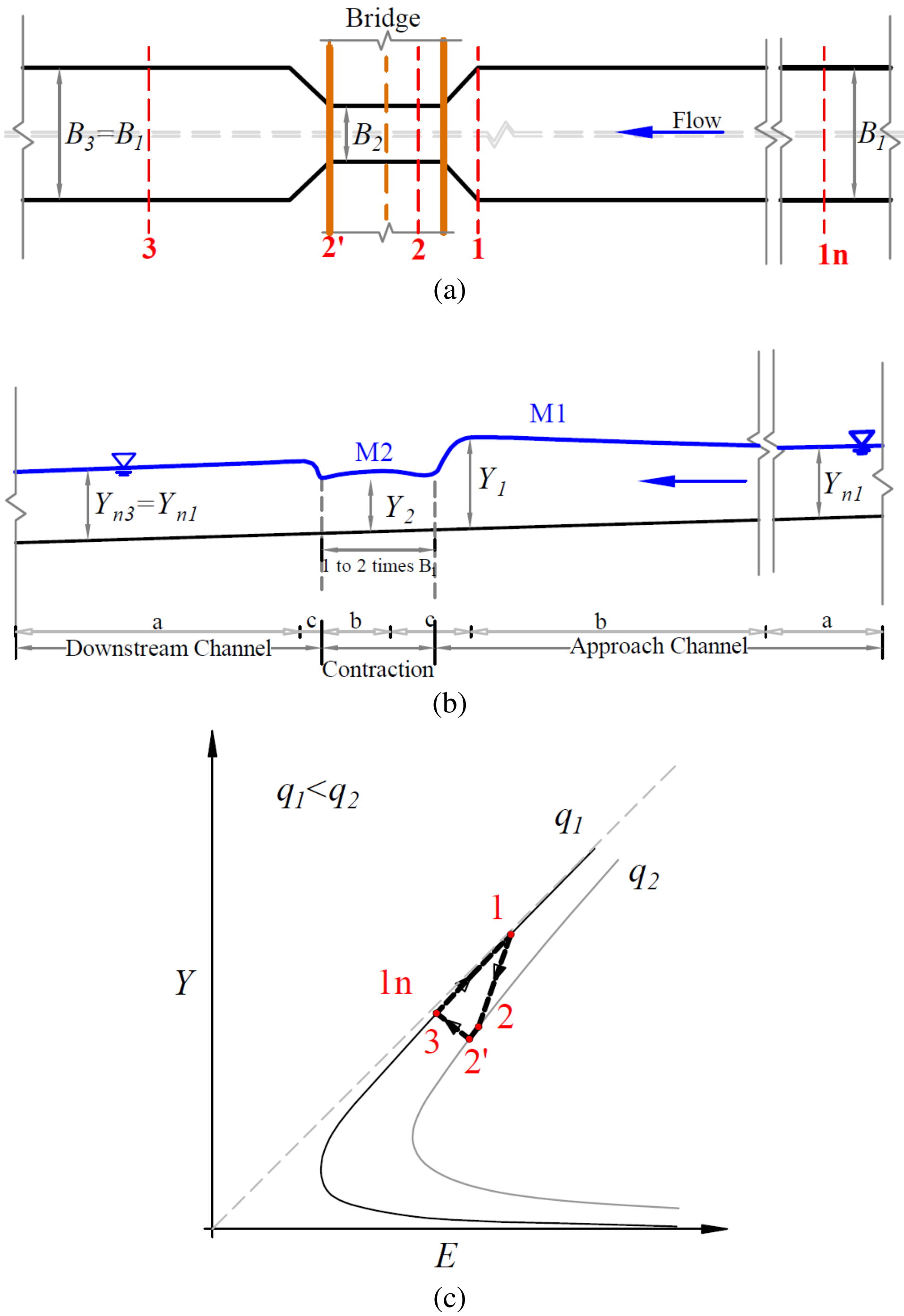

Figure 2.4. Pre-scour flow profile zoning for a short contraction: (a) plan view; (b) centerline cross-section; and, (c) energy diagram. Note the sub-reaches in (b): "a" is uniform flow, "b" is gradually varied flow (GVF), and "c" is rapidly varied flow (RVF)

Specific energy, E, is defined as (e.g., Henderson 1964)

$$E = Y + \frac{V^2}{2g} \tag{3.1}$$

Values of E are measured vertically from the local invert or bed elevation of a channel. By neglecting the energy loss associated with flow resistance along the contraction (the contraction is of short length) the specific energy balance between sections 1 and 3 in Figure 2.4 is

$$E_3 = E_1 - \Delta E \tag{3.2}$$

with,

$$\Delta E = h_{L\ contraction} \tag{3.3}$$

Here,

E_1 = specific energy at section 1

E_3 = specific energy at section 3

ΔE = total energy loss

$h_{L\ contraction.}$ = local headloss for flow through the contraction (like flow through a valve)

The specific energy diagram in Figure 2.4 is useful for describing how the flow profile develops along a contraction. When the flow approaches and enters the contracted channel, the flow may form a backwater curve (M1 profile) along the approach to the contraction, because additional energy (water depth of head) is needed to overcome the local energy loss (headloss) associated with flow passing through the contraction (Figure 2.4c). The energy loss depends on several factors, including the shape of the contraction entrance. The normal flow depth of the approach flow, Y_{n1}, consequently increases to Y_1, and the approach-flow specific energy, E_{1n}, correspondingly increases to E_1. For conditions of modest contraction (like at most bridges) and slight backwater formation, then $Y_1 \approx Y_{n1}$. This approximation often is assumed by bridge engineers estimating depth of contraction scour and can be reasonable (and practical) when the approach channel comprises a main channel with extensive floodplains, which can store water otherwise stored by a flow that develops a marked M1 (or backwater) profile.

The energy increase associated with the backwater development (or with augmented discharge from floodplain drainage) is consumed as headloss as the flow passes through the contraction. Part of this headloss is attributable to increased boundary-resistance as flow velocity increases along with the vena contraction formed in the contraction entrance. Tracking flow specific energy changes (Figure 2.4c), the flow depth moves from 1n to 1 and (as it enters the vena contracta) from 2 to 2', attaining specific energy E_2'. In short-contractions, flow depth Y_2 cannot be sustained as normal flow, because the energy gradient (friction slope) of the flow exceeds the bed slope. Therefore, the flow is non-uniform. Manning's flow-resistance equation (metric units) confirms this effect; i.e.,

$$V = \frac{1}{n} Y_2^{\frac{2}{3}} S_f^{\frac{1}{2}} \tag{3.4}$$

For GVF, friction slope, S_f, exceeds bed slope, S_0. The hydraulics outcome (sub-zone b) is flow depth decreases and flow velocity increases along with the contraction, once the vena contracta formation extends to the full width of the contracted channel.

Where flow re-enters the main channel, flow specific energy then returns to the value associated with the normal depth of flow along the main channel (section 3) as flow continues along the original channel. Herein, the hydraulic properties of cross-section 3 are taken to be the same as for cross-section 1, because the original channel had a constant width of flow.

2.3.2.2. Hydraulics of Intermediate-length Contractions

A contraction is of intermediate length when turbulence structures at the entrance of the contracted channel do not interact with the turbulence structures at the channel's exit, and when the contraction's length produces appreciable energy losses. Additionally, the contraction is not long enough for flow to reach a normal depth, Y_{n2}, along the contracted section.

The energy losses affect the M2 and M1 profiles developed by the contraction. Due to the variation of the M2 curve with contraction length, the backwater depth at the upstream end (entrance) of the contraction varies too, because of the additional resistance to flow along the contraction. The comment made above regarding the approximation, $Y_1 \approx Y_{n1}$, also applies to contractions of intermediate length.

Figure 2.5 illustrates flow along a contraction of intermediate length. The energy balance between sections 1 and 3 in Figure 2.5c is

$$E_3 = E_1 - (h_{L\,ent.} + h_{L\,exit}) - L(S_f - S_0) \tag{3.5}$$

Here,

E_1 = specific energy at section 1

E_3 = specific energy at section 3

$h_{L\,ent.}$ = local headloss at contraction entrance

$h_{L\,exit}$ = local headloss at contraction exit

L = contraction length

S_f = energy gradient

S_0 = bed slope

Figure 2.5b indicates that increasing the length of the contraction channel increases the backwater depth. Also, Figure 2.5c uses a specific energy diagram to show how increasing resistance along the contraction increases flow depth at section 1.

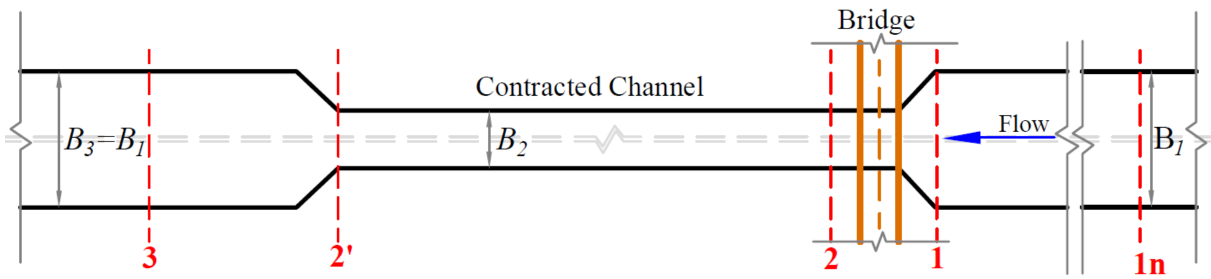

(a)

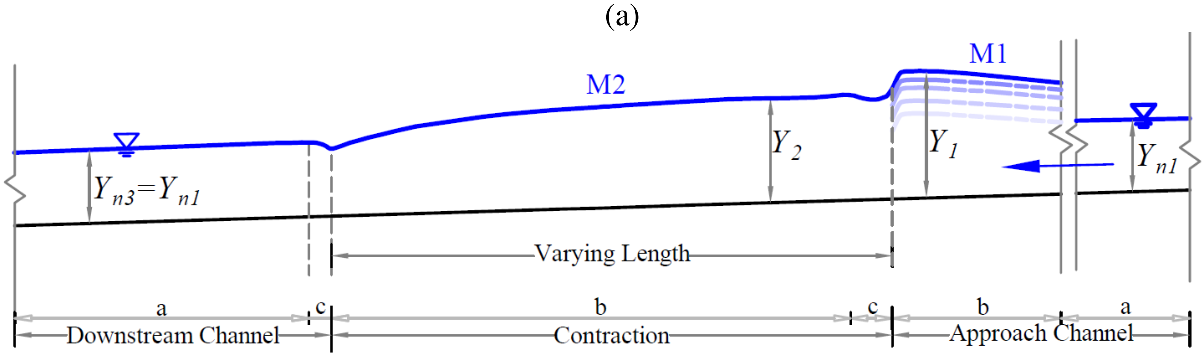

(b)

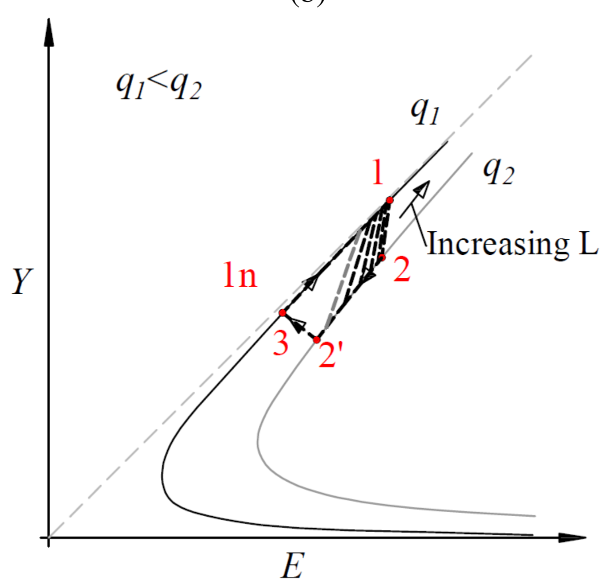

(c)

Figure 2.5 Pre-scour flow profile zoning for an intermediate-length contraction: (a) plan view; (b) centerline cross-section; and, (c) energy diagram. Note the sub-reaches in (b): "a" is uniform flow, "b" is gradually varied flow (GVF), and "c" is rapidly varied flow (RVF).

Essentially all previous experiments (e.g., Dey and Raikar 2005; Webby 1984) investigated a condition of intermediate-contraction scour and erroneously assumed this condition to be long-contraction scour. As mentioned above, the length of an M2 flow profile along an intermediate-length contraction affects scour depth along the contraction. It is useful to reiterate here that all bridge waterways fall into the short- and intermediate-contraction categories, and most bridge waterways form short contractions.

2.3.2.3. Hydraulics of Long-length Contractions

A long contraction occurs when the contraction length is sufficiently long that flow attains its normal depth, Y_{n2}, along the contraction. As the flow attains its normal depth, contraction length no longer affects the water depth at the upstream end of the contracted section. Consequently, the maximum depth of scour along the contraction no longer depends on the length of contraction. Due to attaining normal depth along the contraction the flow control would move from downstream end of contraction (section 3) to the section with normal depth (section 2), as Figure 2.6 shows.

The energy balance between sections 2 and 1 is

$$E_2 = E_1 - (h_{L\,ent.}) - L(S_f - S_0) \quad (3.6)$$

For small distances, e.g. transitions, the term $L\,(Sf - S_0)$ is negligible,

$$E_2 = E_1 - (h_{L\,ent.}) \quad (3.6)$$

Here,

E_1 = specific energy at section 1, which for the shown configuration equals the specific energy at section 3

E_2 = specific energy at section 2

$h_{L\,ent.}$ = local headloss at contraction entrance

Figure 2.6 shows this contraction-scour condition, for which the scour depth results from difference in the initial elevation of the bed and the bed elevation associated with flow resistance along a loose-bed channel of width equivalent to that of the contracted channel.

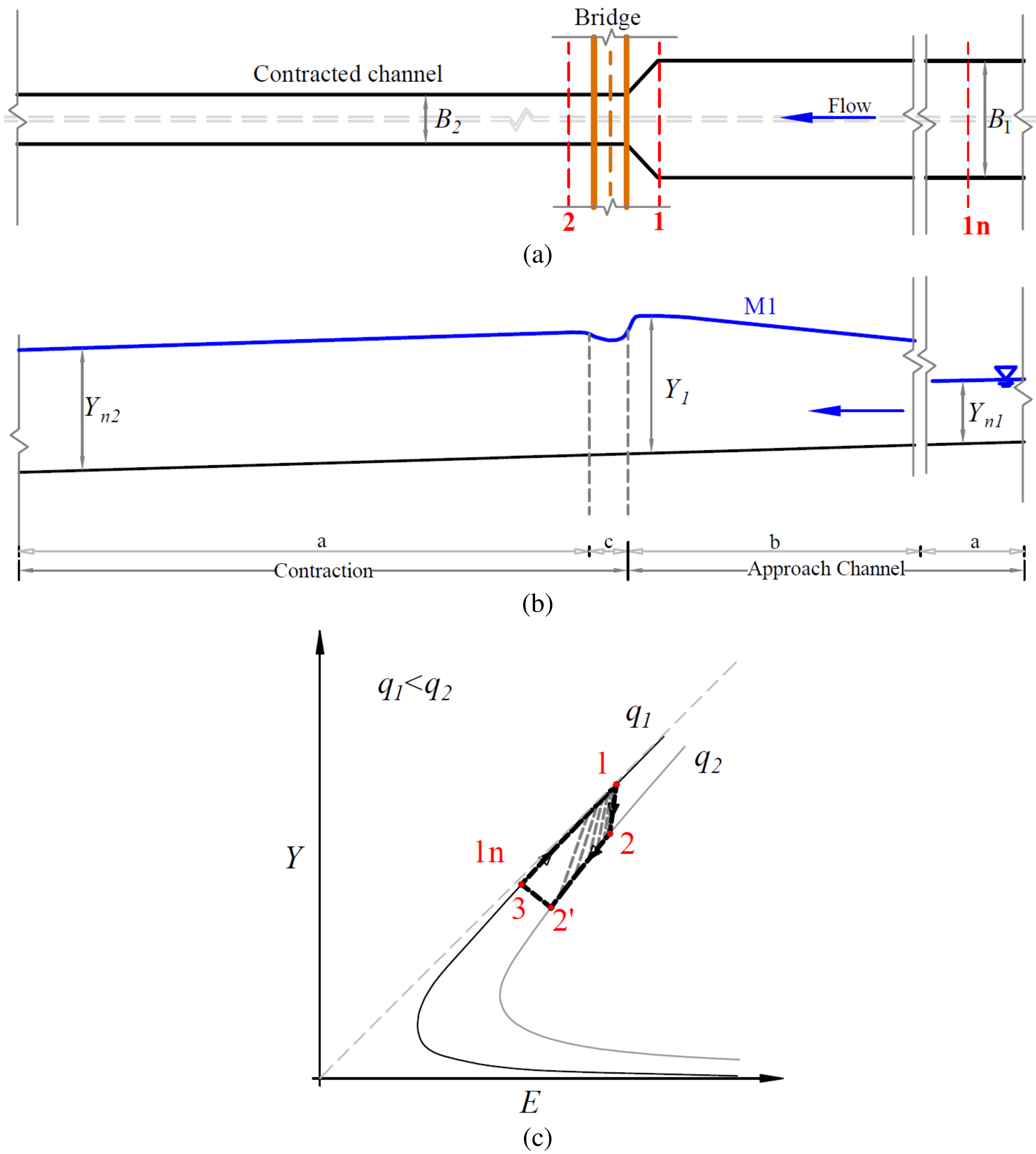

Figure 2.6. Pre-scour flow profile zoning for a long contraction: (a) plan view; (b) centerline cross-section; and, (c) energy diagram. Note the sub-reaches in (b): "a" is uniform flow, "b" is gradually varied flow (GVF), and "c" is rapidly varied flow (RVF)

2.4. Location and Influence of Flow Choking

As mentioned above, flow choking alters the local flow field at and within the entrance of the contracted channel, causing supercritical flow to occur through the entrance of the contracted channel. Supercritical flow implies greatly increased flow velocity and bed shear stress within the entrance and changes the form of flow separation at the entrance. The ease at which choking may occur at intermediate-length contractions and short contractions leads to a loose categorization of channel contractions: tight contractions, medium contractions and mild contractions. Tight contractions choke most readily. Bridge waterways usually are in the latter two categories, except when subject to natural blockages from accumulated woody debris or ice. The bridge-deck blockage is also another possible factor in upstream choking

In intermediate-length or long contractions, choking may happen at the exit or entrance ends of the contracted channel owing to the extensive distance between the exit and entrance ends. Section 2.2.1 describes the conditions leading to choking. Figure 2.7 shows that the flow depth decreases to the critical depth within the contraction entrance when choking becomes severe (e.g., due to bridge-beam and -deck blockage of flow). Potential outcomes of the increased values of flow velocity and bed shear stress (inferred by Figure 2.7) are increased scour depth and altered and spatially varying dimensions of bedforms. Scour and bedforms may, in turn, affect the initial choking at a contraction entrance, but this consequence requires further investigation and was beyond the scope of the present study. In the design of the present experiments, there was no assurance that scour, by increasing the cross-sectional area of flow within the entrance, would alleviate choking. Studies of scour at short-span arch bridges indicate that choking is not substantially relieved by scour (Solan et al. 2020).

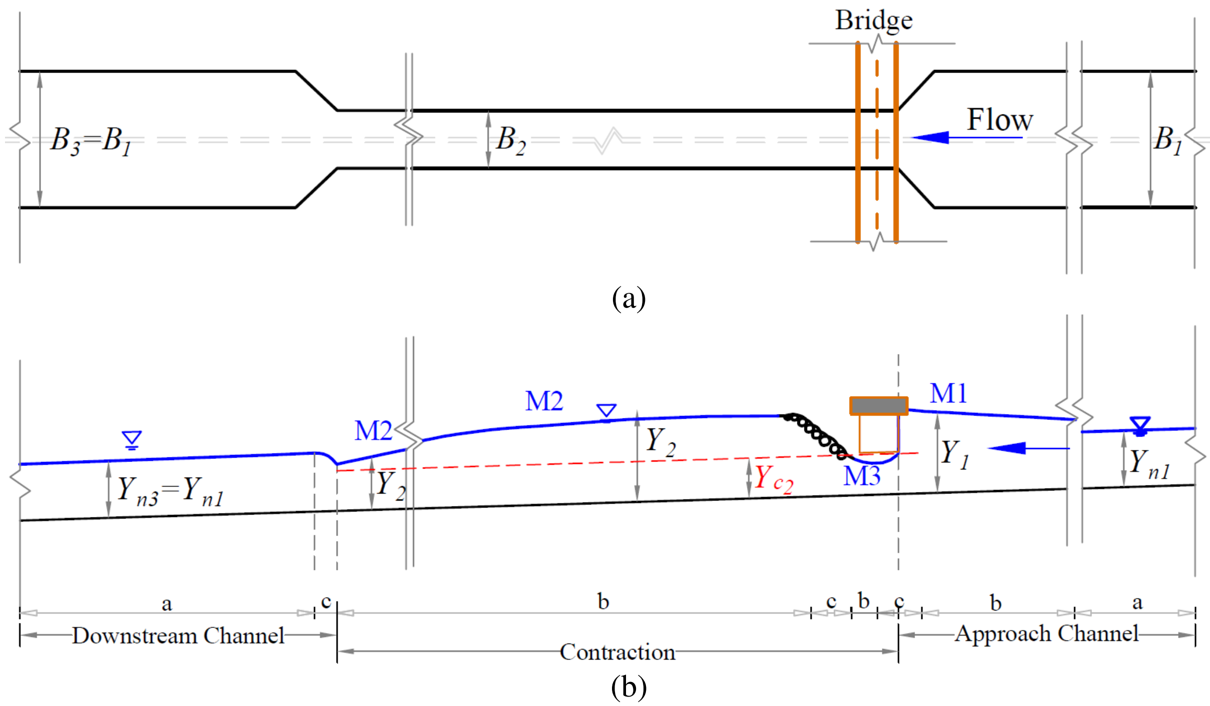

Figure 2.7. Sub-critical flow along a contraction of intermediate length and with choking occurring at the contraction exit: (a) plan view of the contracted channel; and, (b) water-surface profile along the channel with contraction. Also indicated here is choking at the entrance (possibly due to bridge-beam and -deck blockage of flow).

Figure 2.8 uses the specific energy to show the occurrence of choking at a contraction. Beyond point of incipient choking (2') the flow enters the supercritical flow condition. This condition is common for flow in short-span bridges prone to congest flow. Flow choking at the upstream end of the contracted section makes contraction scour depth largely independent of the contraction length because flow control shifts from the contracted channel's downstream end to the channel's upstream end, as Figure 2.8 shows. An approach flow may get choked in a contracted section when the specific energy at the upstream section, E_1, is lower than the minimum energy at the contracted section, E_{min2}. By assuming no energy loss through these sections, the energy level, E_1, water depth, Y_1, at the upstream section will increase until the energy reaches to the minimum energy at the contracted section, E_{min2}. In regular waterways, choking may happen when the contraction ratio reduces to a choking limit. This situation is not a desirable design situation for a bridge waterway, but it could occur owing to debris or ice congestion of a waterway.

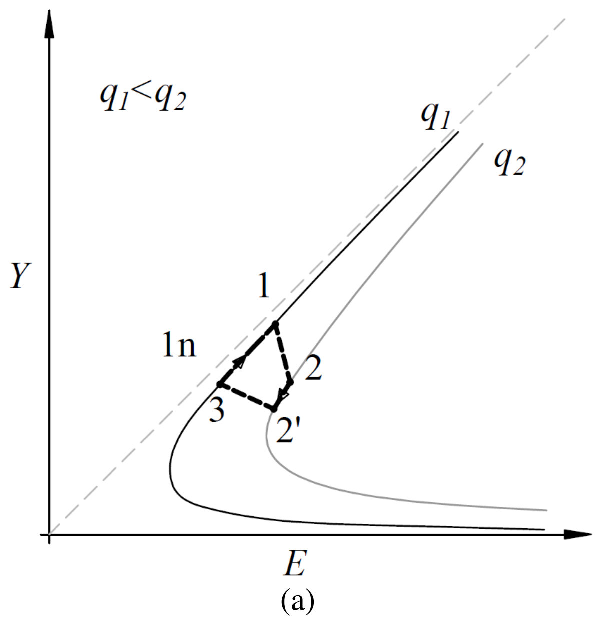

Figure 2.8. Choking effect on flow depth:(a) unchoked condition (b) choked condition

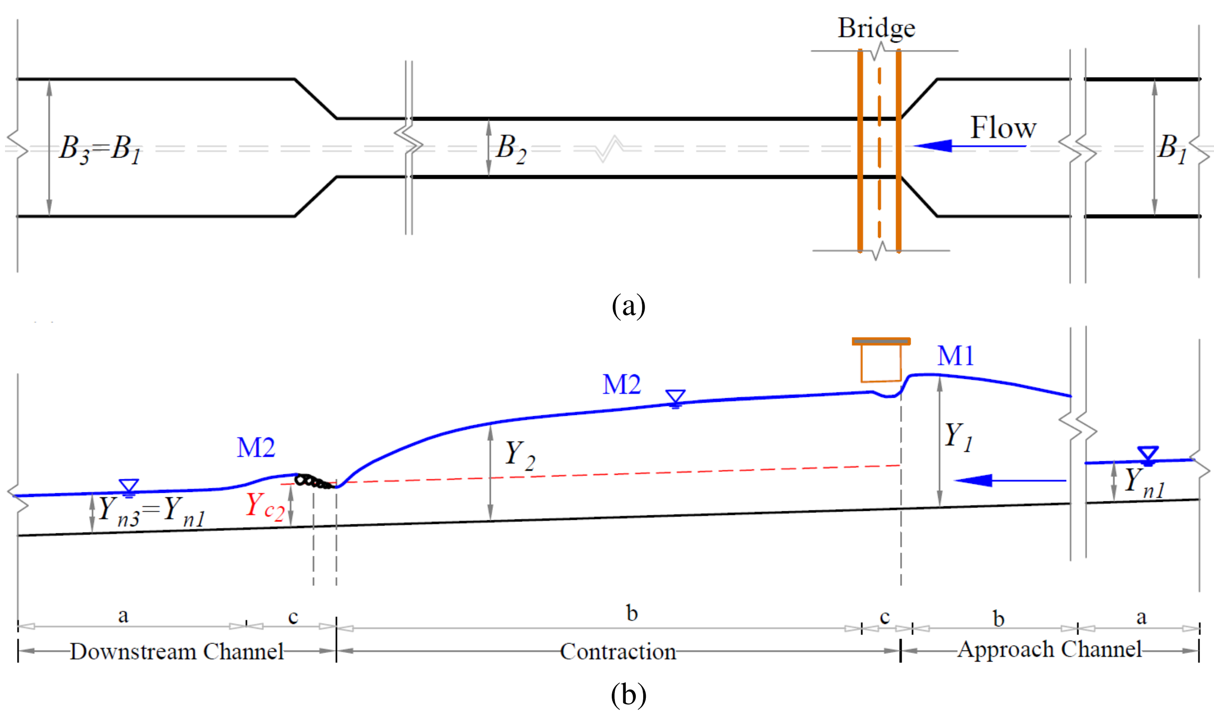

Figure 2.9. Sub-critical flow along a contraction of intermediate length with flow choked at the contraction entrance: (a) plan view of contracted channel; and, (b) water-surface profile along the channel with contraction.

The magnitude of choking or water-level rise varies from negligible to substantial, depending on the geometry of the contraction and the length of the contracted channel. Overall, the choked condition will increase the scour depth in comparison with the unchoked condition, owing to the increased flow velocity through the contraction.

Figure 2.9 shows exit choking, for which the specific energy at the exit, E_3, is less than the minimum energy at end of the contracted section, $E_{min2.}$ It is important to note that, as shown in Figures 2.7 and 2.9, flow has an M2 curve due to losing energy as flowing downstream or in other words gaining energy from downstream to upstream. Consequently, in channels for which no-choking condition applies at the downstream end, it is very unlikely that upstream end chokes owing to flow condition or contraction ratio. However, it is possible to have upstream choking occur due to other processes like the accumulation of ice rubble, woody debris, or bridge-beam and -deck blockage.

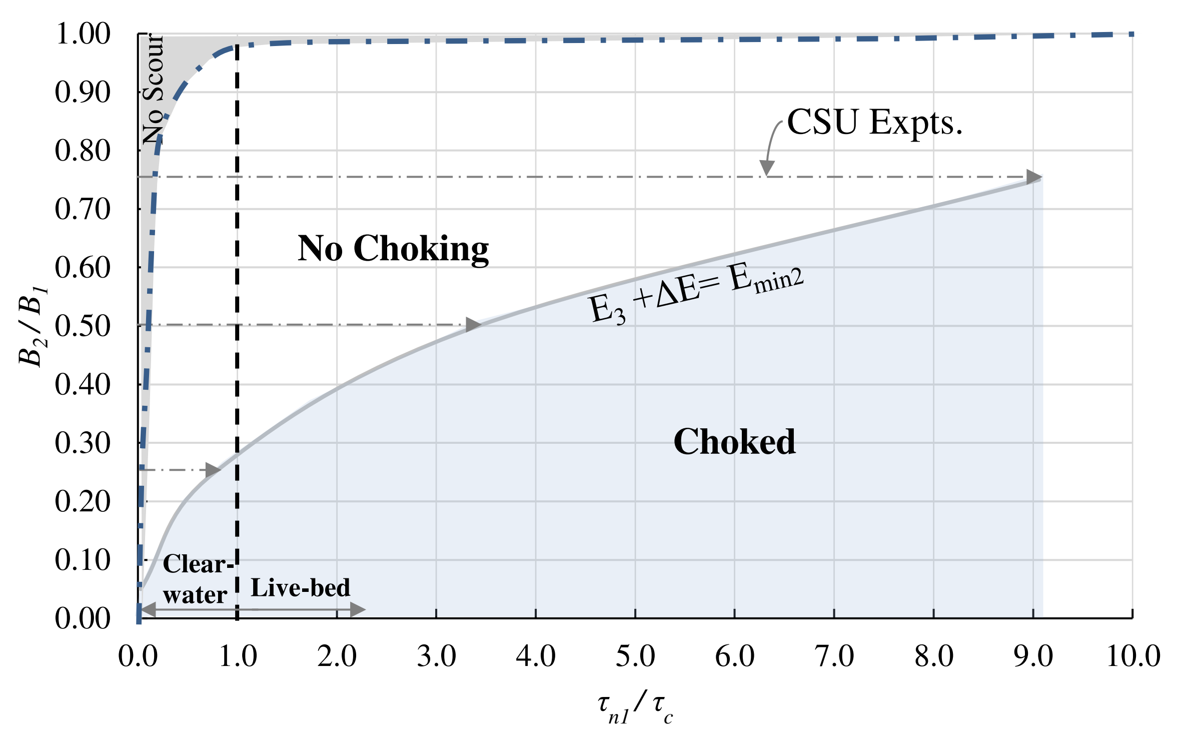

Figure 2.10. The short-contraction choking condition (downstream) outlined in terms of values of the contraction ratio, B_1/B_2, and shear-stress ratio, τ_{n1}/τ_c. This figure also indicates (using arrows) the three values of B_1/B_2 used in the CSU experiments.

As mentioned above, because choking will aggravate the scour depth, it was important for this study to avoid choking. Figure 2.10 was used in designing the experiments so as to avoid a choked condition during the experiment setup process.

The choked condition also can be delineated in terms of the Froude number of the approach channel for different contraction ratios, as Figure 2.11 illustrates. The tight contractions would get choked in lower Froude numbers (i.e. lower velocities) of flow. It is useful to note that the boundary line between choked and no choking condition may encounter a small shift by changing the shape of the exit transition, i.e., local energy loss (ΔE).

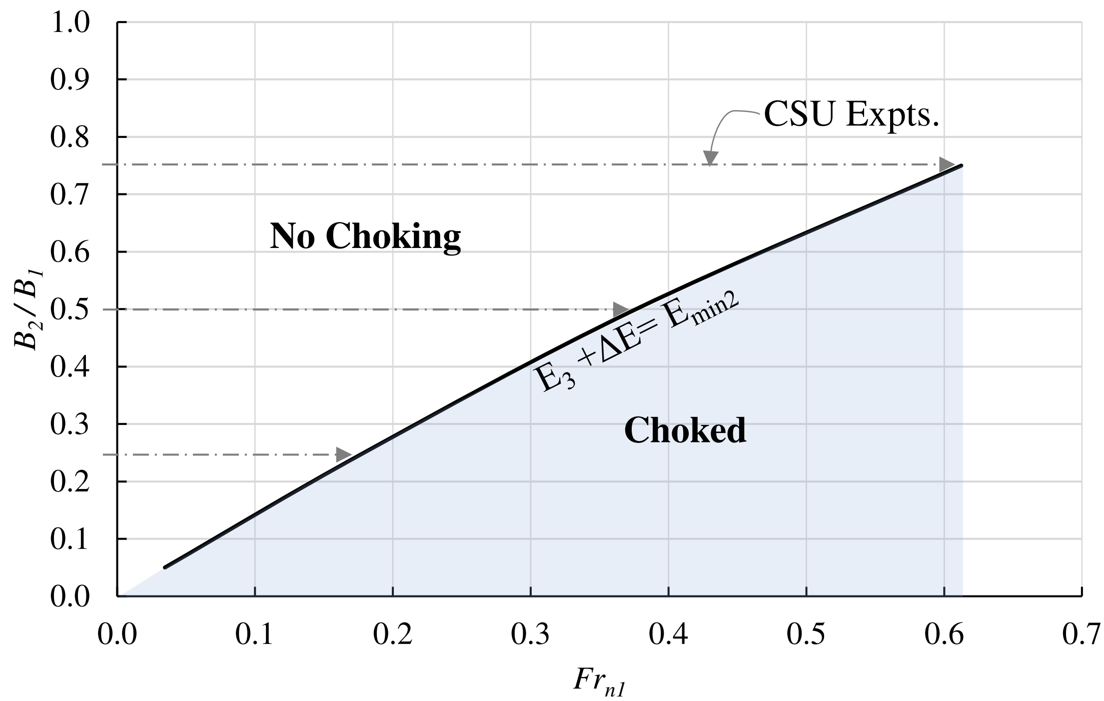

Figure 2.11 The short-contraction choking condition (downstream) outlined in terms of values of the contraction ratio, B_1/B_2, and Froude number Fr_{n1}. This figure also indicates (using arrows) the three values of B_1/B_2 used in the CSU experiments.

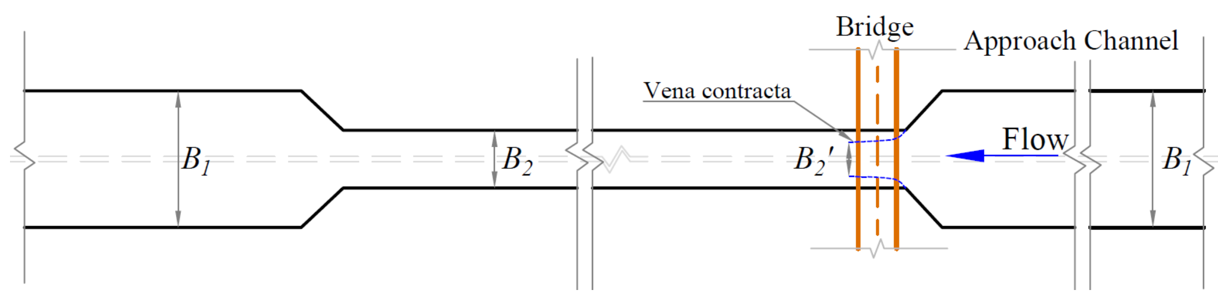

Figure 2.12. Vena contracta formed in the entrance of a contracted channel

A short contraction is typically categorized as an upstream contraction owing to the formation of a *vena contracta*, which affects the exit loss from a contraction. The entrance contraction ratio, B_2'/B_1, is always smaller than the ratio at contracted section, B_2/B_1. A short-contraction has a bigger obstruction at the entrance than exit and the contraction length is not long enough to let the flow gain energy due to the bed slope, see Figure 2.12. By assuming a range of contraction coefficient (B_2'/B_2) between 0.6 to 0.9, the short contraction choking condition becomes a real concern, see Figure 2.13.

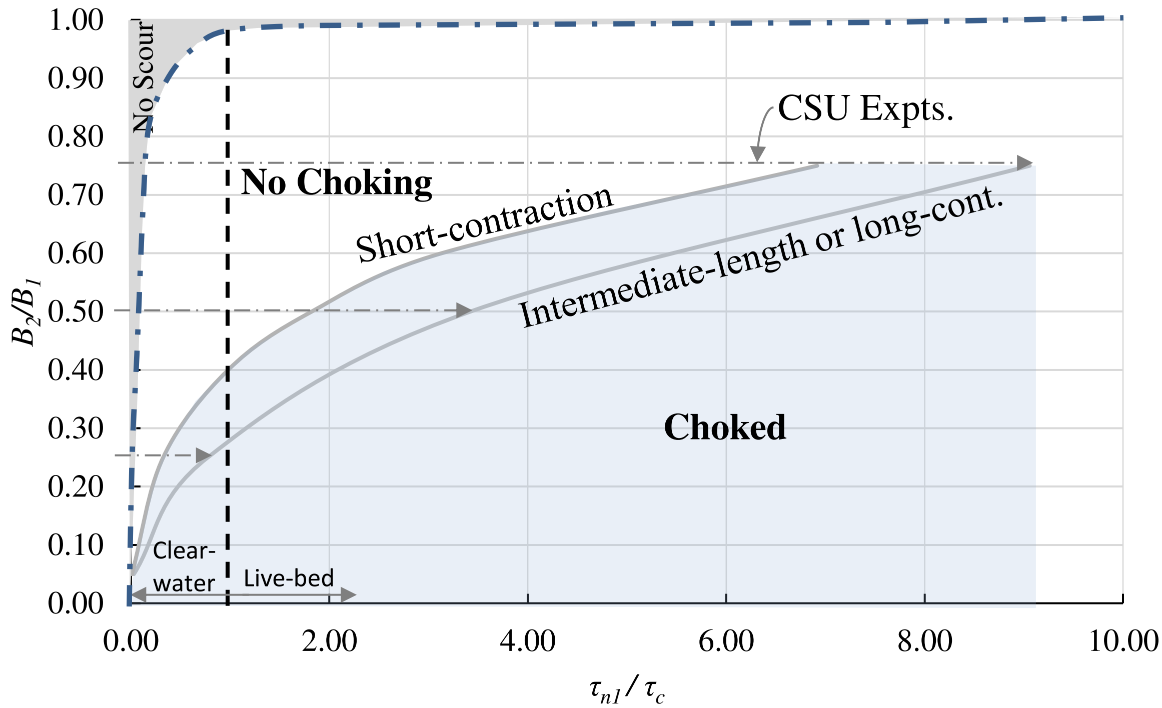

Figure 2.13. The short-contraction choking condition outlined in terms of contraction ratio, B_1/B_2., and shear-stress ratio, τ_{n1}/τ_c.

2.5. Bed shear stress

The bed shear stress (proportional to the square of mean velocity) exerted by a flow influences the scour pattern in a contraction. A bed will scour in clear-water condition when the bed shear stress, τ_b, is larger than the critical value of bed shear stress, τ_c, for the incipient motion of the bed materials. For live-bed conditions, scour occurs when the rate of outflow of bed sediment exceeds the rate of inflow of bed sediment. Webby's (1984) experimental data, together with the numerical model HEC-RAS, can be utilized to illustrate how the shear stress varies in contracted flow along a rigid bed, and to show the hydraulics difference between intermediate and long-contraction scour which is brought in details in Chapter 3.

2.6. Loose-Boundary Consideration

The waterways have loose beds formed of alluvium that respond to changes in flow conditions. Therefore, flow to and through channel contractions is typically unsteady, because the channel bed (and possibly channel banks) experiences erosion, sediment deposition, and changes in bed roughness, bed slope and hydraulic radius.

Contraction scour commences once flow velocities and the hydrodynamic forces associated with turbulence exceed a threshold condition for the erosion of the bed material (and possibly the banks). Consequently, scour begins quite readily as flow rate increases. As scour occurs, the specific energy at the contraction changes and flow hydraulics adjusts. Eventually, as scour deepens, the value of specific energy at the contraction increases and so does the flow depth (Figure 2.14). However, as mentioned above, it is unclear to what extent that scour affects the value. The flow field at the contraction entrance changes in form as scour develops.

It is well-known (e.g., ASCE 2008) that clear-water scour refers to the condition where an alluvial reach does not carry any appreciable quantity of sediment or the sediment remains in suspension during the flow, and that live-bed scour refers to when an alluvial channel conveys sediment and the channel's bed is in an active state of deposition and erosion cycle. Equilibrium for live-bed scour occurs when there is a balance between erosion of bed sediment and deposition of bed sediment in the scour region.

Owing to having a backwater curve at the downstream end of the contracted section, rapidly varied flow at the contraction entrance/exit, and the contraction length as a variable for different cases of contraction; scour depth is expected to vary along the contracted channel, as Figure 2.14 indicates.

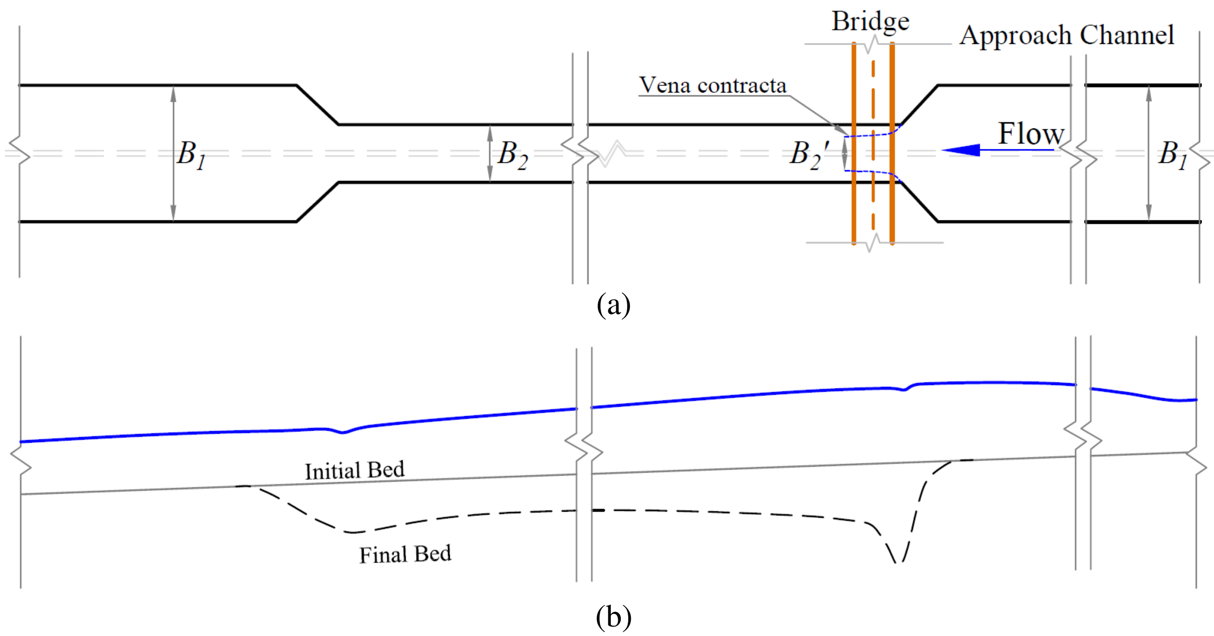

Figure 2.14. General scour pattern along a contracted channel of intermediate-length (as categorized above).

3. Literature Review

3.1.Introduction

As Chapter 2 shows, the hydraulics of open-channel contractions is complicated by considerations related to contraction geometry and loose-boundary flow in alluvial channels. These complications were known before this study (e.g., Keller 1977), but were inadequately addressed in the literature on contraction scour at bridge waterways.

To discuss the literature on contraction scour it is useful to develop a framework formed from considerations that build upon the hydraulics and loose-boundary concepts Chapter 2 presents. This approach can be done by means of dimensional analysis, which then can be used to indicate the shortcomings associated with prior formulations and data trends the literature contains. The ensuing section presents an analysis of dimensional and similitude parameters associated loose-bed open channel contracted by a bridge waterway or a series of other hydraulic structures built at an initially unbridged channel of uniform width. The subsequent sections review the literature and assess the contributions made by prior studies and explain the major gaps prompting the present study.

3.2. Dimensional analysis and similitude

The ensuing dimensional analysis and similitude identifies the main parameters associated with flow and bed scour along a straight open-channel contraction of intermediate length and uniform width (Figure 2.5). The dimensional analysis entails several assumptions, made to aid the clarity of the analysis. Figure 3.1 presents a schematic view of the contraction layout and indicates the main variables the analysis considers. Additionally, this figure indicates that the water-surface profiles of flow through the contracted channel may adjust as the bed of the contracted channel erodes.

The contracted channel is taken to be rectangular in cross-section, smooth-sided, and to have sidewalls resistant to erosion. The flowrate along the approach channel is assumed to be steady and uniform (well upstream of the contraction). It is noted here that the flow immediately upstream of the contraction may be non-uniform, because of the increased resistance created by the contraction. Moreover, the contraction may cause flow choking (Figure 2.7) if the approach has insufficient initial energy to pass the flow into the contraction; the flow depth increases until the requisite energy amount is attained. Furthermore, sub-critical flow entering the contraction develops a vena contracta narrower than the width of the contracted channel, then widens (after some development length) to the full width of the contracted channel. Flow at the exit of the contraction is taken to return to a channel whose width is the same as that of the channel approaching the contraction. Uniform or (hydraulically) normal flow depth occurs along the exit channel.

The channel bed consists of cohesionless sediment, initially leveled to form a bed of constant slope to and through the contraction. The particle shape and specific gravity of the bed sediment are taken to be typical of alluvium found in rivers and streams. In Figure 3.1, λ is bedform wavelength and H is bedform height,

The transition from the approach channel to the contracted channel is a vertical wall set at an angle (plan) of 45^{o}. The analysis assumes that the shape of the transition, by influencing the extent of the vena contracta and the turbulence generated at the contraction entrance, affects the depth of scour and the length of scour or (altered bed) along the contraction. In particular, the analysis assumes that the shape of the transition affects the variation of flow depth along the upstream (or entrance) portion of the contraction. The analysis presupposes that the transition shape affects the flow field at the contraction entrance and that turbulence structures generated in the flow field are advected along the contraction. The depth of uniform or (hydraulically) normal flow depth along a lengthy contraction is independent of the geometry or the shape of entrance, because that depth depends only on the resistance characyeristics of the contracted channel.

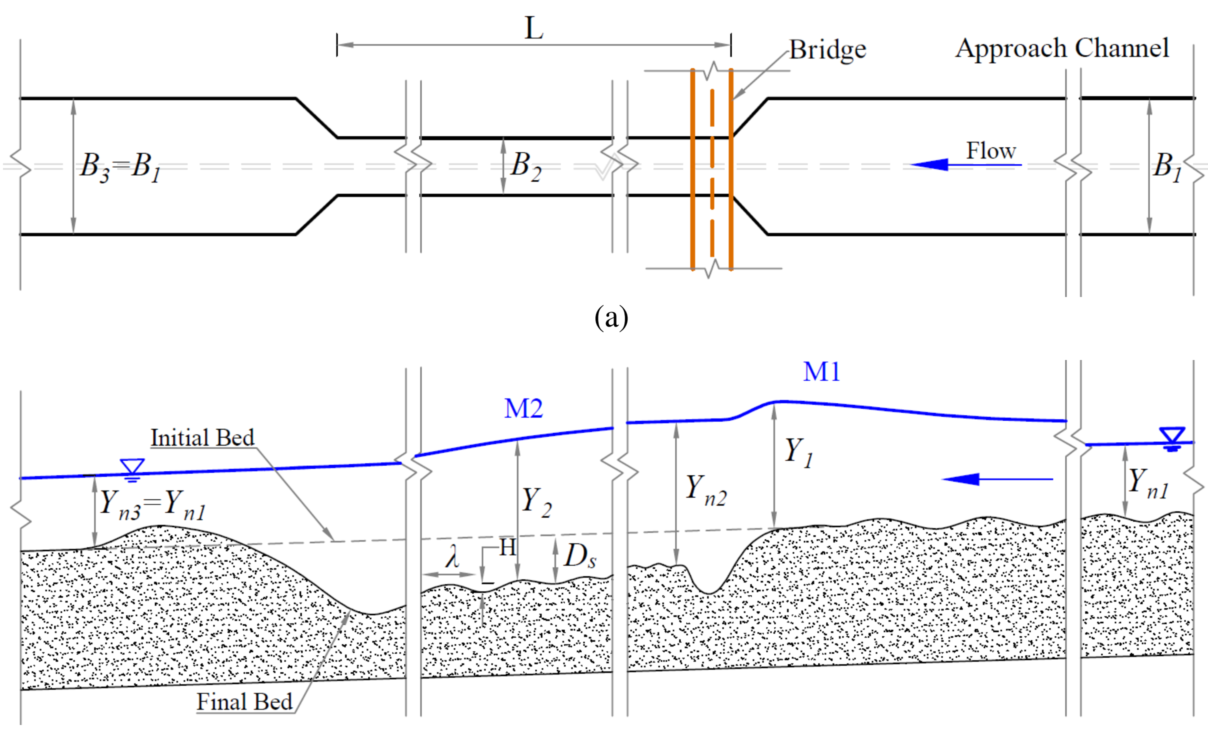

(b)

Figure 3.1. The main variables associated with an intermediate-length contraction of a rectangular open channel formed with a loose, alluvial bed: (a) plan view; and, (b) side elevation.

Table 3.1 lists the independent kinematic, dynamic, and geometric variables taken here to be involved in contraction scour. The variables are then cast in terms of non-dimensional parameters that characterize the influences the variables exert on the development of contraction scour.

Table 3.1. The independent variables considered when analyzing flow and sediment transport through a contraction. (Note: more variables could be considered than are listed here).

Variable	Symbol
Width of approach channel	B_1
Width of contracted channel	B_2
Angle of the contraction transition	α
Normal depth of flow along uncontracted section	Y_{n1}
Bed slope of the approach channel (and contracted channel)	S_1
Length of contraction	L
Shape of the contraction entrance (non-dimensional)	*entr. shape*
Shape of the contraction exit (non-dimensional)	*exit shape*
Median diameter of bed sediment	d_{50}
Geometric standard deviation of bed sediment diameter	σ_g
Sediment density	ρ_s
Density of water	ρ
Gravity acceleration	g
Critical bed shear stress for entrainment of bed sediment	τ_c

The dependent variable of primary interest for this analysis is scour depth at several locations along a contraction. The equilibrium scour depth, D_s, associated with flow along a contraction of intermediate length can be written functionally as

$$D_s = f_1(B_1, B_2, Y_{n1}, S_1, L, d_{50}, \sigma_g, \rho_s, \tau_c, \rho, g, t, entr.shape, exitshape) \quad (3.1)$$

Restated in terms of non-dimensional parameters, Eq. (3.1) becomes,

$$\frac{D_s}{Y_{n1}} = f_2\left(\frac{B_1}{Y_{n1}}, \frac{B_2}{B_1}, \frac{L}{Y_{n1}}, \frac{d_{50}}{Y_{n1}}, \sigma_g, \frac{\rho_s}{\rho}, \frac{\rho g Y_{n1} S_1}{\tau_c}, entr.\ shape, exit\ \ shape\right) \quad (3.2)$$

In Eq. (3.2), D_s/Y_{n1} is a dependent parameter whose value is influenced by the independent parameters within the brackets. In accordance with the hydraulics analyses presented in Chapter

2, the value of D_s varies with position along the contraction. For the temporal development of scour depth, Eq. (3.2) should include a time parameter.

The three repeating variables used to form Eq. (3.2) are Y_{n1}, τ_c, and ρ. In Eq. (3.2), the parameters B_1/Y_{n1} and B_2/Y_{n1} are combined to form B_1/Y_{n1} and $B_2/B1$, as the latter parameter is convenient for describing the contraction ratio for the contracted channel. The terms $\rho g Y_{n1} S_1$ can be replaced with τ_1, the shear stress exerted on the bed by uniform flow along the approach channel. Note that, as discussed in Section 2.3, Y_{n1} and τ_1 pertain to uniform flow along the approach channel. At the upstream end of the contraction, the flow depth and bed shear stress are reduced, owing to the backwater (M1) water-surface profile created by the contraction (Figure 2.4). When the approach flow is subcritical along a river channel of constant geometry, and the bridge waterway is placed in the river channel, Y_{n1} and τ_{n1} also apply to the flow condition at the exit of the contraction.

Eq. (3.2) reduces to

$$\frac{D_s}{Y_{n1}} = f_3\left(\frac{B_2}{B_1}, \frac{L}{Y_{n1}}, \frac{\tau_{n1}}{\tau_c}, \frac{d_{50}}{Y_{n1}}, entr.shape, exit.shape\right) \tag{3.3}$$

The average equilibrium depth of contractions cour, D_s, normalized with approach-flow depth, Y_{n1}, is shown to be a function of contraction ratio, B_1/B_2, values of contraction length and sediment diameter normalized with Y_{n1}, shear-stress ratio (state of bed sediment mobilization), and the contraction's entrance and exit shapes. Eqs. (3.2) and (3.3) do not include factors associated with the non-rectangular form of a channel.

Additionally, the values of D_s and Y_2 are affected by the formation of a vena-contracta within the entrance to the contracted channel. The parameters in Eq. (3.3) influence the width and length of the vena contracta, though the relative importance of each parameter varies.

3.3. General Comments

General observations of the prior studies indicate that several major difficulties regarding contraction-scour estimation are evident. The difficulties are identifiable in terms of Eqs (3.3) and (3.4) and the open-channel hydraulics described in Chapter 2. The main difficulties, which much of the prior literature inadequately addresses, are as follow:

Prior studies indicate several major difficulties regarding contraction-scour estimation. The difficulties are identifiable in terms of Eqs (3.3) and (3.4) and the open-channel hydraulics described in Chapter 2. The main difficulties are as follow:

1. The flow depth used to normalize scour depth is Y_1, typically measured after contraction scour was considered. The difficulty with using Y_1 is that this depth is not an independent variable, because Y_1 varies with scour depth (flow resistance through the contraction) and is in a region of non-uniform flow (a backwater or M1 profile). In other words, contraction-scour depth is normalized using a dependent (not an independent variable);
2. The mean velocity of flow is treated as an independent variable without being related to the overall (fixed) slope and geometry of the channel containing the contraction. Yet the formulations of contraction scour invoke the Manning's equation for values of D_s/Y_{n1} vary with the contraction length parameter, L/Y_{n1}, which is not considered in the prior studies;

3. The resistance of the bed along the contraction varies with the characteristics of loose-boundary flow along the contraction. Besides, describing relative particle roughness and state of bed motion, respectively, the parameters d_{50}/Y_{n1} and τ_{n1}/τ_c describe the variation of flow resistance developed along the contracted channel. Figure 3.1 illustrates this complication for sand bed. A sand bed develops bedforms, whose dimensions are described in terms of bedform height, H, and wavelength, λ, as defined in Figure 3.1. Those dimensions vary with flow over a bed;
4. The shape of the entrance and the shape of the exit to the contraction influence the flow field in the contraction entrance and the contraction exit. These shape configurations affect energy-loss considerations, and the entrance shape affects turbulence advected into the contraction; and,
5. Contracted channels can choke. The combined effect of the dependent parameters can cause the flow to choke at the exit or the entrance of a contraction. Choking at either location substantially alters the flow through a contraction. A common example of choking at bridges occurs with scour at short-span masonry bridges (Solan et al. 2020). A further example arises with severe accumulations of ice and debris at bridges. The occurrence of choking requires doing the analysis Chapter 2 presents; an analysis not done by prior studies.

None of these considerations was considered in the formulation method leading to the equations in Arneson et al. (2012), the widely used design guide for estimating scour at bridge waterways. Furthermore, the considerations bring into question the customary divisions of contraction scour into the categories of clear-water and live-bed contraction scour. This division is arbitrary (as

Chapter 6 of this dissertation explains) and inadequately reflects the physics of loose-boundary resistance to erosion, such as occurs along an open channel of narrowed width.

The ensuing review of prior studies in contraction-scour literature uses the four points listed above when examining the data and scour relationships those studies have produced. Appendices A through D concisely summarize prior studies on clear-water contraction scour, live bed contraction scour, field studies of contraction scour, and numerical-model studies of contraction scour.

3.4. Review of Prior Flume Studies and Formulations

A useful approach to evaluating the insights attained by prior studies with flume is to examine the soundness of the contraction-scour equations resulting from the studies. As the studies essentially build chronologically upon the results of the earlier studies, it is useful to proceed by reviewing the studies in essentially chronological order. Table.3.2 summarizes the values of the parameters Y_1/B_1, B_2/B_1 and L/B_1 used in prior laboratory-flume studies. This table also lists reported values of Y_2/B_2, though these values should be regarded as being only approximate.

Additionally, the prior studies used relatively small values of L/B_1 (or contraction length). In effect, it could be claimed that most of the prior studies only examined short contractions and were unaware (so far as they report) of the hydraulics of contracted channels. Also, the prior studies report using backwater depth (measured at the contraction entrance), Y_1, when presenting their results even though (as Chapter 2 points out) Y_1 itself varies with contraction conditions and does not indicate the onset of flow choking. Among the consequences of Y_1 varying are that bed shear stress and bed sediment transport at Y_1 also vary. Appendices A and B give more detailed information about the range and number data developed by the prior studies' data are shown in histogram format. Chapter 8 compares these data with findings from the present study.

Table 3.3 summarizes the main aspects of the equations emanating from each study. The equations currently recommended in the leading design guide used in, HEC-18 (Arneson et al. 2012) stem from a review of information from the preceding studies.

Table 3.2. The summary of prior lab studies and data.

	Y_1 / B_1	B_2 / B_1	L / B_1	Y_2 / B_2
Live-bed scour				
Straub (1934)	0.05 to 0.19	0.7	6	0.2 to 0.7
Ashida (1963)*	-	0.2, 0.5	-	-
Komura (1966)	0.07 to 0.22	0.3, 0.45, 0.7	10	0.5 to 1.5
Gill (1981)	0.05 to 0.10	0.66	2.4, 3.2	0.1 to 0.25
Rana (1986)*	-	0.3,0.45,0.7	-	-
Clear-water scour				
Gill (1981)	0.03 to 0.11	0.66	2.4, 3.2	0.08 to 0.226
Webby (1984)	0.05 to 0.08	0.33	2.8	0.22 to 0.32
Dey and Raikar (2005)	0.11 to 0.23	0.4, 0.5, 0.6, 0.7	1.67	0.22 to 1.17

* Ashida's paper and Rana's thesis are in Japanese. The data are extracted from Lim and Cheng (1998). However, the channel width and length of those experiments are not mentioned in Lim and Cheng (1998).

The earliest formulation of contraction scour was published by Straub (1934), who treated equilibrium of live-bed contraction scour in terms of continuity of bed-sediment transport as bedload passing through the contracted flow section. He conducted a series of flume experiments (Y_1/B_1 was varied; $B_2/B_1 = 0.7$; and, $L/B_1 = 6$) and used the Du Boys bedload (sediment) transport formula in estimating of the bedload transport rate in the approach-flow and contracted sections.

The Du Boys, or shear-stress excess, formula is one of the earliest formulas for estimating sediment load, and is described in ASCE (2008). Straub's work initiated the notions of a "long contraction" scour and of "clear-water" and "live-bed" equilibrium contraction scour. These terms were adopted by subsequent studies. Inspection of Straub's formulation reveals that it responds to none of the four difficulties listed at the outset of this chapter.

The now classic formulations were by Laursen (1960, 1963). Laursen (1960) followed essentially the same formulation approach to that by Straub, though applied his own sediment transport formula to the live-bed case with the result shown in Table 3.3 His approach is commonly known as the Laursen live-bed contraction scour formula and forms the crux of subsequent formulations in which sediment transport occurs along the approach bed. For compound channels, Laursen assumed that the sediment transport occurs only in the main channel. His formula considers both bed-load and suspended-load transport of bed sediment; the coefficient p (see Table 3.3) varies in accordance with the relative proportions of bed load and suspended load to the total sediment transport rate. For an overbank flow contraction with a bank-line abutment, Table 3.3 indicates that Laursen's dimensionless formula for scour depth depends on (Q_t/Q_c), whereas for flow limited to the main channel it depends on B_1/B_2. Table 3.3 defines the terms in these parameters.

Laursen (1963) additionally used the notion of a long contraction when considering clear-water scour. He assumed that the shear stress on the bed of the contracted section reduced until attaining the critical value τ_c associated with the incipient motion of the sediment forming the bed in the contraction. Thereupon, equilibrium depth of scour occurred. Further, Laursen (1963) used the Manning's flow-resistance equation for the approach flow and the contracted flow to obtain a ratio of τ_1/τ_c that, when combined with the flow-continuity equation, yielded his formula for equilibrium depth of clear-water contraction (Table 3.3) though Laursen's formulas for equilibrium depths of live-bed and clear-water contraction scour seem logical, they like Straub's (1934) formula, do not address the four difficulties mentioned above. Laursen and Straub, for instance, inadequately took into account loose-boundary hydraulics and evidently did not consider the effects of flow-choking.

An aspect of Laursen's work is that he did not do any flume experiments on contraction scour. Instead, he relied on the assumed merits of his formulations and data from Straub (1934). Only subsequently (Laursen and Alawi 1989) did he perform flume experiments. Those experiments, however, involved a short flume and instruments that were awkward to use in the murky conditions often associated with live-bed scour.

In the 1960s, Komura (1966) examined the influence of armouring on live-bed depth of contraction scour. He argued that the ratio of sediment sizes on the approach-flow bed and the contracted-channel bed influences the equilibrium depth of contraction scour for large values of B_1/B_2 and σ_g. His argument, though obvious and sound, did not address the four points mentioned at the start of this chapter. Komura applied dimensional analysis to interpret the results from a series of flume experiments on live-bed and clear-water contraction scour for the range $L_c/B_1 = 10$. The length of his contraction relative to contraction width, L_c/B_1, was the longest of prior studies. His interpretation led to a formula in which dimensionless, equilibrium depth of contraction scour depends on F_1, B_1/B_2 and σ_{g1}, as Table 3.3 shows. Komura's equation, however, is not used these days, because of the empirical origin.

A series of experiments clear-water contraction scour was done by Keller (1977, 1983) regarding scour in a contracted alluvial channel. Though he named the channel a "long contraction", the contracted channel was only 2.8 times the width of the approach channel (i,e.,

L_c/B_1 = 2.6), and the flume's slope was fixed. Keller defined a "long contraction" as pertaining when $L_c/B_1 \geq 2$. He kept the contraction ratio set at $B_2/B_1 = 0.33$, but varied Y_1/B_1, by varying water flowrate, Q. His flume data did not fully agree with the clear-water scour relationship proposed by Laursen (1963), indicating deeper scour occurred in a localized region at the contraction entrance. Also, he noted that especially deep scour near the corners of the contraction. His work was extended by Webby (1984), as noted below.

Next, Gill (1981) generalized the Straub formula for live-bed scour by assuming that the rate of sediment transport is proportional to bed shear stress excess raised to some power; i,e., $(\tau_1 - \tau_c)^\beta$, where β is an exponent equal to 3 for the Einstein-Brown formula and 1.5 for the Meyer-Peter and Mueller formula. This adjustment further reflects the use of earlier, shear-stress excess (Du Boys) expressions for bed sediment transport. Gill ran series of flume experiments, for which the largest value of L_c/B_1 was 3.2. Table 3.3 gives Gill's formula.

The analytically derived equations assume a uniform approach flow (e.g., Laursen 1960, 1963) and sediment transport rates based on uniform flow. However, as mentioned above, there is no clear definition as to whether prior studies used the uniform flow depth, Y_{n1}, or backwater depth, Y_1. It is evident from the pertinent publications that the studies used the post-scour water depth in the approach channel at the cross-section where the contraction starts; i.e., they used the backwater depth at an equilibrium-scour condition, which typically is lower than the backwater depth of the pre-scour condition. They assumed a uniform approach flow but used the post-scour depth (of the backwater water-surface profile) to develop their empirical equation or validate their analytical equation. Webby (1984) was the only experimental study that reported the evolution of both the bed and water-surface profiles through time. In Table 3.3, Y_1 is used to indicate the approach flow depth, which the prior studies take (erroneously) to be uniform. However, whether this depth was pre- or post-scour is not stated by the studies.

Table 3.3. Contraction scour formulas.

Author(s)	Formula(s)	Comment
Straub (1934)	$\frac{Y_2}{Y_1}=\left(\frac{B_1}{B_2}\right)^{6/7}\left[\frac{\tau_c}{2\tau_1}+\sqrt{\left(\frac{\tau_c}{2\tau_1}\right)^2+\left(1-\frac{\tau_c}{\tau_1}\right)\frac{B_1}{B_2}}\right]^{-3/7}$	*Live-Bed Scour;* τ_c = critical shear stress; Based on the DuBoys bedload transport formula Where $B_2 = (1-\alpha)B_1$
Laursen (1960)	$\frac{Y_2}{Y_1}=\left(\frac{Q_t}{Q_c}\right)^{6/7}\left(\frac{B_1}{B_2}\right)^{p_1}\left(\frac{n_2}{n_1}\right)^{p_2}$	*Live-Bed Scour*; Q_c = approach flowrate in main channel ; Q_t = total flowrate through bridge opening main channel; n = Manning's resistance coefficient; p_1, p_2 = exponents from Laursen's total sediment transport formula depending on whether sediment load is mostly bedload, mixed load, or mostly suspended load; B_1 = approach main channel width; B_2 = bridge main channel width.
Laursen (1963)	$\frac{D_s}{Y_1}=0.13\left(\frac{Q}{d_{50}^{1/3}\,Y_1^{7/6}\,B_2}\right)^{6/7}-1$	*Clear-Water Scour*. Shear stress in contracted section equal to the critical shear stress τ_c at equilibrium. The formula is in U.S. customary units.

Author(s)	Formula(s)	Comment
Komura (1966)	$\frac{Y_2}{Y_1} = 1.45\ Fr_1^{1/5}\ \left(\frac{B_1}{B_2}\right)^{2/3}\ \sigma_{g1}^{-1/5}$ *Or* $\frac{Y_2}{Y_1} = \left(\frac{B_1}{B_2}\right)^{\frac{6}{7}} \left(\frac{\tau_1}{\tau_2}\right)^{\frac{2}{7}}$ *Live-bed* $\frac{Y_2}{Y_1} = 1.60\ Fr_1^{1/5}\ \left(\frac{B_1}{B_2}\right)^{2/3}\ \sigma_{g1}^{-1/2}$ *Or* $\frac{Y_2}{Y_1} = \left(\frac{B_1}{B_2}\right)^{\frac{6}{7}} \left(\frac{\tau_{c1}}{\tau_{c2}}\right)^{\frac{2}{7}}$ *Clear-water*	*Live-Bed and Clear-Water Scour.* **F**$_1$ = approach flow Froude number; σ_{g1} = geometric standard deviation of sediment size distribution in approach channel. Includes effect of armouring in contracted section.
Gill (1981)	$\frac{Y_2}{Y_1} = 1.2\ \left(\frac{B_1}{B_2}\right)^{\frac{6}{7}} \left[\frac{\tau_c}{\tau_1} + \left(1 - \frac{\tau_c}{\tau_1}\right)\left(\frac{B_1}{B_2}\right)^{1/3}\right]^{-3/7}$	*Live-Bed Scour.* Sediment transport rate assumed proportional to $(\tau - \tau_c)^{\beta}$
Webby (1984)	$B_2Y_2\left[\frac{B_2Y_2}{B_2 + 2\left(\frac{n_w}{n_b}\right)^{\frac{3}{2}} Y_2}\right]^{\frac{1}{6}} = \frac{n_bQ}{\sqrt{\tau_{*c}\ (GS-1)D_{50}}}$	*Clear-water scour.* *Gs=specific gravity,* n_b*= Mannings n of the channel bed,* n_w*=Manning's n of the channel walls,* τ_{*c}*= critical shields stress*
Froehlich (1995)	$D_s = \left[\frac{Q}{\frac{1}{n}\sqrt{\tau_{*ca}(G_s-1)D_a}B_2}\right]^{\frac{6}{7}} - Y_1$	*Clear-water scour.* Extended Laursen (1963) to consider bed armoring; D_a= Mean diameter of armor particles. n= Manning's n τ_{*ca}= Dimensionless critical shear stress for the smallest particle in armor layer.

Author(s)	Formula(s)	Comment
Laursen and Alawi (1989)	$\frac{Y_2}{Y_1} = \left(\frac{B_1}{B_2}\right)^{P_1} \left(\frac{C_2}{C_1}\right)^{P_3}$	C is the bed shear factor as follow: $C = \frac{\tau_1/\tau_c - 1}{\tau_1/\tau_c}$ p_1, p_3= exponents from Laursen's total sediment transport formula depending on whether sediment load is mostly bedload, mixed load, or mostly suspended load; B_1 = approach main channel width; B_2 = bridge main channel width.
Lim and Cheng (1998)	$\frac{Y_2}{Y_1} = \left(\frac{B_1}{B_2}\right)^{0.75}$	*Live-Bed Scour.* Sediment transport rate assumed proportional to $(V - V_c)^4$ Compared with lab data for both live-bed and clear-water scour.
Briaud et al. (2005)	$\left(\frac{D_s}{Y_1}\right)_{unif} = 1.41\left(1.31\frac{B_1}{B_2}Fr_1 - Fr_c\right)$ $\left(\frac{D_s}{Y_1}\right)\left(1.38\frac{B_1}{B_2}Fr_1 - Fr_c\right)_{max}$ $L_c/B_1 > 3$	*Clear-Water Scour* of Porcelain Clay. unif = uniform scour depth; max = maximum scour depth; Fr_1 = approach flow Froude number; Fr_c = Froude number with critical velocity
Dey and Raikar (2005)	$\frac{D_s}{Y_1} = 0.368Fr_{1e}^{0.55}\left(\frac{d_{50}}{Y_1}\right)^{-0.19}\left(\frac{B_1}{B_2}\right)^{1.26}$	*Clear-Water Scour* ($0.9<V_1/V_c<1.0$) $Fr_{1e} = (V_1 - V_{1c})/[(SG - 1)gY_1]^{1/2}$; SG = specific gravity; V_{1c} = approach flow velocity when $V_2 = V_c$ at beginning of scour.
Julien (2018)	$\frac{D_s}{Y_1} = \left[\left(\frac{B_1}{B_2}\right)^{\frac{1-b}{c-b}} - 1\right]$	The Live-bed equation based on Simons-Lee Fullerton sediment transport equation. The coefficients b, and c are related to the Simons-Lee

Author(s)	Formula(s)	Comment
		Fullerton equation which can be found in Julien (2010).
HEC-18	$\frac{Y_2}{Y_1} = \left(\frac{Q_2}{Q_1}\right)^{6/7} \left(\frac{B_1}{B_2}\right)^{p}$ *Live-Bed* $D_s = \left[\frac{K_u Q_2^2}{d_m^{2/3} B_2^2}\right]^{3/7}$ *Clear-Water*	The live-bed formula is the same as Laursen (1960) with the ratio of Manning's *n* removed; *p* = sediment transport factor = 0.637-0.857. The clear-water formula is derived from $Y_2 = q_2/V_c$ and it is different in form, but not in principle, from Laursen (1963) because it does not involve the approach flow section. K_u = 0.025 (SI); 0.0077 (EN); *dm* = 1.25 d_{50}

The experiments published by Webby (1984) reveal the importance of entrance shape in affecting depth of contraction scour, especially at the entrance corners of the contraction. His experiments used basically the same flume as Keller (1977 and 1983), though the flume's downstream was extended 1.0m to distance the tailgate from the contracted channel. Keller had found that water-surface drawdown associated with tailgate proximity affected the water-surface profile through the contraction, and thereby affected the scour depths he obtained.

Webby extended Keller's experiments by conducting twelve experiments investigating clear-water contraction scour in a flume whose contraction length was 2.8 times the width of the approach channel width (L/B_1). He set B_1/B_2 = 0.33, and used uniform, fine gravel particles with a mean diameter, d_{50} = 2.15 mm. The first six experiments were done with a relatively streamlined entrance (the approach channel narrowed at a plan angle equivalent to 3 streamwise to1 transverse) and the next six experiments were done with a blunt entrance (plan angle of 90°). Figure 3.3 shows the temporal evolution of water surface and bed level for Experiment 1 (streamlined entrance), and Figure 3.4 shows the temporal evolution of the water surface and bed for Experiment 11 (blunt entrance). Keller and Webby found that the maximum depth of contraction scour downstream of the contraction entrance was 1.2 times larger than that estimated using the formula proposed by Laursen (1963). They indicate that these scour depths were measured at $1.0B_1$ to $1.25\ B_1$ downstream of the contraction entrance. Additionally, Webby (1984), like Keller (1977, and 1983), observed the formation of the deepest scour at the entrance of the contraction. Keller's observation is echoed by Bettess (2002), who mentioned the formation of a vena contracta in the entrance of contractions and who states that the then-current methods for estimating contraction scour depth are likely to underestimate scour depth. Webby described the bed evolution with time throughout two experiments, as illustrated in Figures 3.3 and 3.4.

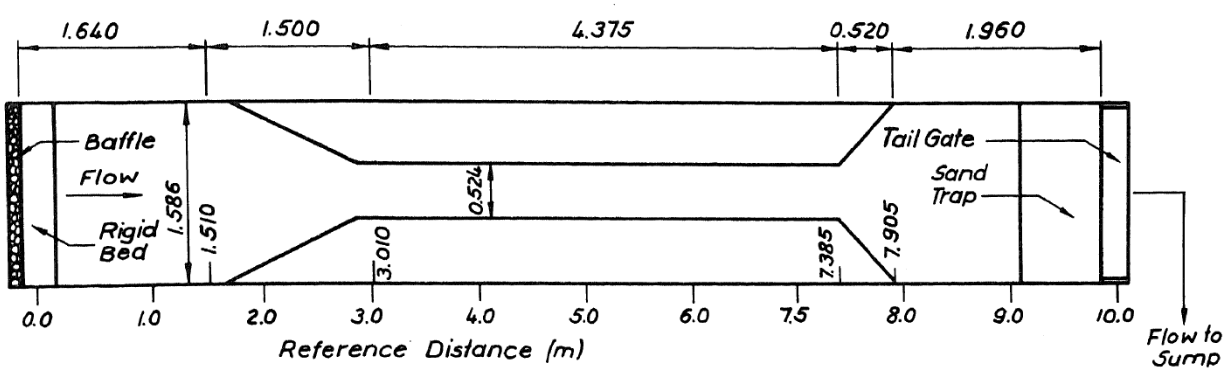

Figure 3.2. Flume layout with streamlined entrance used by Webby (1984). This flume is an extension of the flume used by Keller (1977, 1985).

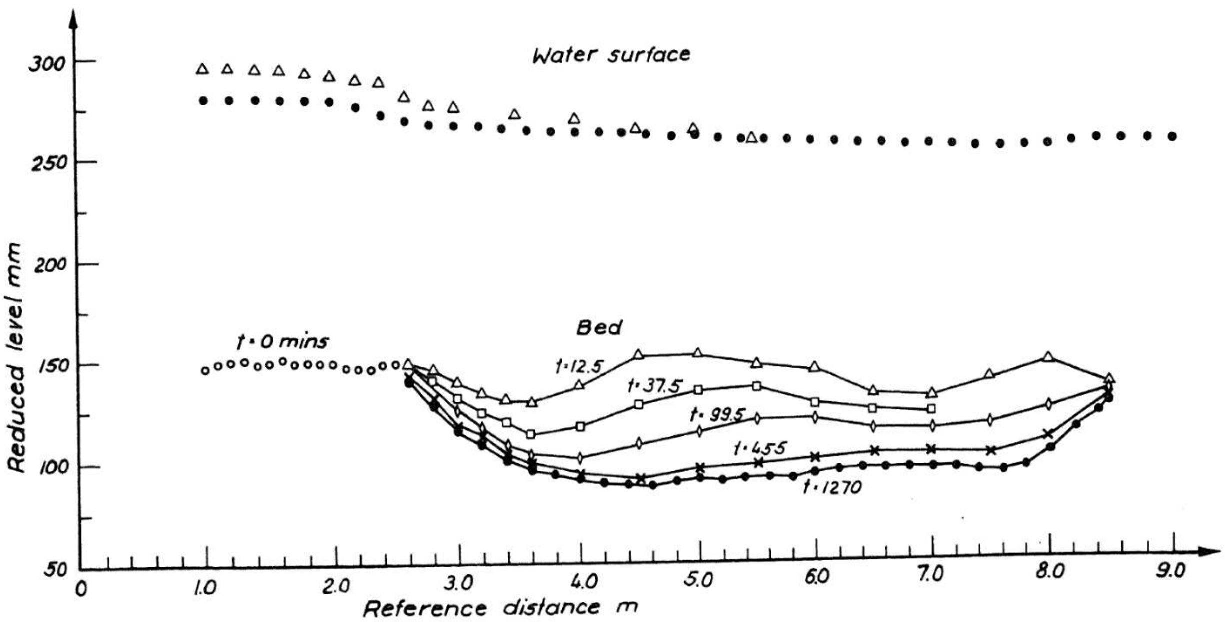

Figure 3.3. Experiment No. 1 (streamlined entrance), water-surface and bed-profile evolution. (Webby 1984)

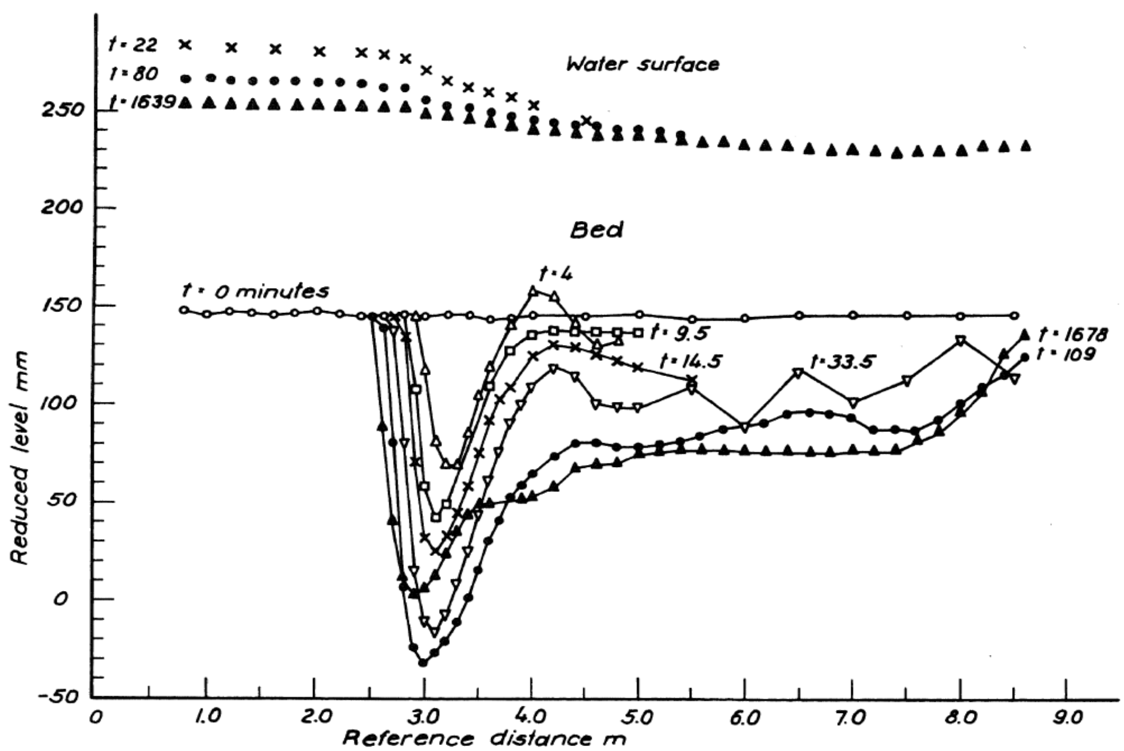

Figure 3.4. Experiment No. 11 (blunt entrance), water-surface and bed-profile evolution. (Webby 1984)

Laursen and Alawi (1989) extended Laursen's live-bed equation by adding the effect of the shear stress difference between uncontracted and contracted sections to the Laursen (1960) live-bed equation. They showed that for live-bed situations contraction scour depth would decrease slightly as the shear stress ratio (τ_1 / τ_c) increases beyond a value of one. Their finding was in accordance with the previous studies by Straub (1934) and Gill (1981). Both studies, and that by Laursen and Alawi (1989), explained that the decrease would occur because rate of bed sediment inflow would be such that the value of τ_1/τ_c in the scour region would have to remain larger, thereby resulting is shallower scour. This suggested trend, not evident in the HEC 18 equation for live-bed scour, was investigated further during this study.

Gill's work was extended by Lim and Cheng (1998), who derived a long contraction scour formula for live-bed scour. Lim and Cheng used $\beta = 4$ to produce an equation in which the equilibrium depth of live-bed contraction scour depth depended on B_1/B_2 alone, as Table 3.2 indicates. Lim and Cheng, who themselves did no flume experiments, compared their formula with several sets of laboratory data for long contractions. They concluded that their formula agreed reasonably with live-bed scour data and several sets of clear-water scour laboratory data.

The topic was expanded further by Briaud et al. (2005), who conducted flume experiments on clear-water scour of a bed of cohesive sediment (a porcelain clay) set in a long contraction, for which $L_c/B_1 = 0.25$ to 3.87. Their interpretation of the data they obtained led them to propose a formula for maximum dimensionless depth of contraction scour depth, d_s/Y_1, that depends on the variable Fr_1, B_2/B_1, and the critical value of the approach flow Froude number, Fr_{1c}, as shown in Table 3.2. They concluded that contraction length has no influence on the scour depth, when $L_c/B_2 \geq 0.25$. In addition, their results showed no influence of the transition angle on scour depth. The values of F_1 translate to values of $\tau_1^{1/2}$ and $\tau_c^{1/2}$. Their findings differ from the observed the scour behavior reported by other studies and can be attributed to the manner of clay failure under flowing water. As Briaud et al. (2005) show, the clay failed in clumps of bed material plucked by the flow, rather by the entrainment of discrete, fine clay particles. The sizes of the clumps were influenced by the contraction width. Consequently, caution is needed when appraising the data presented by Briaud et al. (2005).

Dey and Raikar (2005) conducted a set of flume experiments on clear-water contraction using both sand and gravel beds, and varied σ_g; $1.4 < \sigma_g < 3.0$. They maintained flow conditions such that $0.9 < V_1/V_c < 1.0$, or $0.81 < \tau_1/\tau_c < 1.0$, and the contraction geometry was set as $L_c/B_1 = 1.67$. The formula they produced (see Table 3.3) applied to maximum clear-water depth of contraction scour. Their results, not surprisingly, showed a significant effect of sediment gradation. Bed armoring reduced scour depth to 25% of the depth value obtained for a bed of uniform sediment. The value of the exponent on (B_1/B_2) in their formula is 1.26, which is somewhat larger than the value proposed by Laursen (1966) and other prior studies (see Table 3.3).

In Table 3.3, it is seen that, the current edition of HEC-18 (Arneson et al. 2012) uses the live-bed scour equation is identical to that proposed by Laursen (1960), except that the Manning's n ratio is not present in the HEC-18 equation. For live-bed scour (Arneson et al. 2012) assumed that $n_2 = n_1$. This assumption becomes questionable for tight contractions (differences in local values of n can become important for small values of B_2/B_1) and consequent deformation of the loose bed in the contracted channel. However, given all the other sources of uncertainty, this assumption may be reasonable for bridges of relatively high values of B_2/B_1.

Additionally, the equation HEC-18 recommends using the existing depth in the contracted section before scour, Y_0, when calculating the final scour depth. This slight change is:

$$\frac{Y_2}{Y_1} = \left(\frac{Q_2}{Q_1}\right)^{\frac{6}{7}} \left(\frac{B_1}{B_2}\right)^{p} \quad (3.\ 5)$$

$$D_s = Y_2 - Y_0 \quad (3.6)$$

Where,

Y_1 = average depth in the upstream main channel

Y_2 = average depth in the contracted section

Y_0 = existing depth in the contracted section before scour

Q_1 = flow in the upstream channel transporting sediment

Q_2 = flow in the contracted channel

B_1 = bottom width of the upstream main channel that is transporting bed material

B_2 = bottom width of the main channel in contracted section less pier width(s)

p = an exponent relating the proportions of bedload and suspended-load transport of bed sediment

Similarly, Arneson et al. (2012) developed an equation for estimating equilibrium depth of contraction scour based on the clear-water scour equation proposed by Laursen (1963), which assumed that the shear stress on contraction-scoured bed equals the critical shear stress ($\tau_2 = \tau_c$). By combining shear stress, Manning, and Strickler's equation Laursen (1956) showed that,

$$\tau_2 = \frac{V_2^2\, d_{50}^{\frac{1}{3}}}{30\, Y_2^{\frac{1}{3}}} \quad (3.7)$$

They assumed $\tau_c = 4d_{50}$, then inserted this relationship into equation (3.7), which resulted in

$$Y_2 = \left[\frac{K_u Q^2}{d_m^{2/3} B_2^2}\right]^{3/7} \tag{3.7}$$

And

$$D_s = Y_2 - Y_0 \tag{3.8}$$

Where,

Y_2 = average equilibrium depth in the contracted section after contraction scour

Q = discharge through the bridge or on the set-back overbank area at the bridge associated with the width W

d_m = diameter of the smallest non-transportable particle in the bed material ($1.25d_{50}$) in the contracted section

d_{50} = median diameter of bed material

B_2 = bottom width of the contracted section less pier widths

Y_0 = average existing depth in the contracted section

K_u = 0.0077 in standard U.S. units and 0.025 in standard international (SI) units

Equations (3.5 and 3.7) presently are extensively used by engineers to estimate depth of contraction scour at bridge waterways. Considerations regarding the loose-boundary, open-channel hydraulics involved in flow through contractions, however, indicate that these equations need to be better supported, or modified, using insights and data obtained from a series of flume experiments conducted with the objectives stated in Section 1.2.

3.5. Insights from Field Data and Observations

For several reasons mainly to do with site complexities, field data and observations have not contributed substantially in developing insight into contraction scour at bridge waterways. Comparatively few field studies have been done and they ran into a lengthy list of practical complications:

a) The loose-boundary, open-channel hydraulics involved in contraction scour was not adequately understood;

b) Bridge waterways are essentially short contractions (e.g., Keller 1983), with all the sensitivities associated with short contractions (e.g., the important influence of entrance shape on scour depth);

c) Bed sediments usually are not of uniform size composition;

d) Bridge sties tend to be quite two-dimensional in flow-field behavior;

e) Distinguishing the depth of contraction scour from other types of scour at bridge waterways is not straightforward. Local pier scour is often separated from contraction scour using a concurrent ambient bed surface for the cross-section which is essentially a graphical estimate of the cross section that would exist without pier scour at the time of the cross section measurement (Landers and Mueller 1996). After elimination of pier scour, field contraction scour is determined as the difference between the average bed elevation of the contracted bridge section and an assumed average bed elevation that would have existed without the bridge (uncontracted section). The uncontracted bed elevation can only be estimated from plots of the concurrent bed profile both upstream and downstream of the bridge (Landers and Mueller 1996); and,

f) Existing field data are based either on measurements made after the flood event causing the scour. Typically, values of some parameters are unknown (e.g., the parameters influencing the extent of vena contracta at the contraction entrance), and temporal values of scour depth development may not coincide with the occurrence of maximum temporal scour depth.

Benedict (2003) measured purported values of clear-water contraction scour at bridge sites in the South Carolina Piedmont as the depth of remnant scour holes in the floodplain. As flow data were not available for many of the sites, the 100-year peak discharge was taken as being representative; alternatively, the historic peak discharge was used at bridge sites where it had been measured or could be estimated from nearby gages. The Laursen equation was shown to greatly over-predict the measured depths of contraction scour. An envelope curve for ostensible data on depth of contraction scour was recommended for use, instead of the HEC-18 equations using the geometric contraction ratio $1 - B_2/B_1$. The contraction scour depths were shown to vary from nearly zero to the limit of the envelope for all values of the geometric contraction ratio without any apparent trend. Benedict (2003) concluded that "because the envelope was developed from a limited sample of bridges in the (South Carolina) Piedmont, scour depths could exceed the envelope".

In a follow-up study of live-bed contraction scour in South Carolina's Piedmont (hilly) region and the state's coastal plain, Benedict and Caldwell (2009) used ground-penetrating radar to estimate the elevations of buried scour surfaces. They proposed eliminating Q_2/Q_1 from the Laursen live-bed scour equation by assuming that all flow remains in the main channel in order to justify an envelope curve for the contraction scour depth, which depended only on the geometric contraction ratio. By comparing the maximum depth of scour with soil boring data, they concluded that the Piedmont data for scour depth were limited by a scour-resistant subsurface layer that consisted primarily of bedrock, but in a smaller number of cases it was composed of gravel or clay. Bridge sites in coastal plain had a similar scour-resistant layer, although some scour-cutting into this layer was evident. The layer was about 1.6 m thick.

Mueller and Wagner (2005) analyzed available, though still sparse, field data on contraction scour at bridge waterways. They compared field data with contraction scour estimates from the formulas proposed by Straub, Laursen, and Komura. In general, the results of their analysis were mixed, with over-prediction of scour-depth in most cases, but instances of scour-depth under-prediction also occurred. More detailed real-time measurements of flow velocities and bed elevations were available for a flood in 1997 on the Pomme de Terre River in Minnesota. The velocity data were not reproduced well using HEC-RAS, because flow to and through the bridge waterway was not one-dimensional. The depth of contraction scour for the bridge was significantly under-estimated using the equations recommended in HEC-18. This comparison may have been muddled by an attempt to separate abutment scour and contraction scour. Mueller and Wagner (2005) concluded that future efforts for computing contraction scour (and abutment scour) require greater consider of the two- and three-dimensional nature of field conditions at bridge sites.

On occasion, hydraulic models are used to replicate scour at specific bridge sites. Hong et al. (2006), for instance, used a 1:45 length-scale model of a bridge on the Ocmulgee River in Macon, Georgia. The bathymetry of a 750m reach of the river in the vicinity of the bridge was reproduced in the model. Good agreement was obtained between model and prototype velocity distributions for the 1998 historical flood of 1,840m3/s (the 50-year flood peak = 2,240 m3/s). The maximum clear-water contraction scour in the laboratory (setting $V_1/V_c = 1$) agreed well with the measured maximum depth field depth of contraction scour measured at the bridge sites; the difference was only 5%.

3.6. Insights from Prior Numerical Studies

To date, relatively few numerical models have been used to gain insight into contraction scour, likely because of the non-uniform, unsteady and loose-boundary flow conditions that typically prevail at bridge waterways. The studies have involved fixed boundaries and sought to determine the values of maximum velocity associated with the contraction. Common difficulties encountered involve replicating the unsteady turbulence structures at the flow-separation zone at the contraction entrance, and the deformation of the alluvial bed along the contraction.

However, an advantage of numerical models is that they can be configured relatively quickly (and inexpensively) to investigate how changes in contraction geometry and flow variables affect contraction flow. Over time further advances in modeling will help strengthen the advantages and overcome difficulties. A brief review of prior studies regarding application to contraction scour ensues.

Two-dimensional, depth-averaged-flow numerical models have been used by Weise (2002), Morales and Ettema (2013) and Zey (2017), among others, to investigate flow entry into contractions formed by bridge waterways. These studies show the utility of two-dimensional models, which are becoming increasingly used in designing bridge waterways. Morales and Ettema, for example, used the commercially available model FESWMS to determine the velocity of flow through bridge openings of bridges in compound or rectangular channels. Their modeling shows quantitatively how abutment length dominates flow contraction and affects the flow field at the entrance of a bridge waterway.

Zey used the code SRH-2D to investigate flow entry into contractions. His investigation focused on the magnitude and location(s) of maximum velocity of flow entering a contraction. He determined the effective flow width at the entrance of a contraction and the maximum lateral velocity at the contraction entrance were also investigated. The responses of these flow characteristics were studied as values of contraction ratio, channel roughness, bed slope, and transition geometry were varied. The numerical model produced significant new insights. The factors affecting the values and distribution of velocity in a contraction include channel slope, bed roughness, and contraction shape. The magnitude and location of maximum velocity in the contraction varied with contraction ratio. For contraction ratios milder than approximately 0.5 the velocity maximum occurred at two locations, and at one location for tighter contractions. At a contraction ratio of 0.5, lateral velocity reached a maximum and effective flow width a minimum. Channel slope and bed roughness affect the values and distribution of velocity in a contraction, as did contraction shape. These findings have engineering significance for explaining and estimating contraction scour within the entrance of bridge waterways.

Three-dimensional, computational fluid dynamics models have been used to examine various aspects of flow fields at abutments and entrances to bridge waterways. This review does not include several studies (e.g., Koken and Constantinescu 2007) looking at the flow field at bridge abutments), but instead focuses on channel contractions. Lai and Greimann (2010) give a useful summary of two- and three-dimensional (CFD) numerical models used for illuminating flow through bridge waterways. They compare the results from both types of models and indicate the strengths and limitations of prior models, such as the models described by Weise (2002) and Marek and Dittrich (2004) using two-dimensional models; Bihs and Olsen (2007), and Duc and Rodi (2008), and Koken (2017) who used CFD models.

The present study used one- and two-dimensional numerical models to illuminate certain aspects of the flow field evident during the flume experiments. The water flow was either too unsteady or slightly murky, thereby impeding insight as to how the flow field was developing at a contraction. Additionally, as shown in the next section, this study used the one-dimensional model HEC-RAS to examine how the design of a flume experiment would affect the information produced by the experiment. The flume study reported by Webby (1984) was used for this purpose. Also, HEC-RAS was used to assist in the design of the flume experiments done for the present study.

3.7. Numerical-Model Extensions of Webby (1984)

To extend the insights from the flume experiments reported by Webby (1984), judged here to have been the most useful flume experiments, the one-dimensional model HEC-RAS was applied to his flume and a lengthened version of his flume. The extension demonstrated the significant effects that contraction entrance and length of contracted channel may exert on the variation of bed shear stress along the contracted channel Webby used.

Figure 3.5 shows the flume configuration for Experiments 1 and 11 mentioned above. The main difference between these experiments was the shape of the contraction entrance and the downstream water depth. The flow characteristics entered into the numerical model calculate the flow profile, shear stress and other flow characteristics based on momentum, continuity, energy, and shear stress equations. The resulting streamwise variation of bed shear stress along the contraction is shown in Figure 3.6.

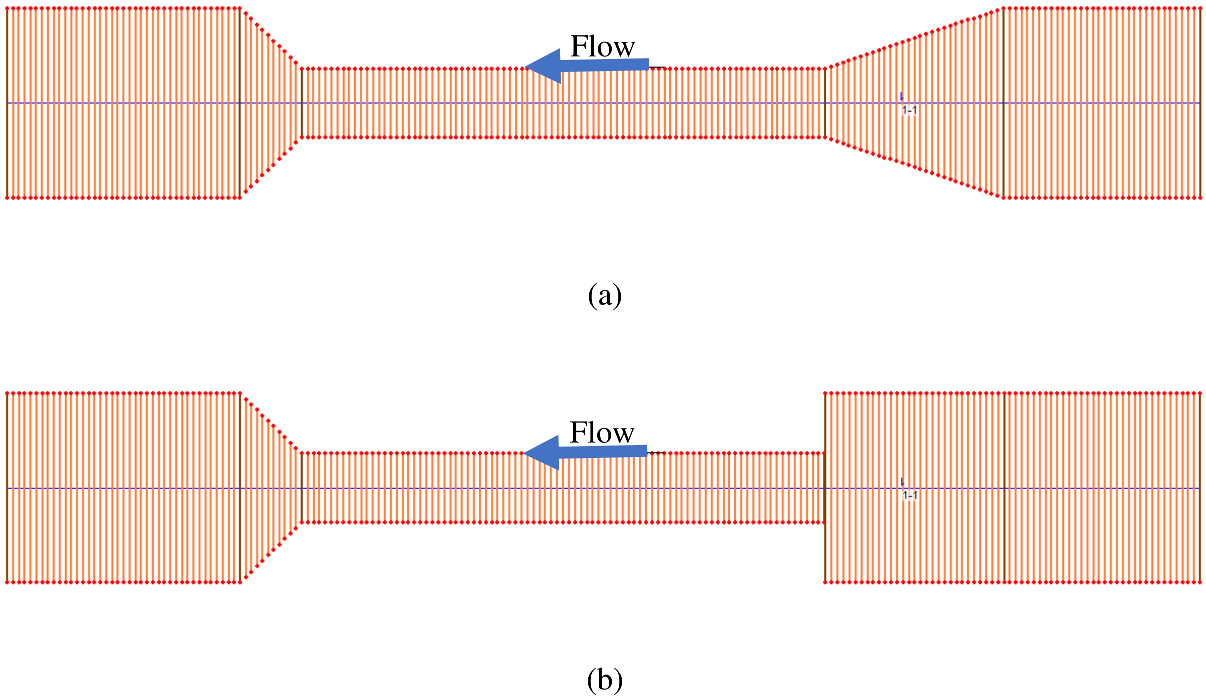

Figure 3.5. Modeled experiments geometry: (a) a fairly smooth transition, (b) an abrupt transition.

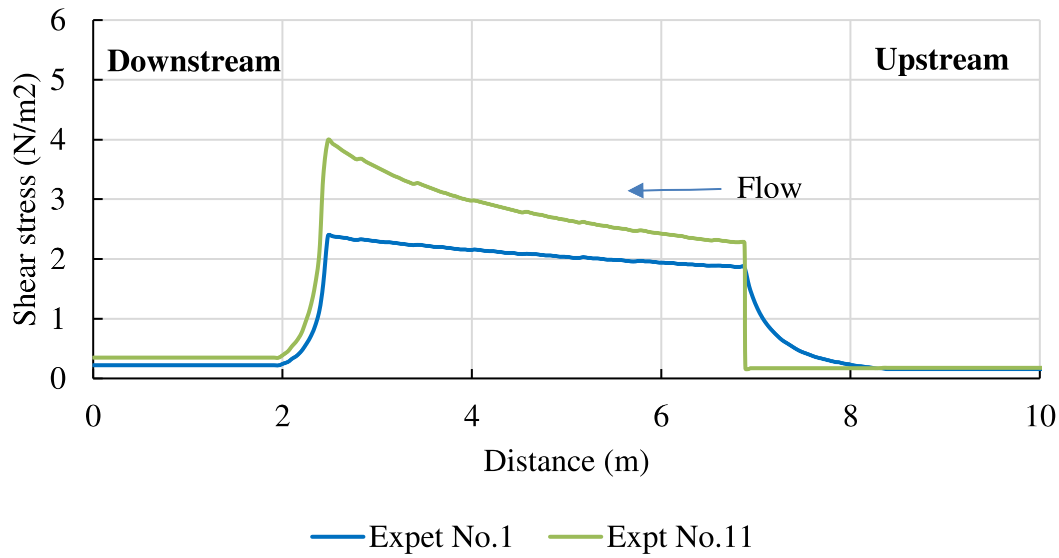

Figure 3.6. One dimensional shear stress distribution along the centerline of the flume bed.

The first result from the simulation is the occurrence of higher shear stress at the downstream end of the contraction. This result does not agree with the scour pattern along the bed (Figures 3.3 and 3.4) but is explainable in terms of the decreasing depth of flow (see Figure 2.4) associated with flow along an M2 water-surface profile.

When the model was adjusted to include the vena-contracta formation at the mouth of contraction, the shear stress varies even more. The vena contracta was simulated using an extra contracted section with a constant contraction ratio of 0.9 for Experiment No.1 (streamlined entrance) and 0.7 for Experiment No.11 (blunt entrance). The use of a contracted extension is illustrated by Figure 3.7 for Experiment 1. The consequent effect on shear stress distribution is shown in Figure 3.8 for Experiments 1 and 11. It is useful to mention that the present study found the formation of a vena contracta to be an important part of contraction scour.

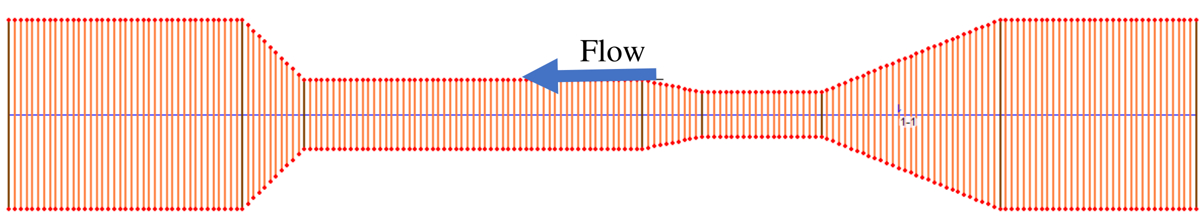

Figure 3.7. Webby's Experiment 1 geometry with an extra contracted section replicating a vena contracta (Cc=0.7).

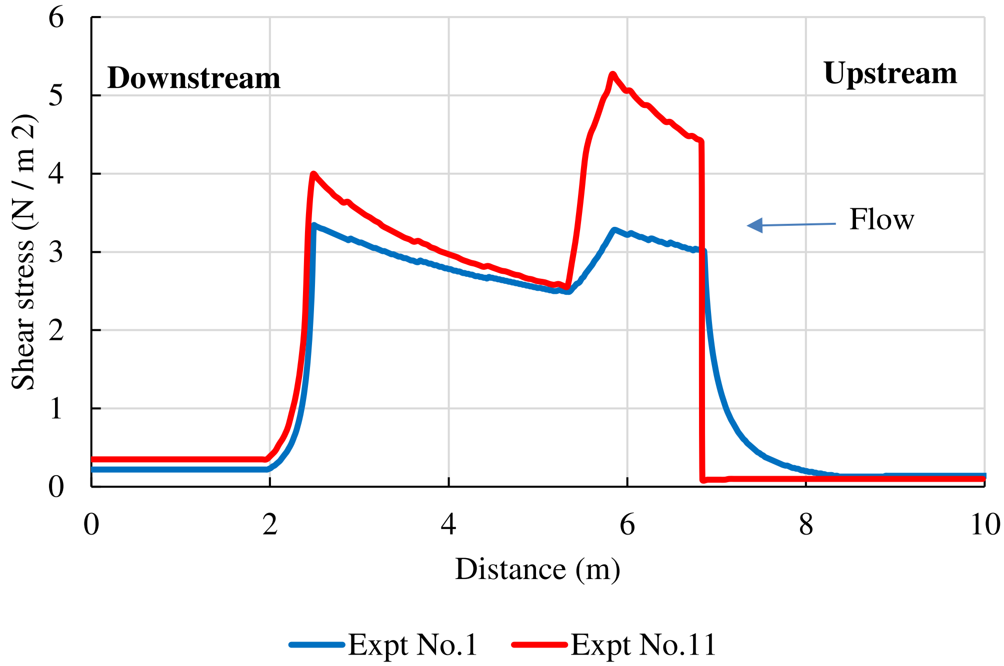

Figure 3.8. Shear stress along the contraction. (Expt. No.1 with Cc=0.9 and Expt. No.11 with Cc=0.7).

This figure shows that the shear stress distribution becomes more like the variation of scour depth (and overall scour pattern) for in Experiments 1 and 11. Moreover, as expected, the values of the bed shear stress at the upstream and downstream ends of the contraction fitted with these two conditions were not the same. This result illustrates the two-dimensional nature of the flow field within the entrance of an intermediate-length contraction.

If the length of Webby's contracted channel were extended from 4.375 m to 300.0 m, and not including the vena contracta effect on flow at the contraction entrance, the numerical simulation with HEC-RAS shows that flow reaches the normal depth along the contracted section. This length was chosen (via trial and error) to ascertain an approximate value of the contraction length needed to establish normal flow conditions along the contraction. The shear stress along the bed centerline is shown in Figure 3.9. As Figures 3.7 and 3.9 demonstrate, the values of shear stress at the downstream end of the contraction are the essentially the same for intermediate-length and long contractions, But the values of shear stresses at the upstream end differ in accordance with the shape of the entrance.

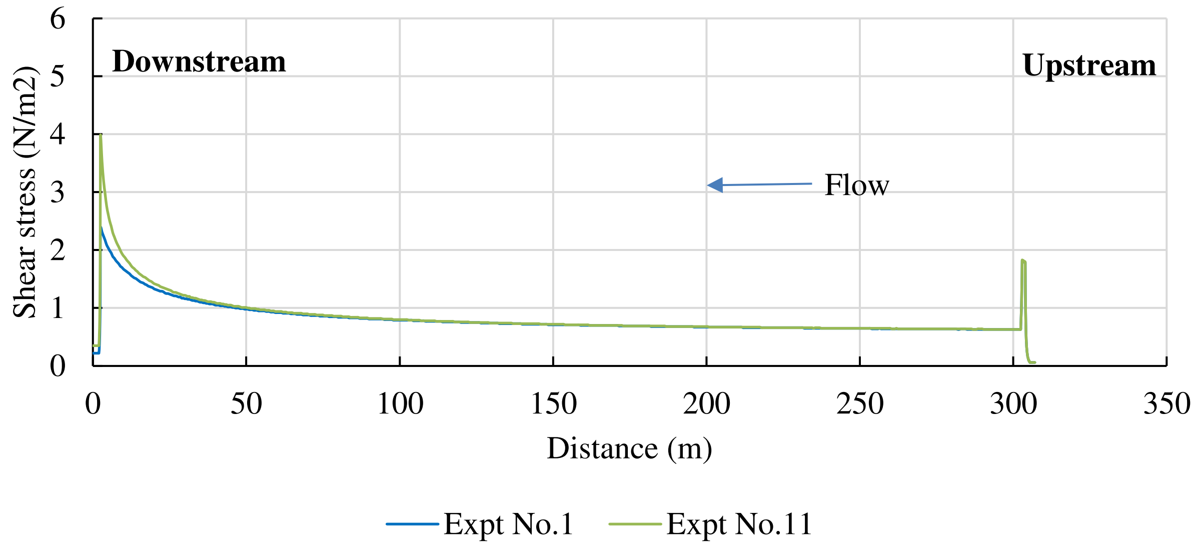

Figure 3.9. Shear stress distribution along a rigid bed in a long contraction (Expt. 1 and 11 are the smooth and the abrupt entrance shapes, respectively.)

Furthermore, comparison of Figures 3.8 and 3.9 shows, the shear stress at the contraction entrance of the original length of contraction used by Webby is about 3 times larger than the shear stress for the long contraction.

Note, the shear stress decreases along the long contraction, see Figure 3.9, until it attains a constant amount when the flow reaches the normal depth. The model's results illustrate that a long-contraction (as defined in Chapter 2) will have a lower (or even no-scour depth) in comparison with the scour depth obtained by Webby, because the flow depth along the contracted channel becomes the normal depth of flow along the contracted channel treated as a narrowed, long channel.

4. Flume Experiments

4.1. Introduction

The flume experiments were conducted to provide data and observations addressing the study's objectives and confirming and expanding the theoretical insights Chapter 2 presents. In particular, the experiments focused on the general case of contracted channels that can be considered as being of intermediate length; i.e., contraction length affects the water-surface profile and, thereby, scour along the channel. The experiments avoided the condition of flow-choking at the downstream end of the channel.

CSU's Hydraulics Laboratory, located at CSU's Engineering Research Center, was used for conducting the experiments, which were deliberately conducted at relatively large scale (using a flume accommodating an ample cross-section dimension and length of contracted channel) to give detailed insights addressing the objectives stated in Section 1.1; i.e., insights into the hydraulics and scour processes associated with contraction scour at bridge waterways. Consequently, the experiments attempted to side-step the hydraulics deficiencies of earlier investigations (notably, shortness of channel and the mixing of choked and unchoked conditions of flow) and the lack of specification as to where the reported scour depths were measured. These deficiencies reduce the usefulness of the data sets resulting from those studies. A consideration, however, with the experiments is that a minimum of two people was required to conduct them. Additional labor was needed in building the experiment set-up, including forming the sand bed before each experiment.

The present experiments entailed the collection of detailed information regarding the morphology of the contracted channel and stating where the reported values of scour depth were measured, as well as assessing the influence of measurement location on magnitude of reported scour depth.

4.2. Experiment Design and Layout

CSU's 2.44-m wide, 60.00-m long and 1.22-m deep, non-recirculating flume was used for the experiments. The contracted channel was formed using two internal walls placed within the flume. Figure 4.1 is a schematic diagram giving the geometric features and dimensions of the experiment layout. The views in Figure 4.2 illustrate the flume.

During early or preliminary experiments, several alterations had to be made to the experiment layout, mainly to ensure suitably adjustable control of the downstream control for flow through the contraction and to prevent leakage beneath the adjustable sidewalls forming the contraction. The layout comprised a 9.15-m long approach channel that contracted to a 25.93-m long narrowed channel (including the contraction). The length of the contracted channel was 10.63 times the width of the approach channel. Figure 4.3 shows the approach channel leading to the contracted channel, and Figure 4.4 shows the contracted channel for the three contraction ratios used. As explained shortly, these were tight ($B_2/B_1 = 0.25$), medium ($B_2/B_1 = 0.5$), and modest ($B_2/B_1 = 0.75$).

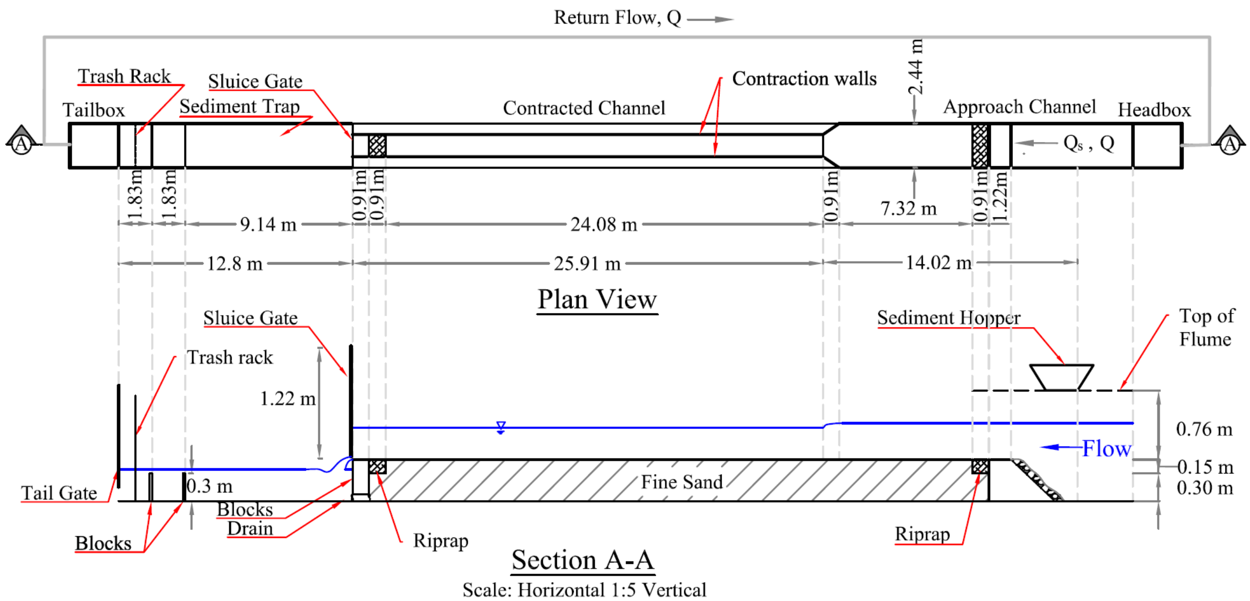

Figure 4.1. Plan and elevation views of the flume set-up used for the experiments.

The flume set-up, shown in Figure 4.1, had a sediment hopper, which fed bed sediment into flow at the flow's upstream end during the live-bed experiments. The selected rating curve, relating discharges of bed sediment and water is further explained subsequently in this section. Riprap rock was used at the upstream and downstream ends of the experiment layout to fix the bed elevations at these locations and to prevent sand erosion at both these boundaries.

A sluice gate was positioned and adjusted at the downstream end of the contracted channel to set the selected depth of flow at the channel's exit, the control section for open-channel flow along the contracted channel. The selected depths of flow were mainly the flow depth in the channel reach downstream of the contracted channel (intermediate-length channel) and the normal depth of flow along the contracted channel (long contraction). The flow depth in the channel reach downstream of the contraction equaled the normal depth of flow in the approach channel; i.e., $Y_{n3} = Y_{n1}$ as per Figure 2.4. The normal flow depth in the long contraction was estimated using flow resistance equations in the one-dimensional, numerical code HEC-RAS.

Several options for the form geometry of the contraction's entrance were considered. Eventually, a tapered, vertical wall set at angle of 45° was chosen for the experiments, as this angle approximately reflected the angle of an abutment shoulder, most notably the angle used for the side wings of a wing-wall abutment.

A two-stage sediment trap was placed downstream of the experiment section to catch sediment as it exited the end of the contracted channel. The first compartment caught the bedload transported bed sediment, whereas the second compartment caught much of the suspended bed sediment. This configuration was fairly effective, though some bed sediment was conveyed into the pump-pit where the flume's pumps were located.

Flow to the flume was provided by a 125-horsepower (hp) pump, which had a maximum discharge capacity of 0.452 m^3/s and was judged sufficient to cover the range of discharges used for the experiments. The pumps drew water from a pump pit (into which the flume's poured) and passed the flow of water along a 0.92-m diameter pipe to the flume' headbox located about 17.00 m upstream of the contracted channel. Flow from the headbox then discharged flow across the full width of the flume. The value of the normal depth of approach flow Y_{n1} was expressed (in accordance with Manning's flow resistance equation) in the selected combination discharge, flume slope, flow geometry and boundary roughness used for each experiment. In effects, the hydraulics variables associated with flow through the layout were checked by means of established analytical relationships for open-channel flow (e.g., Henderson 1966) and numerical simulation of flow through the contracted channel. The numerical simulation was done with the widely used one-dimensional-flow model HEC-RAS. Both checks involved the assumption that the contraction had a fixed flat bed. The checks pertained to the flat-bed or pre-scour condition of each experiment.

The flume had an adjustable (bed) slope, which could be set between horizontal (S = 0) and a maximum slope of S = 0.02 (a 2 percent slope). Adjustment of the flume's slope was done by means of electric motors that altered the elevation of two, threaded shafts. Adjusting the flume's slope required clearing personnel away from the flume, then operating the motors until the slope setting was attained. This process had to be done carefully, given the size of the flume.

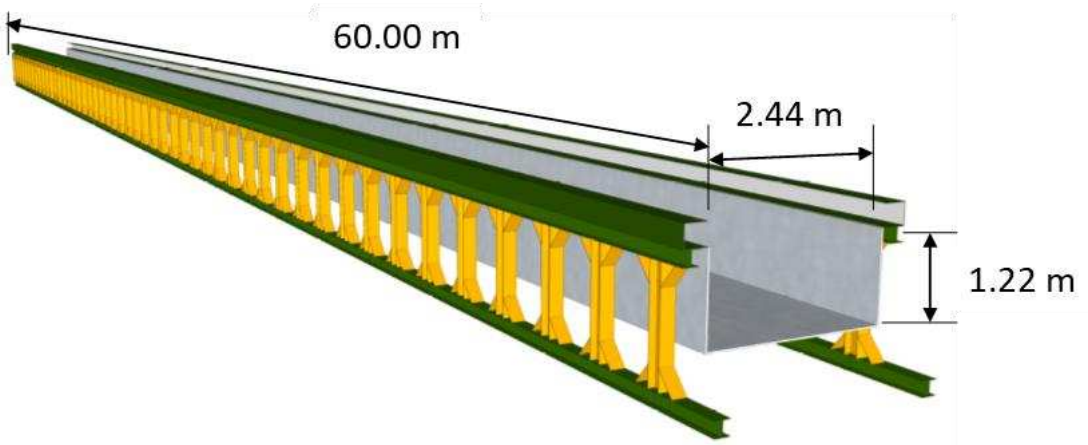

(a)

(b)

Figure 4.2. CSU's 2.44-m-wide, 60.00-m-long, non-recirculating flume: (a) a schematic view; and, (b) a photograph showing a general view.

(a)

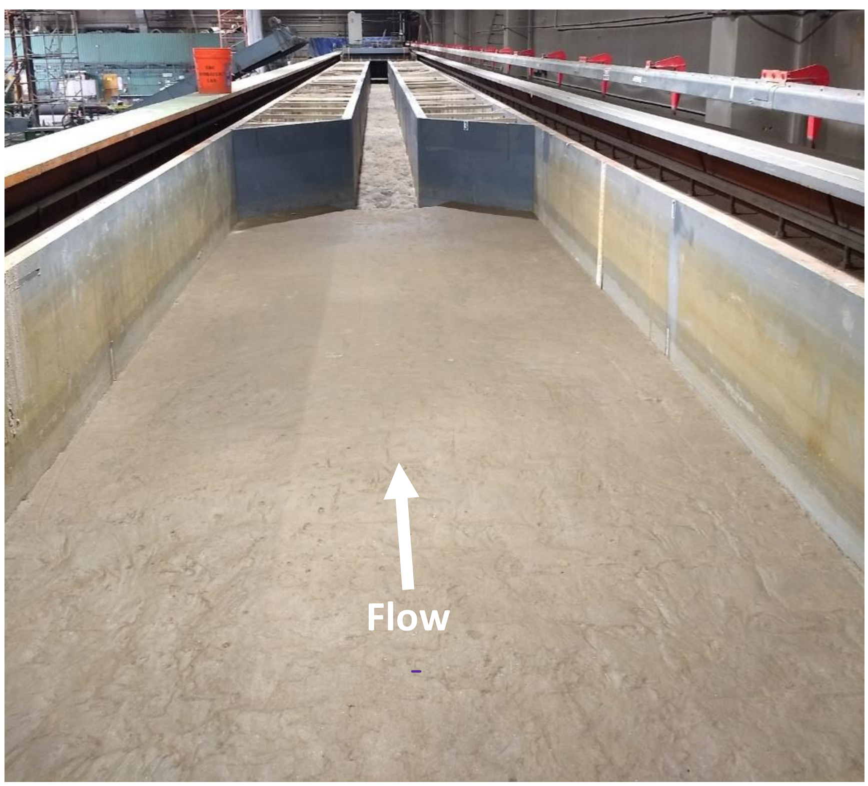

(b)

Figure 4.3. Views of the approach channel; (a) a general overview looking upstream; and, (b) a view of the approach channel to the contracted channel (set for B_2/B_1 = 0.25, the tight-contraction experiments).

(a)

(b)

(c)

Figure 4.4. Views of the contracted channel for each of the three contraction ratios used: (a) $B_2/B_1 = 0.25$*; (b)* $B_2/B_1 = 0.50$ *and, (c)* $B_2/B_1 = 0.75$*.*

Construction of the model construction began with the tight contraction ($B_2/B_1 = 0.25$), as this ratio was expected to produce the deepest scour. Figure 4.5 depicts the contraction under construction. After finishing the wall construction, the contracted area was filled with sand. Figure 4.6 shows the conveyor belt used to convey sand from a Bobcat into the flume, where the sand was then spread by shovel and leveled using a leveling board.

The use of fine sand as bed sediment (selection described below) initially led to the occurrence of multiple sand leaks beneath the constructed walls of the contraction. Different methods were used to caulk the leaks (e.g. sand-cement mortar and silicone gel), but eventually two layers of filter cloth were placed as lining of the bed to and along the contracted channel. The cloth successfully retained the fine sand and inhibited flow leakage beneath the wall.

After finishing the experiments with the tight contraction ($B_2/B_1 = 0.25$), the sand was removed from the contracted area and contracted channel's walls were moved to the next position. The sequence of wall spacing used was tight ($B_2/B_1 = 0.25$), medium ($B_2/B_1 = 0.50$) and modest ($B_2/B_1 = 0.75$). Typically, each reconstruction of the contracted channel took about one month to complete.

Figure 4.5. Construction of the wood frames supporting the sidewalls of the contracted channel. The view is looking into the entrance of the contracted channel; $B_1/B_2 = 0.25$.

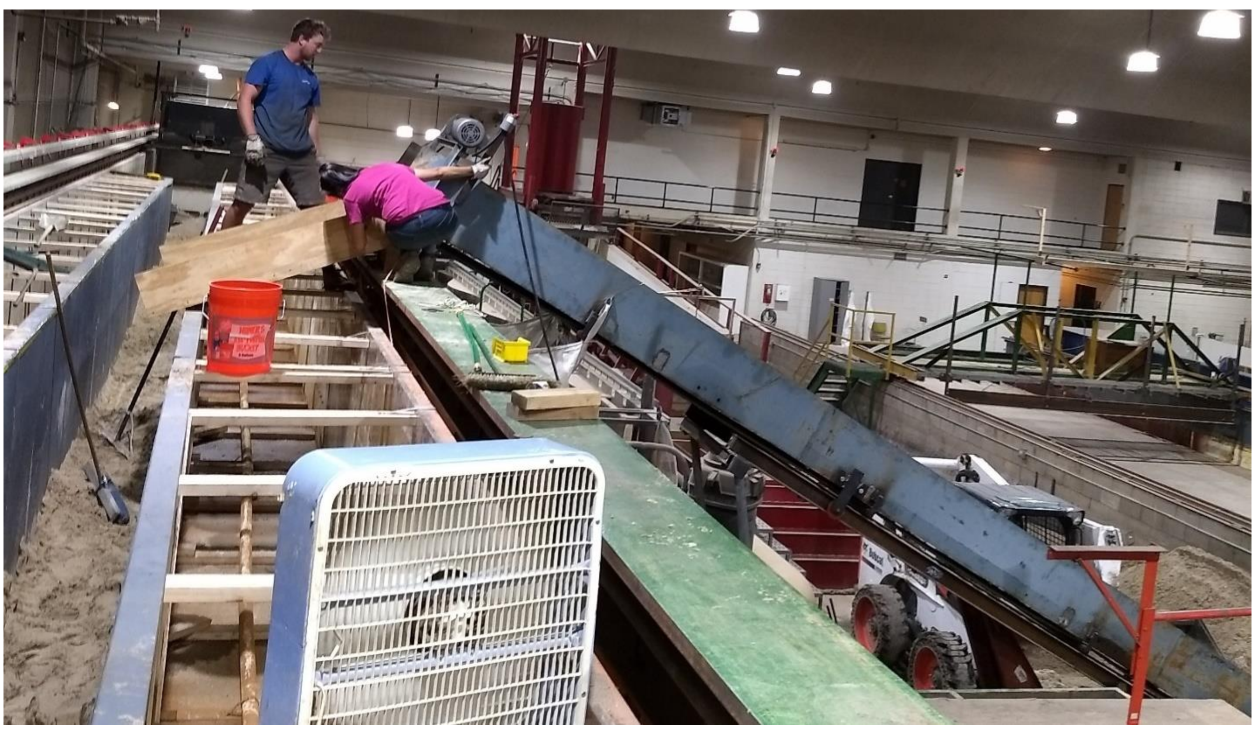

Figure 4.6. Conveying sand to the flume and placing the sand along the bed of the contracted channel; $B_1/B_2 = 0.25$.

4.3. Sediment size

The experiments used uniform-sized, fine sand as bed sediment along the channel. Fine sand was chosen because a large amount of sand was needed for the experiment; about 65 cubic meters (about eight dump-truck loads for the widest contracted channel). Uniform sand available in this quantity inevitably caused the selection of sand to be in the fine-sand size range. It was not economically feasible to acquire an equal volume of suitably uniform sand in the medium-size range for sand. Also, concerns for flow choking had to be kept in mind when selecting the size of sand for the experiments.

The sand's median diameter, d_{50}, was 0.26 mm and the sand's geometric standard deviation, σ_g, was 1.55, making the sand sufficiently uniform in size for the present experiments. Figure 4.7 gives the grading curve for the particle-size distribution of the sand used in the experiments and the grading curve provided by the commercial supplier of the sand. Two tests were done at CSU to determine the actual particle-size distribution of the sand used for the experiments. The actual values d_{50} of σ_g and differed slightly from the values the sand's supplier had indicated; i.e., the supplier had indicated d_{50} = 0.28 mm and σ_g = 1.36. But the sand was deemed sufficiently suitable for the experiments.

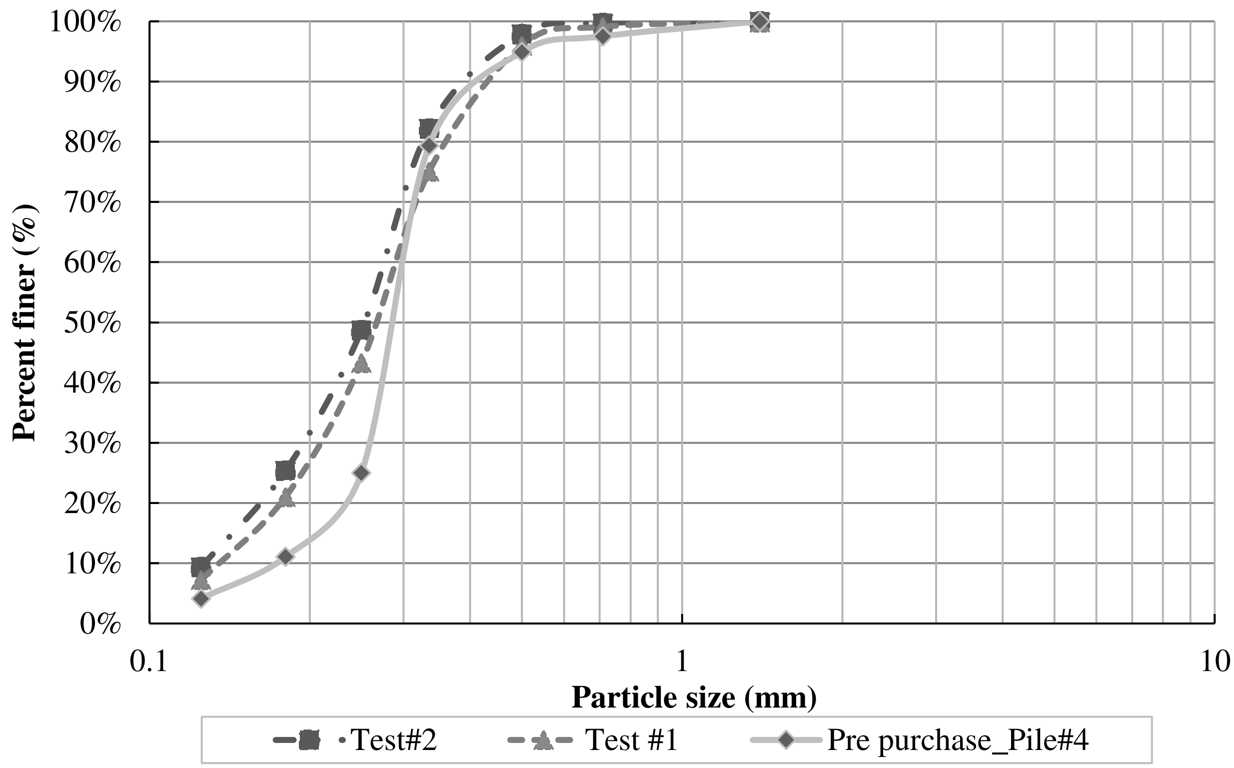

Figure 4.7. The particle-size distribution of fine sand used for the bed of the contracted channel.

4.4. Measurements and Instrumentation

The flume experiments involved the following measurements and instrumentation:

1. The water-surface profiles for each contraction configuration were measured to determine the hydraulic conditions upstream, through and downstream of the contracted section before and during scour. For all the experiments, the time-variation of water-surface profile was measured and documented during the experiments. These measurements were made using a distance sensor produced by Massa (MassaSonic PULSTAR Ultrasonic Sensor). This sensor sampled the water surface at a sampling frequency of 150 kHz and has a precision of ± 0.1% of target range. The sensors were mounted on the end of the flume's mobile carriage.

Water-surface profiles were collected along the flume's centerline and along a streamwise transect near the contraction's right sidewall (facing downstream). The water-surface elevations were measured, at 13 cross-sections along the contraction, see Figure 4.9. The resulting data aided evaluation of the existing current scour-depth equations in HEC-18 (Arneson et al. 2012), which compute scour as the difference between the flow depths on the initial bed and scoured bed in the contracted reach;

2. The experiment's design had included acquisition of time-varying data on bed elevation variation during each experiment. An array of small, cylindrical SeaTek 2MHZ ultrasonic probes had been configured for this purpose (Figure 4.8). However, preliminary experiments revealed that the signals from these probes drifted during the first approximately 6 hours of each experiment, because during those experiments (done during winter) the water temperature typically increased from 57°F to about 67°F. This temperature increase in turn increased water compressibility, and thereby increased the speed of sound through the water column at measurement locations. Consequently, errors were introduced into the measurement of the local elevation of the bed in the contraction. These transducers had been used during several earlier studies at CSU, including the conduct of NCHRP Project 24-26, "Effects of Debris on Bridge Pier Scour" (Lagasse et al. 2010), though the issue of signal stability evidently was not considered in the earlier studies.

   However, a Seatek transducer was used after several hours of running the flume to ascertain whether scour had reached its greatest depth, which was always at the entrance corner. Several measurements were made to confirm that equilibrium depth had been reached. Along the middle of the contraction entrance (as discussed in the next chapter) the formation and small shifting of dunes hampered the acquisition over time of a steady value of scour depth.

3. Once an equilibrium scour depth was confirmed as having been attained, the equilibrium scour hole was LiDAR-scanned using CSU's TOPCON TLS System LiDAR scanner. This instrument had a measurement precision of 0.15% of full scale.
4. Flow-velocity data were obtained using a Nortek, 3-D Acoustic Doppler Velocimetry (ADV) probe. The measurements were made for most runs at the moment when the scour process was reasoned to have reached its equilibrium-depth profile. These velocity data were used in the diagnostic explanation of scour development along the channel contraction. The precision of the Nortek ADV was ±1mm/s.
5. The flow field was more extensively measured at the end of the rigid-bed experiments with the tight contraction (B_2/B_1 = 0.25), see Figure 4.10. These measurements, made with the ADV probe, acquired data on velocity profiles taken at transects 1 through 6 indicated in Figure 4.5. The data were taken at seven points on each cross-section. The resulting velocity information was used to aid calibration of the 1-D and 2-D numerical models run to expand the insights obtained from the experiments. Velocity values were taken at elevation of 0.6 of the flow depths measured down from the water surface. This elevation coincided with the mean velocity of the flow-velocity distribution at the measurement vertical.
6. The flow field at the water surface of flow into the contraction entrance was measured using Large-scale Particle Velocimetry (LSPIV). The LSPIV measurements were done usually at the end of each run when the bed had reached its equilibrium profile. This process entailed seeding the flow surface with paper tracers (about 2 mm in diameter)

and taking a video of the water surface seeded with the tracers, then using the video and computer software to obtain the flow field as seen at the water surface. The detailed description of the steps in this process is given by Fakhri (2020), who's Master-Degree thesis focused on this part of the experiments.

7. Other visualization methods and photography used, as necessary, to provide diagnostic and documentary insight into the processes and extent of contraction scour. Not to be discounted in this part of the experiment was the direct viewing and interpretation of the forms of the water surface and the bed.

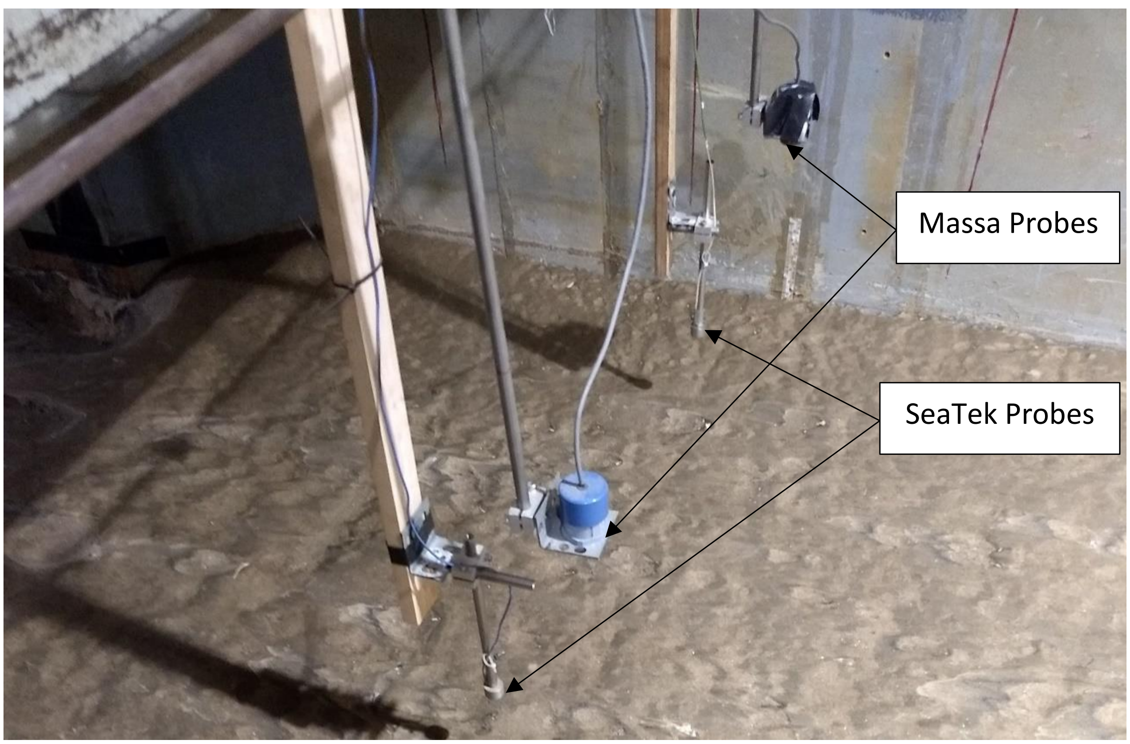

Figure 4.8. Location of instrumentation probes at one end of the flume's mobile carriage. The probes shown were used for measuring the elevations of the channel bed and the water surface

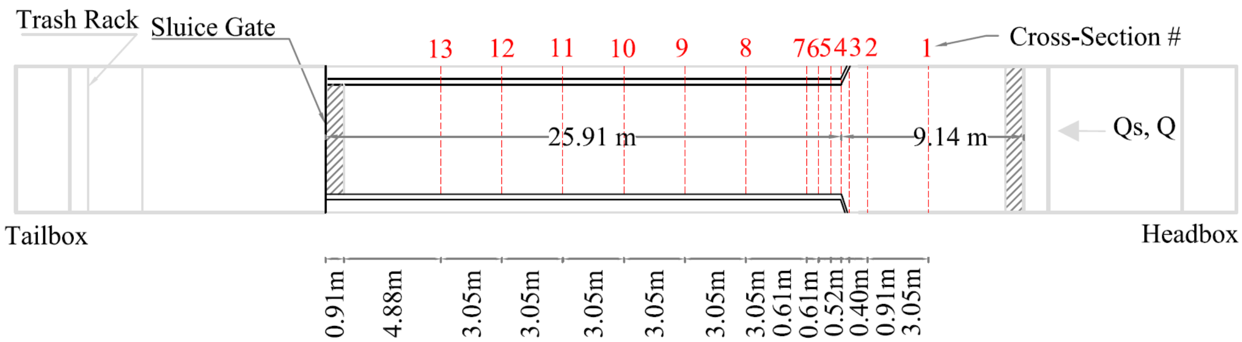

Figure 4.9. The locations of the measurement cross-sections along the flume (this drawing is not to scale).

(a) (b)

Figure 4.10. The tight contraction fitted with a fixed bed formed of plywood: (a) view along the contraction; and, (b) plan view showing the use of dye to delineate flow separation at the contraction entrance.

The sediment-feed hopper used for the present study is shown in Figure 4.11. The hopper was placed on a mobile, sediment storage bin, and positioned upstream of the fixed section leading to the approach bed. The rate of sediment supply to the flume during the live-bed experiments was regulated by means of a motor-speed controller that adjusted the angular speed of a rotating slotted pipe at the base of a hopper bin from which dry sediment was fed to a fan-shaped chute. Sediment passing down the chute was spread across much of the width of the flow along the flume. The rate of sediment feed was calibrated in terms of the mass of sediment collected for given periods of hoper operation.

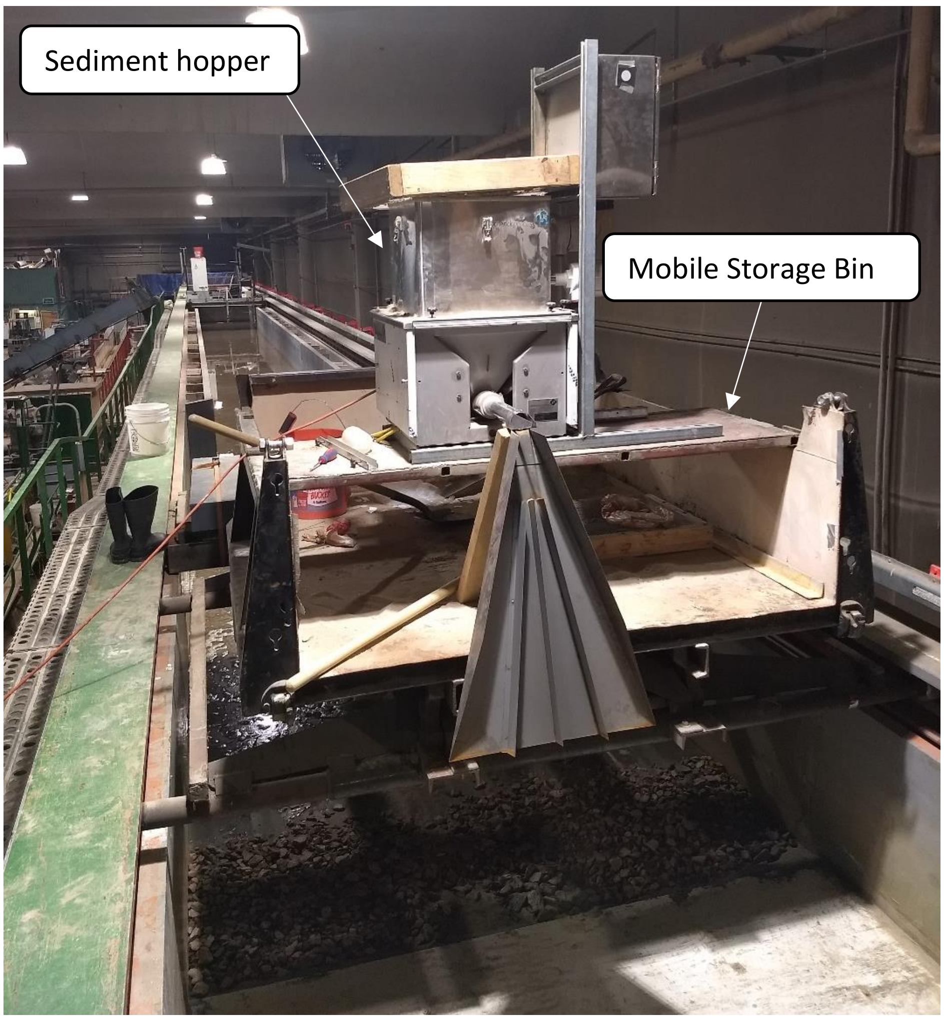

Figure 4.11. Positioning of the sediment hopper on the mobile, sediment-storage bin on the 2.44 m wide flume.

4.5. Ranges of Shear Stress and Velocity Parameters Used

The experiments required selecting values of the following parameters to be used in the experiments: Y_{n1} and, V_{n1}/V_c or τ_{n1}/τ_c . Here, Y_{n1} is the normal depth at uncontracted section, V_{n1} is the velocity related to the normal depth at uncontracted section, and V_c is the critical velocity at the incipient motion of bed material. Note, due to the relationship of V_{n1}/V_c and τ_{n1}/τ_c either one of them can be known. Here, τ_{n1} is the bed shear stress associated with uniform flow along the uncontracted approach channel, and τ_c is critical shear stress at incipient motion. Values of τ_c were determined in the following manner (Julien 2010):

$$\tau_c = (G-1)\gamma_m \, d_{50}\tau_{*c} \quad (4.1)$$

where,

$$\tau_{*c} \approx 0.3\, e^{-\frac{d_*}{3}} + 0.06\, tan\phi \,(1 - e^{-\frac{d_*}{20}}) \quad (4.2)$$

and,

$$d_* = d_{50}\left(\frac{(G-1)g}{\upsilon_m}\right)^{\frac{1}{3}} \quad (4.3)$$

Here, G, γ_m, τ_{*c}, d_*, g, υ_m respectively are specific gravity, specific weight of water-sediment mixture, critical shields parameter, dimensionless particle diameter, gravitational acceleration, and kinematic viscosity of water.

Estimation of critical velocity calculation is complicated by the relationship assumed to link shear stress to velocity distribution. The estimates, however, differ only slightly. The following relationship sequence was used:

$$\frac{V_c}{u_{*c}} = \frac{1}{\kappa}\ln\left(30\frac{Y_{n1}}{k_S}\right) \quad (4.4)$$

With

$$u_{*c} = \sqrt{\tau_c/\rho} \quad (4.4)$$

Here u_{*c} = critical values of shear velocity, κ = von Kárman constant equal to 0.41; and, roughness height, $k_S = 2.5d_{50.}$ The velocity for normal depth at uncontracted section, V_{n1}, was estimated as

$$\frac{V_{n1}}{V_c} = Predefined \quad (4.6)$$

The discharge, Q, was determined as

$$Q = Y_{n1}B_1V_{n1} \quad (4.6)$$

The shear stress along the uncontracted section, τ_{n1}, was calculated as

$$\frac{\tau_{n1}}{\tau_c} = \left(\frac{V_{n1}}{V_c}\right)^2 \quad (4.6)$$

The bed slope of the uncontracted section, S_1 was

$$S_{f1} = S_1\ (uniform\ flow) \rightarrow S_1 = \frac{\tau_{n1}}{\gamma_m R_{n1}} \quad (4.6)$$

Where,

$$R_{n1} = \frac{Y_{n1}B1}{B_1+2Y_{n1}} \quad (4.6)$$

And values of Manning's n for the approach flow were estimated as

$$n_1 = \frac{1}{Q} B_1 Y_{n1} R_{n1}^{\frac{2}{3}} S_1^{\frac{1}{2}} \quad (4.6)$$

The normal depth at contracted section, Y_{n2} was determined as

$$Q = \frac{1}{n_2} B_2 Y_{n2} R_{n2}^{\frac{2}{3}} S_2^{\frac{1}{2}} \quad (4.6)$$

Trial-and-error methods were utilized to reach to the normal depth. It was assumed that Manning's n and bed slope, *S*, are constant for the contracted and uncontracted sections; i.e. $n_1 = n_2 \; and \; S_1 = S_2$.

The value of the shear stress along the contracted section, τ_{n2}, was estimated as

$$\tau_{n2} = \gamma_m R_{n2} S_2 \quad (4.6)$$

Further calculations enable the backwater depth, $Y_{backwater}$, to be estimated; i.e.,

$$E_{backwater} = E_{n2} + h_f \quad (4.6)$$

Where

$$E = Y + \frac{V^2}{2g} \quad (4.6)$$

It was possible to calculate the maximum back water depth at the upstream end of the contraction by utilizing specific energy equation and trial and error methods. Here, *E* is specific energy and h_f is the local headloss between two sections.

The field study reported by Benedict and Caldwell (2009) indicated the range of V_1/V_C values typical of rivers in South Carolina. The present study assumed this range to be representative of rivers generally. Therefore, the clear-water and live-bed experiments were run for the range

$$0.30 \leq \tau_1/\tau_C \leq 6.25$$

or

$$0.55 \leq V_1/V_C \leq 2.5$$

As Figure 4.12 indicates, this study covered the shear stress ratio for more than 90 percent of channels in the coastal-plain region and more than 80 percent of the piedmont region of South Carolina. To be sure, the range can extend beyond the above range (Figure 4.12). However, there are flume limitations, notably in the discharge capacity of the pump and the available depth of the sand to be scoured before scour extended to the flume's fixed floor. Moreover, going beyond this range, though, quickly leads to the issue of choking, which the experiments diligently avoided, because the contraction flow field changes substantially. Additionally, this range covered more than 90 percent of the values of τ_1/τ_c used in the prior laboratory-based studies (see Appendices A and B).

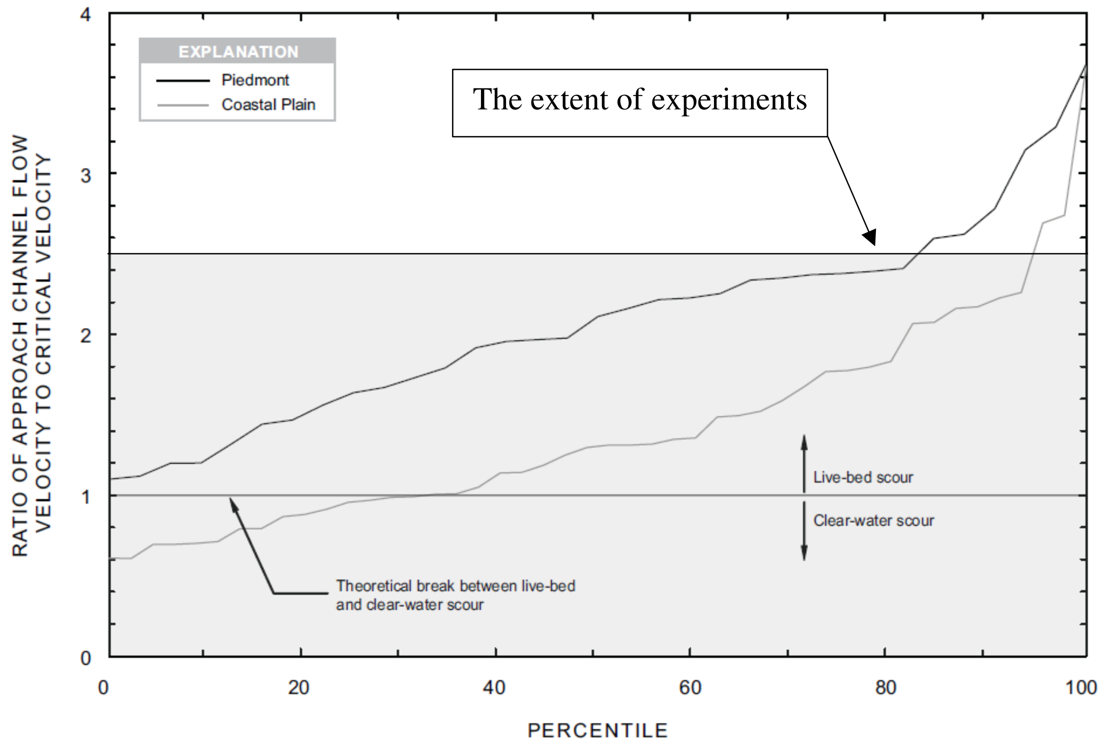

Figure 4.12. Distribution of V_1/V_C values for selected bridges in the coastal plain and piedmont physiographic provinces of South Carolina (Source: Benedict and Caldwell (2009). Also shown (the shaded area) is the range of values used in the present experiments

4.6. Rating Curve for Sediment Discharge

Consequent to the non-uniform and unsteady flow conditions along the contraction, the experiments involved non-uniform and unsteady transport of bed sediment along the contraction. For the live-bed scour experiments, bed sediment had to be fed into the upstream end of the contraction model. This task was done using the sediment hopper described above. An issue to be resolved was the requisite rates at which sediment should enter the flume.

The experiments used the sediment-flow rating curve developed by Guy et al. (1966), relating sediment discharge to water discharge. This curve was developed with the same 8.0ft flume used for the present study, and involved essentially the same sand; i.e., Guy et al used a uniform-sized 0.27mm fine sand, whereas the present experiments used as uniform-sized, 0.26mm.

Figure 4.13 presents the sediment-flow rating curve used for the present experiments, and compares the rating curve developed by Guy et al. with the rating curves suggested using two, well-known methods for estimating bed sediment transport compare with the rating curve:

- Modified Laursen (Madden 1993)
- Yang (1973), as presented in HEC-RAS

The curve associated with the data from Guy et al. (1966) begin at lower transport rates, likely because the fine sand involved quickly developed bed forms (ripples and dunes) that slowed the sediment discharge. As the water discharge increases, the sediment discharge increases more rapidly than indicated by two methods listed above. After careful deliberation, it was decided to use the curve provided by Guy et al. because it was developed using the same sand in the same flume as the present experiments. Part of this consideration was the thought that predictive equations for rates of sediment transport are known to give rather differing estimates of transport rate. The influence of variable transport rate on contraction scour is discussed in Chapter 5.

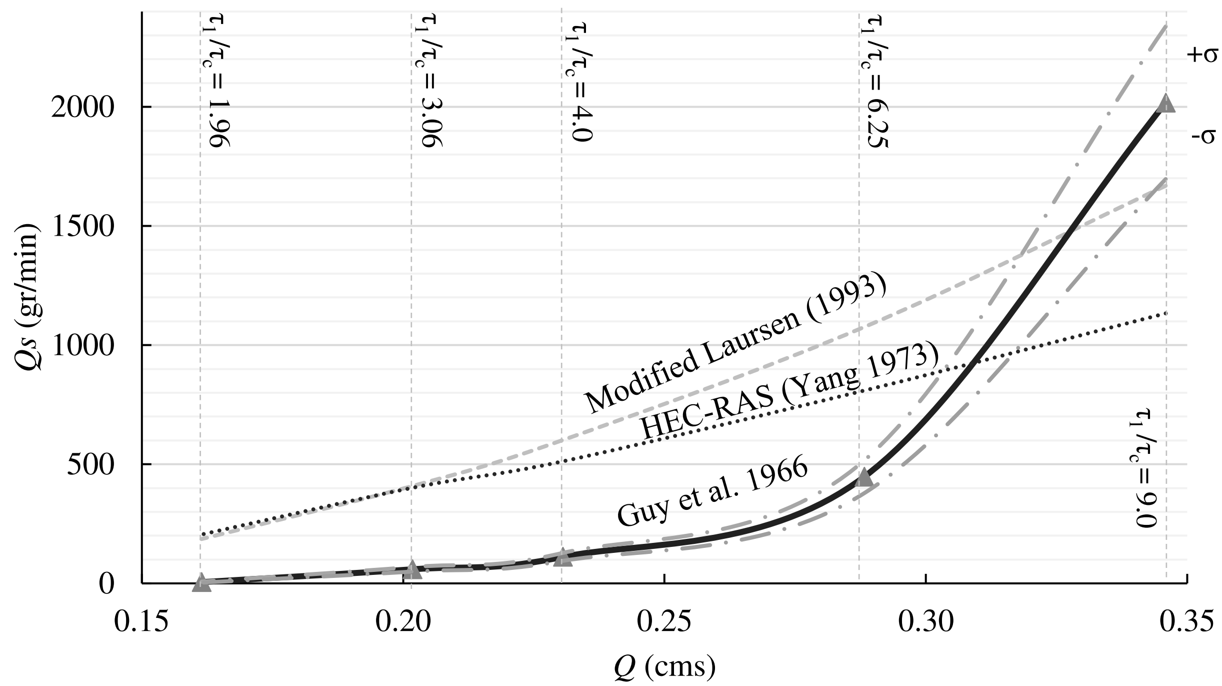

Figure 4.13. Sediment transport rating curve. Several sediment-transport relationships are plotted, indicating the range of values estimated using three relationships.

4.7. Program of Experiments

The bulk of the experiments were conducted with the downstream water depth set at downstream water depth at uncontracted section ($Y_{n3} = Y_{n1}$), which pertains to flow along an intermediate-length contraction. This arrangement aligns with the experiments' design in that the experiments simulated flow along a rectangular channel of uniform width that was then contracted by the construction of a bridge waterway. Tables 4.1 and 4.2 give the variables used. Section 3.2 and Figure 3.1 define the variables in these tables.

For two experiments, the downstream depth of the contraction flow was set as the normal depth of flow in the contraction (Y_{n2}). This arrangement replicated flow along a long-contraction (Figure 2.5), see Table 4.1.

Table 4.3 compares the range of values in Tables 4.1 and 4.2 with the ranges used in prior studies of contraction scour. Table 4.3, therefore, gives context to the present experiments relative to the prior experiments. The ranges coincided with those of prior studies, though the experiments for the present study included measurements made with a non-erodible (for selected cases when B_2/B_1 = 0.25).

The experiment was designed to quantify the influences of the main parameters affecting contraction scour. Eq. (3.3) gives these parameters. Consequent to the constraints and limitations associated with the experiments, the experiment also involved evaluating supportive information (e.g., size distribution of bed sediment), invoking facilitating assumptions (e.g., uniform size of bed sediment), and considering the relationships describing open-channel flow along a contracted loose bed (e.g., specific energy).

The parameters of interest are the contraction ratio B_2/B_1, and the state of bed-sediment motion on the approach channel, τ_1/τ_c. The supportive information related to sediment used as bed sediment (d_{50}, ϕ), the approach-flow characteristics (Y_1, Y_3 and S) and the entrance form of the contraction. Here (as defined above), d_{50} is the mean diameter of the bed material, ϕ is the angle of repose for bed material, B_1 is the width of the approach channel, and B_2 is the width of the contraction. Also, the bed was taken to comprise cohesionless sediment of uniform particle size. The main assumptions concern the relationship between flow characteristics with flume slope and flow resistance. The design of the experiments assumed the channel to have constant slope to and through the contraction, and downstream of the contraction. Additionally, the uncontracted channel (upstream and downstream of the contraction) was uniform in width (B_1=B_3). If $B_1 \neq B_3$, a different flow depth at the downstream end of the contraction would occur than the normal depth associated with the approach flow. The hydraulics of this arrangement is acceptable for the experiments, provided the flow does not choke. Avoiding choking and calculate the initial flow and bed condition throughout the contraction involved estimating the uniform flow condition in the approach channel.

Tables 4.1 and 4.2 list the experiments run for this study. The flow characteristics in the two tables were calculated using the relationships presented above. The numbering of each experiment was based on the shear stress ratio (τ_{n1}/τ_c), width ratio (B_2/B_1). For instance, *CW-0.25-0.81* means, clear-water ($\frac{\tau_{n1}}{\tau_c} < 1$) experiment, with B_2/B_1 = 0.25, and τ_{n1}/τ_c = 0.81. Table 4.3 summarizes the values of the variables used in the experiments Tables 4.1 and 4.2 list the experiments run for this study. The flow characteristics in the two tables were calculated using the relationships presented above. The numbering of each experiment was based on the shear stress ratio (τ_1/τ_c), width ratio (B_2/B_1). For instance, *CW-0.25-0.81* means, clear-water ($\frac{\tau_1}{\tau_c} < 1$) experiment, with B_2/B_1 = 0.25, and τ_1/τ_c = 0.81. Table 4.3 summarizes the values of the variables used in the experiments.

Table 4.1. Program of clear-water contraction scour experiments.

No.	Clear-water expt. #	B2 (m)	B_2/B_1	Y_{n1} (m)	Q (cms)	S_f	V_{n1} (m/s)	V_{n1}/V_c	τ_{n1} (N/m^2)	τ_{n1}/τ_c
1	CW-0.25-0.56	0.610	0.25	0.178	0.087	0.00007	0.20	0.75	0.104	0.56
2	CW-0.25-0.30	0.610	0.25	0.178	0.064	0.00004	0.15	0.55	0.056	0.30
3	CW-0.25-0.42	0.610	0.25	0.178	0.076	0.00005	0.17	0.65	0.078	0.42
4	CW-0.5-0.30	1.219	0.50	0.178	0.064	0.00004	0.15	0.55	0.056	0.30
5	CW-0.5-0.42	1.219	0.50	0.178	0.076	0.00005	0.17	0.65	0.078	0.42
6	CW-0.5-0.56	1.219	0.50	0.178	0.087	0.00007	0.20	0.75	0.104	0.56
7	CW-0.75-0.56	1.829	0.75	0.178	0.087	0.00007	0.20	0.75	0.104	0.56
8	CW-0.75-0.72	1.829	0.75	0.178	0.099	0.00009	0.23	0.85	0.134	0.72
9	CW-0.75-0.90	1.829	0.75	0.178	0.111	0.00011	0.26	0.95	0.167	0.90
10	CW-0.25-0.81*	0.610	0.25	0.152	0.087	0.00011	0.23	0.90	0.150	0.81
11	CW-0.25-0.98*	0.610	0.25	0.152	0.096	0.00014	0.26	0.99	0.182	0.98

*Long-contraction cases; the downstream control depth for these two cases where Y_{n2}.

Table 4.2. Program of live-bed contraction scour experiments.

No.	Live-bed expt. #	B2 (m)	B_2/B_1	Y_{n1} (m)	Q (cms)	S_f	V_{n1} (m/s)	V_{n1}/V_c	τ_{n1} (N/m^2)	τ_{n1}/τ_c
1	LB-0.5-1.44	1.219	0.50	0.178	0.138	0.00018	0.32	1.20	0.267	1.44
2	LB-0.5-1.96	1.219	0.50	0.178	0.161	0.00024	0.37	1.40	0.363	1.96
3	LB-0.5-2.72	1.219	0.50	0.178	0.190	0.00033	0.44	1.65	0.504	2.72
4	LB0-0.5-4.00	1.219	0.50	0.178	0.231	0.00049	0.53	2.00	0.741	4.00
5	LB-0.75-1.44	1.829	0.75	0.178	0.138	0.00018	0.32	1.20	0.267	1.44
6	LB-0.75-1.96	1.829	0.75	0.178	0.161	0.00024	0.37	1.40	0.363	1.96
7	LB-0.75-2.72	1.829	0.75	0.178	0.190	0.00033	0.44	1.65	0.504	2.72
8	LB-0.75-4.00	1.829	0.75	0.178	0.231	0.00049	0.53	2.00	0.741	4.00
9	LB-0.75-6.25	1.829	0.75	0.178	0.288	0.00076	0.66	2.50	1.157	6.25

Table 4.3. Variables used for the experiments.

<table>
<tr><th>Parameter</th><th colspan="3">Values Used for This Study</th><th>Range of Previous Studies</th><th>Comments</th></tr>
<tr><td>Particle size D_{50}</td><td colspan="3">0.26 mm</td><td>0.35 to 14.25mm</td><td>The large size of the expt. set-up required the use of a fine, uniform sand</td></tr>
<tr><td>Contraction ratio, B_2/B_1</td><td>0.25</td><td>0.5</td><td>0.75</td><td>0.25 to 0.70</td><td>-</td></tr>
<tr><td>Dimensionless length, L/B_1</td><td colspan="3">10.6</td><td>1.0 to 10.0</td><td>-</td></tr>
<tr><td>Approach velocity ratio, V_{n1}/V_c</td><td colspan="2">0.55</td><td>2.5</td><td>0.38 to 3.07</td><td>Includes choked and unchoked conditions</td></tr>
<tr><td>Approach shear stress ratio, τ_{n1}/τ_c</td><td colspan="2">0.3</td><td>6.25</td><td>0.14 to 9.4</td><td>Includes choked and unchoked conditions</td></tr>
</table>

4.8. Experiment procedure

The procedure for each experiment involved three phases:

1. Conduct of experiment;
2. Post-experiment measurements; and,
3. Preparation for the next experiment.

An early step during the conduct of an experiment entailed filling the flume slowly with water, beginning with water entering the flume at its downstream end. A flexible hose, 4.0 in in diameter, was used for this purpose. Water was added until the water level reached a designated depth equivalent to the Y_{n1} at the downstream end of the contraction. Then the pump was turned on and the discharge increased to the designated flowrate for each experiment, while the downstream depth of flow was kept constant at the normal depth of flow for the original, uncontracted channel. This action was done by adjusting the downstream sluice gate. The average time-period for this phase was about one hour, see Figure 4.1.

After reaching the designated downstream depth and discharge, the actual conduct of the experiment began as did data collection. This second phase of conducting an experiment lasted between 7 to 48 hours, depending on the experiment setup and whether the experiment was clear-water or live-bed. Scour depths at the corners and vena-contracta region (these specific locations along the contracted channel will be discussed in detail in chapters 6) were checked to determine if equilibrium depth had been attained at those locations. For the live-bed experiments, that along the vena-contracta region reached equilibrium quicker than for the clear-water experiments. The early clear-water experiments were run for 48hrs. By draining the flume and measuring the bed elevations, it was determined that the bed along the vena-contracta region had reached equilibrium within 15 hours of running flow. It was decided to run all subsequent experiments for 18hrs to ensure equilibrium conditions prevailed in the vena contraction region and at the corners of the contraction entrance. The live-bed experiments initially were run for 12 hrs, but no significant change occurred in the vena-contracta region or the corners after about 6 hrs of flow (subsequent Figure 5.25 shows the temporal development of scour). These experiments were then run for 7 hrs, to ensure no additional deepening would occur. However, the bed along the middle of the contracted channel did experience slight adjustments as bedforms passed through this region.

At the end of each experiment, the discharge was decreased slowly, the sluice gate was closed simultaneously, and the flume was drained slowly to keep the bedforms intact and prevent further scour. In total, each experiment took about 9 to 50 hours to complete.

The end of each experiment involved LiDAR-scanning the bed to obtained detailed information regarding the erosion of the bed. The LiDAR scans were collected from both sides of the contraction, up- and downstream end of the contracted section. This setup assisted us to capture all aspects of the bed; i.e., the complete topography of the bed surface. The survey resolution at 10-meter radius around the scanner was 0.1 inch, i.e. the distance between two point in surveyed area around the scanner is 0.1 inch.

Once the scanning was completed, the bed was re-leveled, the sensors readjusted. Then, the bed LiDAR was re-scanned to capture the initial state of the bed in preparation for next experiment. This effort required recovering sand from the sediment trap and augmenting the bed with sediment held in storage. The re-leveled bed had to be compacted, saturated and compacted further to ensure that the bed did not settle during the early stages of an experiment. Typically, preparation for the next experiment took several days.

5. Presentation of Flume Results

5.1. Overview

This chapter presents the results of the experiments. The results comprise data on scour depths, LiDAR scans of the bed bathymetry along the flume, and observations of the flow and the bed bathymetry. To be kept in mind is that the present experiments involved flow contractions that did not choke the approach flow at either the downstream or upstream ends of the contracted channel, because flow choking would have altered the flow field along a contraction and at a contraction entrance. Figures 2.9 and 2.11 delineate the no-choking limits for the experiments.

The results are presented in three categories based on contraction ratio B_1/B_2:

1. Tight contraction, $B_1/B_2 = 0.25$;
2. Medium contraction, $B_1/B_2 = 0.50$; and,
3. Mild contraction, $B_1/B_2 = 0.75$.

All the experiments concern contractions of intermediate length, as defined in Chapter 2. Also, note that the categories include clear-water and live-bed conditions of contraction scour. As explained in Chapter 6, these conditions essentially are portions of curves defining trends in contraction scour.

Though the experiments were limited in number, they produced the data and observations needed to address the study's objectives. Table 4.1 summarizes the flow characteristics associated with each of these experiments. Note that the data and observations for the contractions of intermediate length apply to a channel that was originally of uniform cross-section and conveyed a normal depth of flow, but subsequently was contracted (narrowed).

The first category of experiments listed comprised eight experiments that examined contraction scour development in terms of how flow control affected scour and flow distribution during scour. Three of these experiments involved the downstream control set as Y_{n1} and two where the downstream control was set at normal flow depth for flow along the contraction, Y_{n2}. In effect, these experiments entailed three intermediate-contraction cases and two long-contraction cases. To avoid the choking limitation mentioned above, all the experiments were conducted in the clear-water-scour range. A further experiment was run with the contraction bed was fixed (with plywood) to obtain insights into the variation of flow velocity and water-surface profile to and along the contraction.

The second category listed consisted of seven experiments (clear-water and live-bed) run with the downstream control set Y_{n1}. Three clear-water and four live-bed experiments were run (as per Tables 4.1 and 4.2). The third category listed entailed eight experiments, of which three were clear-water-scour conditions and five were live-bed-scour experiments (as per Tables 4.1 and 4.2). The results of the experiments are documented in Appendix D. Note that the acronyms CW and LB are refer to clear-water and live-bed conditions of scour, respectively.

The process used to locate and measure the vena-contracta scour is discussed in Chapter 6, Analysis. As that chapter elaborates, the formation of dunes and ripples non-uniformly spaced along the vena-contracta introduced uncertainty into the measurements. Additionally, measurements revealed that the streamwise length and width of the vena contracta varied as the contraction ratio and water discharge varied.

The results of the LSPIV measurements are presented at the end of this chapter. They were obtained and evaluated in the course of a companion study (Fakhri 2020), which fully documents them and presents the analysis involved in obtaining the results. The LSPIV results are used in Chapter 6, which considers how to improve the HEC-18 equations.

5.2. The Tight Contraction, $B_2/B_1 = 0.25$

This section gives the results from three experiments conducted for contraction scour produced by the tight contraction, set here as $B_2/B_1 = 0.25$. For two of the experiments presented here, the downstream control for the experiments was the normal depth, $Y_{n3} = Y_{n1}$, for flow along the uncontracted channel downstream of the contracted channel. The third experiment was done with the downstream control being commensurate with the long contraction condition; i.e., the normal depth, Y_{n2}, of uniform flow along a lengthy contracted channel, such as would occur for a channel constricted by a series of instream channel-control structures (e.g., rock vanes or barbs).

As flow-choking would have occurred for live-bed approach flows to the tight contraction $B_2/B_1=0.25$, as Figure 2.9 indicates, the described experiments are limited to clear-water approach flow upstream of the contracted channel. Flow-choking at the downstream or upstream ends would alter the flow field through the contraction, complicating comparison of data and observations.

5.2.1. Overview

Tight contractions typically are not used in the design of bridge waterways, but contractions considered tight can arise when the entrance to a bridge waterway becomes partially blocked by drifting objects like woody debris or ice floes, or when a channel is lined with instream structures that intrude extensively into the channel; a recommended intrusion sets these structures at a third to a fifth of the channel width (e.g., Siefken et al. 2020). The results from the tight contraction essentially set a contraction-scour limit in terms of B_2/B_1 for contraction scour development during the present experiments, because the scour depths were greatest for this contraction ratio.

The data and observations give insights into intermediate-contraction experiments in which the downstream control was set at Y_{n1} (normal depth of flow in the uncontracted channel) and the values of the shear-stress ratio τ_1/τ_c were 0.30 and 0.56. Additionally, the data and observations show the effect of setting the downstream control as Y_{n2} (normal depth of flow in the contracted channel). For this latter case, choking had been estimated not occur at the contracted channel's downstream end when $\tau_1/\tau_c = 0.98$, because of the greater depth of flow along the contracted channel; i.e., $Y_{n2} > Y_{n1}$. Choking otherwise readily occurs in tight contractions.

Further, paving the contraction's flat bed with non-erodible plywood (producing the same Manning's roughness as the sand bed; $n = 0.011$), enabled velocity measurements to be made for flow along a contraction having a flat bed, in effect, this arrangement was similar to flow and bed condition at the beginning of an experiment. The results of these measurements aid numerical simulation of the initial flow field through the contraction.

The data presented for each experiment associated with the abovementioned categories of channel contraction include the following measurements:

- LiDAR scans of the initial condition, i.e., flat bed, and equilibrium scoured bed
- The temporal evolution of bed profile and the water-surface profile (along the centerline of the flume and along the right side [looking downstream] of the flume)
- Variation of the maximum depth of scour along the contraction centerline. This value of scour depth was found to occur along the centerline near the contraction entrance and to coincide with what is herein termed *vena-contracta scour*. The next chapter, Chapter 6, discusses how this depth location varied for the experiments
- Variation of the maximum depth of scour at the corners of the contraction entrance. This scour depth is herein termed *corner scour*. A pronounced feature of the experiments was that this scour depth greatly influenced scour along the contraction, especially at the contraction entrance

To aid tracking of the experiments, the experiments are labelled as listed in Table 6-2 and indicated in the appendices. At certain times, the details of the labels are elaborated in this presentation of results.

5.2.2. Intermediate-length contraction: CW-0.25-0.30

For this experiment the downstream control was set as the normal depth of flow along the uncontracted section (i.e., at Y_{n1} = 0.18cm (7 inches)) for the flume slope adjusted as Table 4.1 describes. The shear stress ratio along the normal depth of the uncontracted approach flow (of depth Y_{n1}) was set to produce the shear-stress ratio τ_1/τ_c = 0.30 associated with the uniform flow. The duration of this experiment was 18 hours. However, after 12 hours of running the experiment, measurements of the bed-surface profile showed that the contracted channel had reached the equilibrium condition.

Figure 5.1 illustrates the scoured bed with views looking upstream and downstream along the contracted channel. Scour at the contraction entrance developed to form essentially a step or abrupt drop in bed elevation. Therefore, the whole entrance scoured practically an equal amount, producing a level scour step.

(a)

(b)

Figure 5.1. Views of the scoured bed at the end of experiment: (a) view looking at the contraction entrance and downstream along the contraction; and, (b) view looking upstream along the contraction.

A comparison of the LiDAR-scanned bed before and after the experiment (18 hours of run time) is shown in the Figure 5.2. The comparison reveals that the scour predominantly occurred within the entrance of the contracted channel. The red region used for the scour scale indicates the location of deepest scour along the contracted channel.

The profiles of the bed and water surfaces along the flume centerline, measured at the same time (using the SeaTEK and Massa sensors), are shown in Figure 5.3. The scour depth at the contraction entrance developed very fast due the increase in flow velocity and to the presence of turbulence structures at the entrance. The bedforms along the contracted section started to migrate to the downstream and bed has reached to the equilibrium condition.

Figure 5.2. The LiDAR scan of the flume bed (CW- 0.25-0.30) after the 18th hour of running. The red area indicates the region of deepest scour (The units of the scale are meters, and C2C means Cloud to Cloud, and is a term included in the LiDAR software used)

.

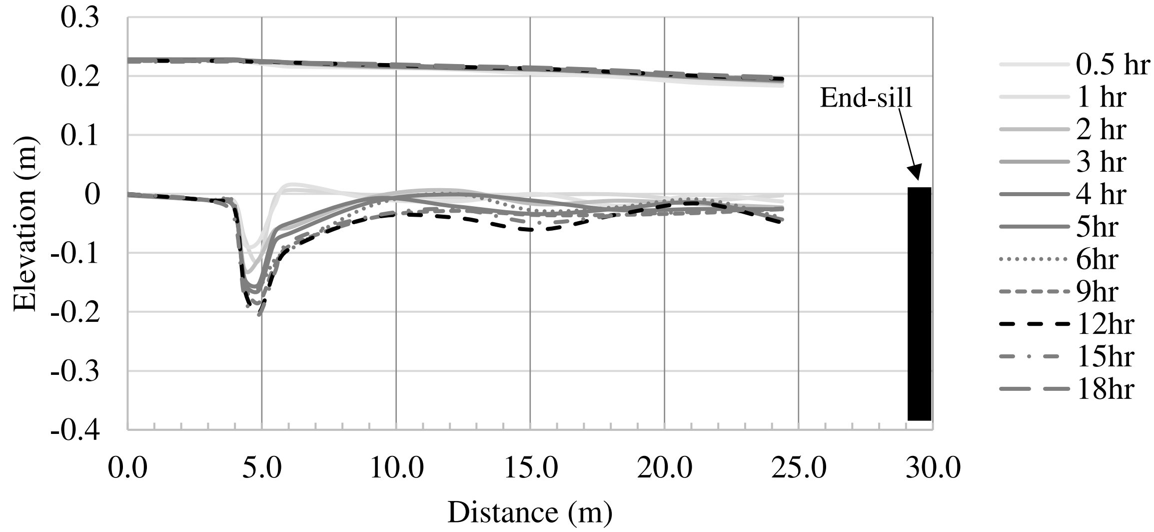

Figure 5.3. The temporal variations of the centerline profiles of the bed and water surface (CW-0.25-0.30). The downstream control water depth was Y_{n1}.

5.2.3. Intermediate-contraction: CW - 0.25 - 0.56

For this experiment, the downstream control was set as the normal depth of flow along the uncontracted section, Y_{n1}. As mentioned in Chapter 4, $Y_{n1} = 0.18$cm (or 7 inches). The shear stress ratio along the uncontracted approach flow (depth Y_{n1}) was set at the shear-stress ratio $\tau_1/\tau_c = 0.56$. The duration of this experiment was 30 hours. Figure 5.4 shows two views of the bed of the contracted channel after the experiment.

(a) (b)

Figure 5.4. Views of the scoured bed (CW-0.25-0.56): (a) view at the entrance; and, (b) view along the whole contraction. The initial elevation of the bed is indicated by the black line along the wall of the contracted channel.

Though measurements show that the maximum depth of scour at the entrance was reached within 12 hours, the bed downstream of the contraction entrance continued to undergo minor changes as bed forms adjusted in position and height. These minor adjustments happened along the major portion of the contracted channel downstream of the vena-contraction region. The extent to which the changes occurred was affected by the value of the shear-stress excess at the downstream end of the contracted channel; such variations were observed when the shear stress exerted by the flow exceeded the critical shear stress associated with the entrainment of the sand forming the bed. Figure 5.5 shows LiDAR scans of the channel bed at three times during the experiment. The red area in the scans indicates the dominant area of scour, typically in the entrance of the contracted channel.

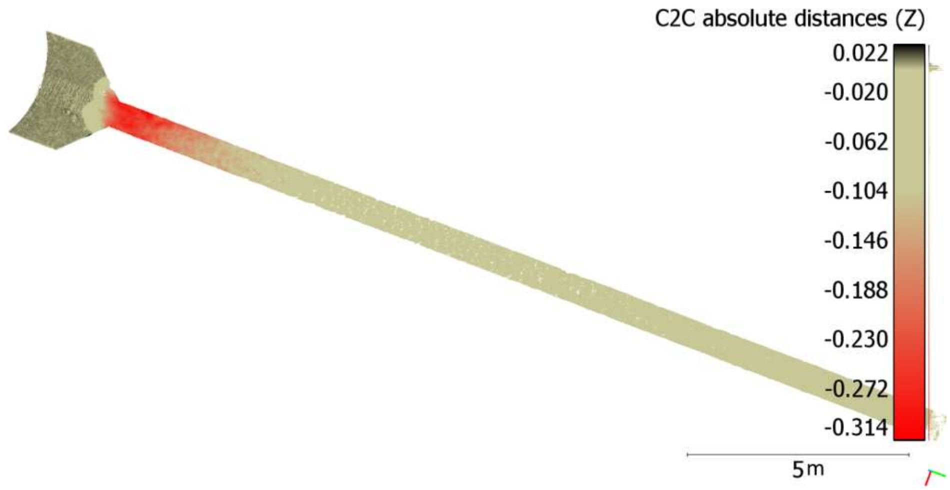

(a)

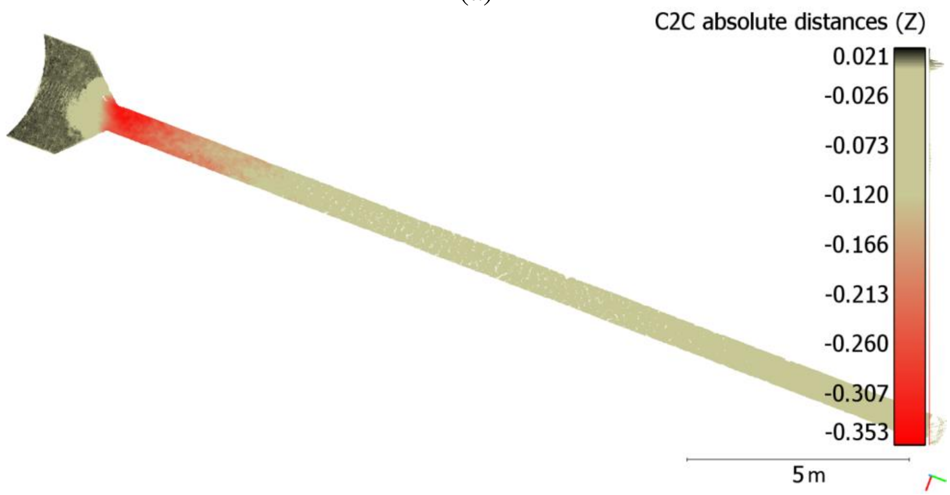

(b)

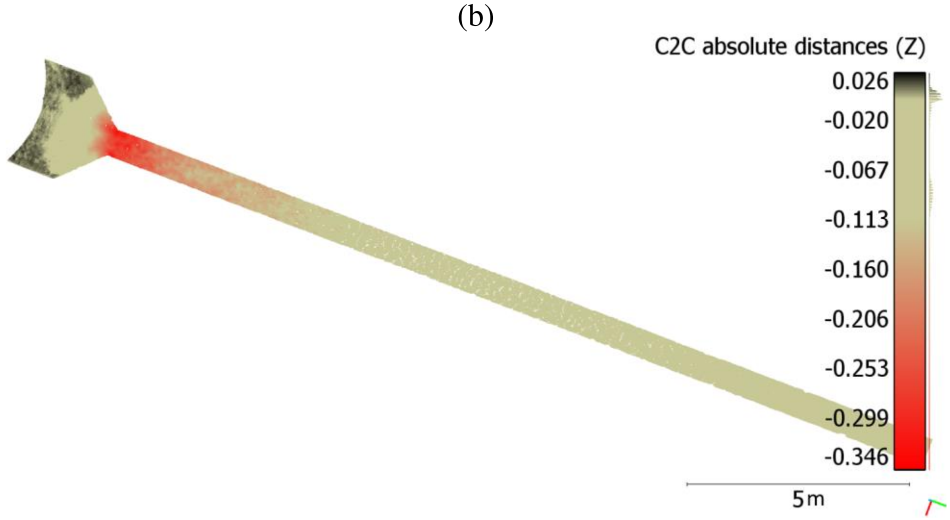

(c)

Figure 5.5. The LiDAR scans of the flume bed at different times during experiment (CW-0.25-0.56): (a) after the 12th hour; (b) after the 24th hour; and, (c) after the 30th hour. LiDAR was used to scan about 20 meters of contracted section.

Figure 5.6 shows centerline profiles of the bed surface and water-surface. The profiles were taken using the Massa and SeaTek probes placed at flume cross-sections 1 through 13, and they were coordinated in time. Due to the physical limitation (space need) of getting the flume carriage suitably located near the end of the contracted channel, there was a gap in the data between end-sill; i.e., between the sluice gate, and cross-section number 13. However, the elevation of the end-sill was fixed and known. Therefore, the data located near the end of the contracted section were not used in the analysis of results, because those data potentially were affected by the presence of the end-sill and fixed elevation of bed. This trimming of data at the end of contraction did not affect the capacity of the experiments to help in addressing the study's objectives listed in Section 1.2.

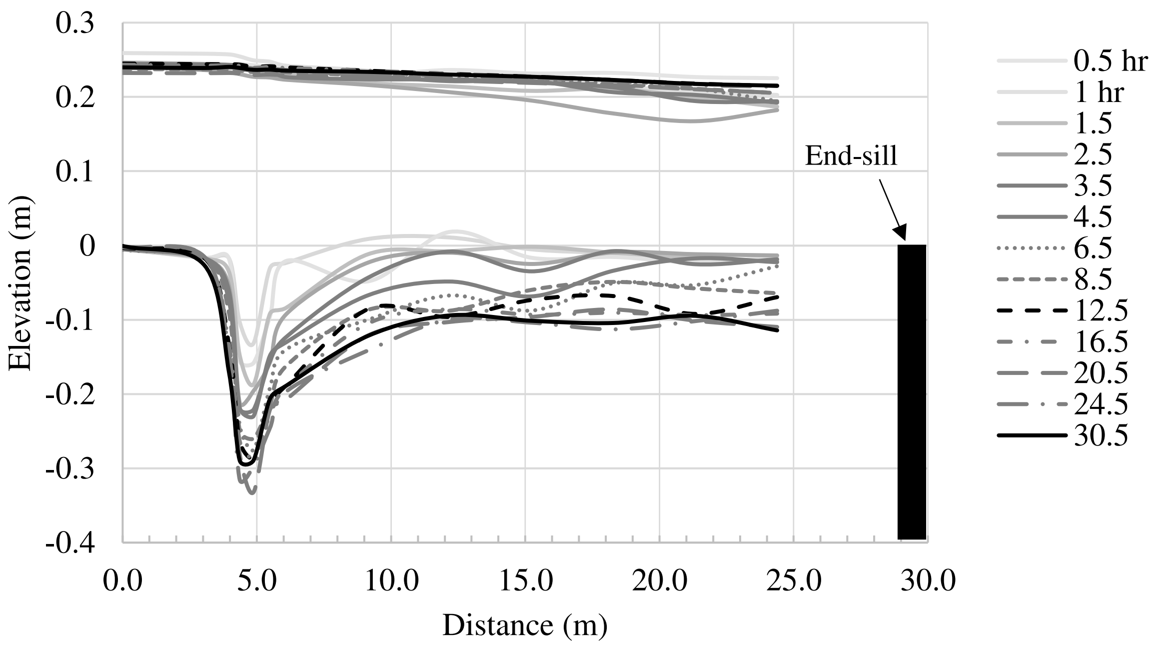

Figure 5.6. The temporal variation of the centerline profiles of the bed surface and water surface. The downstream control was set at Y_{n1} (CW - 0.25 - 0.56). The position of the end-sill (and control gate) is indicated.

5.2.4. Long-contraction: CW - 0.25 - 0.98

The results for the tight contraction with the water depth at the downstream of contracted section was set at Y_{n2} (the normal depth of uniform flow along the contracted channel) to investigate the influence of this control condition of flow control. Now, $\tau_1/\tau_c = 0.98$, as the deeper flow increased the specific energy at the entrance of the contraction (Chapter 2). A higher value of τ_1/τ_c than this value would have led to the live-bed condition of scour.

This experiment ran for 30 hours. Though the maximum depth of scour at the entrance was reached within 12 hours, the bed along the major portion of the contraction continued to be affected by the shear-stress excess at the downstream end of the contracted channel. However, the extended observations and measurements indicated that changes along the major portion of the contracted channel were marginal (minor) and attributable to adjustments of the bedforms (mainly ripples) occurring non-uniformly in terms of position along the bed of the contracted channel.

This experiment showed that no scour occurred along the middle of the contracted section and the only area of scour occurred within the entrance to the contraction. The latter location for scour developed because of the turbulence structures (from the separation region) enhanced the abrasiveness of flow accelerating into the vena contracta formed within the contraction entrance. The turbulence was generated as flow-separation vortices formed at the contraction entrance. The bed sediment scoured from entrance (especially its corners), then deposited to form a mound at a distance about one width, B_1, of approach channel downstream from the contraction entrance.

Figure 5.7 is a sequence of LiDAR scans portraying the bed evolution over 30 hours of run time. The corner scour at the contraction entrance basically attained an equilibrium depth and form after about 12 hours of run time. However, some negligible adjustment in maximum depth of scour occurred when sand accumulated to form the deposition mound slowly eroded, such that the mound flattened and elongated during the remainder of the experiment (12 hours to 24 hours, and then 24 hours 30 hours). This flattening and elongation of the deposition mound was monitored to check whether it would the maximum depth of scour at the contraction entrance; no deepening effect was detected. The area covered by the LiDAR scan extended between flume cross-sections 1 and 13. Figure 4.9 gives the locations of the cross-sections. With the passage of time and owing to turbulence generated by flow passing over the deposition mound, ripples appeared on an increasing area of the bed.

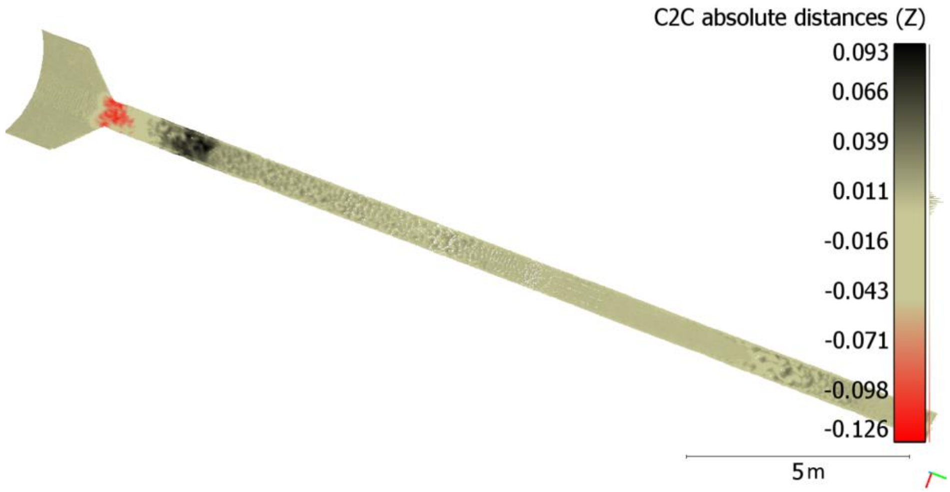

(a)

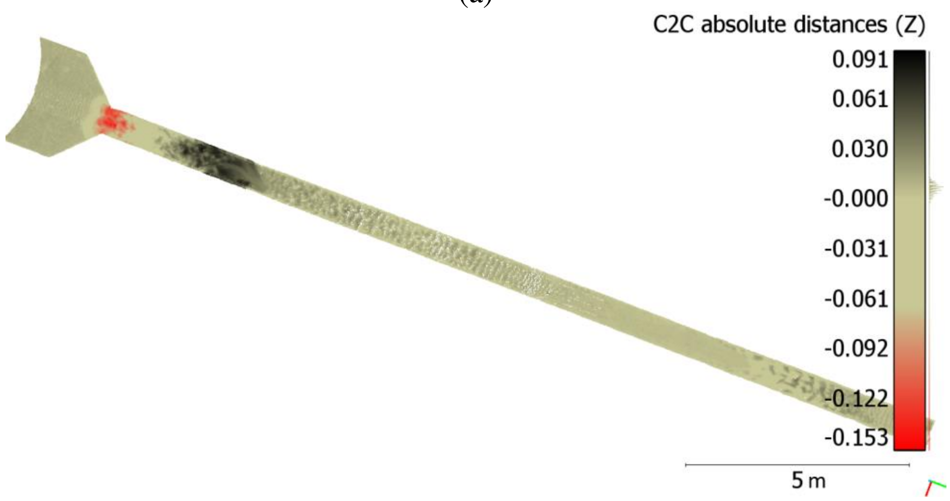

(b)

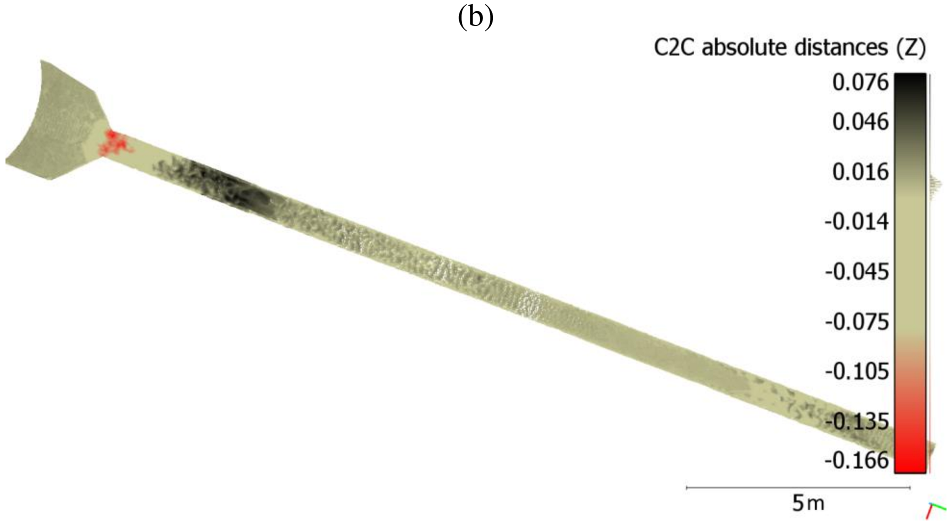

(c)

Figure 5.7. The LiDAR scans of the flume bed at different times during experiment (CW - 0.25 - 0.98): (a) after 12 hours; (b) after 24th hours; and, (c) after 30 hours. The red area indicates the region of greatest scour, whereas the dark area indicates the deposition mound that marked this experiment.

As also shown in Figure 5.8, there is an area near the middle of the contracted channel where the sand did not move at all and the bed surface remained smooth during the duration of the 30 hours of running the experiment. This sub-reach of the flat-bed occurred because the increased flow depth in the contraction coincided with the value of τ_2/τ_c being less than one.

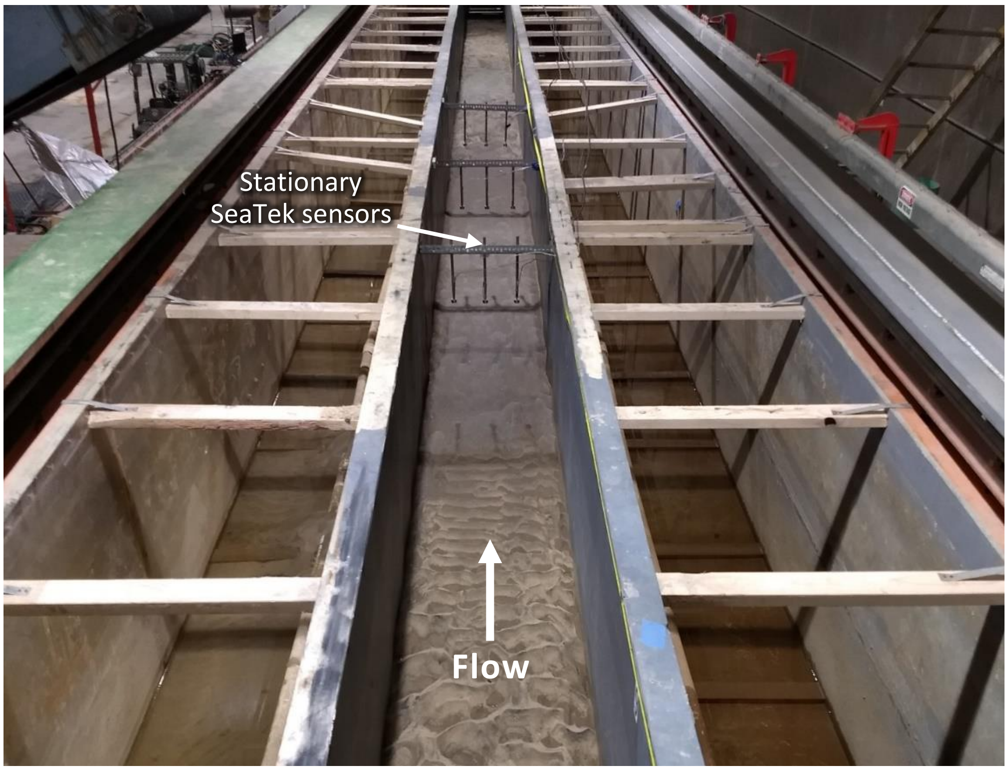

Figure 5.8. No bed elevation changes (mean values) were observed along the middle portion of the contracted channel, even after 30 hours of running the experiment (B_2/B_1 = 0.25).

As Figure 5.8 shows, for the first two, long-contraction experiments the SeaTek acoustic sensors were used. They were stationary and mounted at the middle of contracted channel, where only minor if any changes in bed elevation happened. However, to get more insights from the experiment, it was decided to mount the sensors on the flume's instrument carriage, which enabled collection of the time variation of the bed and water surface at the designated cross sections.

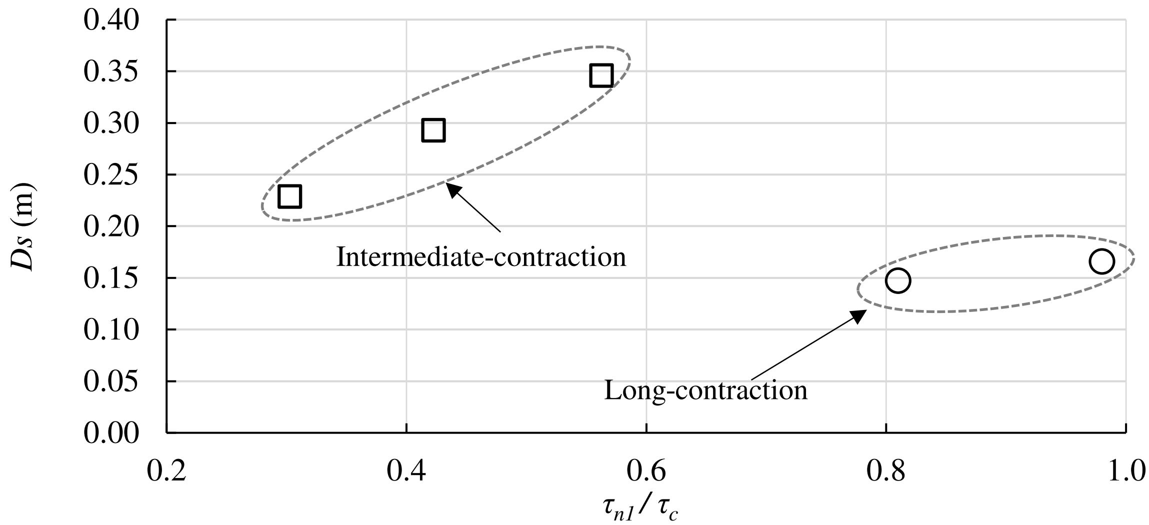

Figure 5.9. The variation of the maximum depth of vena-contracta scour, D_s, for intermediate-length and long- length contraction control conditions set at the downstream end of the contracted channel (B_2/B_1 = 0.25). The control conditions were Y_{n1} and Y_{n2}, respectively for the two control conditions.

As Figure 5.9 shows, the two experiments in which the downstream control for flow along the contraction was set in accordance with uniform (or normal) depth of flow in a long contraction condition, Y_{n2}, yielded lesser maximum depths of scour, even though these latter experiments used values of τ_1/τ_c = 0.81 and 0.98. The lesser values of maximum depth of contraction scour can be attributed to the deeper flow along the contraction, as $Y_{n2} > Y_{n1}$, and the consequent reduction in range of velocity magnitudes and shear stress (hydrodynamic forces generally) at the contraction entrance. This result is somewhat analogous to the effect on maximum scour depth that would be exerted by choking of flow at the exit of the contracted channel.

5.2.5. Tight contraction: fixed-bed experiment

To obtain data regarding the water-surface profile along the contraction and the corresponding velocity-profile distributions, prior to contraction scour development, the bed was covered with sheets of treated plywood which was estimated to have about the same value of Manning's n as did the flat bed of sand; i.e., $n = 0.11$. Figure 5.10 is a view of the contraction fitted with the plywood. The top of the plywood corresponded to the original top of the sand bed.

Figure 5.10. The contracted channel and its entrance covered with sheets of plywood that fixed the flat bed of the contracted section.

The water surface profiles associated with the range of discharges and τ_I/τ_c passed through the contraction are shown in Figure 5.11. The results show that by increasing the shear stress ratio (i.e., discharge when flume slope is adjusted), while keeping the downstream control depth constant, the water depth through the contracted section slightly increased. In other words, the M2 curve of open-channel water-surface profile altered slightly. As expected, when the flow depth at downstream control and steepening the channel to increase the discharge, the backwater curve elevated along the contraction. The increased discharge created a deeper scour in the entrance region of the contracted channel.

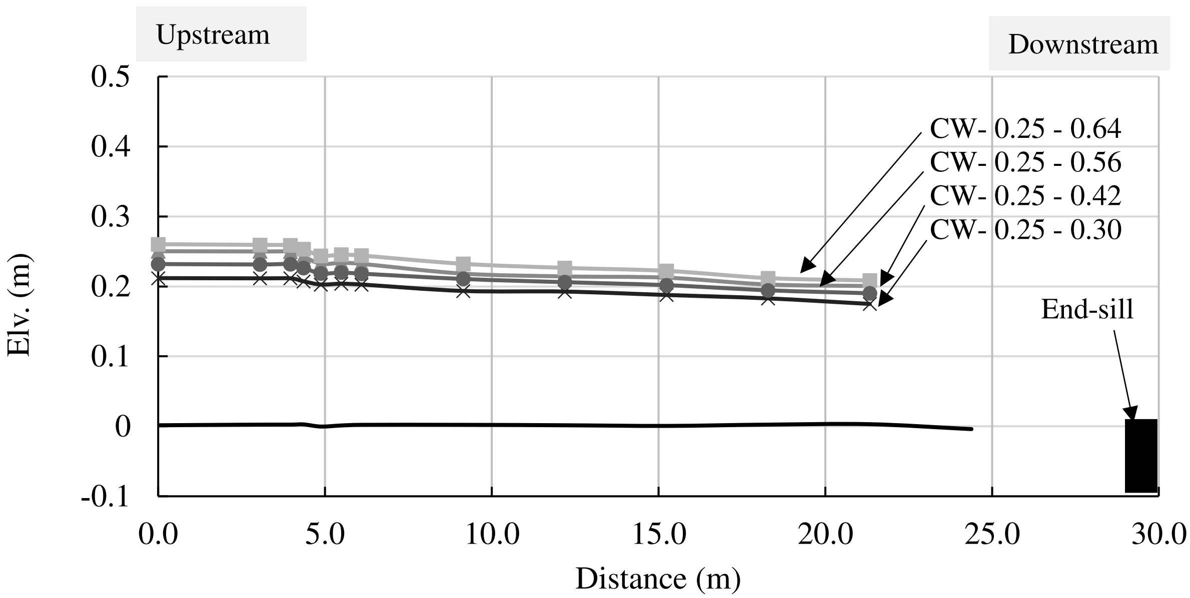

Figure 5.11. Profiles of water-surface elevation along the flume bed for the different values of τ_1/τ_c used in the experiments (B_1/B_2 = 0.25). The starting point (zero) given relates to cross-section 1, defined in Figure 4.9.

The depth-average (2D) values of velocity were collected for each shear stress ratio at cross-sections 1 to 6 in the vicinity of the contraction entrance. Figure 5.12 shows the average magnitude of the velocity and the turbulent intensity for the condition $\tau_1/\tau_c = 0.56$. Note, to facilitate the collection of more velocity data, two additional cross-sections were added between cross-sections 4, 5 and 6; i.e. at cross-sections 4.5 and 5.5.

Some transverse variations in depth-average velocity were noticed in the measurements, and some of the measurements were repeated. However, it was detected that slight differences in approach-channel geometry, and in the surface elevations of the plywood, became reflected in the transverse distributions of velocity. For example, the riprap at the beginning of the plywood-covered entrance to the contracted channel caused the slight variations at cross-sections 1 and 2. These variations continued into the contracted channel (cross-sections 5 and 6). The flow-separation zones at the entrance to the contracted channel (Figure 5.12) caused substantial unsteady fluctuations of flow velocity, evident in the distributions at cross-sections 4 through 6. The LSPIV showed that, once scour occurred in the sand bed, the flow entered symmetrically into the contracted channel (Fakhri 2020). Additionally, the profiles of the eroded bed through the contraction, though variably uneven locally, were essentially similar along several streamwise transects of the channel. However, the bedforms along the contracted channel were markedly three-dimensional in morphology. This three-dimensionality locally affected flow-velocity distribution through the entrance of the contraction.

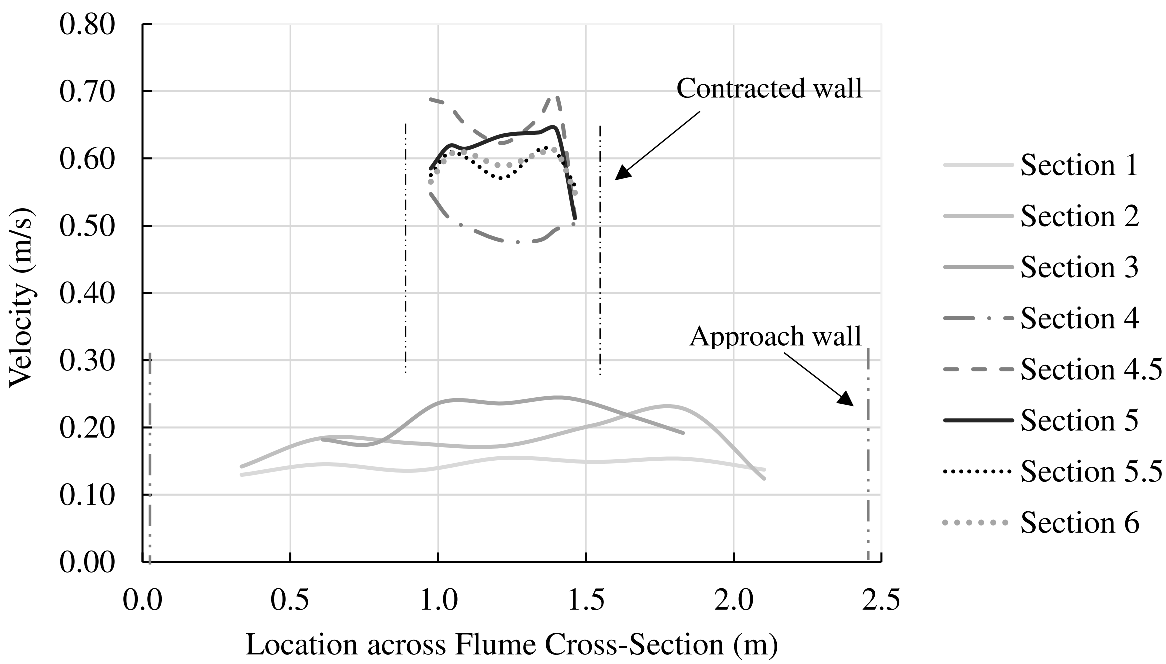

Figure 5.12. The depth-average magnitude of velocity at several cross-sections for the experiment CW-0.25-0.56.

To better characterize the turbulent fluctuations of the flow to and through the contracted channel, estimates were made of the turbulence intensity, *I*, at each position of velocity measurement. The local value of *I* was calculated as follows:

$$I \equiv \frac{u'}{U} \tag{5.1}$$

Here, I is the turbulence intensity, $u'$the root-mean-square of the turbulent velocity fluctuations and U is the mean velocity. (ANSYS, 2018). The value of u' was determined from the measurements as being

$$u' \equiv \sqrt{\frac{1}{3}\left({u'_x}^2 + {u'_y}^2 + {u'_z}^2\right)} \tag{5.2}$$

and,

$$U \equiv \sqrt{U_x^2 + U_y^2 + U_z^2} \tag{5.3}$$

The turbulence cases were divided into three groups:

I. High turbulence cases, where $5 < I < 20$ percents;

II. Medium turbulence cases, where $1 < I < 5$ percent; and,

III. Low turbulence cases, where $I < 1$ percent.

Figure 5.13 shows high turbulence intensity near the contraction walls and medium to low turbulence intensity at the centerline. This finding is to be expected, because of the greater shear stress at the channel boundaries. Turbulence intensity is also another indicator to indicate the separation zone, due to having high turbulence and eddy shed in the separation zone. The high intensity turbulence can be indicating the higher scour depth at the separation zone, i.e. corner scour.

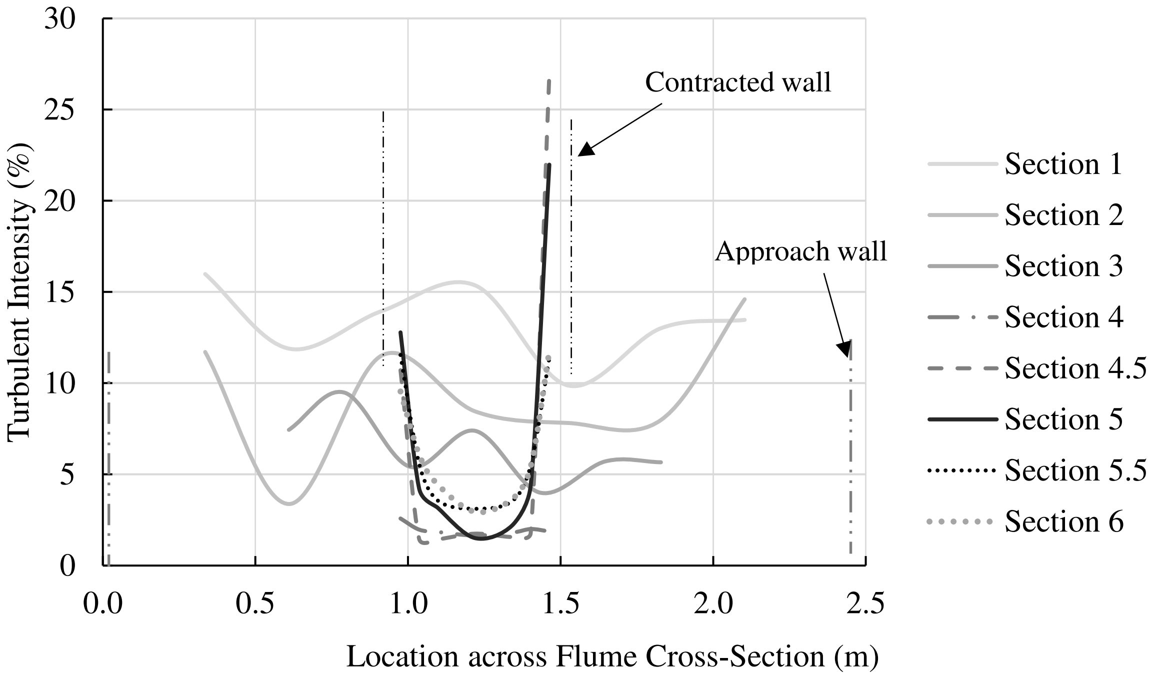

Figure 5.13. Values of turbulence intensity, I, across selected cross-sections of the flume for experiment CW-0.25- 0.56.

5.2.6. Tight contraction: scour at the corners of the contraction entrance

The maximum depth of scour at the contraction's entrance corners are given in Figure 5.16. Two sets of data are shown: depths for the intermediate-contraction experiments and for the long-contraction experiments. The trend shows that scour depth increased as the shear stress ratio, τ_1/τ_c, increased. Further, the trend essentially corresponds to the increase in flow velocity (or discharge) associated with the increases in the shear-stress ratio. However, to be observed are the differences in the magnitude of the scour between intermediate- and long-contraction. The velocities associated with the two control conditions differed (being less for the long contraction) and therefore the scour depths differed, even within the entrance of the contracted channel.

As mentioned above (and elaborated in Chapter 6) for all contraction ratios, a local maximum depth of scour occurred at the centerline of the channel within a distance equivalent to the width of the approach channel, B_1. The distance was measure downstream from the contraction entrance, see Figure 5.14.

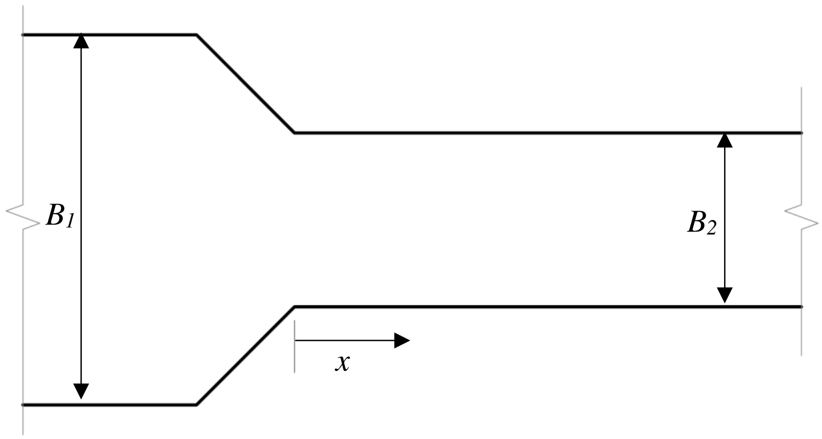

Figure 5.14. The position of the narrowest cross-section of the vena-contracta, was measured distance x from the start of the contracted channel (width B_2).

This maximum scour depth was related to the formation of a vena-contracta within the contraction entrance and to the dimensions encompassed by the vena contracta (Chapter 6). Due to the flow interaction of the recirculation areas at the entrance of tight contraction, the contraction entrance bed was scoured so as to be practically flat across the entrance within the contracted channel. Figure 5.15 illustrates the interference of corner scour with the vena-contracta area for tight contraction (B_2/B_1 = 0.25). Consequently, as shown, a single scour hole formed in the contraction entrance, and that scour hole merged up to the downstream bed by means of a relatively a smooth, upward slope that showed no further local maximum depth of scour; i.e., vena-contracta scour could not be delineated in this area. Consequently, it is reasonable to assume that, for tight-contractions, the corner scour depth and vena-contracta scour depth work together to develop the a single region of scour, as shown in Figure 5.15.

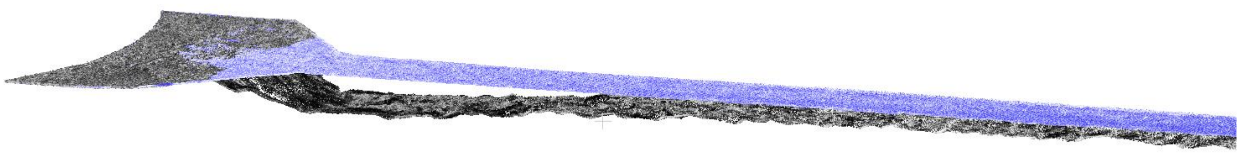

(a)

(b)

Figure 5.15. A comparison of the LiDAR scan of the flume bed before and after scour (CW- 0.25-0.56). (a) isometric view of the bed; and, (b) side-view of the bed. (B_2/B_1 = 0.25).

Also, it is clear from Figure 5.16 below that the downstream boundary condition (i.e., Y_{n2} or Y_{n1}) affected the maximum depth of scour formed in the vena contracta. The long-contraction control, Y_{n2}, led to substantially shallower scour depths in this region. This trend indicates that the intermediate- and long-contraction scour depth increased by as the shear stress ratio increased, but the intermediate-contraction scour involved higher values of the ratio because the flow depth was less (and the velocities higher) than was the case for the long-contraction control.

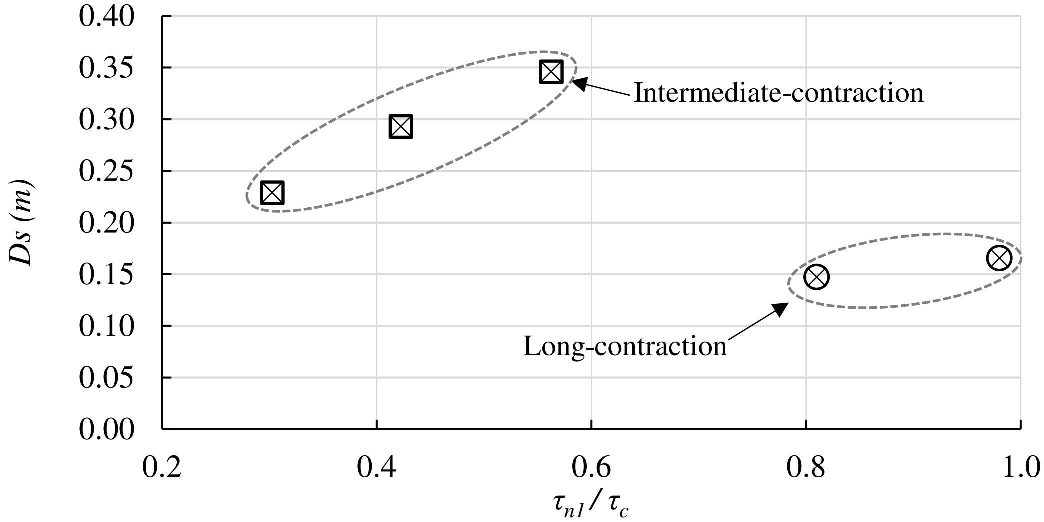

Figure 5.16. The maximum depth of corner scour for intermediate- and long-contraction experiments for the tight contraction. The hollow symbols are the vena-contracta scour depth and the cross symbols are for the corner scour depth (B_2/B_1 = 0.25).

5.3. The Medium Contraction (B_2/B_1 = 0.50)

This section presents the results from the series of experiments regarding contraction scour associated with the medium contraction, set here as $B_2/B_1 = 0.5$. The downstream control for the experiments was the normal depth of flow, Y_{n1}, for the uncontracted channel downstream of the contracted channel. The experiments involved clear-water and live-bed conditions of flow along the approach channel.

5.3.1. Overview

The contraction ratio for this medium contraction condition was taken as $B_2/B_1 = 0.5$, because this value of B_2/B_1 begins to be more common for bridge waterways than is the tight-contraction condition described in the preceding section. This value of B_2/B_1 is still relatively small for bridge waterways, but it usefully illuminates how the vena-contract scour becomes a local scour maximum and becomes distinguishable from the regions of corner scour.

Presented first are the data and observations for the clear-water condition of scour. The values of the shear-stress ratio τ_1/τ_c used in the presentation are 0.30 and 0.56. Presented subsequently are the four cases of intermediate-contraction with live-bed condition and the values of shear stress ratio τ_1/τ_c set at 1.44 and 4.0. Tables 4.1 and 4.2 list the full set of experiments for the mild contraction ratio (B_2/B_1 = 0.5).

5.3.2. Medium contraction: CW - 0.5 - 0.56

The shear stress ratio for uniform flow along the approach channel was τ_1/τ_c = 0.56 and the water depth at the downstream boundary condition (i.e., the sluice gate) was equal to normal water depth at uncontracted section, Yn_1. The duration of this experiment was 18 hours, because experience with the experiments led to the conclusion that, after 18 hours of run time, the bed of the contracted channel or at least the entrance part (about 2 to 3 times of uncontracted section width, B_1) had reached to the near equilibrium state.

Figure 5.17 shows a LiDAR scan of the flume bed for this experiment. The V-shape area at the entrance of the contracted channel formed due to the combined effects of vena-contraction scour and corner scour. For this experiment, bedforms (ripples and low dunes) developed along the entire length of the contracted channel.

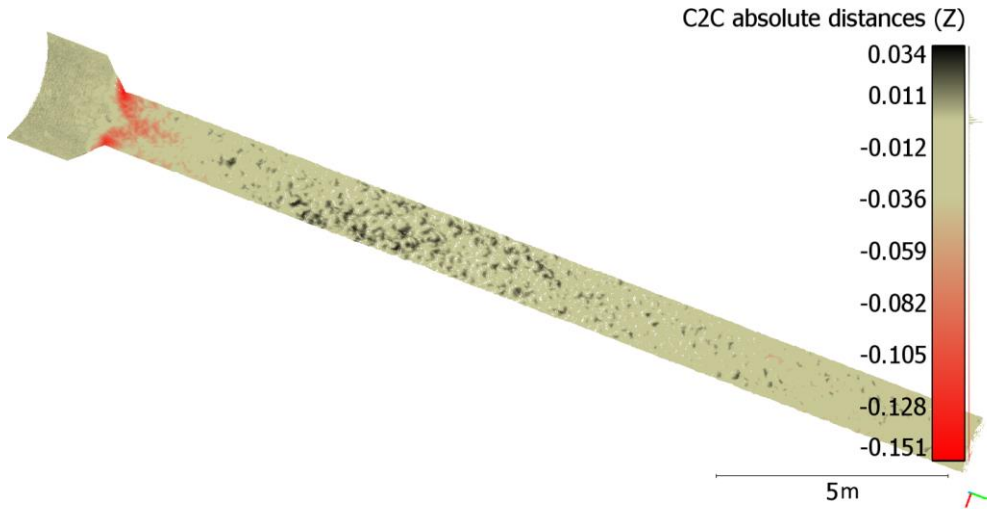

(a)

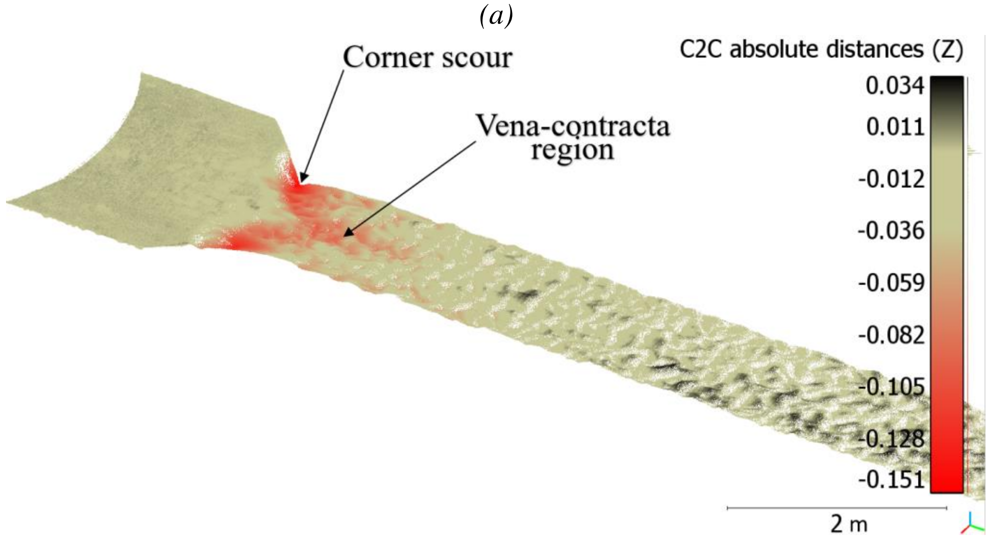

(b)

Figure 5.17. The difference in elevation between the initial bed level and the bed after 18-hours of running the experiment. (CW - 0.5 - 0.56); (a) a view of the full scan along the contraction; and, (b) a view of the portion of the contraction closer to the contraction entrance.

Figure 5.18 shows the corner scour and the vena-contract scour during and after this experiment. A notable feature of the bed is the formation of bedforms, especially in the region of the vena contract. Bedform development introduced uncertainty to measurement of a value of maximum scour depth in the vena contracta. Consequently, the bedforms complicated estimation of the bed profile along the contracted channel, because the bedforms gave the bed surface a non-uniform texture as Figure 5.18 shows.

(a) (b)

Figure 5.18. Views of the scoured bed as viewed from upstream: (a) during the experiment; and, (b) after the experiment (CW - 0.5 - 0.56). The black line along the contraction wall shows the bed elevation before scour.

Figure 5.19 shows the development of profiles of water surface and bed along the centerline of the flume. The water surface and corner scour elevation near the right-side wall is shown in Figure 5.20, which also shows the migration along the flume of dunes. The dunes are evident as undulations in the bed profile downstream of the contraction entrance. The average dune height was about 0.024 m, as determined from measurements made for this experiment. The three-dimensional shape of the bedforms meant that the measurements inevitably entailed some approximation. Herein, it was assumed that the average height of a local dune was about twice of the local fluctuation of the standard deviation of the bed elevation. More information about the dunes and their height variation along the contracted channel is given in Chapter 6.

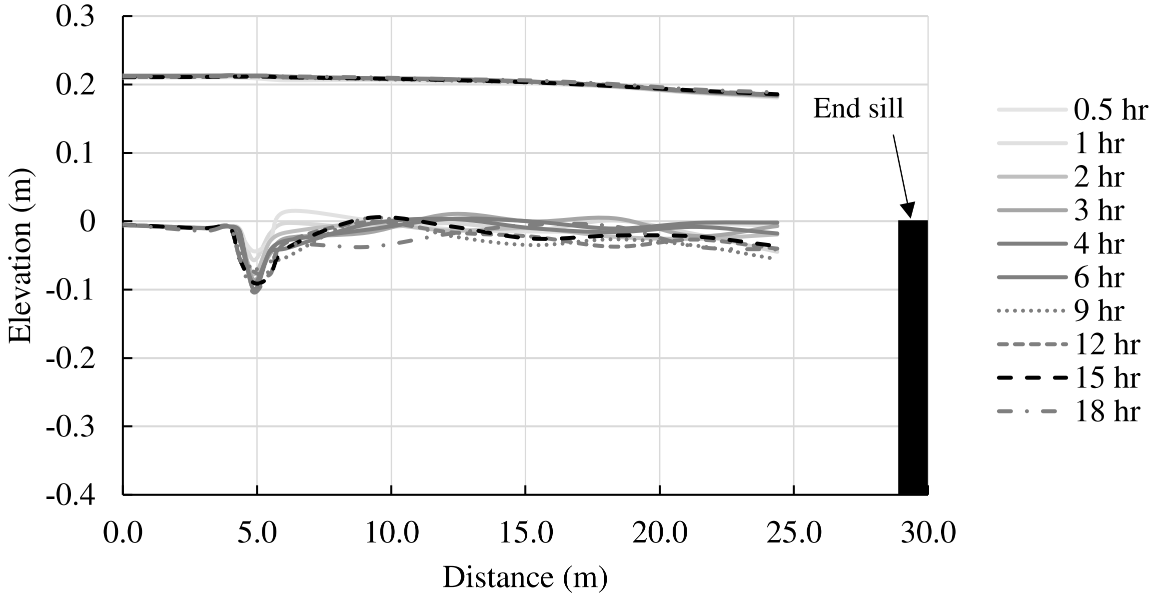

Figure 5.19. Temporal variations in the profiles of water surface and bed elevation along the contraction centerline. (CW - 0.5 - 0.56)

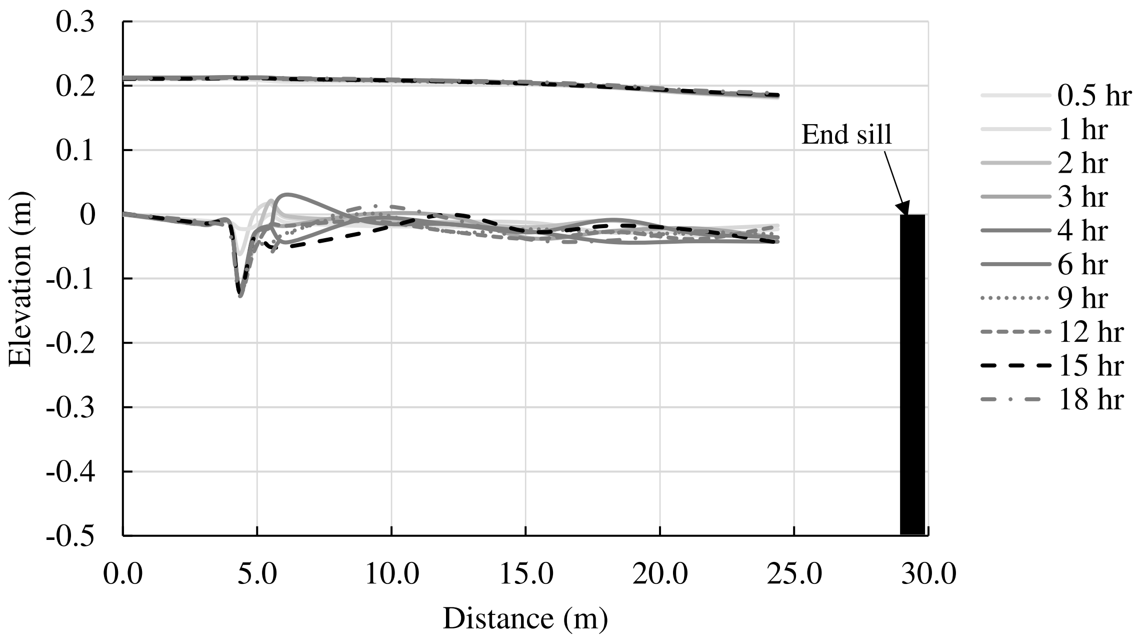

Figure 5.20. Profiles of water surface and bed elevation near the right-side wall for different time-steps. (CW - 0.5 - 0.56)

5.3.2. Medium contraction: LB - 0.5 - 1.44

The shear stress ratio at uncontracted section was τ_1/τ_c = 1.44 and water depth at downstream boundary condition (i.e., sluice gate) was equal to normal water depth at uncontracted section, Yn_1. The duration of this experiment was 7 hours. Figure 5.21 shows a LiDAR scan of the bed after 7 hours of running the experiment. This experiment involved the lowest value of shear stress for the live-bed cases.

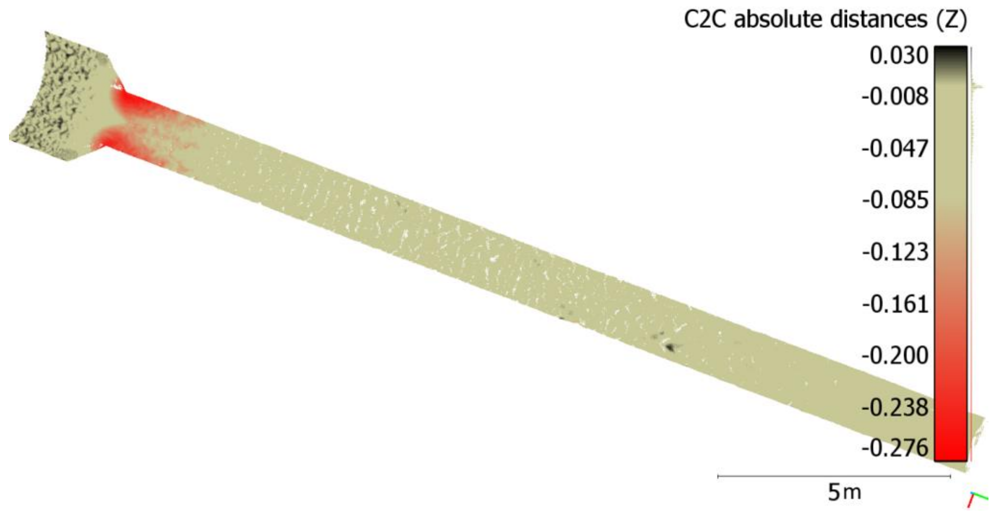

(a)

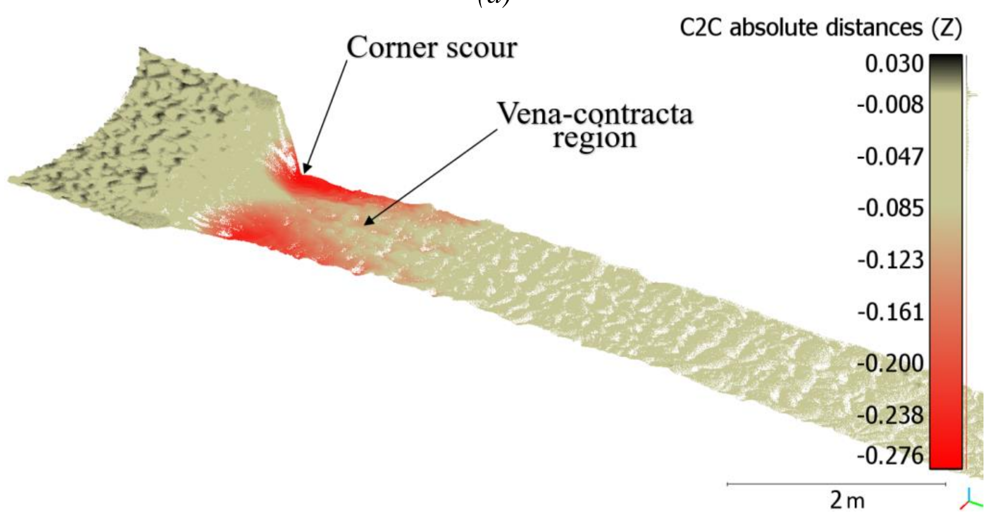

(b)

Figure 5.21. A LiDAR scan of the contracted channel showing the bed surface after 18-hours of running the experiments. (LB- 0.5- 1.44); (a) a view of the full LiDAR along the contraction; and, (b) a view of the portion of the contraction closer to the contraction entrance.

The photographs in Figure 5.22 illustrate the bed surface after 7 hours of running the experiment. The views in the two photographs are looking upstream and downstream, respectively. The two photographs show the two regions of corner scour and the dunes which propagated along the bed. They also show the region of vena-contract scour and give an impression of the difficulty of accurately estimating the maximum depth of vena-contracta scour. As mentioned for the prior experiments, the estimation of scour depth was complicated by the presence of bedforms.

(a)

(b)

Figure 5.22. Views of the scoured bed after completion of the experiment: (a) view looking downstream; and, (b) view looking upstream (LB- 0.5- 1.44). The black line shows the bed elevation before scour.

Figure 5.22 shows the centerline water surface and bed-evolution at different times during the experiment. Dune migration is evident in this figure as varying undulations of the bed surface. The scour depth is shallow due to the low shear stress ratio.

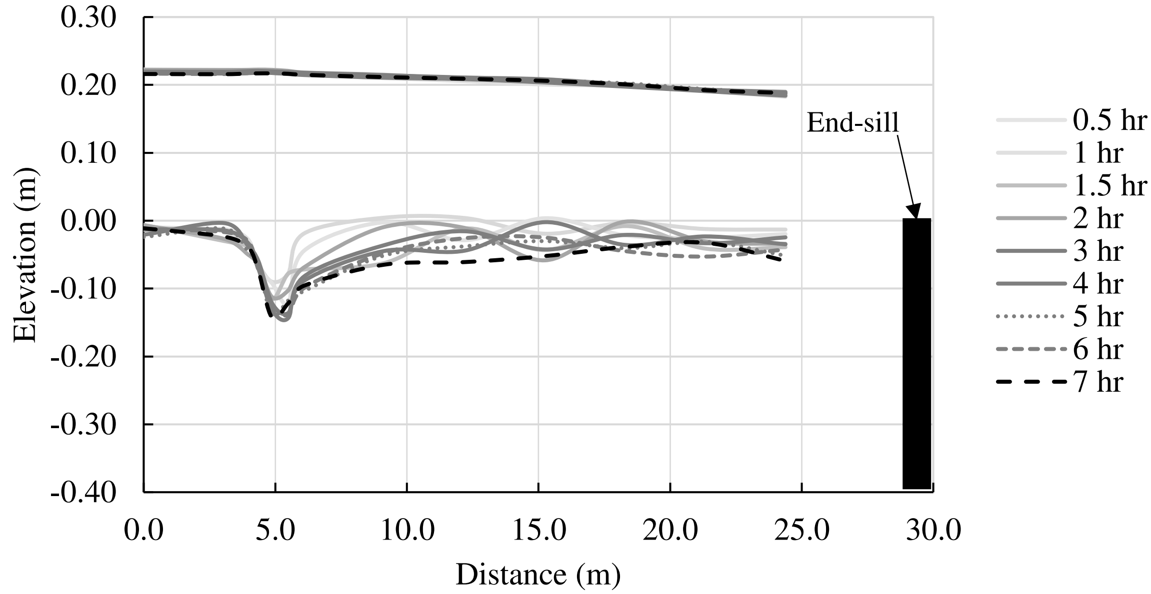

Figure 5.23. Profiles of water surface and bed elevation near centerline for different time-steps. (LB - 0.5 - 1.44)

The temporal development of the water-surface profile and profile of scour elevation near the right-side wall (looking downstream) is shown in Figure 5.24. Each of the two regions of corner-scour attained a maximum equilibrium depth after about 2 hours of running the experiment.

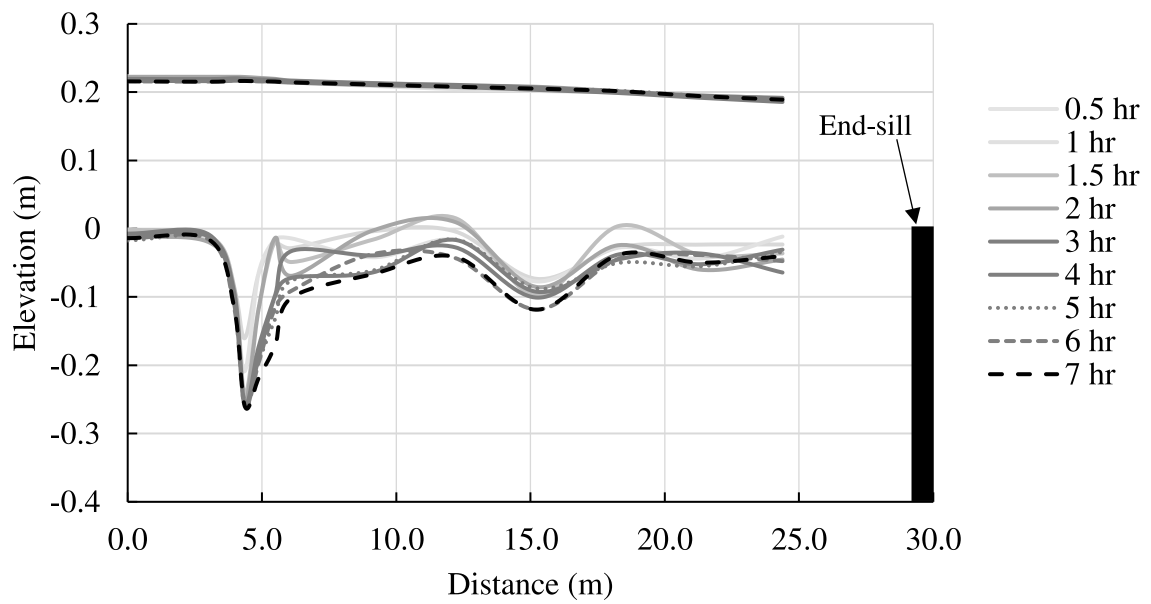

Figure 5.24. Profiles of water surface and bed elevation near the right-side wall (looking downstream) for times during the experiment (CW-0.5-1.44)

5.3.3. Medium contraction: LB - 0.5 - 4.0

The shear stress ratio associated with uniform flow along the approach channel upstream of the contraction was $\tau_1/\tau_c = 4.0$, such that the live-bed condition of scour occurred. The water depth at downstream boundary condition, i.e. sluice gate, was equal to normal water depth at uncontracted section, Y_{n1}.

The duration of this experiment was 7 hours, which the measurements showed to be sufficient for equilibrium scour to develop along the contracted channel, especially within the vena-contract region and at the corners of the contraction entrance. Previous studies have shown that the live-bed cases reached faster to the equilibrium state than clear-water cases. For example, Gill (1981) stated that, for his live-bed experiments with fine and coarse sands, 6 hours was ample time for contraction scour to reach an equilibrium condition.

The bed evolutions at the centerline locations for cross-sections 4, 5, 6 and 8 (encompassing the entrance of contracted channel) are presented in Figure 5.25, which shows that, at about 7 hours, the bed along the contraction reached its lowest elevation at cross-sections 4, 6, and 8. The fluctuations in bed level measured at cross-section 5 is attributable to dune and ripple migration downstream along the contraction. Such fluctuations were typical of the measurements of the bed elevation at a single point along the contracted channel. A source of uncertainty in the measurements arose because a slight change in measurement position could result in the measurement of the crest of a dune instead of the trough of a dune. However, generally at most cross-sections the bed was determined to have reached an equilibrium average profile after 7 hours.

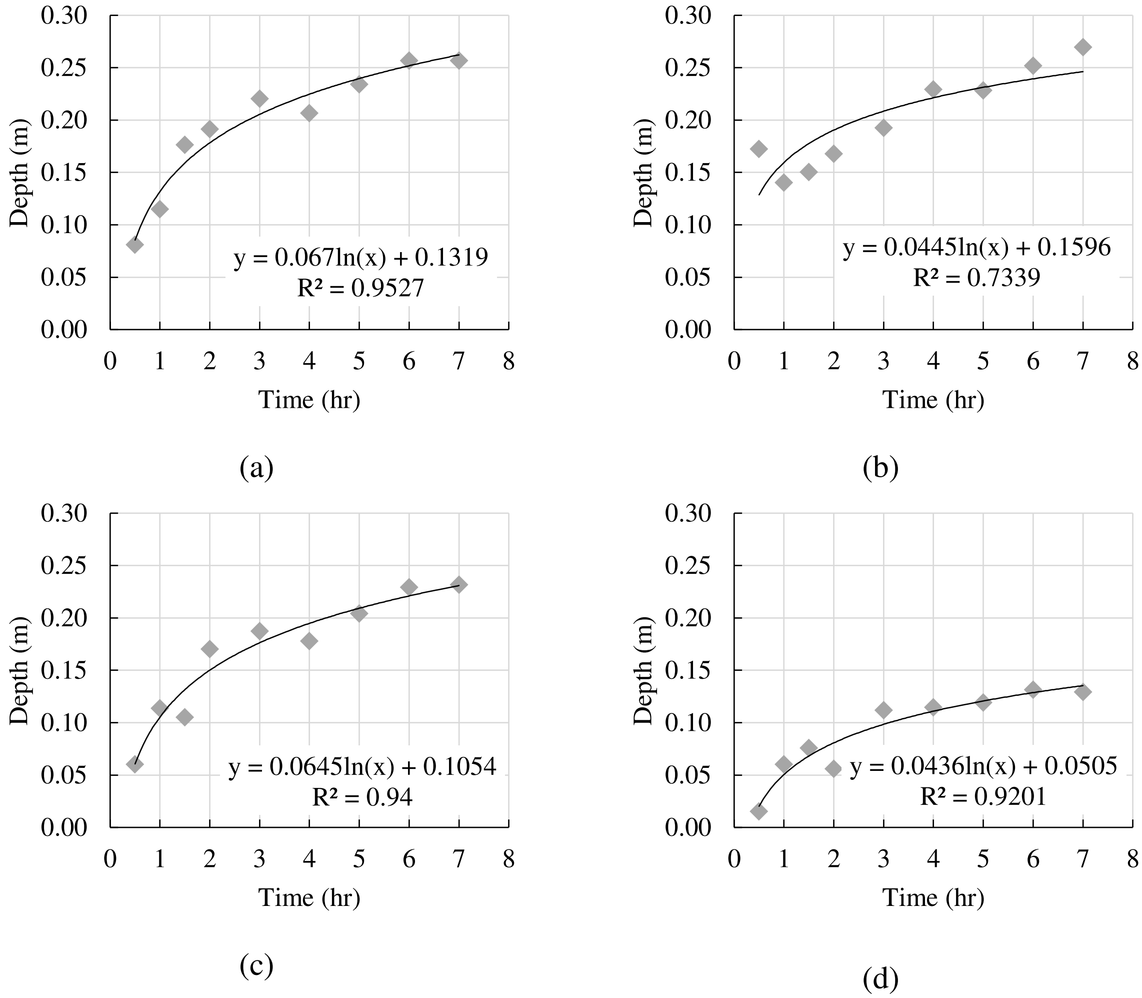

Figure 5.25. The lowering of the bed elevation along the flume's centerline: (a) at cross-section 4; (b) at cross-section 5, (c) at cross-section 7; and, (d) at cross-section 8. Experiment LB - 0.5 - 4.0.

Figure 5.26 shows a LiDAR scan of the bed after 7 hours of running experiment. The contracted channel was marked by scour development at the entrance to the channel, and (as anticipated) by the development of deeper scour at the corners of the contraction. The vena-contracta scour was evident throughout the experiment and was not noticeably affected by the scour development at the entrance corners. The corner scour did not progress fully across the contraction entrance.

The LiDAR scans for this experiment are shown in Figure 5.27. Figure 5.27a depicts the contraction during the experiment, looking downstream. Figure 5.27b shows the channel bed at the entrance of the contracted channel. This latter figure shows the cross-channel encroachment of scour at the entrance corners. Also evident in this figure is the extensive roughening of the bed of the contracted channel. Bedforms developed along the full length of the bed (contracted and un-contracted channels).

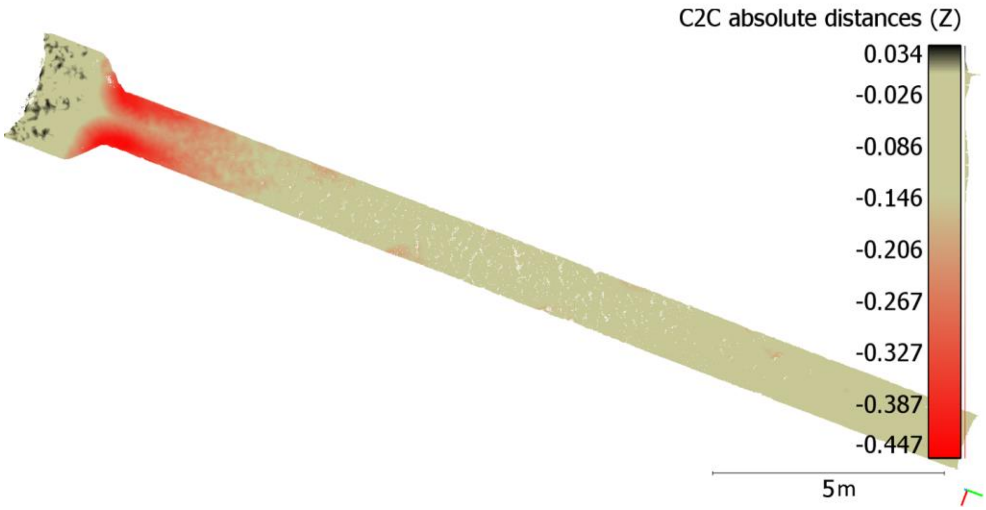

(a)

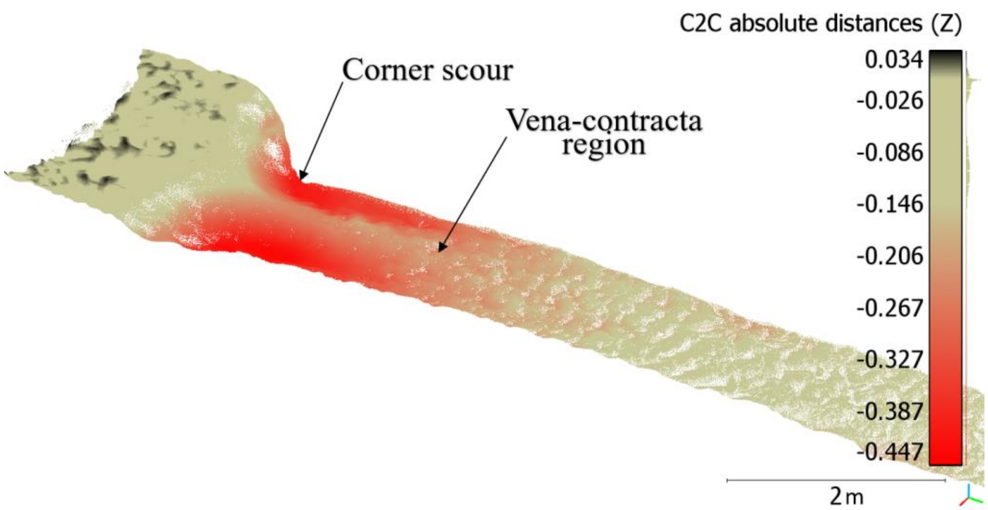

(b)

Figure 5.26. A LiDAR scan showing the bed surface after 7-hours of experiment running. (CW-0.5-4.0) ; (a) a view of the full LiDAR along the contraction; and, (b) a view of the portion of the contraction closer to the contraction entrance.

(a)

(b)

Figure 5.27. Looking downstream of the contraction: (a) during scour process; and, (b) after completion of the experiment (CW-0.5-4.0). The black lines on the walls show the bed elevation before scour.

The turbulence visible in Figure 5.28 indicates the rapid process of scour at corners. This photograph was taken ten minutes after the beginning of the experiment. The suspended sand elevated by turbulence in the flow-separation regions outlines the extent of the vena-contracta formed within the entrance to the contracted channel.

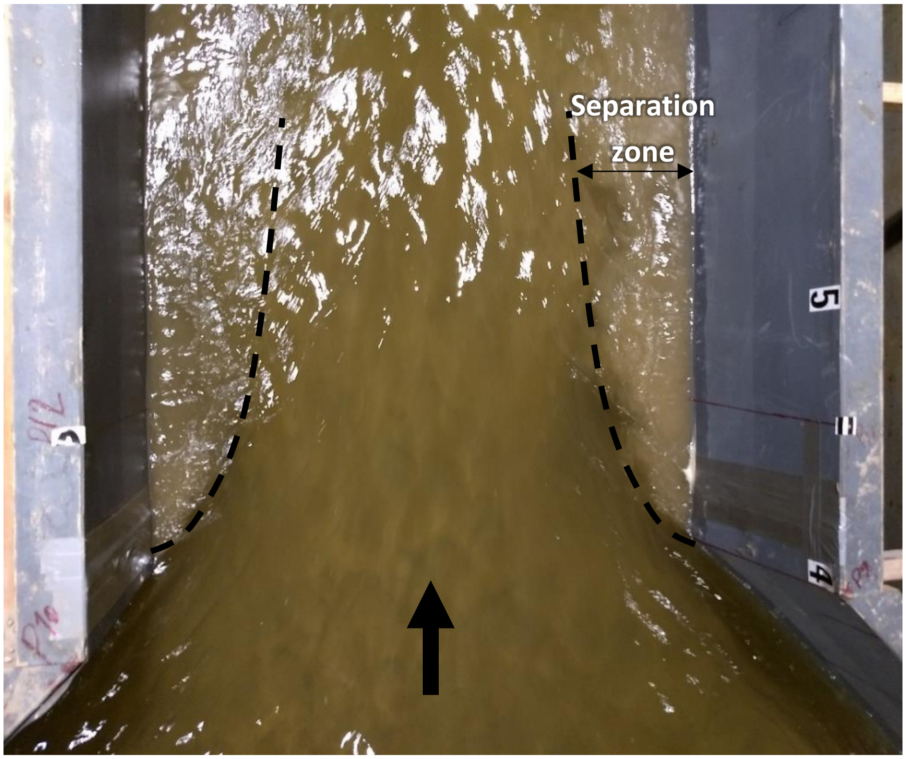

Figure 5.28. Corner scour underway ten minutes after the beginning of the experiment (LB – 0.5 – 4.0).

Figure 5.29 shows the temporal development of the water-surface profile and bed-surface profile as the experiment progressed. The bed lowered relatively rapidly at the entrance to the contracted channel. Further the bed roughened as bedforms developed. The roughening of the bed along the contraction caused the water-surface profile to rise slightly along the lower portion of the contracted channel. Dune migration is evident in this figure, which shows the downstream migration of bed-surface undulations.

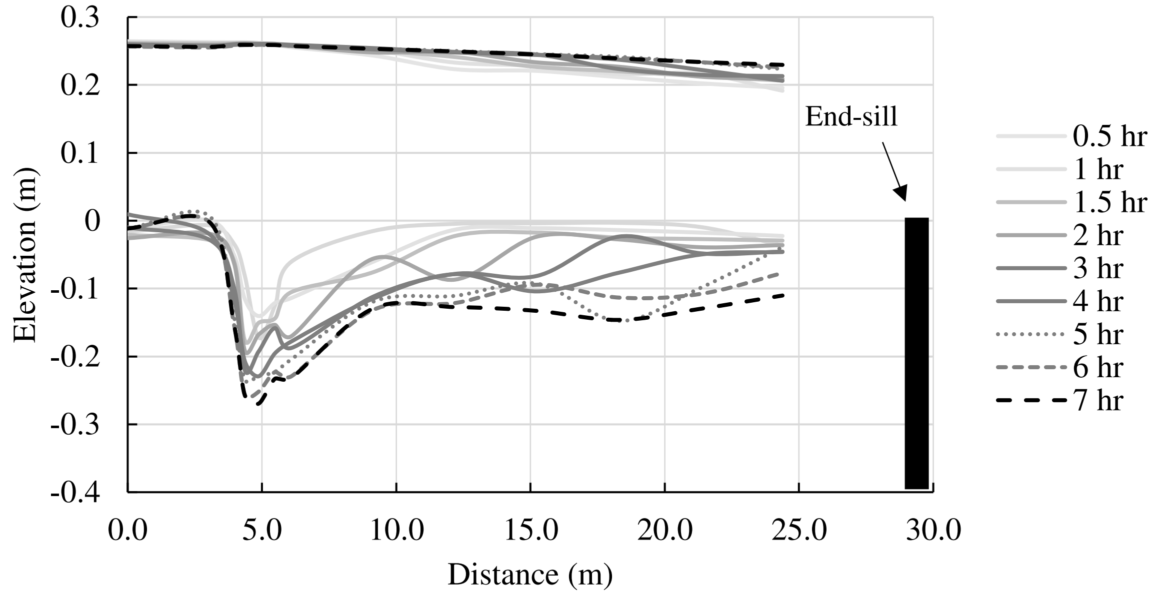

Figure 5.29. Profiles of water surface and bed elevation near along the centerline at different times during the experiment. (LB - 0.5 - 4.0)

The elevation profiles of the water surface and corner scour near the right-side wall are shown in Figure 5.30. The high shear stress ratio used for this experiment, and the turbulence generated in the flow-separation region, caused the corner scour to develop relatively fast and to reach an equilibrium depth shortly after about 3 hours of running the experiment. It was observed too that the water-surface elevation along the contracted channel oscillated (varied with time) due to the relatively rapid migration of dunes along the contracted channel and the generally unsteady nature of scour within the contraction entrance.

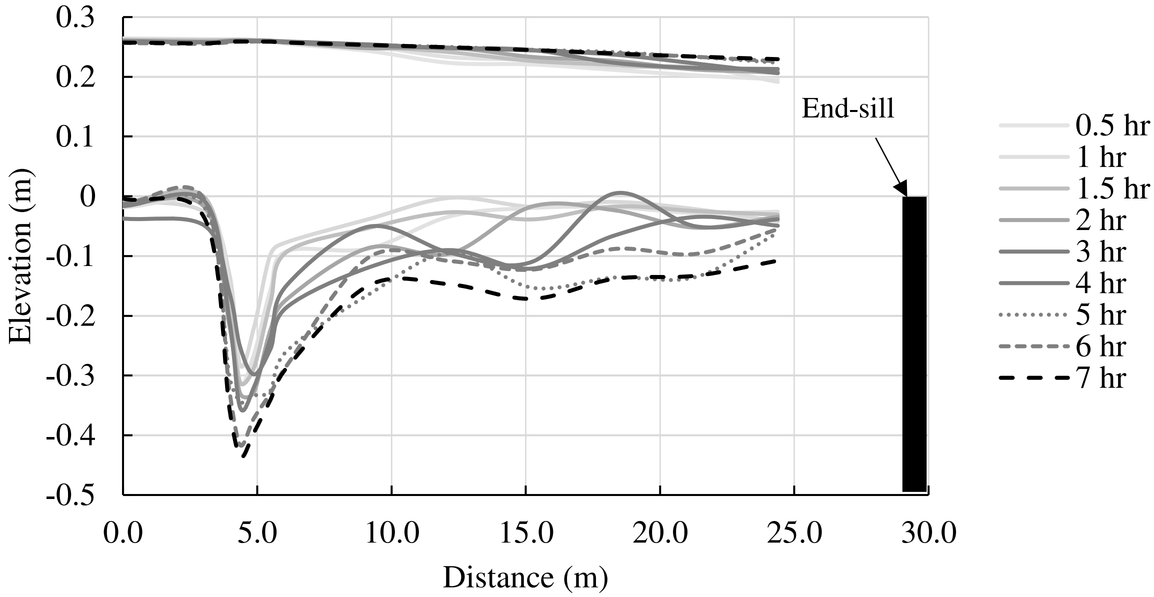

Figure 5.30. Profiles of water surface and bed elevation near the right-side wall (looking downstream) at different times during the experiment. (LB - 0.5 - 4.0)

5.3.4. Scour depth of medium contraction

The maximum values of depth of corner scour and of vena-contracta scour for medium contraction are plotted in Figure 5.31. The corner scour happened near the side walls at the entrance corner, whereas the vena-contracta depth was estimated as developing at a location near the entrance of the contracted channel but along the channel's centerline. The maximum depth of corner scour always exceeded the maximum depth of contraction scour, owing to the influence of the turbulence structures formed in the flow-separation region at each corner. The depths of corner scour were usually about equal, though small (typically negligible) differences were measured. Such differences were attributed to the three-dimensional nature of the scour regions, slight differences in the transverse distribution of approach flow, see Figure 5.12.

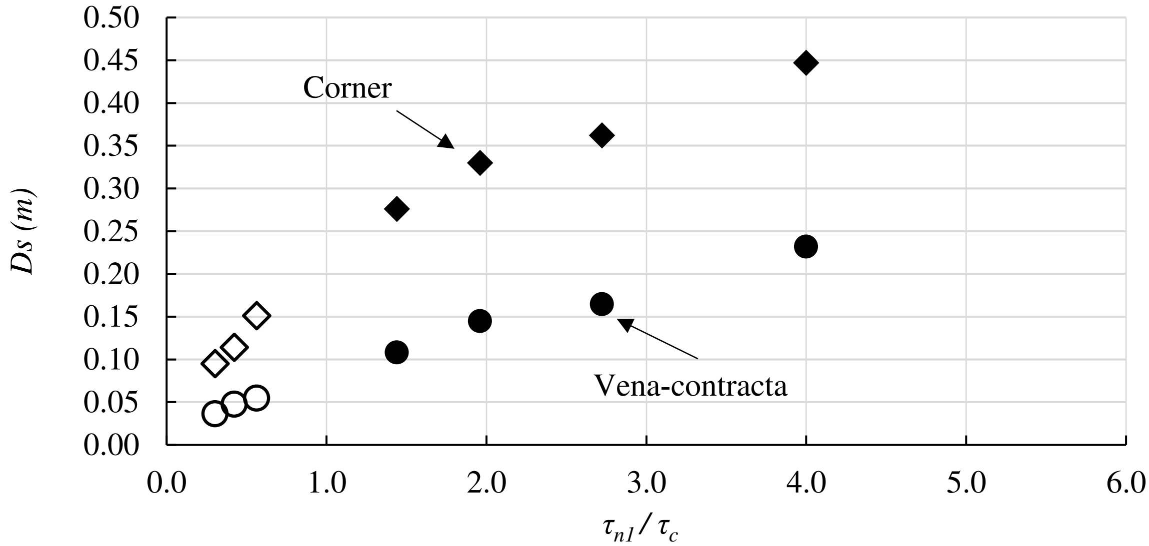

Figure 5.31. The measured depths of maximum scour in the vena-contracta region and the corner region, for medium contraction experiments; clear-water cases shown with hollow symbols, and live-bed cases, shown with solid symbols.

5.4. Mild contraction (B_2/B_1 = 0.75)

This section presents the results from the series of experiments done with the mild contraction, set here as $B_2/B_1 = 0.75$. The downstream control for the experiments was the normal depth of flow, Y_{n1}, for the uncontracted channel downstream of the contracted channel. The experiments involved clear-water and live-bed conditions of scour, as Tables 4.1 and 4.2 summarizes.

5.4.1. Overview

This section presents data and observations on contraction scour formed in the contraction considered herein to be mild (with contraction length defined as in Chapter 2). This magnitude of contraction ratio (0.75), or less, is more representative of contraction ratios associated with the design of bridge waterways than are the previous ratios (0.25 and 0.5).

The data and observations give insights into clear-water contraction scour for intermediate-contraction experiments in which the downstream control was set at Y_{n1} (normal depth of flow in the uncontracted channel). Table 4.1 list the clear-water experiments conducted. Presented here is the clear-water condition when the shear-stress ratio τ_1/τ_c was 0.90. The mild value of the contraction ratio enabled the use of this value of τ_1/τ_c without causing flow choking. The data and observations also yield useful insights into live-bed scour. Presented here are two cases with τ_1/τ_c = 1.44 and 6.25.

5.4.2. Mild contraction: CW - 0.75 - 0.90

The shear stress ratio at uncontracted section is τ_1/τ_c was 0.90, clear-water condition, and the water depth at downstream boundary condition (i.e. the sluice gate) was equal to the normal depth of uniform flow in the approach channel, Y_{n1}. The duration of this experiment was 18 hours.

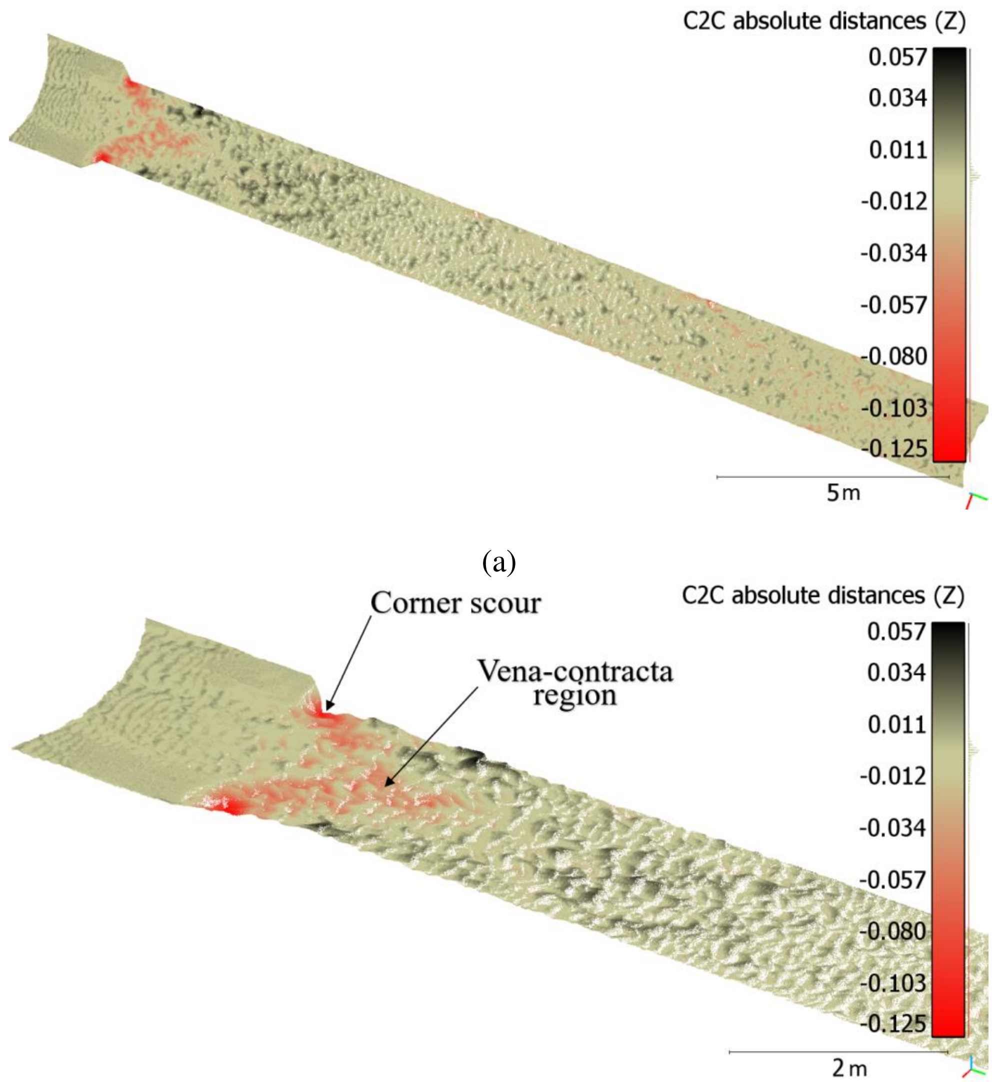

(a)

(b)

Figure 5.32. A LiDAR scan of the bed surface after 18 hours of running the experiment. (CW - 0.75 - 0.90); (a) a view of the full LiDAR along the contraction; and, (b) a view of the portion of the contraction closer to the contraction entrance.

The LiDAR scan of the bed at the end of the experiment shows that, for a mild contraction, the depths of contraction scour (vena-contracta scour and corner scour) were not severe even when the shear stress ratio is near the condition of incipient motion for the bed sediment. Figure 5.32, shows a LiDAR scan of the bed. The photographs in Figure 5.33 show the bed during and after the experiment. Further, the photographs show the development of the vena-contracta scour and the scour at the two corner regions. The development of bedforms in the contraction entrance added uncertainty to the measurement and estimation of the maximum depth of vena-contracta scour. Also, because the shear stress on the approach bed was close to the condition of incipient motion of the bed sediment, ripples and dunes also developed on the approach bed. Several hours of flow were needed for the approach-bed bedforms to develop, but once the bedforms were developed they generally kept their dimensions and grew no further.

(a)

(b)

Figure 5.33. Views of the scoured bed: (a) during scour; and, (b) after the experiment (CW- 0.5 - 0.90).

Figure 5.34 and Figure 5.35 show profiles of the water surface and bed elevation along the flume's centerline and near the flumes right-side wall looking downstream, respectively. The profiles show that the depths of vena-contracta scour and corner scour developed relatively rapidly. Both the centerline and near-wall profiles show little change in bed surface and water surface, except indicating the migration of dunes during the experiment. The migration of dunes is evident as undulations in the bed elevation and very small changes in the water surface elevation.

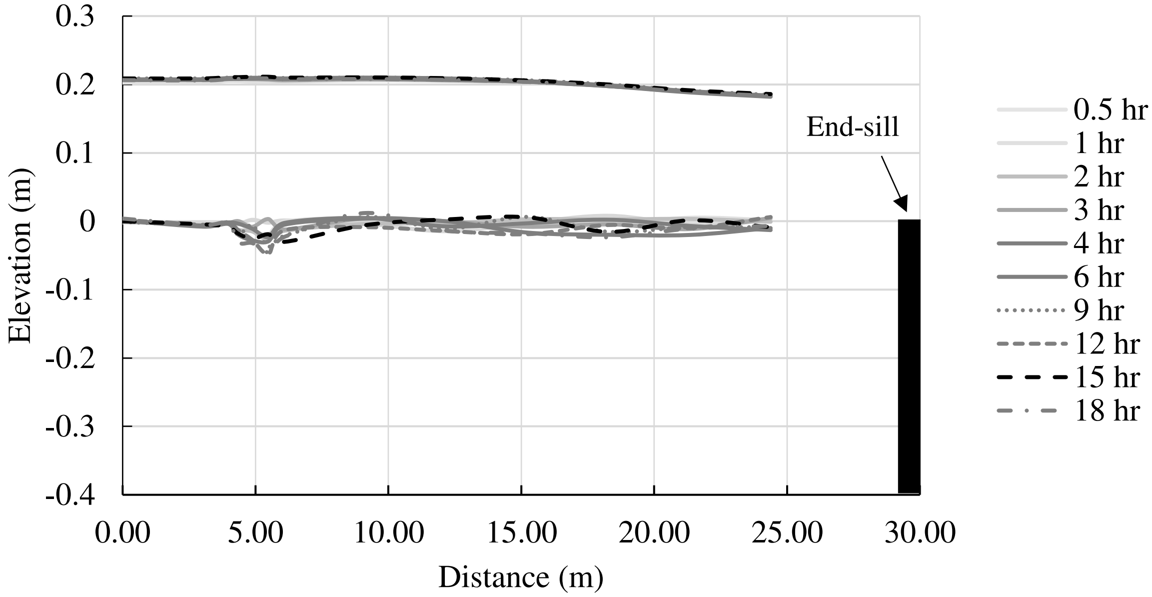

Figure 5.34. Profiles of water surface and bed elevation near centerline for different times during the experiment (CW- 0.75 - 0.90).

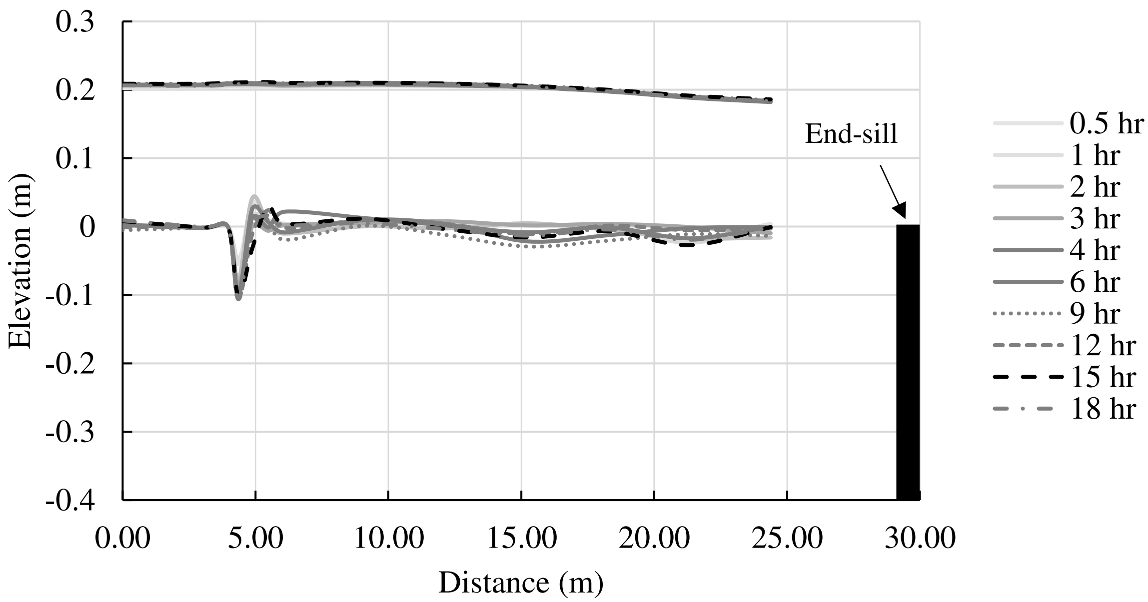

Figure 5.35. Profiles of water surface and bed elevation near the right-side wall (looking downstream) for different times during experiment (CW- 0.75-0.90).

5.4.3. Mild contraction: LB - 0.75 - 1.44

The shear stress ratio associated with uniform flow along the uncontracted approach uncontracted section was τ_1/τ_c = 1.44, live-bed condition, and the water depth at downstream boundary condition (i.e. sluice gate) was equal to normal depth of flow along the approach channel, Yn_1. The duration of this experiment was 7.0 hours. Figure 5.36 shows the LiDAR-scan of the bed once the experiment had ended. This figure reveals that not much sediment moved along the contracted channel, and that a V-shape scour pattern developed at the entrance of the contracted channel. The resulting scour pattern can be attributed to the development of the two regions of corner scour and the development of the vena-contracta scour.

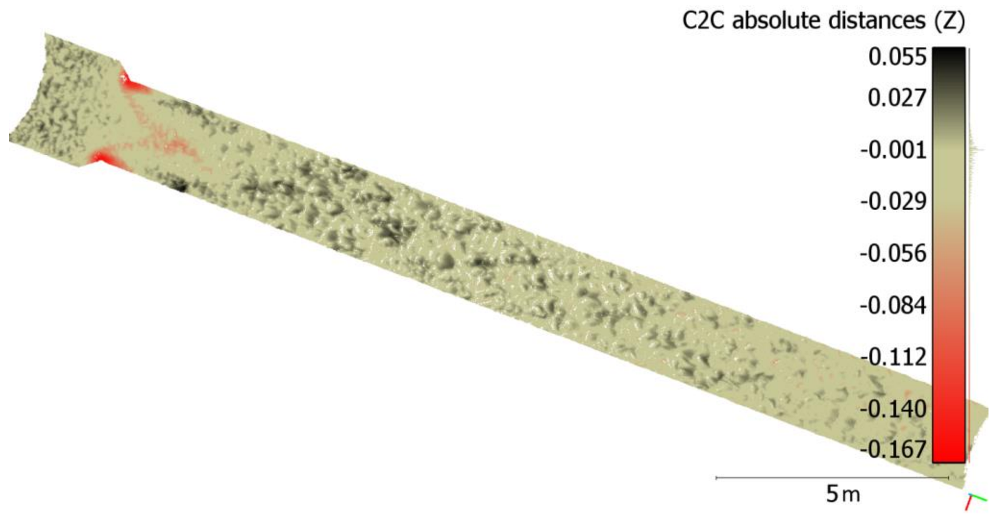

(a)

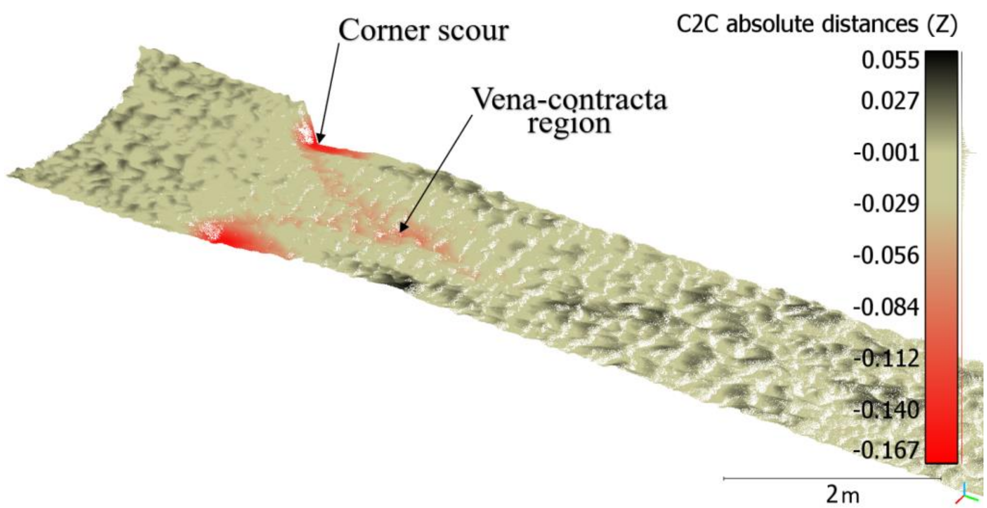

(b)

Figure 5.36. A LiDAR scan of the bed after 7 hours of the experiment. (LB- 0.75 - 1.44): (a) a view of the full LiDAR along the contraction; and, (b) a view of the portion of the contraction closer to the contraction entrance.

The scour process was not as dramatic as indeed is portrayed by the following two photographs in Figure 5.37. The bed along the contraction was only slightly scoured though formed bedforms as evident in Figure 5.35 and Figure 5.36b. As Figure 5.36a illustrates, the flow through the contraction entrance was relatively unremarkable.

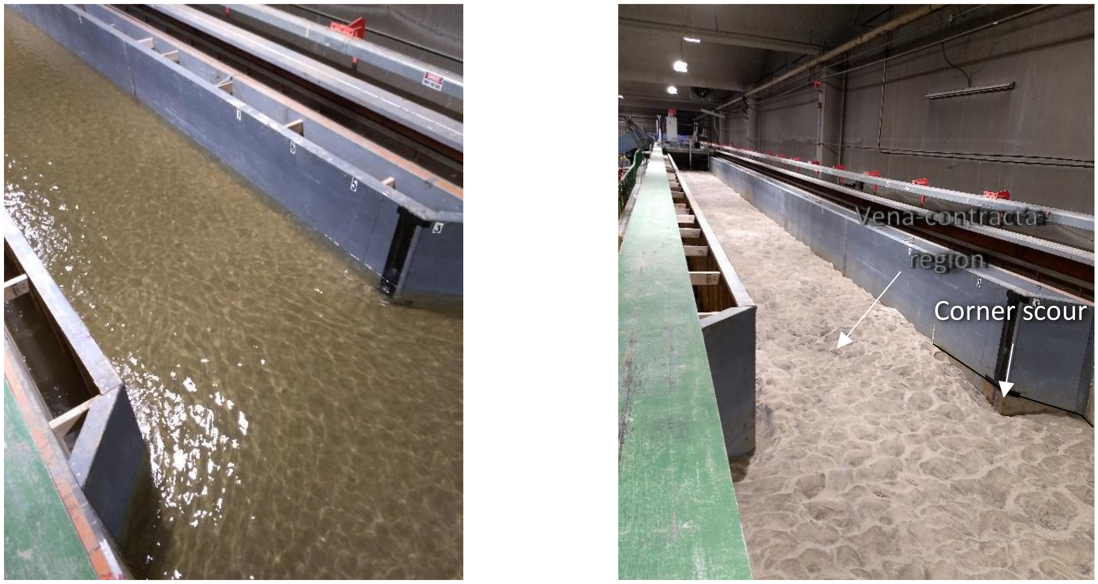

(a) (b)

Figure 5.37. Views of the scoured bed: (a) after 1 hour of the experiment; and, (b) after the experiment was completed (LB-0.75-1.44). The black line shows the bed elevation before scour.

Figure 5.38 shows temporal developments in the profiles of the water surface and bed surface along the flume's centerline during the experiment. The profiles reflect the unsteady nature of contraction scour insofar that dunes formed and moved along the flume bed. The dunes in the approach channel differed in form to those in the contracted channel, although the variation in flow depth (and bed shear stress) along the contraction caused the dunes to vary in characteristics. The dunes formed in the contracted channel relatively quickly (during the first two hours of running the experiment) and, persisted and did not alter the water-surface profile, which was measured once the dunes had formed. The LiDAR scan also shows the dunes. The average height of dunes inside the contraction was determined to be 0.026 m. However, the heights of the dune varied at different locations along the contracted channel. Chapter 6 explains in greater detail the dimensions of the dunes formed along the contracted channel.

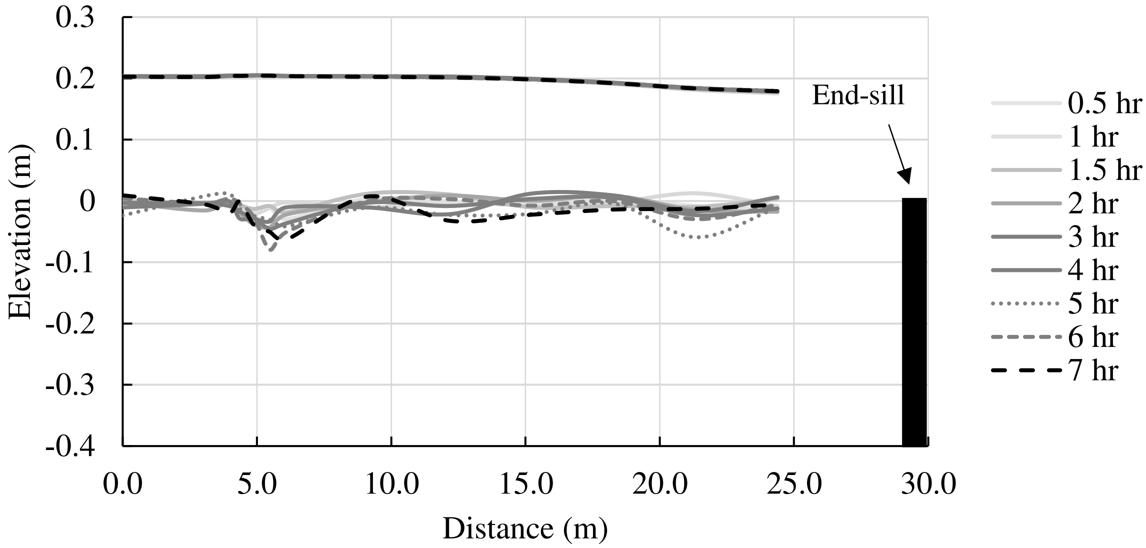

Figure 5.38. Profiles of water surface and bed elevation near centerline for different times during the experiment (LB- 0.75 - 1.44).

The bed evolution near the right-side wall is shown in the following figure. Note, the corner scour reached to the equilibrium stage after almost the first hour of the experiment. As observed for the earlier experiments, scour at the entrance corners was deeper than along the vena contracta formed within the contraction entrance.

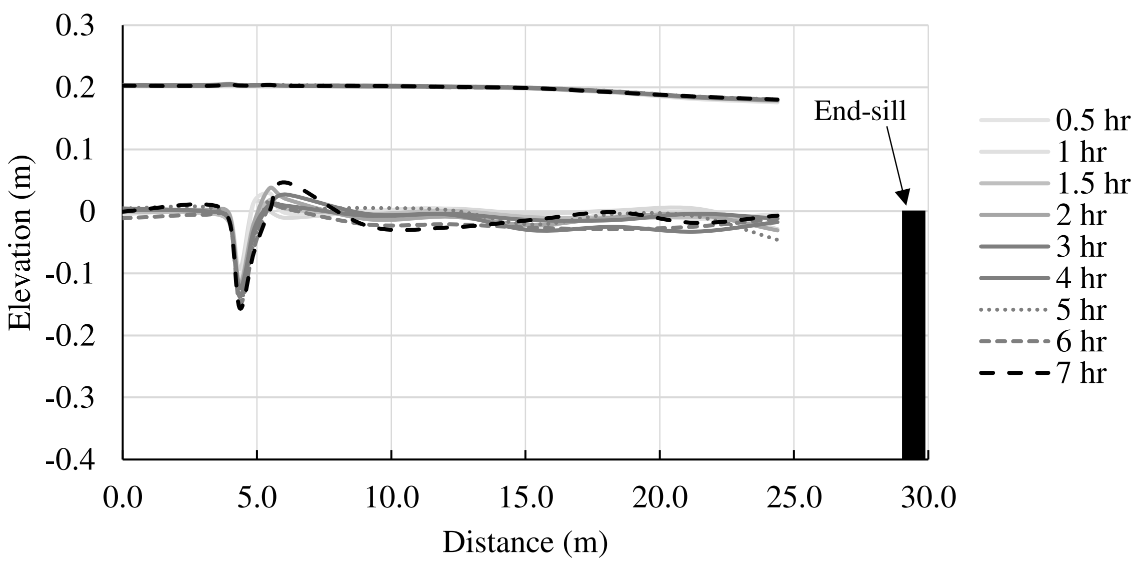

Figure 5.39. Profiles of water surface and bed elevation near the right-side wall (looking downstream) for different times during the experiment (LB- 0.75 - 1.44).

5.4.4. Mild contraction: LB - 0.75 - 6.25

The shear stress ratio associated with normal flow along the uncontracted approach channel was τ_1/τ_c = 6.25 and the water depth at downstream boundary condition (i.e. the sluice gate) was equal to the normal depth of flow along the approach channel, Yn_1. The duration of this experiment was 7.0 hours. The larger value of contraction ratio enabled this experiment to be conducted with the highest value of shear stress ratio selected for the experiments. The value was selected to ensure that no of flow choking would occur at the contraction's exit or entrance.

Figure 5.40 is a LiDAR scan of the bed once the experiment had been completed. The scan shows that the deepest contraction scour occurred as corner scour. The vena-contracta scour was modest, as is shown later in this section of the thesis. The scan also shows that dunes propagated along the approach channel and the contracted channel. The value of τ_1/τ_c in the contracted channel was such that the flow mobilized sand along the entire length of the contraction.

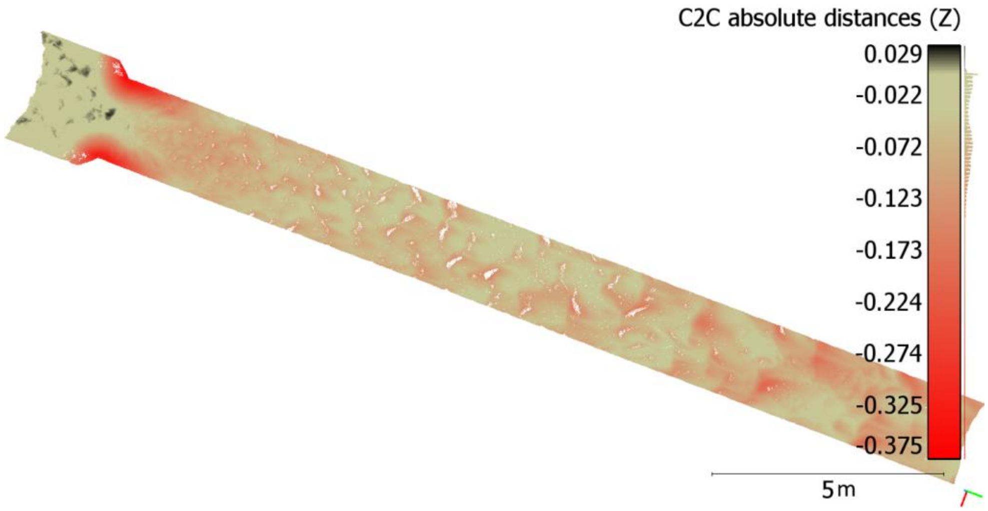

(a)

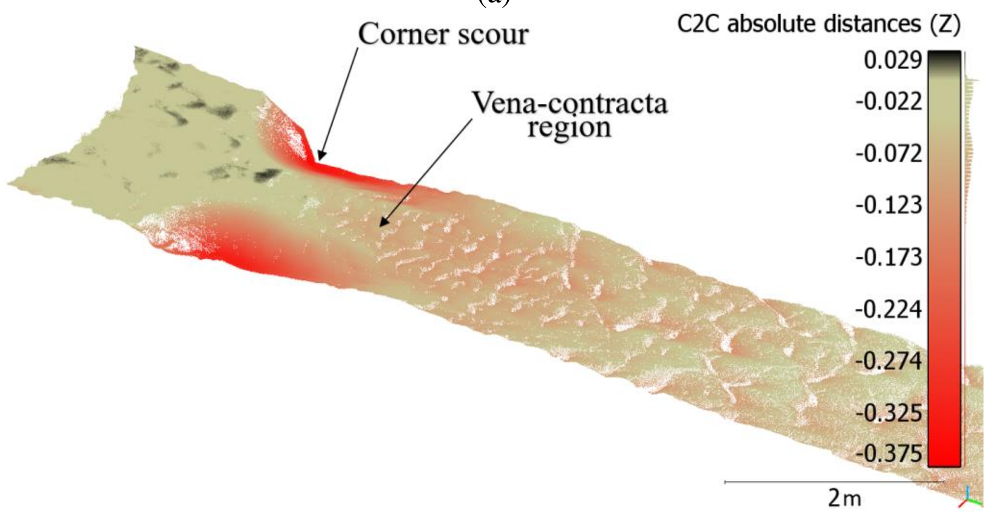

(b)

Figure 5.40. A LiDAR scan of the bed after 7 hours of running the experiment. (LB- 0.75 - 6.25): (a) a view of the full LiDAR along the contraction; and, (b) a view of the portion of the contraction closer to the contraction entrance.

Special care was needed in starting this experiment, because of its high value of τ_1/τ_c, of concern was that, unless the flow was controlled to increase gradually while gradually filling the flume, the flow could cause the undesired rapid erosion of the bed. The flume, therefore, was filled with water from downstream, to prevent bedforms propagation before the experiment. Figure 5.41a shows the careful filling of the flume whereas Figure 5.41b shows the flume bed after the flume was carefully drained. These figures show the scour at the vena contract and scour in the corner regions. The greatest maximum depth of scour was 0.375 m, which occurred at the corners of the contraction entrance, as Figure 5.40 indicates.

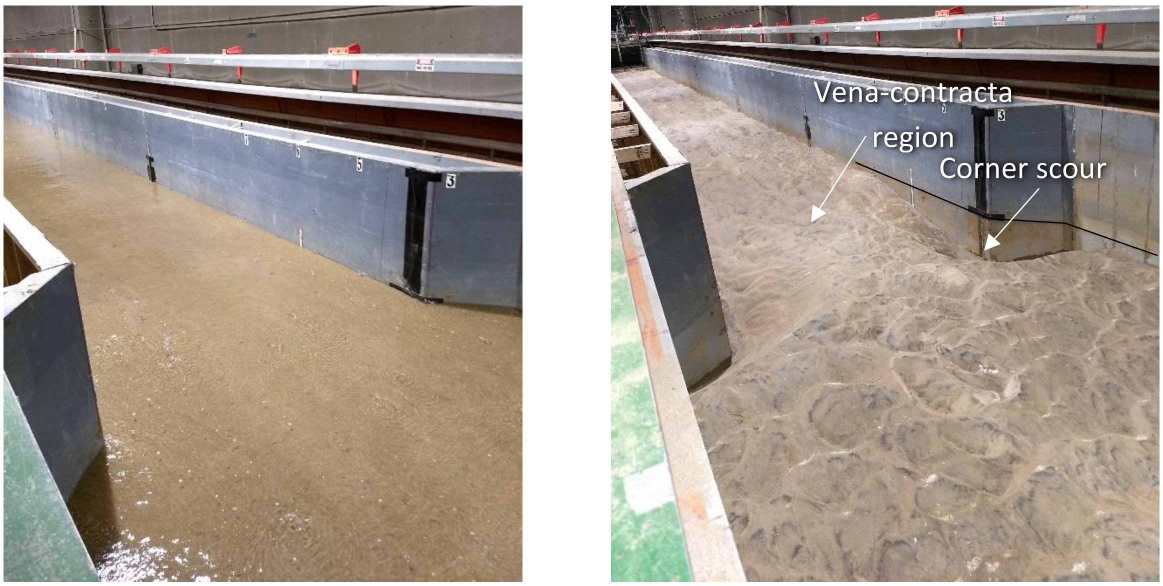

(a) (b)

Figure 5.41. Scoured bed: (a) filling the flume with water introduced from the flume's downstream end at the beginning of the experiment; and, (b) after the experiment (LB- 0.5 - 6.25). The black line on the wall shows the bed elevation before scour.

Figure 5.42 shows the temporal developments of profiles of the water-surface and bed surface along the flume's centerline during the experiment. The oscillations of the bed surface reflect the unsteady nature of scour development along the contraction. In particular, the oscillations indicate how dunes formed and migrated along the entire channel (approach and contracted portions).

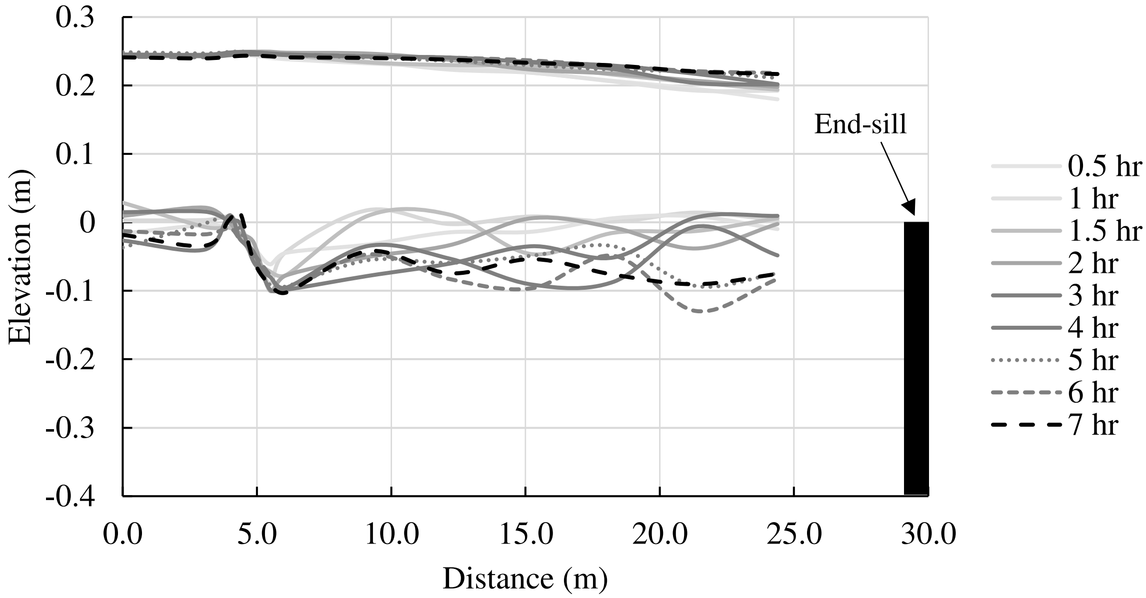

Figure 5.42. Profiles of water surface and bed elevation near centerline for different times during the experiment (LB- 0.75 - 6.25).

Profiles of the water surface and the bed surface near the flume's right-side wall (looking downstream) are presented in Figure 5.43. This figure shows that corner scour at the contraction entrance corners reached a maximum equilibrium depth at about the first hour of the experiment. In this regard, the present experiment shows that, as shear stress ratio (τ_1/τ_c) at the uncontracted section increased, scour developed faster and more quickly attained an equilibrium condition.

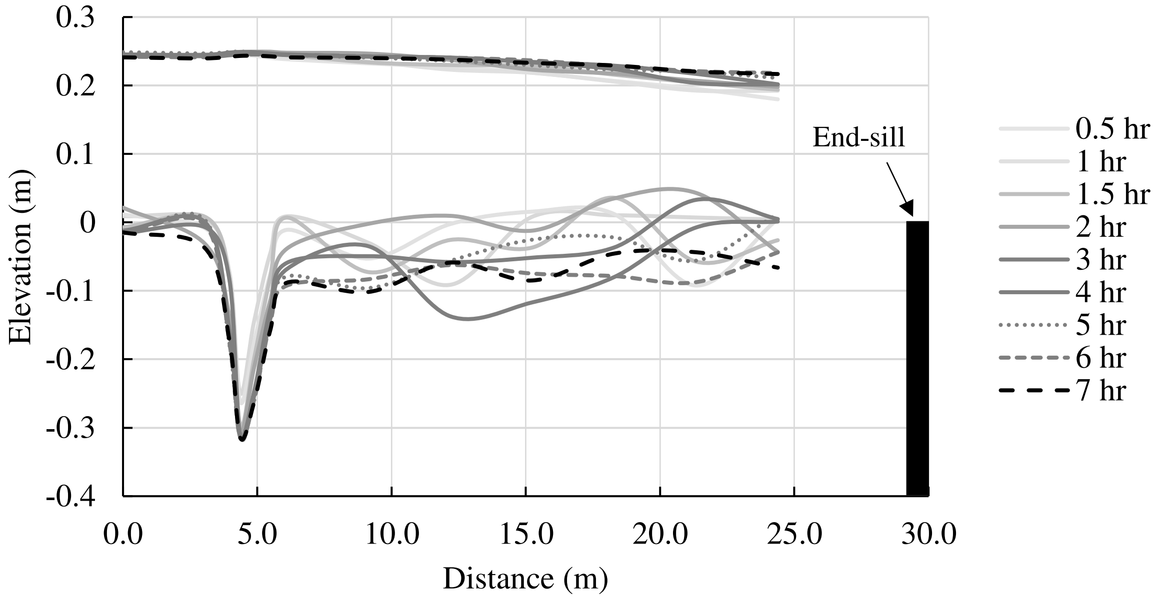

Figure 5.43. Profiles of water surface and bed elevation near the right-side wall (looking downstream) for different times during the experiment (LB- 0.75 - 6.25).

5.4.5. Scour depth of mild contraction

The scour in the mild contraction was due primarily to corner scour and vena-contracta scour. As the value of B_2/B_1 increased, the degree to which these two scour locations interacted decreased. The LiDAR scans of the experiments usefully illustrate this point. The maximum depths of scour occurred at the contraction-entrance corners and in the region of the vena-contracta. The corner scour could be determined more accurately than the depth of vena-contracta scour, because the presence of bedforms in the vena contracta complicated estimation of scour depth there.

Figure 5.44 presents the data obtained for maximum depths of vena-contracta scour and corner scour. This figure shows (as does Figure 5.31 for the medium contraction) that corner scour significantly exceeded vena-contracta scour for the experiment arrangement used here. Both scour forms produced deeper scour as the shear stress ratio τ_1/τ_c increased. However, the variation with τ_1/τ_c of scour deepening diminished for both locations as the values of τ_1/τ_c entered the live-bed condition. The scour depths for the corner scour continued to increase more substantially for the corner scour than they did for the vena-contracta scour. This finding can be ascribed to the fact that bedload sediment from the approach channel would pass through the vena contracta rather than through the region of flow-separation. The lesser amount of sediment in the region of flow separation means in effect that a form of clear-water scour continued beyond the criterion limit $\tau_1/\tau_c < 1$ conventionally set for clear-water scour (e.g., Arneson et al. 2012). However, this limit was more strictly observed for scour and sediment movement in the vena contracta.

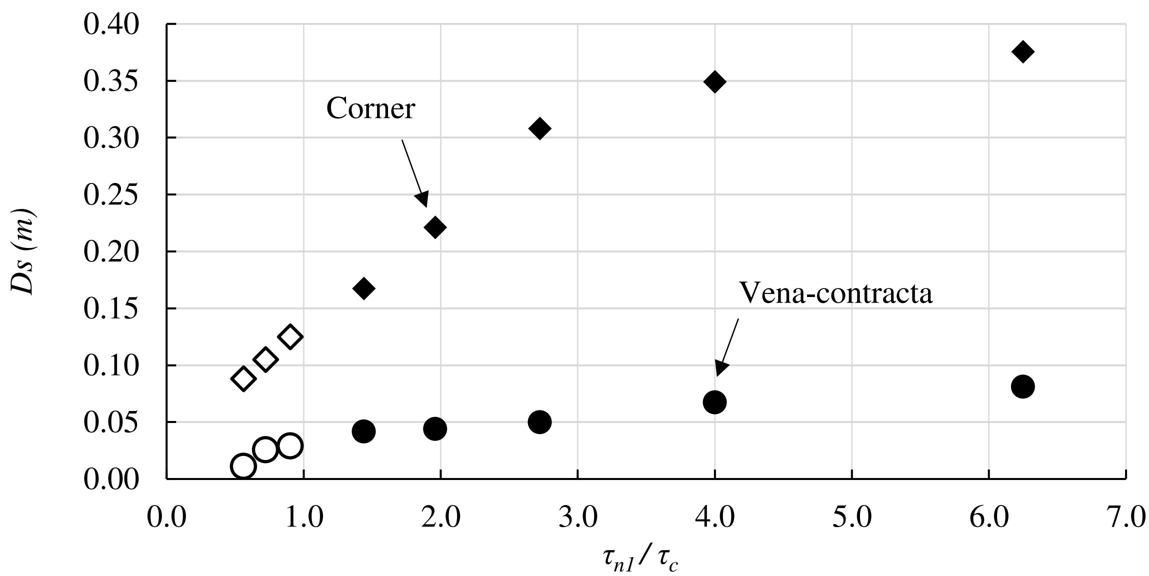

Figure 5.44 The corner and vena-contracta scour depth for mild contraction experiments; clear-water cases shown with hollow points, and live-bed cases with filled points.

6. Analysis of Flume Results

6.1. Introduction

This chapter analyses and discusses the data and observations presented in Chapter 5. The analysis and discussion sought to improve insights regarding contraction scour and provide the commensurate adjustments to the equations commonly used for estimating the equilibrium depth of contraction-scour at bridge waterways. In particular, the analysis leads to modifications of the HEC-18 equations (Arneson et al. 2012), which are widely used in the U.S. and abroad. However, the discussion at the end of this chapter reiterates the practical considerations that make estimating depth of contraction-scour approximate.

The analysis addresses the following aspects of contraction scour:

1. The overall trends relating maximum depth of contraction scour in the vena-contracta region to the parameters B_2/B_1 and τ_1/τ_c, *the main parameters,* varied in the flume experiments;
2. Bed profiles along the contracted channel;
3. Scour-depth variation along the vena-contracta formed by flow entering the contracted channel;
4. The relationship between the scour depths at the corners of the contraction entrance and in the vena-contracta region;
5. Bedform variation along the contracted channel;

6. Adjustments to the equations in HEC-18 (Arneson et al. 2012) commonly used for design estimation of contraction-scour depth; and,
7. An empirical equation for estimating average depth of vena-contracta scour, based on the flume data obtained from the present experiments.

An important aspect of the analysis involved defining the location where the depth of contraction scour should be measured. Chapter 5 (and this chapter) proposes that the location be in the vena-contracta region, which herein is taken to be the narrowest cross-section of flow entering the contracted channel. The companion study by Fakhri (2020) was useful in developing the adjustments to the HEC-18 equations.

The shape of the contraction entrance influences the depths of scour at the contraction entrance and along the vena contracta. The entrance form can be abrupt (90^o), angled (typically 60^o to 30^o), or conformed to the shape of entrance streamlines.

Other factors affect depth of contraction scour depth at the entrance corner or in the vena contracta. Notably, the contraction length and, relatedly, the variation of flow depth in the flow-drawdown profile along the contraction affects scour depth. Also, to be kept in mind (and a complicating factor) is the deformable roughness of the contracted channel's loose bed. Moreover, the bed's roughness varied along the contracted channel, because the bed developed ripple and dune bedforms that varied spatially along the contracted channel.

A further consideration not included in the present experiments concerns the geotechnical stability of the sides of the contracted channel. This consideration, which would limit the depths of scour and the reshape the entrance of the contraction, was not addressed in the layout of the flume experiments.

6.1.1. Bracketing Trends

An important finding from the flume experiments, the hydraulics outlined in Chapter 2, and the similitude considerations presented in Chapter 3, is that the conditions termed "clear-water" and "live-bed" contraction scour actually form bracketing functional trends whereby scour depth and scour profile of contracted, loose-boundary open channel vary with the shear stress parameter τ_1/τ_c for a given contraction ratio (B_2/B_1) and contraction-entrance shape. The trends or relationships are continuous and relate to the vena-contracta formation when flow enters a contraction. This finding must be stated early when analyzing the flume data, because it leads directly to the recommended adjustments to the HEC-18 design relationships widely used for estimating depth of contraction scour (Arneson et al. 2012).

Figure 6.1 schematically depicts the overall trends bracketing the data from the contraction-scour analyses in Chapters 2 and 3 and the findings from the flume experiments. The data and observations obtained from the flume experiments (involving a loose-bed approach flow and contraction) conform to the overall trended labelled "data". To be sure, the present experiments did not investigate conditions when the shear stress ratio, τ_1/τ_c, exceeded a value of one but no bed sediment entered the contracted channel. This condition prevails in certain situations; e.g., when flow passes through a bridge opening on a vegetated flood plain. The lower branch evolves as an approach flow mobilizes a bed's sediment, transports bed sediment into the contraction, partially compensates for the loss of bed sediment in the contraction and, consequently, reduces the magnitude of scour depth compared to the values of scour depth associated with the upper branch (the extended curve for clear-water scour). As mentioned above, the upper branch in Figure 6.1 corresponds to equilibrium scour depth based on the condition whereby bed shear stress essentially equals the shear stress related to the entrainment of the boundary material.

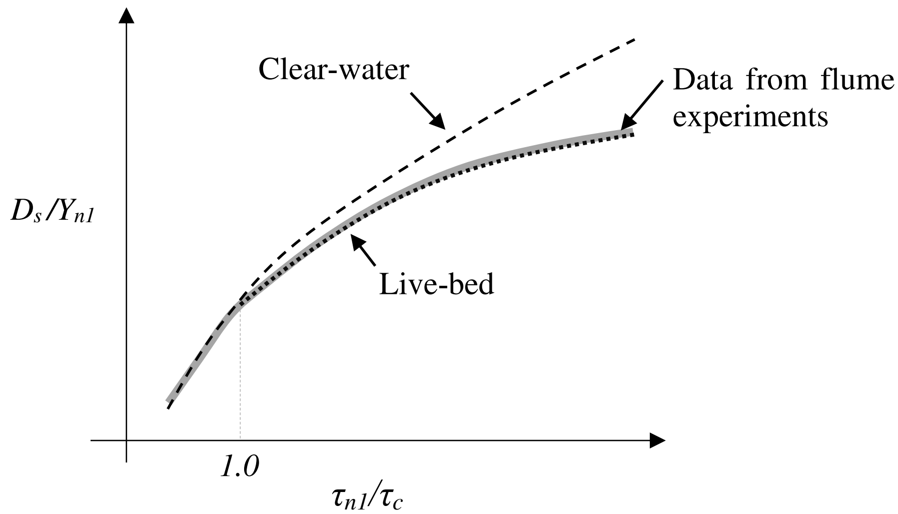

Figure 6.1. A schematic illustration of the variation of the contraction-scour depth parameter, D_s/Y_{n1}, with shear stress parameter, τ_{n1}/τ_c, along the approach channel of the contraction entrance. Indicated are the bracketing trends for clear-water and live-bed scour, and the trend shown by the data obtained from the present flume experiments.

For loose-bed channels typical of rivers, the trends indicated by the two branches shown in Figure 6.1 may become complicated by the spatially non-uniform formation of bedforms along the contraction and the commensurate non-uniform deformation of the contraction bed. Bedforms may also exist also on the approach bed to the contraction. A further complication is that, in rivers, loose beds comprise bed sediment that is non-uniform in size distribution. As mentioned already in this study, bedforms make it difficult to assign accurate values of scour depth, notably when the heights of bed-forms were comparable to nominal depth of scour. These points are elaborated subsequently in this chapter, notably when considering the issues and adjustments needed for the equations HEC-18 (Arneson et al. 2012) currently recommends for estimating depth of contraction scour.

Also complicating the interpretation of the results is the presence of important turbulence structures, flow-separation vortices, formed when flow separated from the corners of the entrance walls leading into the contraction (as Figure 5.28 depicts). These turbulence structures developed at the corners of the 45^{o} entrance convergence used in the experiments and express a major influence on scour depth that entrance shape exerts. Consequent to the formation of these turbulence structures was the formation of the two regions of corner scour. Additionally, two more influences of the large-scale turbulence structures created by flow separation need to be considered:

1. The turbulence structures were advected downstream, thereby influencing bed-sediment entrainment and bed scour downstream of the entrance; and,
2. The size of the separation vortices affected the width of the vena contracta, making the width unsteady and, at times, difficult to determine accurately.

Both additional turbulence-related influences were complicated further by the development of bedforms on the bed. This point also is elaborated later in this chapter.

6.2. Bed Profiles and bedforms along the Contraction

In accordance with the non-uniform profiles of the water-surface along a contracted open channel (Chapter 2), the scour depth varied along the contracted channel in each experiment. These variations along a contraction indicated that the shear stress exerted on the contraction bed should curve the profile of the bed surface along the contracted section; e.g., see Figure 2.13 and Figure 5.23. There indeed was a commensurate variation of bed profile along the contracted channel, though the profiles were complicated by the streamwise variation of bedforms characteristics.

Additionally, the formation of the vena contracta and the two flow-separation zones, at the contraction entrance, influenced scour of the bed along the contraction, augmenting the effect of the spatial variations of bedforms developed along the bed of the contracted channel. The combined effect of the non-uniform hydrodynamic loading of the bed was evident as scour depth variation along the contracted channel. These scour-depth results were anticipated (Chapter 2) and the LiDAR scans confirmed that scour depths (and scour patterns) differed along the contracted channel for the three contraction ratios used in the flume experiments.

As Chapter 5 shows, variations in bed bathymetry were quantified and characterized using the LiDAR scans of the bed along the contracted channel. These LiDAR-scan data were divided into five length-segments of contracted channel:

1. The first segment (the focal segment of the contraction) included the contraction entrance and a downstream length equal to approach-flow width, B_1. This region contained the regions of flow separation and vena-contracta formation. After passing through the vena contracta and a flow length of about B_1, the flow re-attached to the full width of the contracted channel; and,
2. The remaining four, downstream length-segments were divided into four parts (herein termed quartiles 1, 2, 3 and 4) to aid investigation of the variation of bed elevation changes and bedforms along the contracted channel.

Figure 6.3 indicates the locations of the entrance length-segment and the four, downstream length-segments. Scour development along these five length-segments was affected by the three aspects of the flow field mentioned:

1. The formation of a vena contracta;
2. Flow separation at the corners of the contraction entrance; and,
3. Flow reattachment at the full width of the contraction.

Figure 6.2 is a simple sketch outlining these flow aspects. For the flume experiments conducted for the present study, flow reattachment was observed to occur within the downstream distance $x = B_1$ along the entrance segment of the contraction.

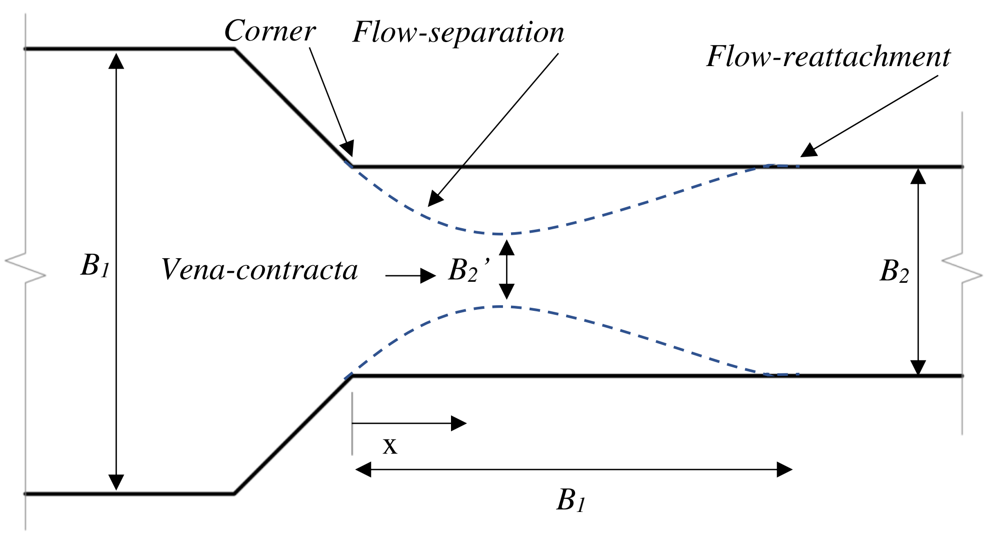

Figure 6.2. The main regions of the flow field observed within entrance to the contracted channel.

The deepest scour always occurred at the contraction corners within the entrance segment. This scour location was caused by the generation of flow-separation vortices at the entrance corners of the contracted channel. The scour in this region is herein called *corner scour*, as mentioned in Chapter5. The scour associated with the vena-contracta is herein termed *vena-contracta scour* (also mentioned in Chapter 5) and happened along a region delineated (streamwise direction) within the entrance segment. The location of the maximum contraction of the vena-contracta shifted downstream as the water discharge increased (for constant flow depth, but adjusted flume slope) and, thereby, the shear-stress ratio, τ_{n1}/τ_c, increased.

Because of the narrowness of the tight contraction (B_1/B_2 = 0.25), the scour along the vena-contracta merged with the corner scour. The separation vortices generated at the two corners dispersed downstream across the major portion of the vena-contracta, causing the two corner scour regions to interact, such that the corner scour and vena-contracta scour, together, produced an essentially level transverse bed at the contraction entrance. This merging of scour regions did not occur for the two larger values of B_1/B_2 used in the experiments, because the maximum scour depth in the vena-contract region always occurred where the vena contracta was least wide; usually within the range 0.5-0.90 B_1. The position of this local maximum depth (the maximum scour depth in the vena-contracta) shifted as the location of the vena contracta shifted downstream when parameters B_1/B_2 and τ_{n1}/τ_c increased.

The value of contraction-scour depth measured at the beginning of the second quartile of the contraction (starting at a distance B_1 downstream from the contraction entrance) gave the maximum depth of scour when the streamlines of contracted flow reattached to the full width of the contracted channel, as Figure 6.3 indicates. However, the measurement of an exact scour depth at this location was complicated by the presence of bedforms, whose amplitude (or height) varied streamwise and laterally and, thereby, introduced substantial uncertainty into the scour-depth measurement.

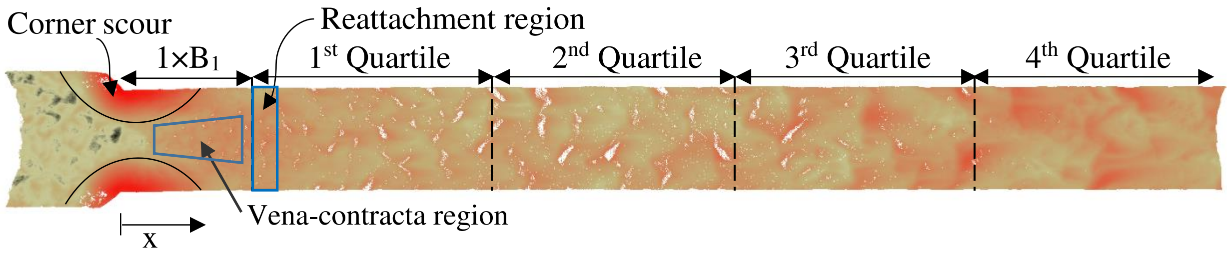

(a)

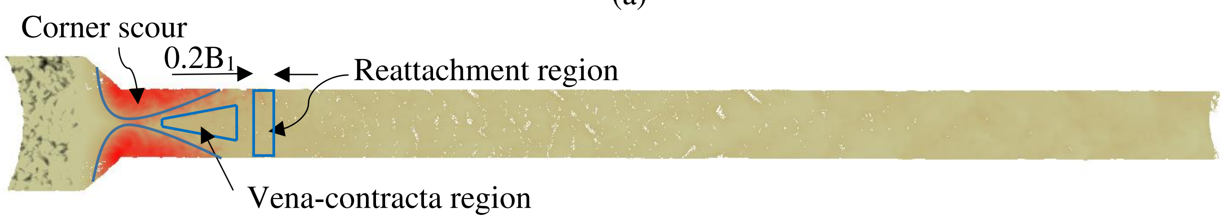

(b)

(c)

Figure 6.3. The composition of scoured areas in the contracted channel: (a) $B_2/B_1= 0.75$; (b) $B_2/B_1= 0.5$; and, (c) $B_2/B_1= 0.25$; A width of $0.2B_1$ was selected for analyzing scour depth at the reattachment region.

The bed-centerline and the near the right wall depth profiles were plotted in Chapter 5 (e.g., Figures 5.26 and 5.27) based on the scour-depth data collected at cross-sections 1 through 13 (Figure 4.9). Because the collected data at these cross-sections did fully capture the detailed variation of bed-elevation throughout the whole area of the contraction, the data were considered inadequate for determining an average value of scour depth at each cross-section. Therefore, the data obtained from the LiDAR scans of the bed were used to obtain the value of the maximum and the average scour depth at each of the segments which was discussed above.

The average elevation of the contracted bed along each quartile is shown in the Figure 6.4. This figure indicates that, in most cases, the average elevation of the contracted bed along the second quartile (flow was now spread across the full width of the contraction) was higher than the average elevation of the bed along the other quartiles downstream of the entrance segment. This finding supports the curved shape bed profile inferred by the hydraulics considerations explained in Chapter 2. Furthermore, this profile of bed along a contraction is in accordance with the shear stress profile that was confirmed from the 1D numerical model simulating the flume experiments conducted by Webby (1984). Figure 3.8 shows this finding from the 1D modeling. The curved profile of the bed developed because the values of the bed shear stress at the vena-contract and exit ends of the contracted channel were higher than those at along the middle of the channel; the bed profile responded to this variation of bed shear stress.

The downstream end of the fourth quartile, i.e. downstream end boundary of the LiDAR scan, was about five meters upstream from the end-sill at the contraction exit, i.e. cross-section 13 which is shown in Figure.4.9. The end-sill helped set the downstream control and, therefore, set the downstream control depth. In a few experiments (those with low shear stress ratio or mild contraction), the curved profile of the bed was not clear (e.g., experiment CW-0.75-0.56), because the flow did not muster sufficient magnitude of bed shear stress to transport bed sediment downstream from the first or second quartiles of the bed of the contraction downstream of the contraction entrance. Additionally, in these experiments the bed shear stresses were barely large enough to form dunes along the contracted bed. When dunes developed, they roughened the contracted bed and, thereby, caused the contraction to dissipate more flow energy. Consequently, less flow energy (and bed shear stress) was available to transport the sediment comprising the bed. As evident in Figure 6.4, some experiments even had deposition at the first and second quartiles of the bed (downstream of the entrance segment), because the bed shear stress declined below a value needed to move sediment substantially.

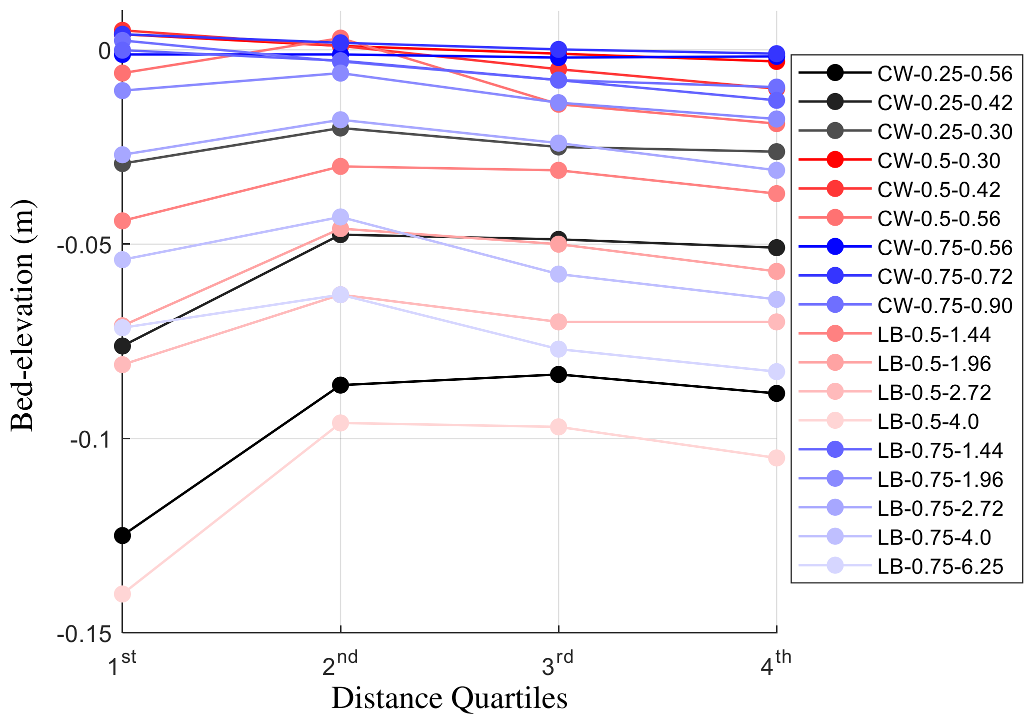

Figure 6.4. The average bed-elevation at each distance quartile along the bed of the contracted channel.

To evaluate the effect of bedform development on scour depth along the contracted channel, values of bedform height were estimated for the bed of each flow condition along the contracted channel. Different methods of estimation were considered and used to find the average dune height for a reach; e.g., hand-measurement of the actual height of a dune's height and length or using twice the standard deviation (STD) of dune amplitudes above the initial elevation of the bed. Twice the STD was chosen as the preferred measure of representative bed height, due to similarity of dune forms when compared with a couple of hand calculated dunes height at the flume centerline. Figure 6.5 illustrates the methods.

The value obtained by using twice the STD of dune amplitudes as the average of the four quartiles was 0.058 m, which agreed well with the hand-calculated value of dune height which was about 0.06 m (Figure 6.5). Figure 6.6 shows the average height of dunes in each quartile. Though for each experiment there is a different trend regarding dune height along the contracted channel and even gets more complicated by the three-dimensional shapes of the bedforms, dune heights along the middle quartiles (quartiles two and three) were on average about 10 percent lower than the heights of dunes in quartiles one and four along the contraction. This trend is attributable to the large values of bed shear stress that prevailed along quartiles one and four; the entrance and exit quartiles. The full LiDAR scan of the bed for experiment LB-0.75-6.25 is shown in Chapter 5.

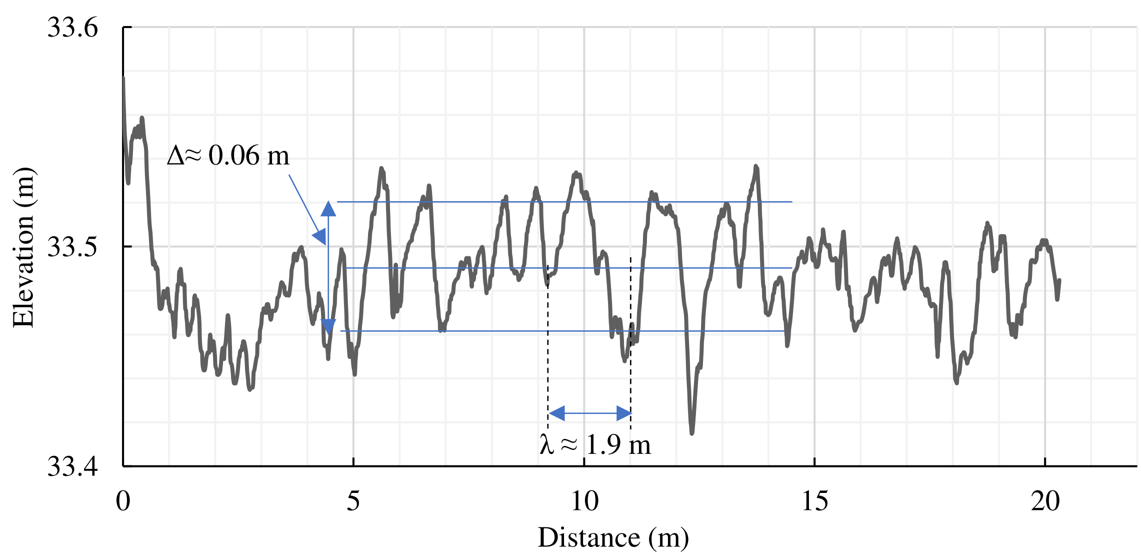

Figure 6.5. The centerline profile of the bed surface elevation along the contracted channel. The profile was extracted from LiDAR data. (LB-0.75-6.25)

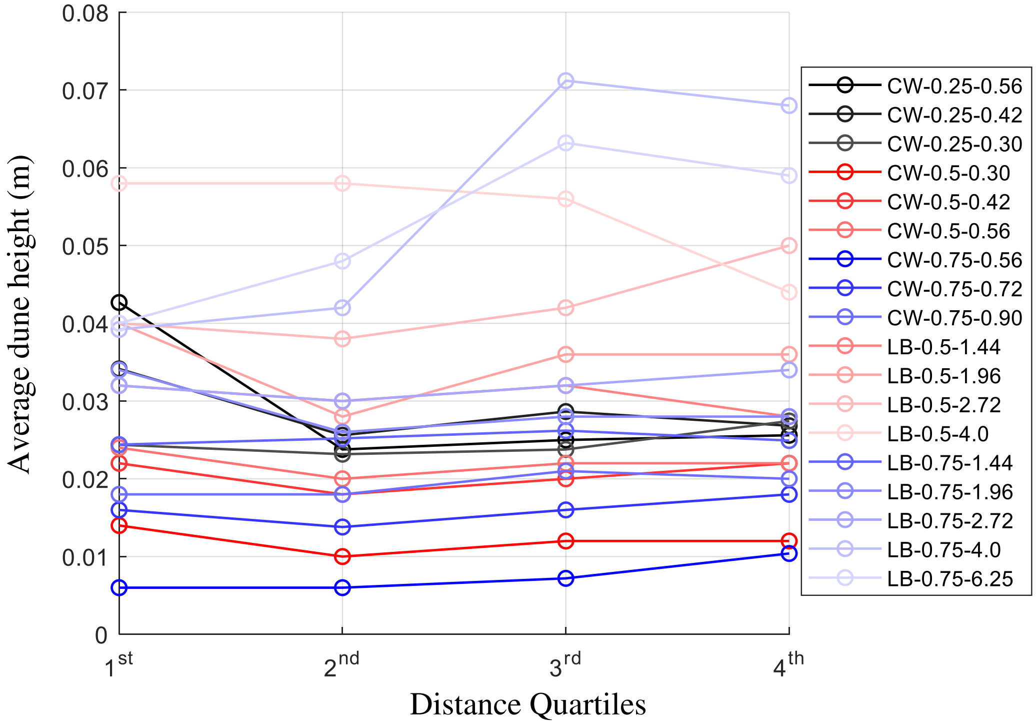

Figure 6.6. The average height of dunes developed along the contracted channel.

6.3. Scour-depth variation in the vena-contracta region

The varying length of the vena-contracta formed for each contraction ratio, B_1/B_2, and shear stress ratio τ_{n1}/τ_c (water discharge for constant depth and adjusted bed slope) introduced uncertainty into the selected values of scour depth along each vena-contracta. The length increased as τ_{n1}/τ_c increased for each value of B_1/B_2. Therefore, the question arose as to the requisite length of vena contracta area over which the scour depth should be determined. To address this question, a sensitivity analysis was done to ascertain how the estimated depth of scour varied with the overall length of the vena-contracta area used to calculate the average scour depth for vena-contracta area. The following measurement lengths, l_{vc}, were considered the length of the region corresponding to the vena contracta, See Figure 6.7. Note, the width of the vena-contracta region is constrained with the corner scour regions.

- l_{vc} = 0.1-0.6B_1
- l_{vc} = 0.2-0.5B_1
- l_{vc} = 0.2-0.6B_1
- l_{vc} = 0.2-0.9B_1

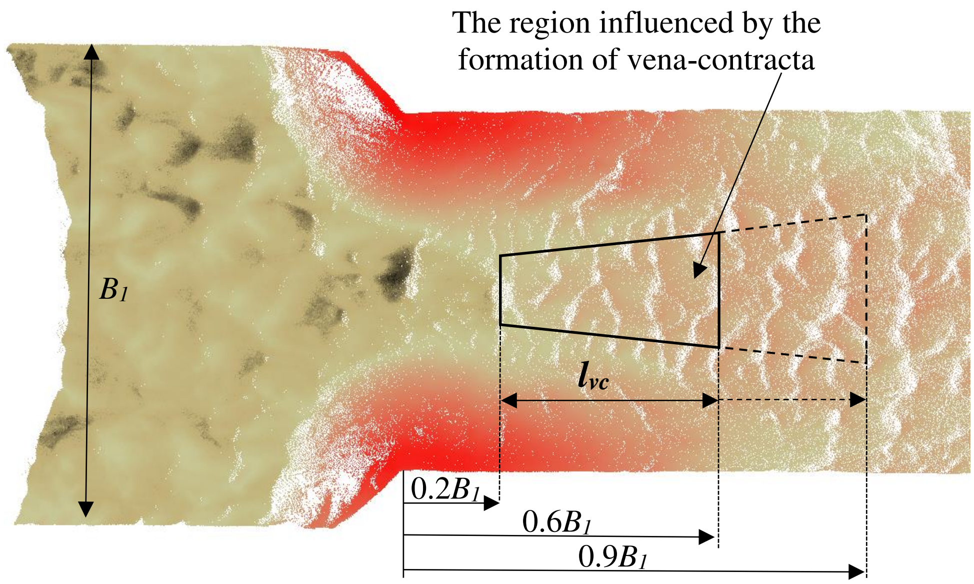

Figure 6.7. The example of scour regions including the vena-contracta and the corners.

Herein, l_{vc} =0 is taken to be the start of the contracted channel, as indicated above. The analysis sought to determine which range would best represent scour depth for the vena-contracta area.

The presence of bedforms complicated determining dune heights and, therefore, measurement scour depth in the vena contracta for these ranges of l_{vc}, was made difficult, because the dune heights (and, therefore, amplitudes) were of significant magnitude compared to the scour depths.

It was judged, therefore, that the occurrence of bedforms added substantial uncertainty to measurements of contraction scour depth at practically at all locations along the contracted channel.

The results of the analysis regarding the selection of l_{vc} are given in Figure 6.8, which shows that there was only about 5% difference between the values of average scour depth estimated for lengths l_{vc} = 0.2 to 0.5 B_1 and to l_{vc} = 0.2 to 0.6 B_1, though the latter range encompassed the longer stretch of the vena contracta. Furthermore, though the other two ranges mentioned above (l_{vc} = 0.1 to 0.6, and l_{vc} = 0.2 to 0.9) yielded scour-depth values that followed the overall trends for the influence of the parameters B_2/B_1 and τ_{n1}/τ_c, these two ranges were considered overly long, because they encompassed more of the vena-contracta than was needed for accurate estimation. The range 0.1 to 0.6 covered too much of the upstream end of the vena contracta, whereas the ratio 0.2 to 0.9 covered too much of the downstream end of the vena contracta. The latter range had the added complication arising from the presence of bedforms. Therefore, the measurements made in these areas were omitted from the selection. The focal sample area extending from 0.2 to 0.6 B_1 was selected for use when determining the scour depth for vena-contracta. The values of vena-contracta scour depth that Chapter 5 reports were taken from this range, as are the values of vena-contracta scour depth reported in the ensuing section of this chapter.

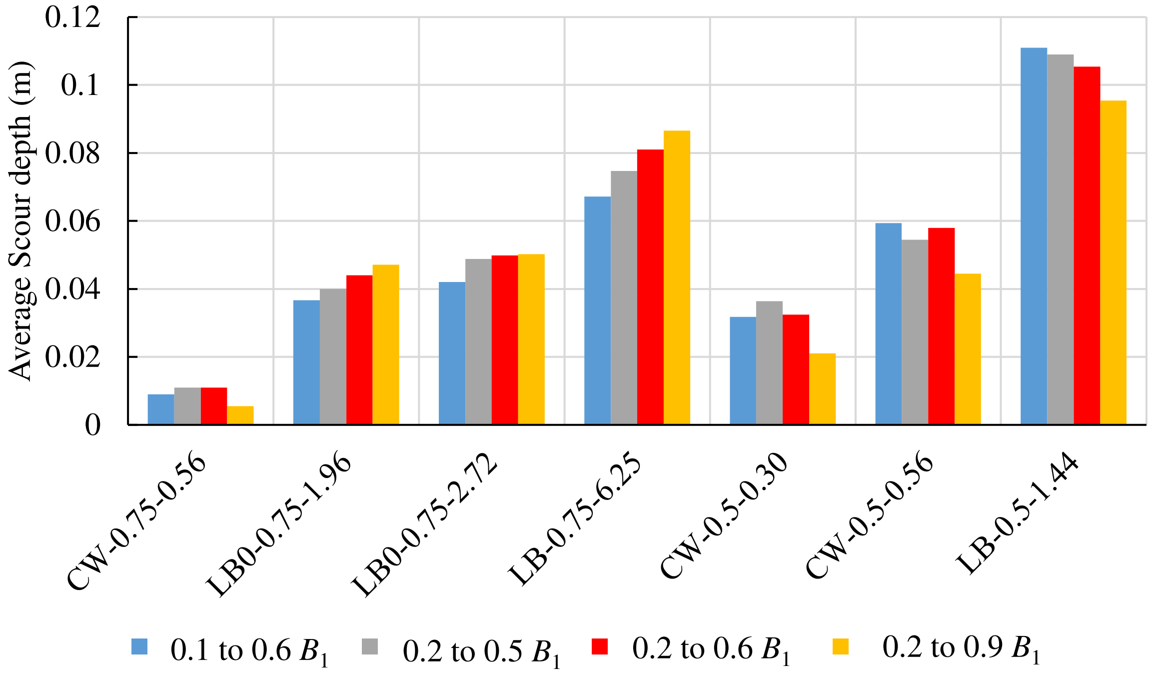

Figure 6.8. Sensitivity analysis on the average scour depth along the vena-contracta region for different ranges of sampling distance along the vena contracta.

Fakhri(2020), who participated in conducting the flume experiments, utilized Large Scale Particle Image Velocimetry (LSPIV) to estimate the minimum width, B_2', of the vena-contracta width, The relationship he developed is presented in Figure 6.9, which includes only two values of experiments when B_1/B_2 = 0.25. At the highest value of τ_{n1}/τ_c for this ratio, the separation turbulence made it difficult to define B_2'/B_2 with assurance; estimate made indicated that the initial-bed curve leveled out. His LSPIV measurements (documented as his master's degree thesis, Fakhri 2020) were taken after the bed had reached to a condition of equilibrium, maximum scour-depth in the vena contracta. He obtained a curve (Figure 6.9) for the variation of B_2'/B_2 with the non-dimensional parameter $(B_1/B_2 - 1)\ Fr$. The ratio B_2'/B_2 was designated as K_v. The parameter, K_v, essentially relates B_2'/B_2 to the amplification of the Froude number, Fr, of the approach flow entering the contraction. Further, the parameter assumes that flow depth plays a negligible role in values of K_v. This assumption requires verification in future experiments but is considered herein as being reasonable for estimating K_v. It should be noted that the curve can be only used for 45° entrance (not unreasonable for bridge abutments, especially wingwall abutments) and that further research also is needed to ascertain whether different entrance shapes affect vena-contracta coefficient, K_v. Note, the research team tried to find this coefficient by using dye or based on 2D velocity profile. However, due to the varying nature of the effective width through time, i.e. by increasing the scour depth the vena-contracta loosens up, it is possible to find two different K_v factors for pre-scour, i.e. rigid-bed, and post-scour, i.e. equilibrium, conditions.

Fakhri (2020) also shows that values of K_v, were generally smaller, as expected, at the start of the experiments (or when the bed is fixed) because the flow is constrained in a lesser area of contracted entrance that after scour has opened up the contraction entrance, doing so by deepening the entrance. Figure 6.8 shows this variation, obtained using the fixed bed experiments though the number of the data collected for fixed-bed condition is very few and consequently inconclusive.

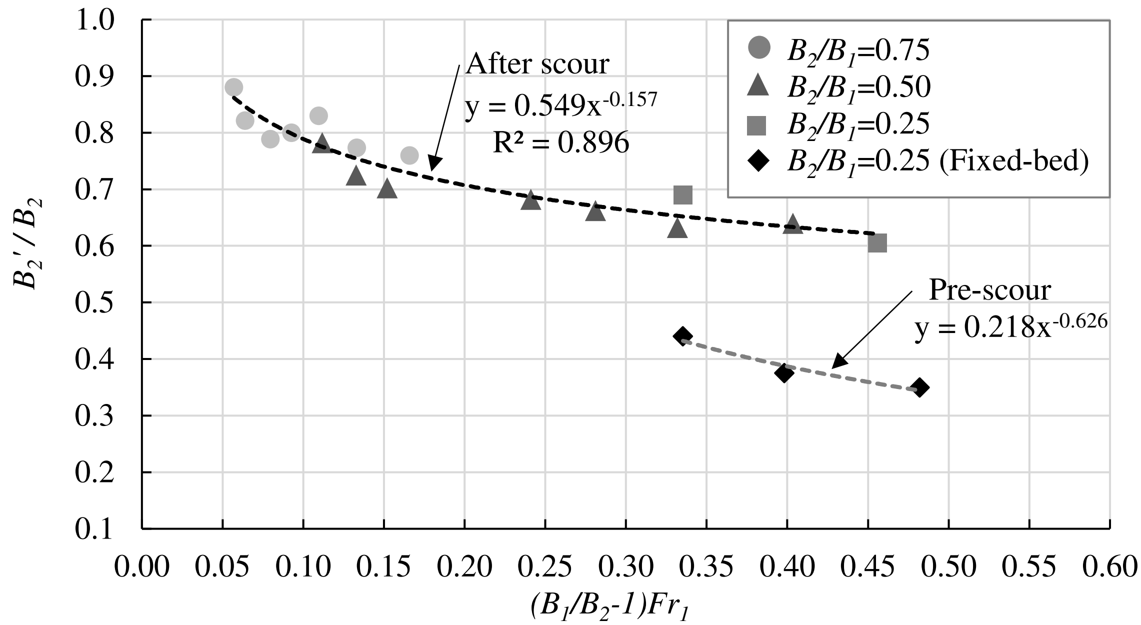

Figure 6.9. Values of vena-contracta coefficient, K_v, for a loose boundary channel with a 45˚ channel entrance. Two curves indicate the value of K_v for Fixed-bed and after contraction-scour developed. Indicated in the legend box are the values of B_2/B_1.

6.4. Trends in measured depths of scour at different regions of the contraction entrance

Two regions of scour within the entrance of a contracted channel were of interest: at the entrance corners; and, along the vena contracta. The two regions of scour experienced similar trends, though the trends diverted during live-bed scour.

Figure 6.10 assembles all the data on the maximum scour depth at the vena-contracta region (measured as described above). When flow entered the contracted section, the flow streamlines separated from the walls and reattached (for all the experiments) at approximately a distance B_1 from the start of the contracted channel. The exact distance to reattachment varied as τ_{n1}/τ_c increased. It is useful to observe that, in previous literature (e.g., Webby 1984), a contracted section was called "long" if was longer than one to two times B_1. Webby stated that, as the flow streamlines reattach to the walls, uniform scour should occur downstream from this point. The results of the present flume experiments showed this statement to be incorrect, and Webby's flume was too short to address this point.

It is important to mention that, in the following graphs, Y_{n1} and τ_{n1} are the depth of the water and bed shear stress associated with normal flow approaching the contraction (also before the presence of a bridge waterway contracts the channel). This condition still prevails at the downstream end of the contraction when $B_1 = B_3$ after constructing the contraction. Recall that the downstream end of the contraction sets the flow controls and determines the scour progress through the contraction. However, the water depth at the upstream end of the contraction is affected by the contraction length, entrance shape, i.e., Y_1 (the backwater depth). The effect of using Y_{n1} or Y_1 on the estimate of contraction scour depth is discussed in sub-section *6.5.3*. The assumption of normal depth and a backwater profile upstream of the contraction was essential for calculating the initial flow and bed conditions and to identify when choking could occur.

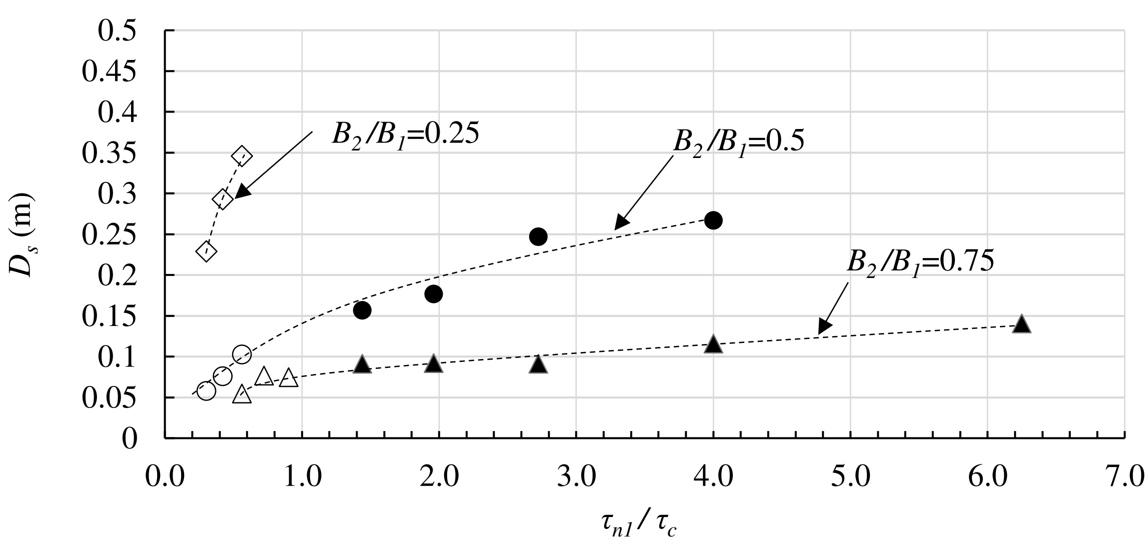

Figure 6.10. The maximum depth of scour in the vena-contracta region. The hollow points indicate the clear-water experiments and the solid points indicate the live-bed experiments.

Figure 6.11 shows the average scour depth estimated for the vena-contracta region for the experiments. For the tight contraction, as mentioned above, the separation vortices influenced scour along the vena contracta, thereby complicating estimation of an average depth of scour at vena-contracta region. The complication makes it difficult to determine an average scour depth purely attributable to flow through the vena contracta region.

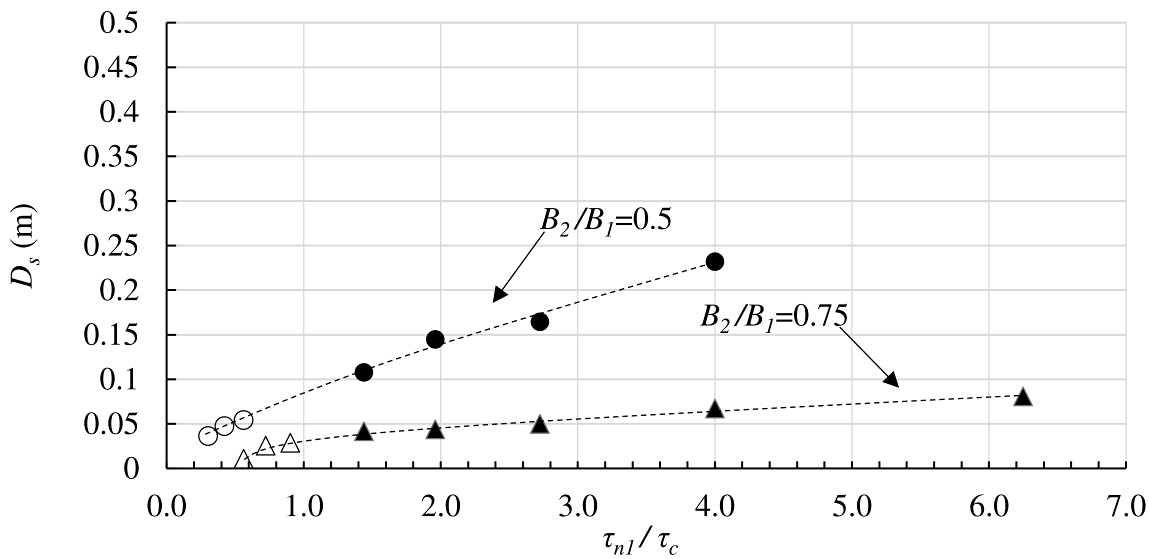

Figure 6.11. The average depth of scour in the vena-contracta region. The hollow points indicate the clear-water experiments and the solid points indicate the live-bed experiments.

Figure 6.12 illustrates the consequence of the intersection of the separation vortices and flow contraction through the vena contracta region (B_2/B_1=0.25). A single scour hole developed, which connected to the downstream bed by way of a continuous slope. Other than the low elevation at the start of the contracted channel, no other locally minimum area developed in this area.

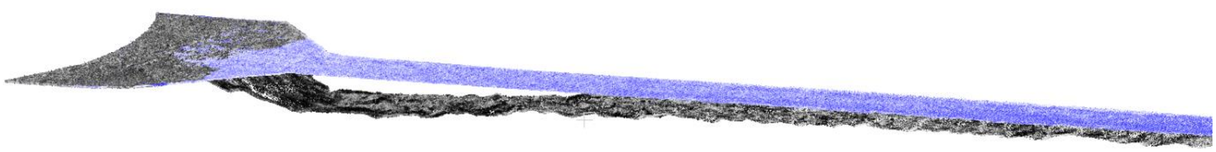

(a)

(b)

Figure 6.12. Comparison of the LiDAR-scanned bed pre- and post-scour along the contracted channel, experiment CW- 0.25 - 0.56: (a) an isometric view of the contracted channel; and, (b) a streamwise-view of the contracted channel.

As shown in Figure 6.4, the bed profile of the contracted channel became curve, in response to the GVF flow. Further, the curve's shape changed as the length of the vena contracta increased or decreased along the contracted section (Chapter 2). Figure 6.13 plots the average depth of scour of the bed (bed lowering) at a cross-section located a distance B_1 downstream of the start of the narrowed width of contracted channel, as shown in Figure 6.3. The scour depth at this cross-section usually had the lowest elevation along the contracted section downstream of this cross-section location. A cross-sectional strip of width about $0.2B_1$ was used for sampling and determining the bed-average elevation at this location for each experiment. Figure 6.13 plots these values.

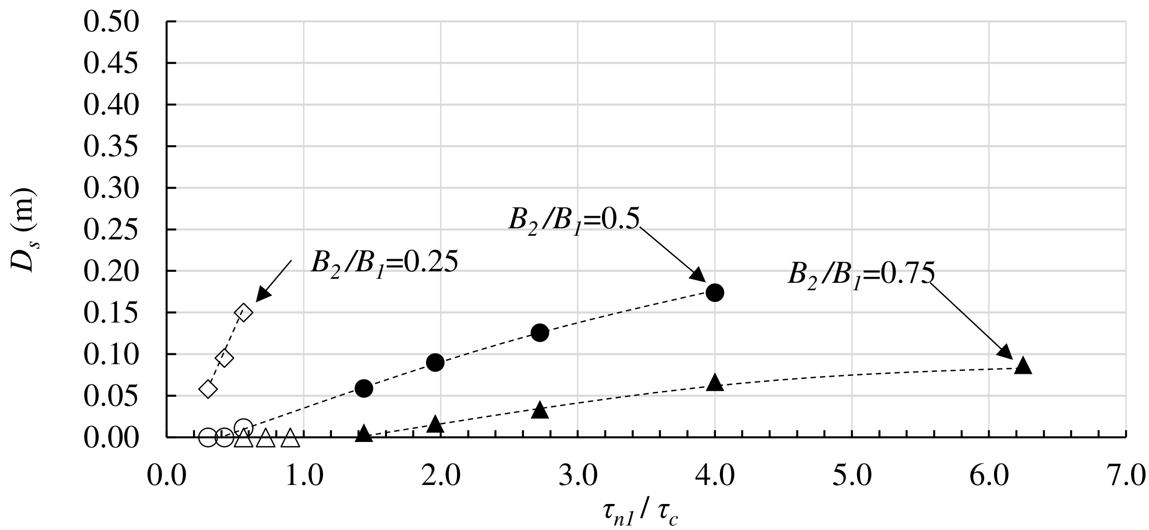

Figure 6.13. The average depth of scour at distance B_1 downstream of the contraction entrance. The hollow points indicate the clear-water experiments and the solid points are related to the live-bed experiments.

Figure 6.13 shows that, for medium and mild contraction categories, the depth of clear-water scour was negligible at reattachment region (at a distance B_1 downstream of the contraction entrance). The flow through the contraction was such that shear stress exerted on the bed was insufficient to move the bed sediment. Additionally, it is useful to note that the scour depth at this area is affected by the length of the contraction (for contractions of intermediate length) such that the bed shear stress gradually increased along the contraction.

The values of corner scour depth generally exceeded the scour depth in the vena contracta because of the hydrodynamic forces exerted by the separation vortices. Generally, there was a slight difference between the maximum scour depth at the right and left sides of the contraction entrance, with the left corner sometimes developing deeper scour. The maximum difference was about 8 cm. This difference resulted from small variations in the flow field and slight asymmetrical variations in the roughness gravel placed at the start of the approach channel. Prior studies, for example Gill (1981), indicate that asymmetry of scour depth at the corners is not unusual. The variation of the depth of corner scour near the right and left corners is shown in Figure 6.14.

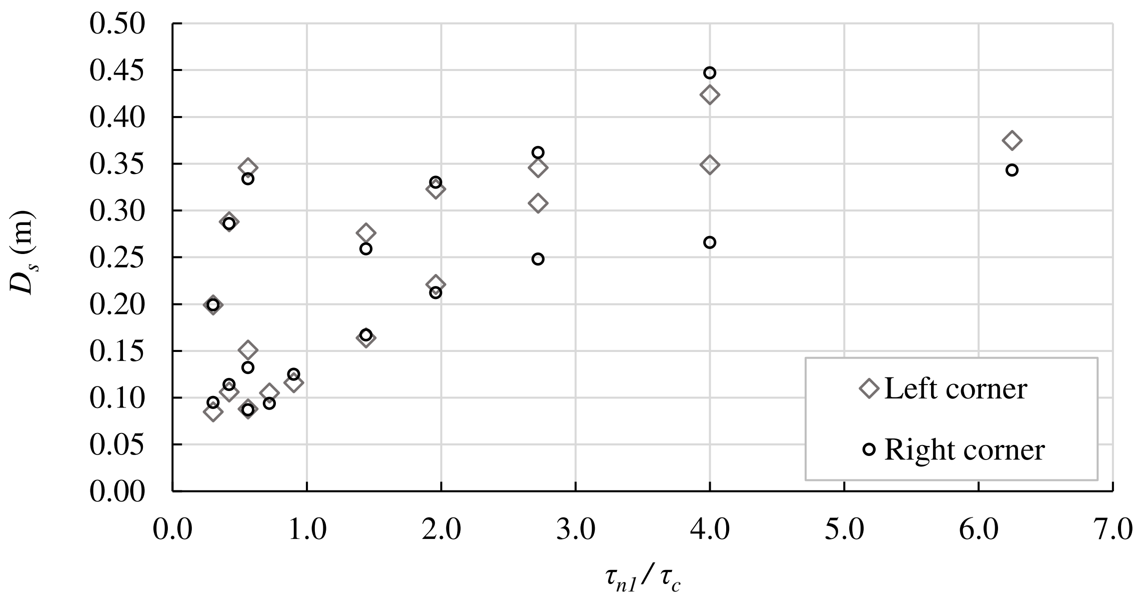

Figure 6.14. Values of the depth of corner scour at the right and left corners of the entrance to the contracted channel.

The maximum depth of corner scour versus τ_{n1}/τ_c is plotted in Figure 6.15. This figure shows the increase of scour depth by increasing the shear stress ratio. However, the rate of scour decreases as the contraction ratio increases. It should be noted that for the experiment CW-0.25-0.30, the maximum of scour depth happened at the centerline of flume entrance.

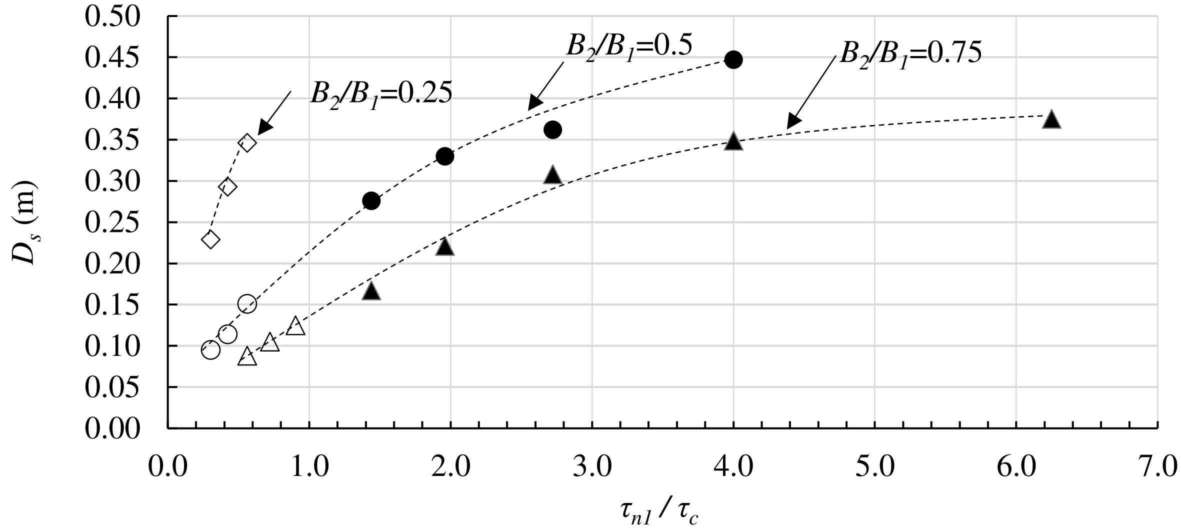

Figure 6.15. The maximum depths of scour at the entrance corners of the contracted channel. The hollow points indicate the clear-water experiments and the solid points are related to the live-bed experiments.

6.5. Adjustments to the Leading Methods for Design Estimation of Contraction Scour

A practical outcome sought from the present research was guidance on improving the HEC-18 equations widely used in engineering design for estimating the depth of contraction scour in a bridge waterway. The hydraulics and the flume experiments indicate how the equations could be adjusted. Practical considerations at usual bridge sites, though, temper the suggestions.

6.5.1. Introduction

As Chapter 3 explains, the leading (and most accepted) methods for estimating depth of contraction scour at bridge waterways are given in the FHWA monograph HEC-18 (Arneson et al. 2012). The methods essentially are modified versions of Laursen's equations (Laursen 1960 and

1963) for the clear-water and live-bed conditions of contraction scour. This section of the thesis uses the insights gained from the flume experiments to develop adjustments to the methods in HEC-18. The adjustments aim to modify or better focus the widely used (and accepted) methods rather than replace the methods with a substantially new equation of pair of equations (for clear-water and live-bed scour). The latter approach is infeasible, given the limited number of flume experiments conducted. Also, the latter approach would be hard to implement in design practice. However, a subsequent section of this chapter takes the flume data and casts them into an empirical equation that may be considered in subsequent research on contraction scour.

The contraction-scour methods in the present edition of HEC-18 are presented without the framework for trends in contraction scour that Figure 6.1 shows. Further, the methods in HEC-18 assume that contraction scour occurs as a so-called long-contraction scour (Arneson et al. 2012). Because the methods incompletely consider the hydraulics of open-channel contraction flows (outlined in Chapter 2), and do not mention the formation of a vena contracta within the entrance of the contracted channel, the methods are inherently incorrect. An important finding that the present study illuminates is that a uniform depth of contraction scour along a contracted channel does not occur, and that the deepest location of contraction scour occurs in the vena-contracta region. As explained in the preceding sections of this chapter (and in Chapter 2), other locations along a contraction may produce comparable or even deeper scour depths (the corners of a contraction entrance and at the exit of a contraction subject to a substantial drawdown of water-surface profile). However, the present section does not address scour depth at those locations.

An additional issue with the methods in HEC-18 is the lack of clarity about using of the approach-flow depth taken near the entrance of the contraction (i.e., the bridge waterway) rather than using the normal depth of approach flow. Flow depth at near the contraction, though, is part of a backwater profile (M1 profile) for water-surface at the approach to a contraction. The backwater profile depends on the extent of flow constriction a contracted channel exerts, and the backwater causes the slope of the energy-grade line to depart from the bed slope of the channel. Therefore, the flow depth near the contraction entrance is itself fraught with variability. Consequently, adjustment of the HEC-18 methods also involves basing them on the normal depth of approach flow.

The present section illustrates the issues with current HEC-18 equations then compares the flume data on vena-contracta scour with predictions from the existing forms of the HEC-18 methods. Finally, this section adjusts the methods and compares the data to predictions from the adjusted methods.

6.5.2. The existing equations in HEC-18

This section outlines the issues associated with the HEC-18 equations for estimating depth of contraction scour and indicates how the issues may affect the depth estimates. The HEC-18 methods involve the following sets of equations for estimating contraction-scour depth associated with clear-water and live-bed conditions (Arneson et al 2012) described below. The equations are repeated here to show how they should be modified.

The clear-water equations HEC-18 recommends for estimating for contraction scour are as follow:

$$Y_2 = \left[\frac{K_u Q^2}{d_m^{2/3} B_2^2}\right]^{3/7} \tag{6.1}$$

and

$$D_s = Y_2 - Y_0 \qquad (6.2)$$

Here,

Y_2 =average equilibrium depth in the contracted section after contraction scour, ft (m)

Q = discharge through the bridge or on the set-back overbank area at the bridge associated with the width W, ft^3/s (m^3/s)

d_m = diameter of the smallest non-transportable particle in the bed material (1.25 d_{50}) in the contracted channel, ft (m)

d_{50} = median diameter of bed material, ft (m)

B_2 = bottom width of the contracted section less pier widths, ft (m)

Y_0 = average existing depth in the contracted section, ft (m)

K_u = 0.0077 in English units and 0.025 in SI units

Before presenting HEC-18 live-bed equation, however, it is necessary to mention the uncertainties implicit in this equation. As pointed out by Laursen (1960) and Arneson et al. (2012; sub-section 6.5), derivation of the equation assumes a uniform reach upstream of the contraction and along the contraction. Additionally, Arneson et al. (2012) mentioned that "both clear-water and live-bed equations calculate contraction scour depth assuming a level water surface ($D_s = Y_2 - Y_0$)". Consequently, the definitions of some of the parameters used in the HEC-18 equation have changed to be in accordance with the parameters this study introduces and used in the original equation proposed by Laursen (1960).

The live-bed equations HEC-18 recommends for contraction scour are:

$$Y_2 = Y_{n1} \left(\frac{Q_2}{Q_1}\right)^{\frac{6}{7}} \left(\frac{B_1}{B_2}\right)^{p} \tag{6.3}$$

$$D_s = Y_2 - Y_0 \tag{6.4}$$

Here,

Y_{n1} = uniform (normal) depth of flow in the main channel approaching the contraction, ft (m)

Y_2 = average equilibrium depth in the contracted section after contraction scour, ft (m)

Y_0 = existing depth in the contracted section before contraction scour, ft (m)

Q_1 = discharge in the upstream channel transporting sediment, ft^3/s (m^3/s)

Q_2 = discharge in the contracted channel, ft^3/s (m^3/s)

B_1 = bottom width of the upstream main channel that is transporting bed material, ft (m)

B_2 = bottom width of the main channel in contracted section less pier width(s), ft (m)

P = exponent related to the intensity of the sediment transport. Table 6.1 indicates the recommended values of p.

Table 6.1. Values for the exponent 'p'(the sear velocity u is associated with Y_{n1})*

Rouse Parameter u_*/ω	p	**Mode of bed-sediment transport**
<0.50	0.59	Mostly contact bed sediment discharge
0.50 to 2.0	0.64	Some suspended bed sediment discharge
>2.0	0.69	Mostly suspended bed sediment discharge

$u_* = (gY_1S_1)^{0.5}$, the shear velocity in the upstream section, ft/s (m/s)

ω = fall velocity of bed sediment, ft/s (m/s). The value of ω is based on the median diameter of bed sediment, d_{50}, and kinematic viscosity, υ_m

υ_m = kinematic viscosity of the water-sediment mixture, (ft^2/s) (m^2/s)

g = acceleration of gravity (32.2 ft/s2) (9.81 m/s^2)

S_{n1} = slope of energy grade line of the approach channel, ft/ft (m/m)

The existing equations in HEC-18 pose substantial issues regarding the variables B_2, Y_0, Y_{n1}, and Y_2. Each of these variables involves approximations and errors, and therefore each is a source of uncertainty in the estimation of depth of contraction scour, D_s. The approximations (and errors) stem from a lack of clarity regarding contraction hydraulics in channels with a loose bed. For instance, mis-selection of approach flow depth, Y_1, leads to incorrect trends for D_s, as mentioned above and elaborated in the ensuing sub-section.

The present study indicates, however, that the major sources of uncertainty that markedly affect the estimation of the contraction scour depth are the correct selection of Y_1 *and* B_2 to be used in the estimation. The difficulties associated with these two variables are elaborated in the ensuing subsections. The other sources of uncertainty are discussed subsequently in this chapter.

6.5.3. Selection of approach flow depth (Y_1)

For scour-depth estimation using HEC-18, the approach flow depth is used to define the approach flow and the approach-bed condition, (i.e., clear-water or live-bed approach-flow conditions). The approach flow depth directly appears in the HEC-18 equation for live-bed scour, Eq. (6.3). There is no clear explanation whether the backwater depth, Y_1, or the uniform flow depth, Y_{n1}, should be taken, though the estimation equations were developed using formulations for uniform flow in open channels and sediment transport equations related directly to uniform flow.

However, this study and its flume experiments showed that the depth of the contraction scour relates primarily to the downstream flow depth (Y_{n3} in Chapter 2), as this flow depth acts as a flow-depth control for subcritical flow along the contraction. Strictly speaking, it is more accurate to use the uniform (normal) depth of flow at the uncontracted section downstream of the contracted channel; i.e., to use $Y_{n1} = Y_{n3}$. Yet, to define the upstream bed-condition, and thereby select the HEC-18 clear-water or live-bed equations, the uniform depth of approach flow, Y_{n1}, should be used. The present edition of HEC-18 does not deny or accepts the validity of using Y_1. A difficulty, though, is that Y_1 is in the backwater region of approach flow, and therefore is affected by the flow resistance posed by the contracted channel. Common practice is for engineers, however, is to use Y_1 (depth of the flow immediately upstream of the contraction) to define the approach flow bed condition. Use of Y_1, however leads to incorrect trends for depth of contraction scour.

To illustrate the result of using Y_1, instead of Y_{n1}, a table of data was developed using a wide range of flow discharges (0.01-0.536 m^3/s) and two different contraction ratios (B_2/B_1 = 0.5 and 0.75) for the same experiment setup as used in the flume experiments (Chapter 5). The water depth and energy-grade line along the backwater profile were simulated by means of the widely used, 1D, rigid-bed numerical model, HEC-RAS. The depth of contraction scour was estimated for each discharge and contraction condition using Y_1 and Y_{n1} as the depth variable defining the approach depth of flow and the approach-flow bed condition. The depth of contraction scour was then estimated using the HEC-18 equation for live-bed scour. Also, values of the ratio Y_{n1} were calculated using HEC-RAS.

Figure 6.16 shows the increase of the ratio Y_1/Y_{n1} as the shear stress ratio τ_{n1}/τ_c increased. When the latter ratio increased (i.e., by increasing discharge for constant $Y_{n1} = Y_{n3}$ and adjusted bed slope), it increased the ratio Y_1 / Y_{n1}. Note that the zigzags or shifts in Figure 6.16 are due to change of the downstream control depth from normal to critical depth due to flow-choking, which occurred. To be sure, flow-choking altered the flow field in the contraction entrance.

A further reason for the trend is due to simplifying the bed slope, which is used in 1D, numerical flow simulations with HEC-RAS. The bed slope for the whole range of the discharges was divided in to four groups and the average of the bed slope for each group is used to make a numerical model for that specific group. However, these small shifts did not significantly affect the overall trends. The four groups of slopes were selected in accordance with the varying depths of normal flow associated with each contraction ratio. To simplify the simulations, instead of making 41 different HEC-RAS models, the 41 normal depths were divided into four groups and the average bed slope of each group. The resulting variations in depth were negligible.

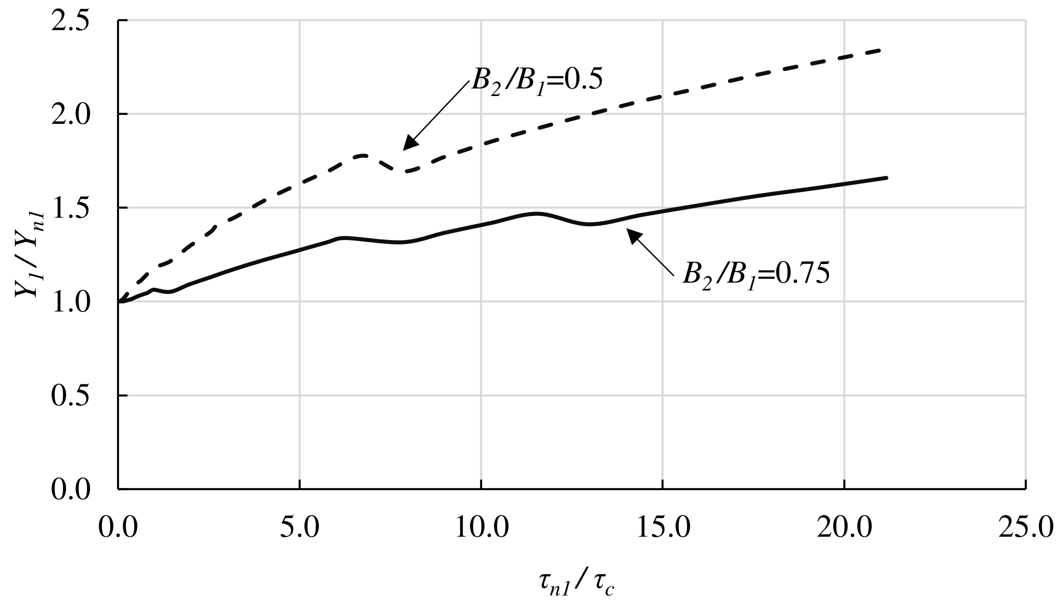

Figure 6.16. Backwater depth change relative to normal depth of approach flow for increasing value of the shear stress ratio for the flume setup; τ_{n1} is the bed shear stress related to the normal depth, Y_{n1}.

The HEC-18 equation for clear-water contraction scour suggests that utilizing Y_1 instead of Y_{n1} does not substantially affect the estimate of scour for clear-water contraction scour. This equation presumes that the shear stress limiting scour-hole deepening attains the critical shear stress for the bed sediment; i.e., $\tau_2 = \tau_c$. However, utilizing a backwater depth instead of the normal depth of flow substantially increases the estimate of scour depth for live-bed estimates of scour depth, because the flow depth, Y_2, associated with the scour directly relates to Y_1.

Figure 6.17 compares the scour depth estimation based on Y_1 with the average values of scour depth evaluated for the vena-contracta region. The results show that the scour depth estimation agrees well with the measured depths. But, because HEC-18 does not include the formation of the vena contract region, and neither does Laursen (1960 and 1963), these equations do not estimate the scour depth in the vena-contracta region. In other words, the use of Y_1 compensates for not using the narrower contraction width occurring in the vena contracta.

However, it is important to mention that the backwater depth, Y_1 is subject to change through time; i.e., Y_1 decreases as the scour depth develops along the contraction. The backwater depth which used to estimate the scour depth in Figure 6.17 is related to the pre-scour condition, i.e., rigid-bed, and the Manning's *n* for the HEC-RAS model was calibrated based on measurements from the experiments. Therefore, there is the risk that using the backwater depth at the scour-equilibrium condition (or using smaller values of Manning's *n*) would result in the underestimation of the scour depth at the vena-contracta.

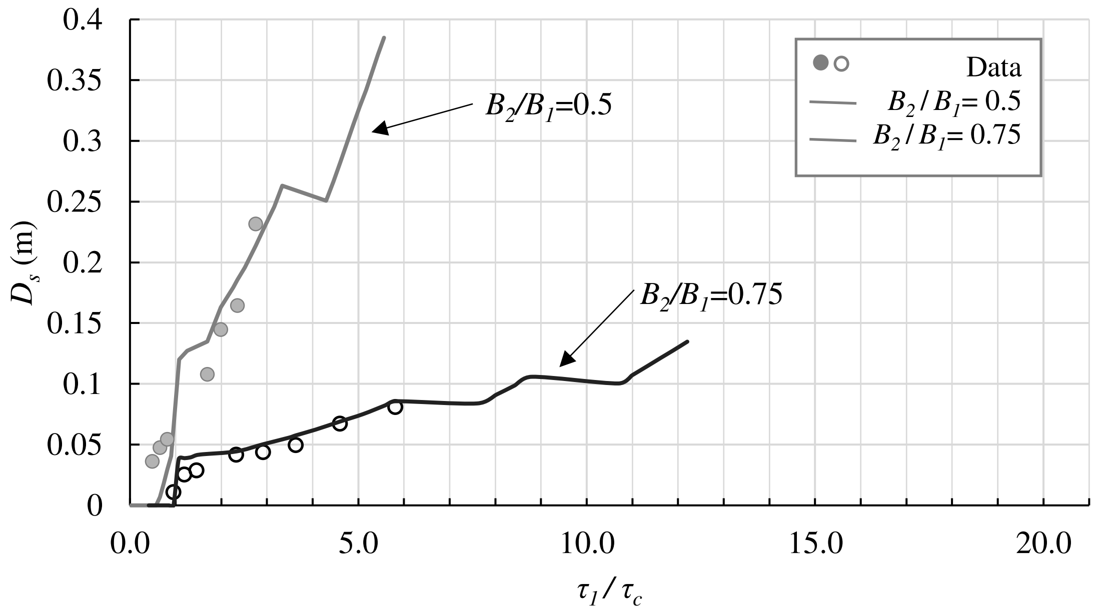

Figure 6.17. Scour depth estimation based on backwater depth and comparing with observed data. τ_1 is the bed shear stress related to the backwater depth, Y_1.

Another issue for estimating scour depth in terms of the backwater depth, Y_1 is that the estimated scour depths for the clear-water and live-bed cases trend upward, even for the live-bed condition of contraction scour. This trend does not agree with data reported by Straub (1934) and Laursen and Alawi (1989).

Figure 6.18 shows values of scour depth estimated using the uniform flow (i.e., normal depth) Y_{n1} compared with the measured values of the average scour depth in the vena-contracta region. This figure indicates that the estimated values of scour depth decrease for the live-bed condition and underestimate the scour depth in the vena-contracta region. This outcome was expected, because the equations do not account for the formation of a vena contracta within the contraction.

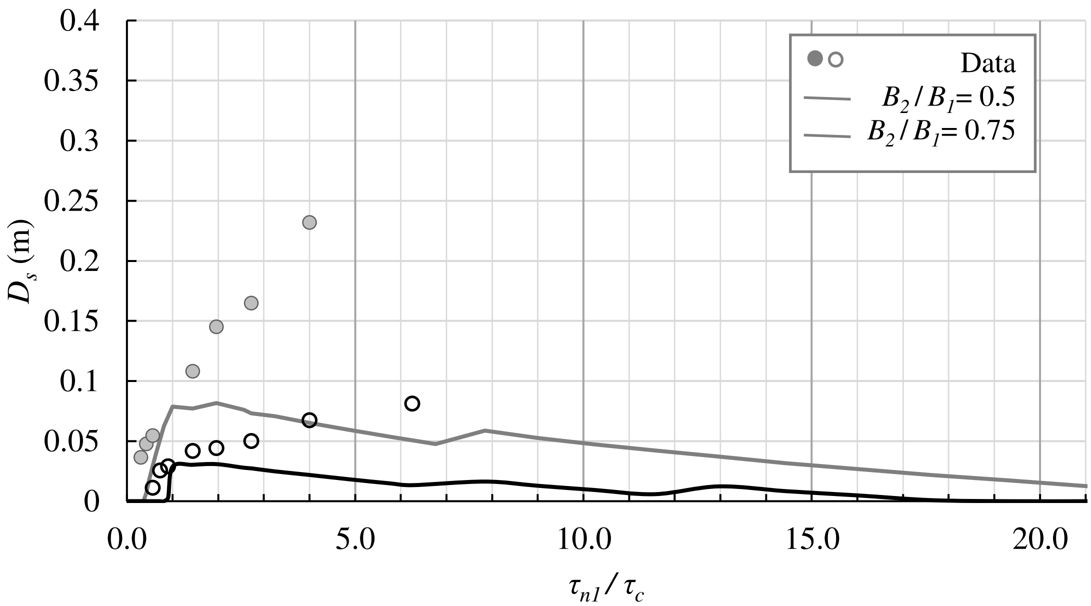

Figure 6.18. Comparison of the scour depth estimated using the normal water depth, Y_{n1}, and the measured scour-depth data.

Figures 6.17 and 6.18 use the same flow discharges, values of Manning's *n*, and downstream control constraint. Consequently, using the backwater adjusted slope and Y_1 gives lesser values of bed shear stress. For example, when the contraction ratio is 0.5, the shear stress ratio is about 8 at Y_1, whereas it is 21 when using Y_{n1}. In actuality, the rather high rate of sediment transport consequent to using the normal depth would be subject to sediment deposition along the backwater region. Also, bed roughness would change. Therefore, the bed elevation would increase at the upstream of the contracted section. However, once the deposition stopped, the sediment transport rate of the whole reach would return to the sediment transport rate related to the normal depth (i.e., uniform flow condition, of that reach). Therefore, use of the backwater depth to define the bed condition significantly underestimates the sediment transport rate which, in turn, may lead to an overestimation of the depth of contraction scour.

Additionally, if it were assumed that flow in the continuing channel the downstream of the contracted channel were the same as uniform flow along the approach channel, the scour depth at downstream end of the contracted channel may exceed scour depth at the upstream end of the contracted channel. This result would occur due to the substantially increased value of the shear stress ratio prevailing at the downstream end of contracted channel; the slope of the hydraulic and energy gradients would be estimated as being steeper than in actuality.

The present analysis indicates that the theoretically correct flow depth to use in the HEC-18 equations is the normal depth of approach flow, Y_{n1}. Strictly speaking, as the flow control is exerted at the downstream end of the contraction, the normal depth of flow at the downstream end of the contraction, Y_{n3}, should be used in the HEC-18 equations. For flume experiments in this study, $Y_{n1} = Y_{n3}$, because the channel was of constant width.

The flume experiments also showed that the bed elevation along the contracted channel varied in response to the variation of the shear stress, as the open-channel flow hydraulics presented in Chapter 2 shows. Consequently, determining an accurate average value of scour depth for the whole length of the contracted channel was difficult. This subject is discussed more in the following sections of this chapter

6.5.4. The width of the vena contracta

The HEC-18 equations use the full width of the contraction, B_2, when estimating the depth of the scour along a contraction. However, as Chapter 2 points out, the depth of flow along a contraction designated as being of intermediate length forms a gradually varied water-surface profile of the M2 type. This profile creates a varying shear stress distribution along the bed. Also, the variation of shear stress changes with the varying length of an intermediate-length contraction. As a result, using an average depth through the whole contraction introduces error in scour depth estimation. The experiments indicate instead that the contraction-scour depth should be estimated for the vena-contracta region.

In the ensuing subsections of this section, the HEC-18 equations for clear-water and live-bed contraction scour are adjusted using the minimum width of the vena-contracta formed. This adjustment entails introducing a coefficient, K_v, to ensure that the equations include the vena-contracta effect on scour depth.

6.6. The adjusted HEC-18 equation for clear-water contraction scour

The present experiments indicate two adjustments to the widely used, HEC-18 equations:

1. Stipulating that the equations apply to the narrowest portion of the vena-contracta region formed as flow passes into a contraction; and,
2. Inserting into the HEC-18 equations a relatively simple coefficient that indicates how the width of the vena contracta varies with contraction-flow conditions.

The HEC-18 method assumes that the bed shear stress along a long contraction (away from the influence of corner scour) scours the contraction bed until the bed is lowered sufficiently that the bed shear stress reaches a value equivalent to the bed shear stress associated with the incipient motion of the bed sediment; i.e., $\tau_2 = \tau_c$. Figure 6.19 compares estimates made with the existing HEC-18 clear-water equation to the average values of scour depth measured for the three regions of scour measured during each experiment with the flume. The comparison shows that there is not a uniform depth of scour along the contraction. This finding was expected, for the reasons explained in the preceding subsection of this chapter; i.e., the drawdown profile of the water surface (the M2 profile) caused the flow depth and, therefore, the shear stress to be non-uniform along the contraction. As mentioned above, a shortcoming of the HEC-18 equations for contraction scour is that is no guidance is provided regarding the region along a contracted, bridge waterway as to where the HEC-18 equations should be applied.

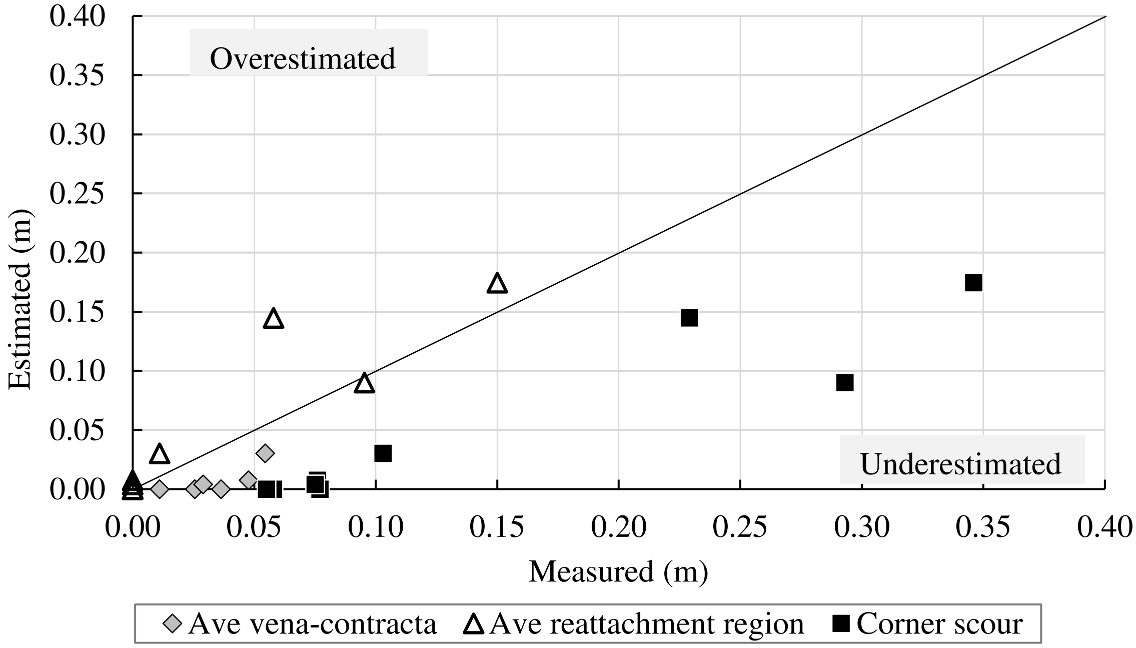

Figure 6.19. Comparison between estimates made with the existing form of the HEC-18 clear-water equation and measured values of contraction-scour depth for three regions along a contracted channel: average depth in the vena-contracta, average depth at the reattachment region, and maximum depth of corner scour.

As Figure 6.19 shows, the HEC-18 equation for depth of clear-water scour works acceptably well when estimating the average depth of scour at the reattachment region, a distance of approximately B_1 downstream of the contraction entrance. However, the HEC-18 equations significantly underestimate the average depth of scour in the vena-contracta region. Additionally, and as expected, the HEC-18 equations do not accurately predict the depth of scour at the entrance corners of the contracted channel; the HEC-18 equations do not include the effect of the flow-separation turbulence structures. Turbulence structures at the entrance corners produce deeper scour than the HEC-18 equations were intended to estimate.

The vena-contracta region is the appropriate region for using the HEC-18 equations to estimate the average depth of contraction scour along a contracted channel of intermediate length. The open-channel hydraulics outlined in Chapter 2, together with the scour-depth data and the observations in Chapter 5 show that flow depth and scour depth vary along the downstream regions of the contraction, thereby weakening the formulations leading to the HEC-18 equations. Therefore, an important adjustment to the existing equations in HEC-18 involves including the flow-concentrating effect of the vena-contracta region. This effect narrows the width at contracted section, B_2, to an effective width, B_2'. The narrowed width of flow through a vena contracta amplifies the shear stress causing scour of the bed.

The effective minimum width of flow through a vena contracta can be estimated as

$$B_2' = K_v B_2 \tag{6.5}$$

Here, K_v is termed the vena-contracta coefficient, as mentioned above. The value of K_v relates to the entrance velocity, contraction ratio and the entrance transition shape and can be related to these variables by means of the dimensional analysis done in Chapter 3; i.e.,

$$K_v = f(Fr_1, \frac{B_2}{B_1}, Entr\_Shape) \tag{6.6}$$

Fakhri (2020) used LSPIV to measure the minimum width of vena-contractas formed in the flume experiments, and he used those widths to determine values of the coefficient, K_v. related to the condition of equilibrium bed profile developed for sub-critical flow along a contraction whose entrance was formed using 45° angled walls. Figure 6.9 shows the values of K_v he obtained. It is noted that the values of K_v were smaller than the values associated with equilibrium scour along a vena contracta. More research is needed to find K_v values for different entrance shapes for the flat-bed and equilibrium-scour conditions of flow entering contracted channels.

By introducing K_v into the HEC-18 equations for estimating depth of clear-water contraction scour, the equations are adjusted as follow:

$$Y_2 = \left[\frac{K_u Q^2}{d_m^{2/3}(K_v B_2)^2}\right]^{3/7} \quad (6.7)$$

and

$$D_s = Y_2 - Y_0 \quad (6.8)$$

Here,

Y_2 =Average equilibrium depth in the contracted section after contraction scour

Q = discharge through the bridge or on the set-back overbank area at the bridge associated with the width W

d_m = diameter of the smallest non-transportable particle in the bed material (1.25 d_{50}) in the contracted section

d_{50} = median diameter of bed material

B_2 = bottom width of the contracted section less pier widths

Y_0 = average existing depth in the contracted section

K_u = 0.0077 in English units and 0.025 in SI units

K_v = vena-contracta coefficient ($K_v \leq 1$)

Fakhri (2020) suggested the following equation to be used for estimating K_v produced by a 45°entrance:

$$K_v = 0.55\left(\left(\frac{B_1}{B_2} - 1\right) Fr_1\right)^{-0.16} \quad and\ K_v \leq 1 \tag{6.9}$$

This equation applies for the equilibrium-scour condition.

Figure 6.20 compares measured values of the average depth of scour depth in the vena-contracta region with predicted values obtained using the adjusted HEC-18 equation (Eq. (6.7)). The adjusted equation produced estimate values that agree well with the measured values of scour depth in the vena contraction. The two low values evident in this figure relate to the effects of bedform development in the vena contracta rather than to scour development owing to shear stress. The vena contract region typically occurs within the length of flow along a bridge waterway.

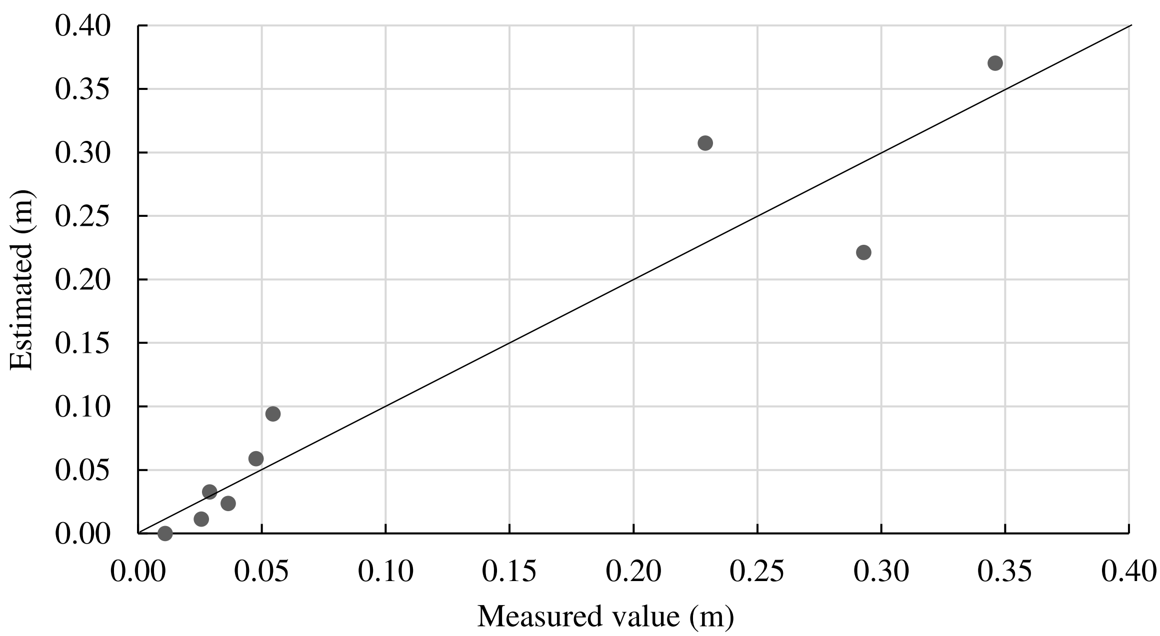

Figure 6.20. Comparison between scour-depth values obtained using the adjusted HEC-18 equation for clear-water scour and the measured values of average scour depths in the vena-contracta region.

6.7. The adjusted HEC-18 equations for live-bed contraction scour

The existing equations in HEC-18 for estimating depth of live-bed contraction scour are based on Laursen's (1960) method. Indeed, the HEC-18 equations essentially are identical to Laursen's equations for estimating live-bed contraction scour. To simplify his equations, Laursen (1960) assumed that, during floods, the shear stress exerted on the bed is much higher than the critical shear stress for bed-sediment entrainment ($\tau_1 \gg \tau_c$). Consequently, Laursen approximated $\tau_1/\tau_c - 1$ as τ_1/τ_c, and used this approximation to simplify his total sediment load transport equation. As a result, his live-bed equation relates only to contraction geometry (the contraction ratio) and sediment-transport condition (i.e., bedload or suspended load of bed sediment).

A comparison of values of contraction-scour depth predicted using the HEC-18 equation for live-bed contraction scour and the measured values of scour is presented in Figure 6.21, which shows poor agreement between the estimated and measured values. However, the estimates do show a trend generally indicating that the estimates under-predict depth of contraction scour.

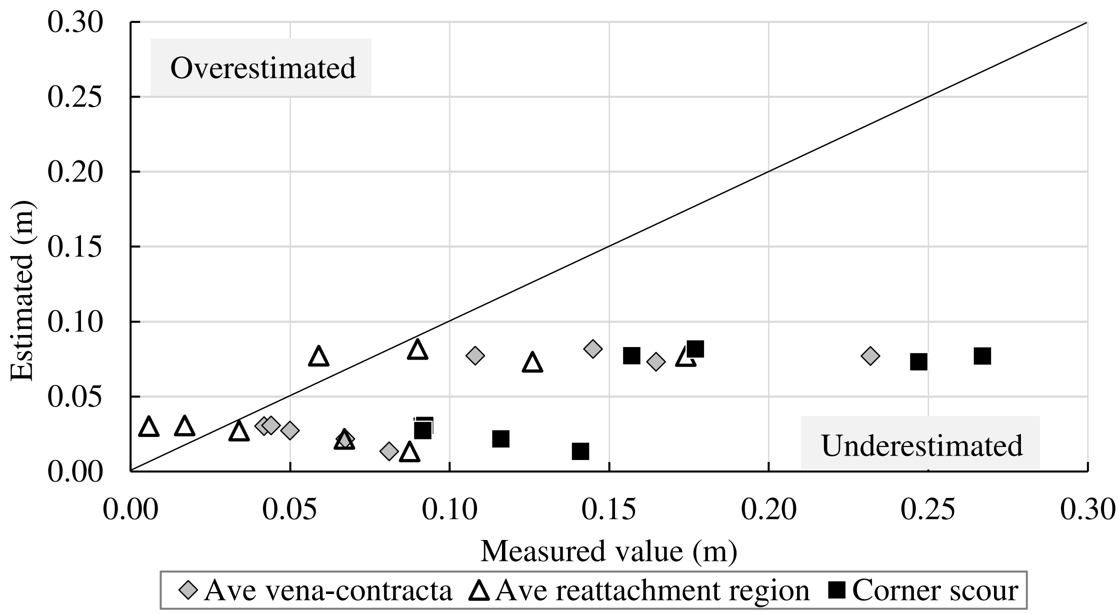

Figure 6.21. Comparison between HEC-18 live-bed equation and scour depth measurements at three regions along the contracted channel: (1) Average depth at vena-contracta; (2) average depth at reattachment region; and (3) Maximum depth of corner scour.

The same adjustment used for the HEC-18 equation for clear-water contraction scour is used here to adjust the HEC-18 equation for live-bed scour. The adjusted equations are:

$$\frac{Y_2}{Y_{n1}} = \left(\frac{Q_2}{Q_1}\right)^{\frac{6}{7}} \left(\frac{B_1}{K_v B_2}\right)^{p} \tag{6.10}$$

$$D_s = Y_2 - Y_0 \tag{6.11}$$

Where,

Y_1 = average depth in the upstream main channel approaching the contraction

Y_2 = average equilibrium depth in the contracted section after contraction scour

Y_0 = existing depth in the contracted section before contraction scour

Q_1 = discharge in the upstream channel transporting sediment

Q_2 = discharge in the contracted channel

B_1 = bottom width of the upstream main channel that is transporting bed material

B_2 = bottom width of the main channel in contracted section less pier width(s)

p = exponent related to the intensity of the sediment transport. Table 6.1 indicates the recommended values of p.

K_v = vena-contracta coefficient ($K_v \leq 1$)

u_* = $(gY_{n1}S_1)^{0.5}$, shear velocity in the upstream section

ω = fall velocity of bed material based on the d_{50}

g = acceleration due to gravity (32.2 ft/s^2, 9.81 m/s^2)

S_1= slope of the energy grade line along the approach channel

The equation developed by Fakhri (2020) was used to estimate K_v, i.e., Eq. (6.9). Note, the value of K_v cannot be more than one ($K_v \leq 1$), because the flow was constrained to the contracted channel. Figure 6.22 compares the measured values of contraction-scour depth to the estimated values obtained using the adjusted HEC-18 equations. This figure shows that the values obtained from the adjusted version of the equations agree better with the measured values. The comparison shows that the adjusted HEC-18 equation works suitably well for the range of flume experiment conducted in this study.

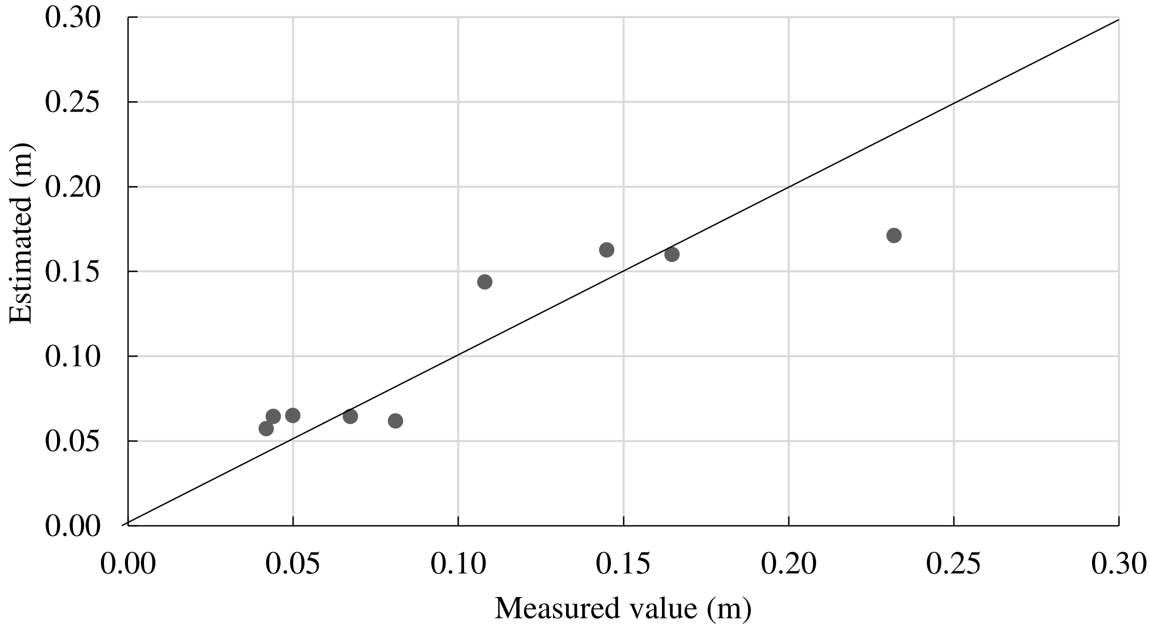

Figure 6.22. Comparison between the scour-depth values obtained using the adjusted HEC-18 equation for live-bed contraction scour and the measured values of average scour depths in the vena-contracta region.

Additionally, it is useful to replot Figure 6.18 using now the adjusted forms of the HEC-18 equations. Figure 6.23 presents the resulting comparison and shows improved agreement over the trends in Figure 6.18. For live-bed scour conditions, when the shear ratio exceeds unity, the scour depth levels off and does not continue increasing as the shear stress ratio τ_{n1}/τ_c increases, because the rate of bed-sediment inflow to the vena-contracta region increases so as to off-set the rate of scour removal of bed sediment. Some variation of this result could occur owing to variations in the bed-sediment transport equation used, and because of the variations in bedform dynamics that may develop consequent to increasing τ_{n1}/τ_c. This aspect of contraction scour requires further investigation.

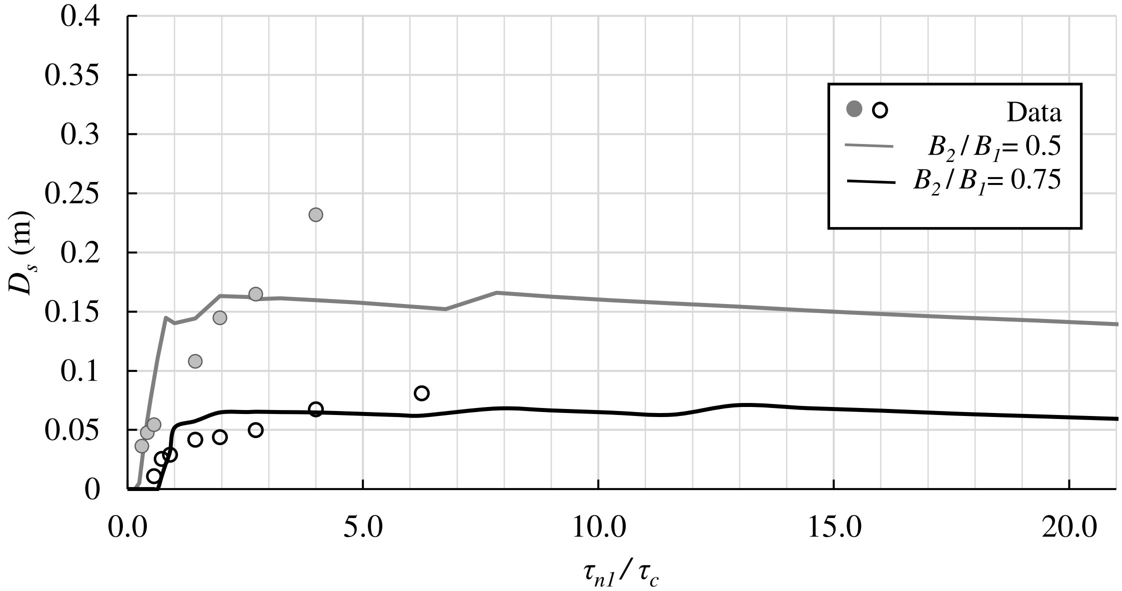

Figure 6.23. Comparison of the scour depth estimated using adjusted HEC-18 equations and the measured scour-depth data.

6.8. An Empirical Equation Fitted to the Flume Data

The dimensional analysis in chapter 3 revealed the relationship between scour depth in a contraction and two most important factors – shear stress ratio and width ratio – to be considered when estimating depth of contraction scour. This sub-section presents an empirical relationship for estimating contraction-scour depth. The relationship was developed by fitting a curve to the flume data obtained during this study.

Previous literature gives analytical methods that discern between clear-water (i.e., no sediment transport along the bed at uncontracted section) and live-bed (i.e., there is erosion and sedimentation along the uncontracted bed) conditions of scour. The sediment continuity equation is a mandatory component for analytical approaches to relate the rate of sediment transport with flow characteristics and finally find the depth of scour. However, due to zero sediment transport along the approach bed during clear-water scour, there is no clear relationship between sediment transport and scour depth so most of the previous literature. For example, Laursen (1960 and 1963), assumed that for clear-water cases the shear stress at contracted section, at the equilibrium, will reach to critical shear stress ($\tau_2 = \tau_c$). The results of this study show that this assumption is not always true; notably along a long, contracted channel. The results show that the sediment continuity equation influences both clear-water and live-bed conditions of contraction scour, and that continuity of sediment movement along a channel is an unsteady process.

Previous studies, e.g., Laursen (1963), Laursen and Alawi (1989), Straub (1934), and Gill (1981), shown that by increasing shear stress ratio of the approach flow, the scour depth for clear-water situation always have an increasing trend. However, for live-bed case by increasing shear stress ratio, i.e. increasing sediment transport rate, the depth of scour starts to slowly decrease. This study showed that by increasing shear stress ratio of approach flow the rate of the scour always increases, with a decreasing rate, for the range of this study. This may bring the argument of the existence of a transitional region between clear-water and live-bed conditions. This argument will be discussed in more details in ensuing section.

The clear relationship between the scour depth measurements, shear stress ratio, and contraction ratio for the range of this experiment is tempting to identify a single equation that addresses both clear-water and live-bed contraction scour for the range of this experiment.

This study sought a relationship between the important, non-dimensional parameters that effecting the scour process. Dimensional analysis showed that shear stress ratio, contraction ratio, sediment size, entrance and exit shape are the parameters that affect depth of contraction scour. In normalized form, the scour depth can be expressed functionally as

$$\frac{D_s}{Y_{n1}} = f\left(\frac{B_2}{B_1}, \frac{d_{50}}{Y_{n1}}, \frac{\tau_{n1}}{\tau_c}, entr.shape, exit.shape\right) \tag{6.12}$$

As this study focuses on the average scour depth in the vena-contracta region, the exit-transition shape of the contracted channel can be omitted from Eq. (6.12). Also, the analysis can be simplified by considering uniform sediment (i.e. one particle size) and a single, 45˚ entrance transition. Eq. (6.12) simplifies further to:

$$\frac{D_s}{Y_{n1}} = \alpha_1 \left(\frac{B_2}{B_1}\right)^{\alpha_2} \left(\frac{\tau_{n1}}{\tau_c}\right)^{\alpha_3} \tag{6.13}$$

Based on the discussion in the previous sections, the scour pattern inside a contraction (quantified in terms of the quartiles) responds to the distribution of bed shear stress along the contraction. The distribution produces a mound shape that may change in accordance with the flow-resistance effect exerted by the length of contraction. However, the scour depth at the vena-contracta produces a local minimum that always (as this study showed) has a higher scour depth compared with scour of the bed along the rest of the contracted section; except scour at the entrance corners. The flume experiments showed that the vena-contracta attained an equilibrium average depth faster than does the rest of the bed downstream. Moreover, the scour depth there was deeper than the remainder of the contracted channel. Accordingly, the vena-contracta area is an acceptably reliable location to represent the average depth of scour inside a contracted channel of intermediate length. This effort was expanded to included selected sets of suitable data encompassing an acceptable range of variables in a way to deliberately omit the factors (especially choking) that may adversely affect the development of a relationship based on the flume data.

The measurements for average depth of scour in the vena-contracta region were used to find the parameters $\alpha_1, \alpha_2,$ and α_3 in Eq. (6.13), by means of a non-linear regression analysis. The resulting equation was as follows and is shown in Figure 6.24.

$$\frac{D_s}{Y_{n1}} = 0.05 \left(\frac{B_1}{B_2}\right)^{3.3} \left(\frac{\tau_{n1}}{\tau_c}\right)^{0.75} \tag{6.14}$$

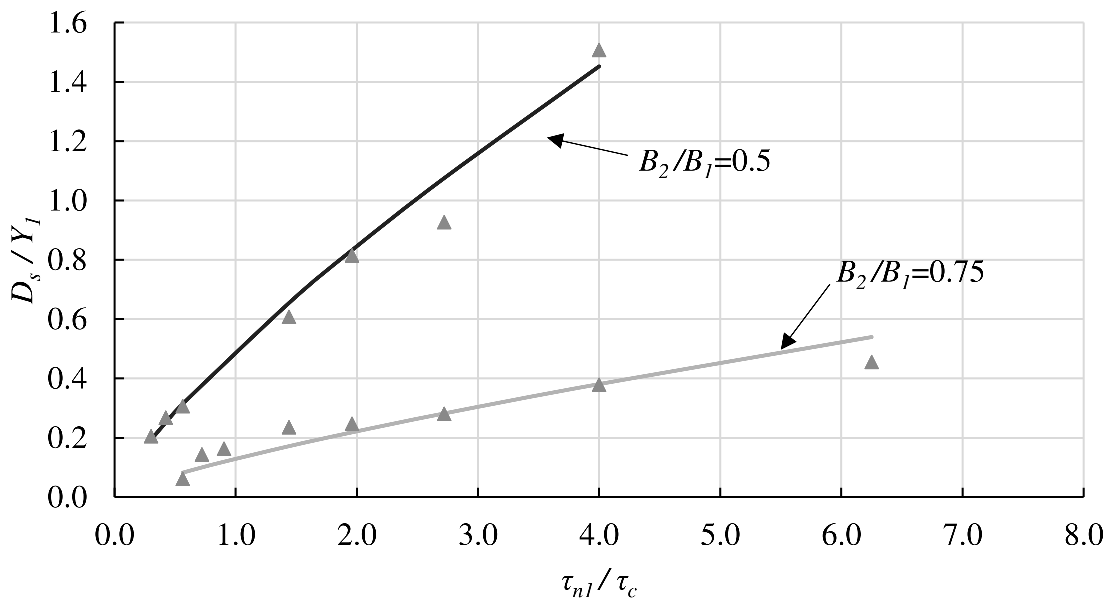

Figure 6.24. A comparison between estimates made with Eq. (6.14) and the measured values of scour depth in the vena-contracta region.

Due to the development of corner scour, flow-separation turbulence affected the vena-contracta scour for the tight contraction experiments ($B_2/B_1 = 0.25$). For these experiments, the average scour depth at vena-contracta merged with the corner scour. However, by comparing the estimated results of proposed equation for tight contraction and the observed maximum abutment scour, it was evident that Eq. (6.9) overestimates the average scour depth for tight contractions. As shown in Figure 6.25, the average scour depth estimated for tight contractions was greater than the corner scour depth at tight contraction. Consequently, Eq. (6.14) overestimates the scour depth for tight contractions. However, it should be reliable and accurate for the sandy bed rivers with shear stresses in the range of this experiment and having medium to mild contractions comparable to the ratios used in the flume experiments (Figure 6.24).

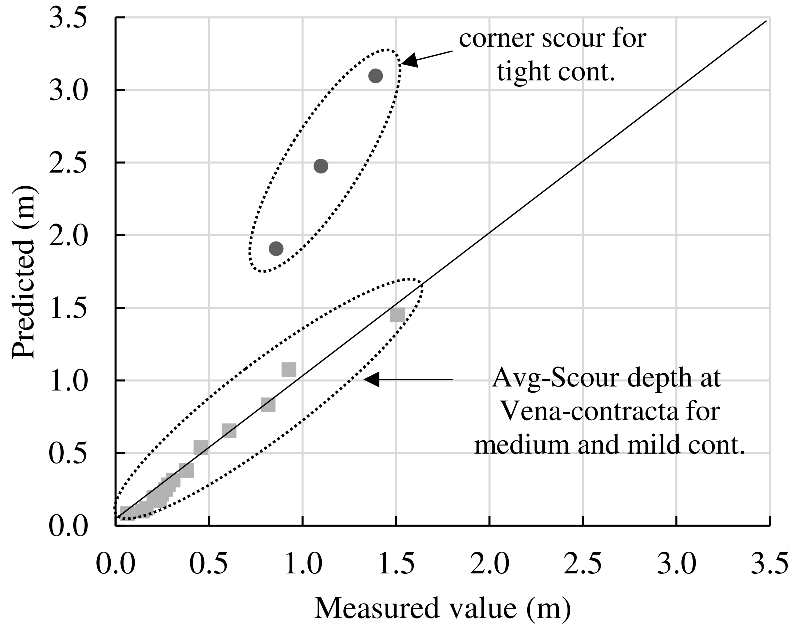

Figure 6.25. A comparison between Eq. (6.14) and measured values of contraction-scour depth in the vena-contracta.

To evaluate the proposed equation further, selected available data available in the literature was also plotted in Figure 6.26. Note, as expected, that the literature data did not exhibit a clear trend, as did the data obtained from this study. The data from previous studies included an extensive number of cases where the flow was choked, and the data were obtained from experiments involving different contraction lengths and various entrance-shapes. Furthermore, it usually was unclear where the scour depth was measured.

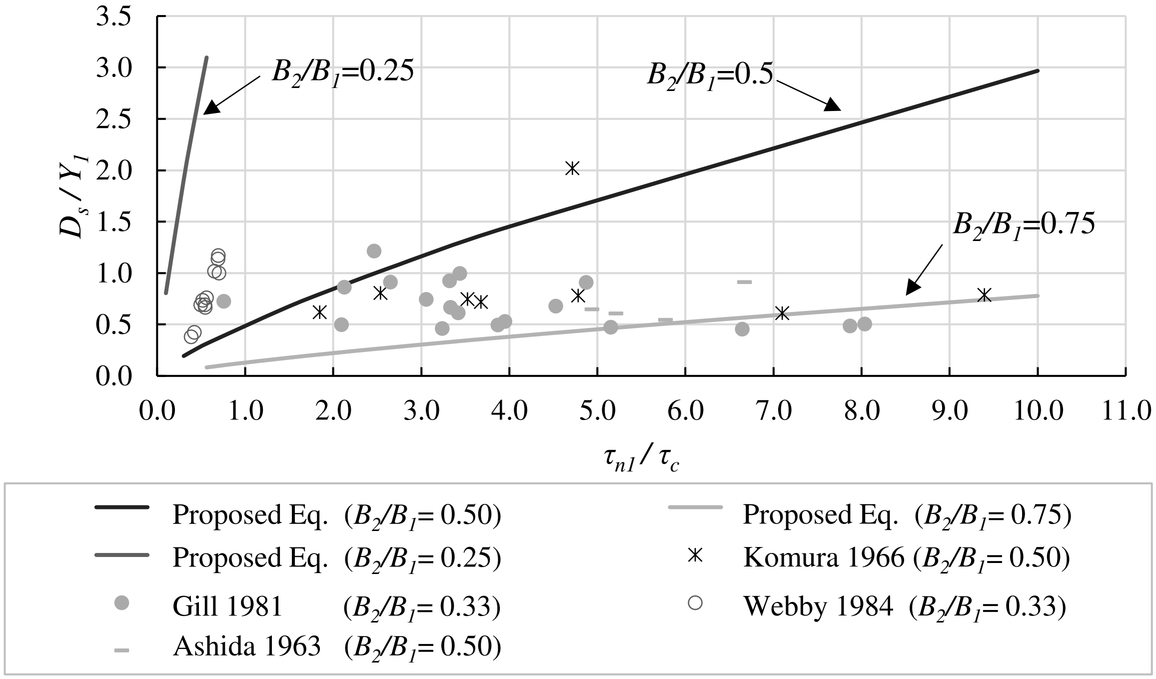

Figure 6.26. A comparison of the proposed equation with the data from prior studies.

However, due to using fine sand size and design the experiments by thorough understanding about the hydraulic of contractions, in a way to prevent choking and mixing different types of the contraction (i.e. short-, intermediate-, and long-contraction) the proposed equation should be able to reasonably estimate the scour depth for intermediate-contractions with medium to mild contractions subject to similar conditions as the present flume experiments.

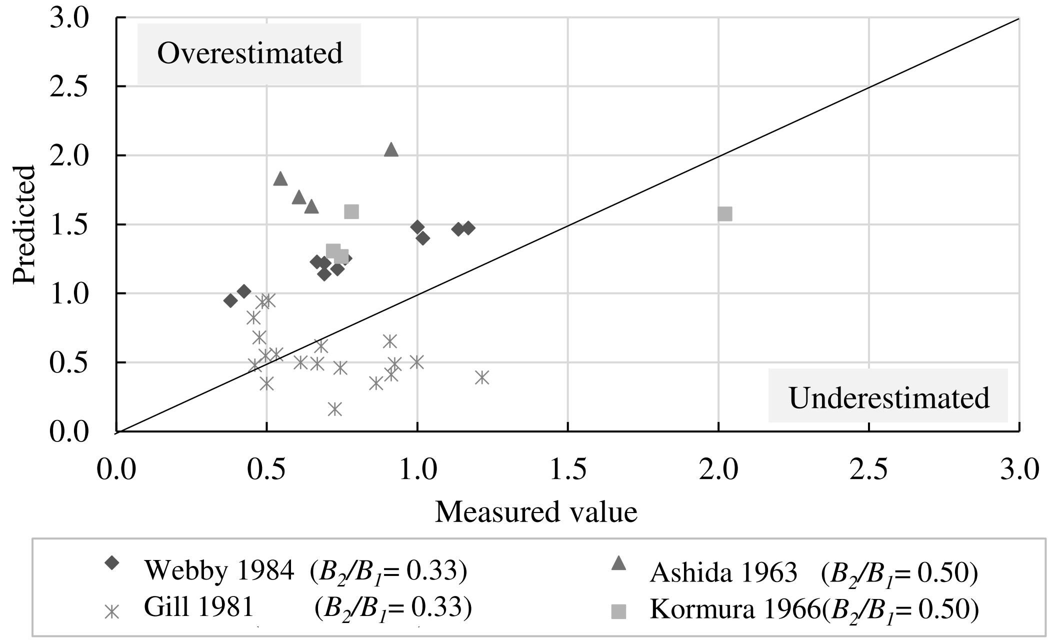

Figure 6.27. A comparison between the scour depth estimation by proposed equation and data from prior studies in the literature.

As it is shown in Figure 6.27, the proposed equation overestimated the scour-depth values reported by Webby (1984), Ashida (1963), Komura (1966) and moderately underestimates Gill's (1966) data. It is not possible to decipher the causes of these over- or under-estimates. Choking of approach flow was a common cause contributing to differences in scour depth. Other factors, such as the location of measurement and the presence of bedforms, also affected the data in the literature.

It was also possible to find a relationship for the maximum depth of corner scour. The relationship was obtained in a same manner as the relationship for average depth of scour in the vena-contracta region. The experiment setup, though, used abutments equivalent to 45˚wingwalls with infinite depth of foundation. In other words, sidewalls of the contracted section were extended to the bottom of the flume. Therefore, the setup did not replicate actual types of foundation depth as used for real bridges. Consequently, the proposed equation for corner scour depth may overestimate the scour depth, though such over-estimation may be on the safe side for design purposes;

$$\frac{D_s}{Y_{n1}} = 0.57\left(\frac{B_1}{B_2}\right)^{1.1} \left(\frac{\tau_{n1}}{\tau_c}\right)^{0.6} \quad (6.15)$$

Figure 6.28 and Figure 6.29 compare estimates obtained using the proposed equation and measured scour depths recorded for the flume experiments.

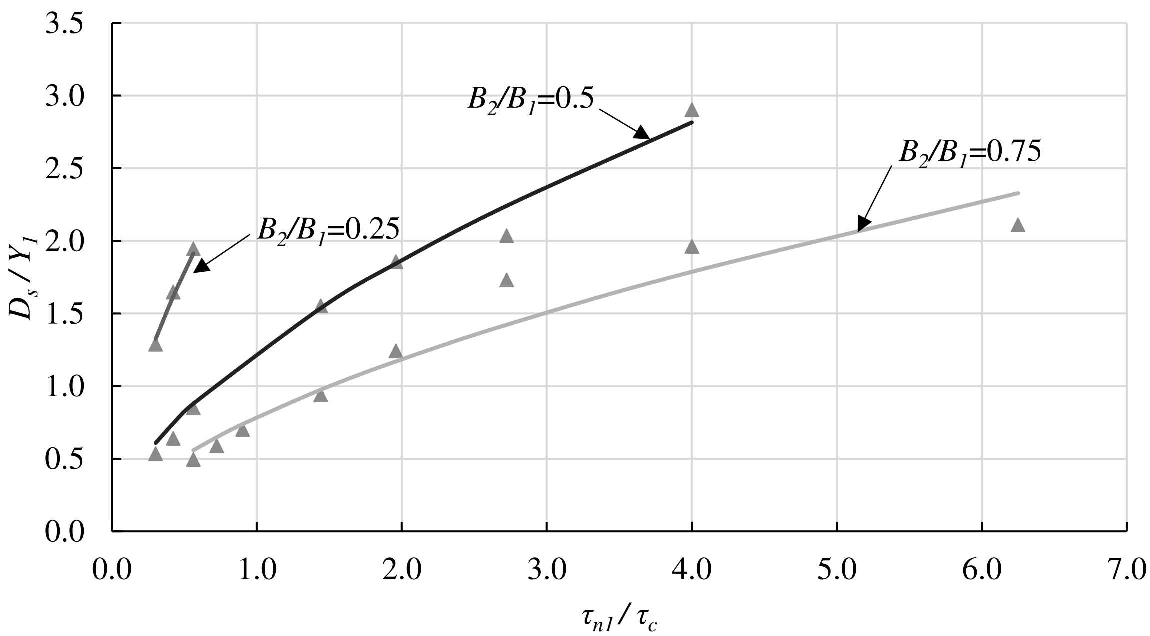

Figure 6.28. Comparison of maximum abutment scour depth estimated and measured.

Eq. (6.15) can be used for the different ranges of contraction ratio. However, due to the dominant effect of entrance shape on abutment scour depth, this equation is only applicable for 45˚ entrance transition. Figure 6.29 compares the abutment scour estimation with observations.

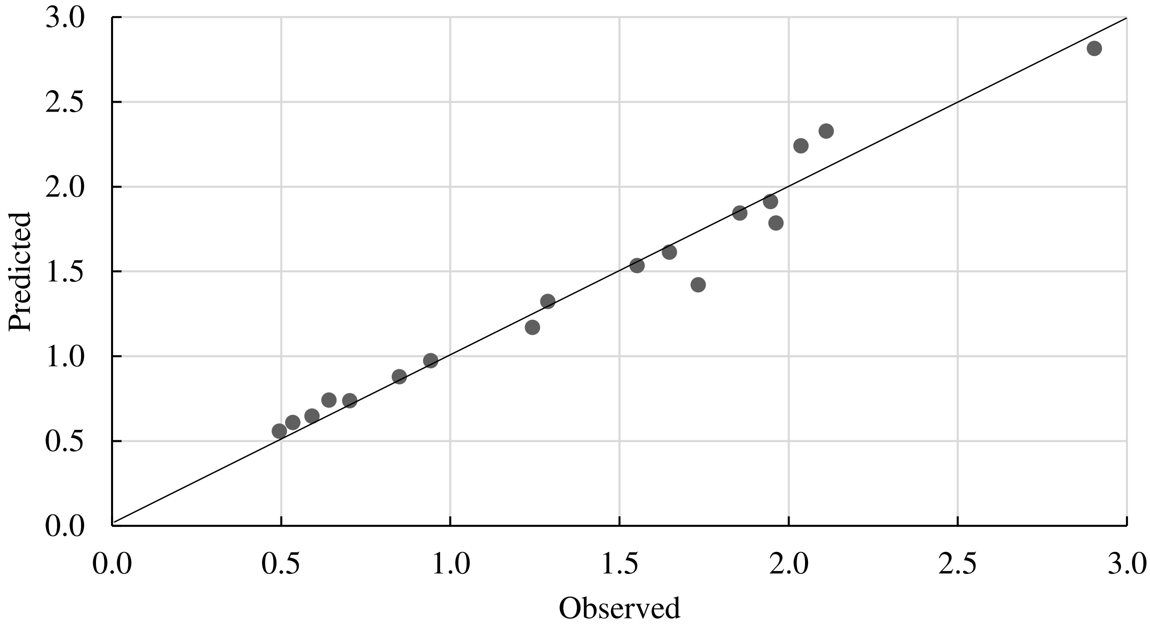

Figure 6.29. Comparison between the abutment scour depth estimation using the proposed equation and measured.

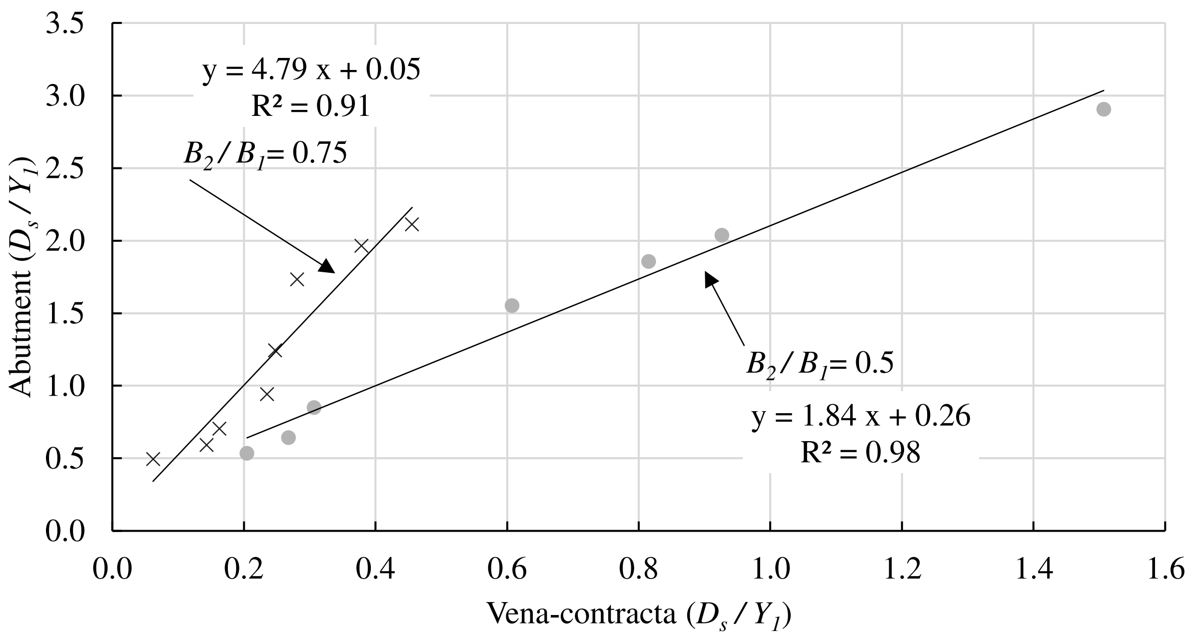

Figure 6.30. Abutment scour amplification factor compared with the average scour depth at vena-contracta.

It is also possible to compare the scour depth at the vena-contracta and the corner scour to find an amplification factor for medium and mild contractions near abutments. Figure 6.30 shows the scour depth amplification factor for a 45° transition wall with infinite depth; i.e., extending to the bottom of the bed in the flume. The corner scour depth was roughly about 1.84 and 4.79 times higher than the average-scour depth at vena-contracta for 0.5 and 0.75 contraction ratios, respectively. This difference reflects the influence on scour exerted by the flow-separation eddies developed at the abutment corners.

6.9. Discussion

Two aspects of the study are discussed here:

1. The advantages and concerns with using Y1 to estimate depth of contraction scour; and,
2. Overall trends evident in the data from the present flume experiments.

6.9.1. Practical Considerations with HEC-18

The resulting equations in HEC-18 are appealing in their apparent simplicity, especially at bridge waterways in river channels. As mentioned at the beginning of this thesis, several considerations complicate the application of more complicated equations. If the existing equations in HEC-18 estimate somewhat deeper scour, then such over-estimation can be acceptable for design purposes.

There are practical advantages in using Y_1 instead of Y_{n1}. Approach-flow depth taken as Y_1 is readily measurable and its use can compensate for the unknown effects related to channel morphology, variability of bed material and the form of the bridge itself. Also, use of Y_1 offsets the issue of assessing the narrowest width of the vena-contracta formed in the contraction entrance. It should be added that scant few field measurements of contraction scour exist for bridges waterways uncomplicated by channel complexities.

However, to be kept in mind is that Y_1 depends on characteristics of contraction and, therefore, can readily vary. Moreover, use of Y_1 to define the sediment transport condition of the approach channel when Y_1 is in a region of gradually varied flow (an M1 or backwater profile) can cause the incorrect estimation of the rate of sediment transport to the contraction. This will lead to using clear-water equation instead of live-bed equation which causes overestimation of the depth of scour. Additionally, if rates of sediment transport in the approach channel are high, the flows causing them likely will form large magnitudes of backwater depth, Y_1. The net initial effect is diminishing rate of sediment transport along the backwater approach to the contraction and deeper scour depth estimated for the contraction. Eventually, over a longer time than needed for the deeper scour to form, sediment deposition along the upstream bed will decrease the bed's slope and the contraction scour will decrease in depth as more bed sediment enters the contraction.

It also should be pointed out that, as Figure 6.17 shows, estimated scour depths for the clear-water and live-bed cases trend upward. For live-bed scour, this trend does not agree with data reported by Straub (1934), Laursen and Alawi (1989) or obtained from the present study's flume experiments. In summary, therefore, although use of Y_1 is attractive and practical for many bridge waterways, there are considerations attendant to Y_1 that should be kept in mind.

6.9.2. Trends from the Flume Data

The experiment results presented thus far are for values of the shear stress ratio τ_{n1}/τ_c varying up to 6.25, the range used in the present flume experiments. However, the insights obtained from the experiments and Chapter 2 make it possible to surmise the extended trend for larger values of τ_{n1}/τ_c. Figure 6.34 extends the trends presented in Figure 6.1 and indicates that, at high values of τ_{n1}/τ_c (well beyond the range used for the flume experiments), the depth of contraction scour may reduce as τ_{n1}/τ_c increases. This trend is further discussed below.

The contraction scour can be divided into two separate categories based on sediment movement in the approach channel; i.e., clear-water scour and live-bed scour. For clear-water scour the lack of sediment entering the contraction, the scour to increase in depth and streamwise extent by increasing the flow velocity, and, therefore, the bed shear stress increases relative to the critical shear stress associated with entrainment of the bed sediment. However, for live-bed scour, bed sediment enters the scour region and offsets the amount of bed sediment eroded during scour. A few publications in the literature suggest that category of scour may become more complicated in its trend, though (e.g., Straub 1935, Laursen and Alawi 1989)

For example, Straub (1935) presented an analytical solution for estimation of the live-bed contraction scour and indicated the scour depth would decrease, though slightly, when the shear stress ratio, τ_{n1}/τ_c, increases beyond one. He argued that, increasing this shear stress ratio from about 1 to about 1.1, would decrease scour depth by about 10%; and, that about a 5% decrease should result in the depth of the scour when the shear stress ratio increases from 2 to infinity. Laursen and Alawi (1989) offer a similar argument.

Alawi (1985) used numerical models to investigate this trend of decreasing scour depth with value of τ_{n1}/τ_c. He used different sediment transport formulas (notably, those by Einstein (1950), Maddock (1976), Laursen (1958), Yang (1973)) to estimate the depth of contraction scour. He found using most of these equations led to the same trend shown by Straub (1935), but the estimated depth of the scour varied depending on which sediment-transport equation was used in his numerical simulation. Laursen and Alawi (1989) also used flume data to show this decreasing trend, but the scour depths they report are of questionable accuracy owing to the manner whereby the scour depth was measured. Their data were from two studies done by Alawi (1981) and Laursen (1988). Both studies used the moderate contraction ratio, $B_2/B_1 = 0.5$. The resulting data are shown in Figure 6.31.

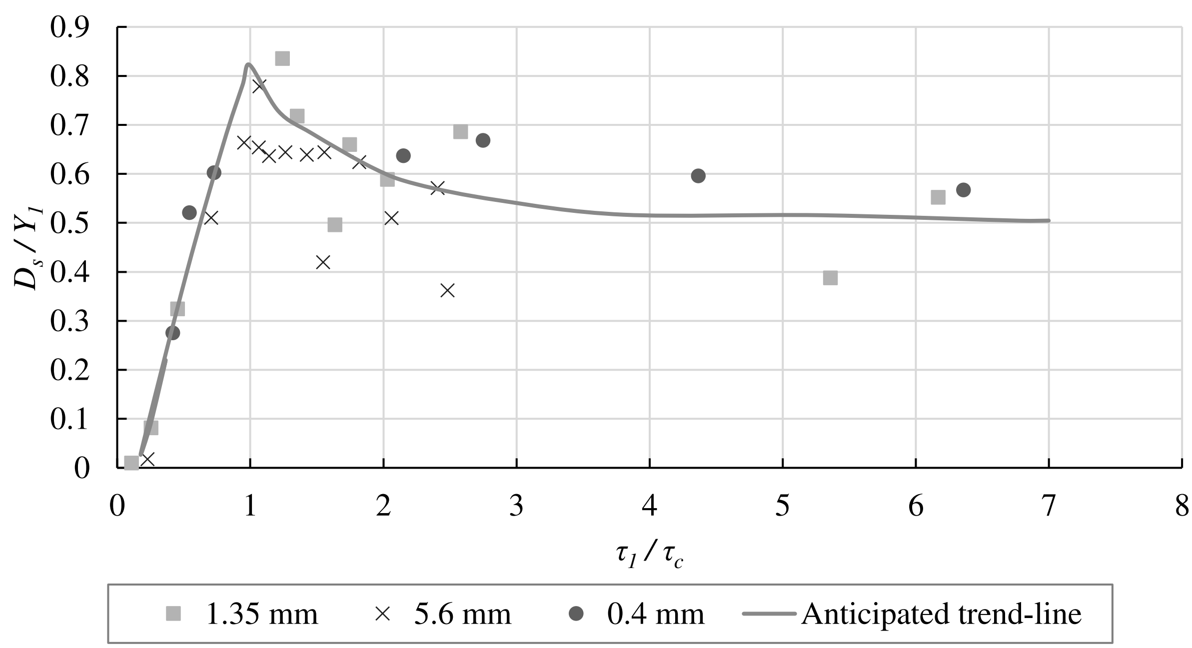

Figure 6.31. Depth of contraction scour as a function of τ_{n1} / τ_c, as per suggestion by Laursen and Alawi (1989). ($B_2/B_1 = 0.5$)

The same approach proposed by Alawi (1985) is here to compare a couple of different contraction scour estimation methods with the measured values, adjusted HEC-18, and proposed empirical equation. Figures 6.32 and 6.33 show the comparison for medium contraction (B_2/B_1=0.5) and mild contraction (B_2/B_1=0.75), respectively.

As evident from Figure 6.32 and Figure 6.33, the estimated scour depth from analytical contraction scour equations is highly susceptible to the sediment transport method which is utilized to derive the equation. This finding reflects both the difficulty in developing a reliable method or formula for estimating bed sediment transport (e.g., ASCE 2008, Julien 2018) and the likely variation of transport mode (along the bed and conveyed in suspension) as the shear stress exerted on the bed increases.

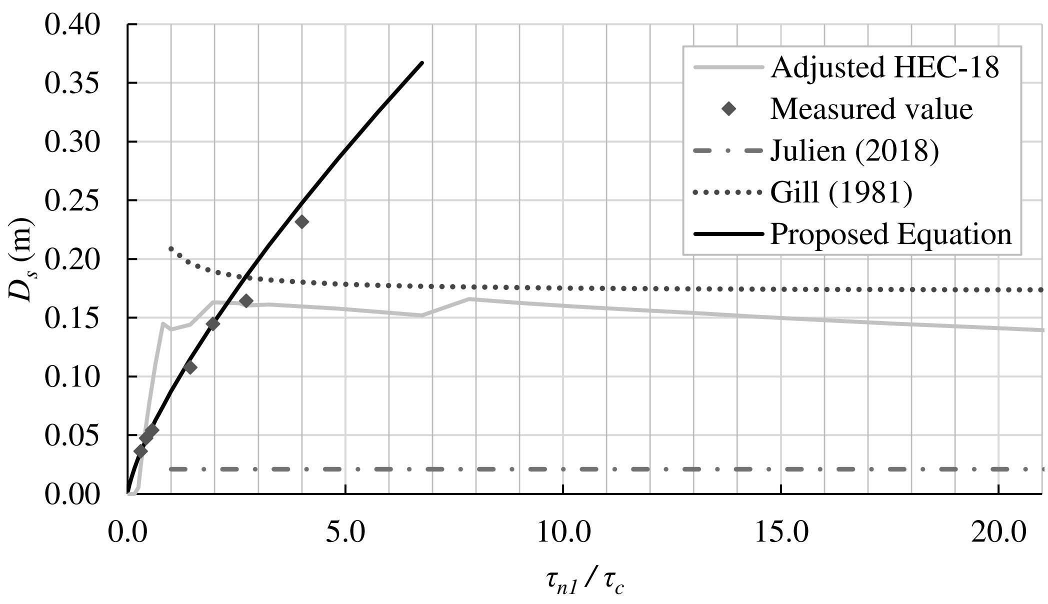

Figure 6.32. Comparison of the different contraction scour equations to estimate the depth of scour at vena-contracta (B_2/B_1=0.5)

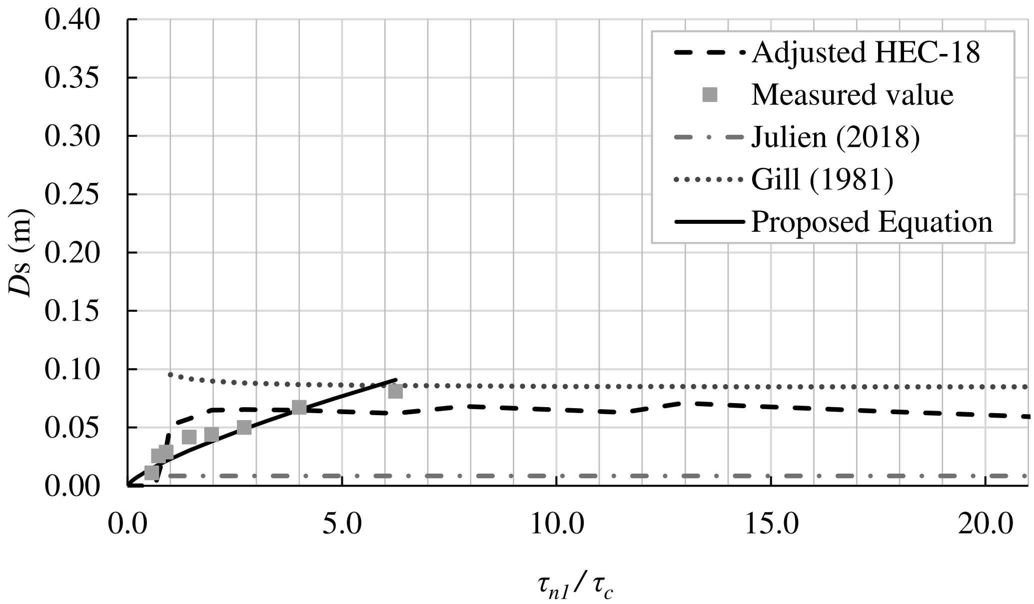

Figure 6.33. Comparison of the different equations to estimate the depth of contraction scour at vena-contracta (B_2/B_1=0.75).

The accuracy of the data reported by Laursen and Alawi (1989) in questionable, as indeed they themselves state. They used point gauges to measure bed elevation on bedform-roughened beds in the murky water. Therefore, they mentioned they had to use their judgment as to whether the point gauge hit the bed. Also, the flume used by Alawi (1981) was short (0.61m wide and only 2.14m long). He used two separate sets of experiments: one involved only an entrance transition plus 1.53 m of contracted section; and, the other experiment included an exit transition downstream of 1.53 m of contracted section at the upstream. Alawi did not report the locations of the scour depth measurements. Moreover, his experiments mixed choked and unchoked flow conditions, thereby introducing additional substantial uncertainty as to the veracity of his data.

In contrast, the results of the present study showed, for unchoked subcritical flows, the scour depth has an upward trend with a decreasing rate for the range of this study. This may bring the argument of the existence of a transitional region between clear-water and live-bed conditions.

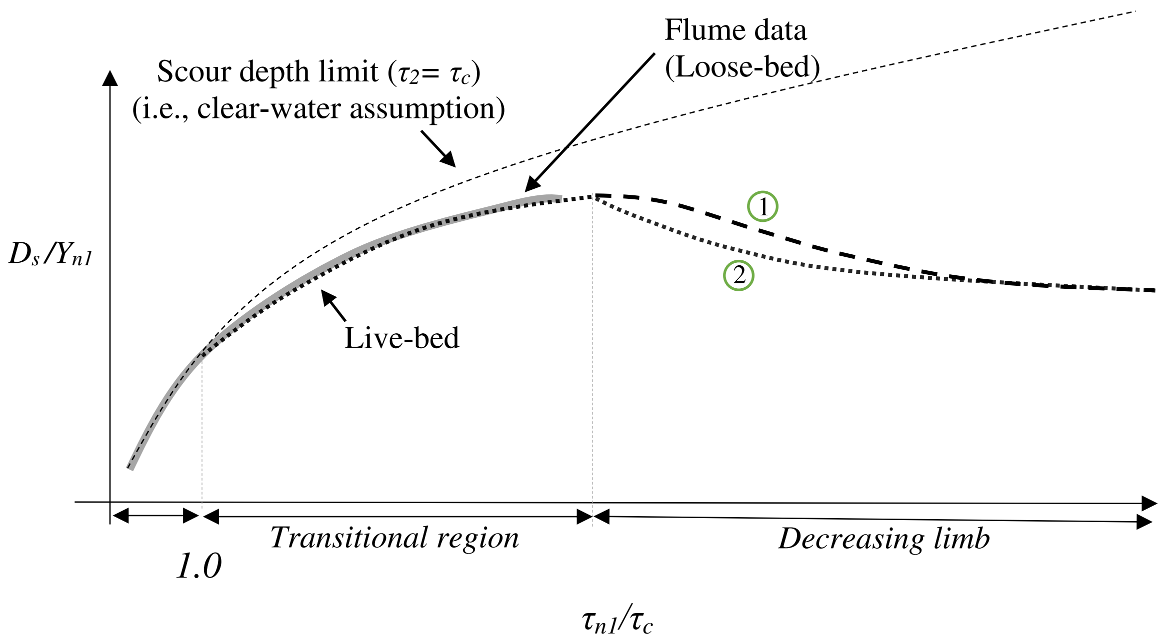

Figure 6.34. A schematic illustration of the variation of the contraction-scour depth parameter, D_s/Y_{n1}, with shear stress parameter, τ_{n1}/τ_c, along the approach channel. Indicated are the bracketing relationships for clear-water and live-bed scour, and the trend shown by the data from the present flume experiments. 1 and 2 are two different possible trends for higher shear stress ratios.

By increasing the shear stress ratio more than one the bed material at uncontracted section, i.e. approach flow, starts to move and bedforms start to develop. The development of bedforms will increase the total flow resistance and consequently will result low sediment transport rate related to the small values of shear stress ratio. In other words, the sediment feed slightly decreases the scour depth limit ($\tau_2 = \tau_c$) however does not have a dominant effect on scour depth development.

For higher shear stress ratios (i.e., higher discharges) the sediment transport substantially increases, and the scour depth decreases substantially, see

Figure 6.34. This trend is also confirmed with numerical model which is brought in Appendix F. However, as the discharge, increases, the mode of sediment transport starts to shift from bed-load to increasing suspended load. This shift in sediment transport mode will bring semi-uniform

scour depth in relation to high shear stress ratios, which is analytically showed by previous literature; e.g., Straub (1934) and Laursen and Alawi (1989).

Further studies are needed to define the continuing trend for live-bed scour for higher values of shear stress ratios. A potentially difficult factor is that such values could be associated with choked conditions and supercritical flows.

Figure 6.34 depicted two different possible trends which the second trend is more consistent with analytical equations. These trends must be verified by further investigation beyond this study.

6.10. Other sources of uncertainty

Other sources of uncertainty arise in the estimation of contraction-scour depth at bridge waterways. The sources form a lengthy list and are briefly explained here:

- Estimation of τ_c
- The approximate treatment of bed-sediment transport
- The non-uniform and unsteady development of bedforms
- The non-uniform and unsteady development of the approach bed
- Bed sediment characteristics
- The possible presence of bridge piers (or various blockage forms) in the vena contracta region
- Choking of flow to and through the contracted channel

- Other natural characteristics of the channel, e.g. having a compound cross-section or curvature.

These sources of uncertainty form topics for further investigation and are beyond the immediate scope of this dissertation, which focused on the objectives stated in Section 1.2.

As many books on sediment transport indicate (e.g., ASCE 2008, Julien 2010), there are different methods to calculate a value of the critical shear stress, τ_c, associated with incipient motion of bed sediment. Additionally, this calculation is itself subject to uncertainty; e.g., the location of particles on a bed, and the influence of the turbulence intensity of a flow. These uncertainties in τ_c values would cause slight but discernable changes in the depth of contraction scour in the vena-contracta region.

There are numerous sediment transport equations, which taken together give substantial variations in estimates of bed-sediment transport rates. The subject of estimating rate of bed-sediment transport is well-known to complications making estimation accuracy elusive. Differences in estimates of rate of bed sediment transport may introduce uncertainties in contraction-scour depth, although the trends for live-bed contraction scour infer that scour depth in the vena-contracta region has reduced insensitivity to shear-stress ratio and, therefore, rate of bed-sediment transport. Figures 6.32 and 6.33 illustrate the range of transport rates related to a small selection of transport predictors.

Due to the non-uniform water-surface profile along the contracted section the development of the bedforms varies spatially along the contracted section. The development of scour makes the flow field unsteady as scour develops and, thereby, can cause unsteadiness in bedform morphology along the contracted channel. Additionally, the elevation of the approach channel bed may change (i.e., sediment deposition in live-bed condition), owing to the backwater effect created at the entrance of the contracted channel. Consequently, the approach bed may change profile, and be further complicated by spatial variations in bedforms developed on the approach bed. Such variations detract from accurate estimation of contraction scour in the vena contracta.

The stratigraphy of the bed forming the contracted channel affects contraction-scour depth. The bed sediment variability along the contracted channel may lead to armoring of the channel's bed. Presently, there are no data or insights regarding contraction scour in channels with beds comprising non-uniform sediment. It can be assumed that trends regarding non-uniformity of bed sediment obtained for scour at bridge piers (e.g., Raudkivi and Ettema 1983, Chiew and Melville 1989). The present experiments showed regions of sediment sorting, where dense fine sediment (specific gravity of 5.2) accumulated on several bedforms. Further work is needed in this regard. Also, the sediment stratification will affect the contraction scour depth. This aspect of contraction scour, and scour generally, has received little attention.

The presence of piers inside the contracted section can reduce the effective width of the contraction and induce vortex shedding. This process needs further investigation, but points to pier presence increasing depth of clear-water contraction scour, as flow velocities increase and the flow conveys increased intensities of turbulence, both of which aid sediment entrainment. It is a process that is unmentioned in the recent NCHRP study (NCHRP 24-37, Sturm et al. 2018), which considered how scour at bridge components combine.

Flow choking alters the flow field at the entrance and along a contracted channel, and thereby affects contraction scour. Chapter 2 of this dissertation explains how choking affects the flow field. For many contractions, choking can occur at sufficiently large values of shear stress ratio and thus alter the trend between scour depth and shear-stress ratio. The altered relationship was overlooked by all prior studies, with the consequence of substantial scatter in data on scour depth.

As a result of the inherently complex nature of contraction scour, the introduced method can only give an approximate estimate of contraction-scour depth. Too many sources of uncertainty compromise estimate accuracy. Yet to be investigated, for example, is contraction scour for conditions when flow passes from a main channel's floodplain(s) through a bridge waterway.

7. Conclusion and Recommendations

Presented here are the main conclusions drawn from the observations of the flume experiments. The conclusions directly relate to the objectives for this study (Section 1.2). Also, presented are recommendations for further research aimed at improving understanding of contraction scour at open-channel contractions, especially bridge waterways. The channel contractions of interest for this study were contractions associated with rivers at bridge waterways. Moreover, the contractions were taken to occur along a river channel that was initially uniform in width. This arrangement is representative of bridge-waterways placed in rivers having a single main channel and no floodplain. Not included in this study are channels with a substantial floodplain or channels with substantial curvature. However, the conclusions and recommendations stemming from this study also apply to such channels.

This study treated contraction scour in terms of three categories based on the water-surface profile produced by sub-critical flow along a contracted channel of varying length; i.e.,

- Short-length contractions, which are shorter than about one to two times of the width of the approach channel and the water surface profile is controlled by the depth of uniform flow downstream of the contracted channel. Open-channel flow considerations associated with rapidly varied flow indicate that these contractions are shorter than about one to two times the width of the approach channel. Further, these contractions are sufficiently short that the flow separation at the upstream end of the contraction extends to the downstream end of the contraction;

- Intermediate-length contractions, for which the water-surface profile is influenced by the length of the contracted channel and controlled by the depth of uniform flow downstream of the contracted channel. Also, for these channels, the flow separation at the upstream end of the contraction is included within the length of the contraction; and,
- Long-length contractions, for which the water-surface profile is controlled by the depth of uniform flow along the contraction. These channels are sufficiently long that they develop uniform flow (normal flow conditions).

Of focal interest for this study was the second category of contracted channel, as this is the more general condition of channel contraction. Contraction hydraulics for this category is influenced by contraction length and applies to bridge waterways involving multiple bridges and channels contracted by a series of channel-narrowing instream structures. Bridge waterways formed by single- or dual-lane results tend to be short contractions, because the bridge waterway is, in most cases, less than about one width of the approach channel.

A review of existing literature shows that all prior studies of contractions scour (e.g., Laursen 1960, 1960) dealt with either short contractions or contractions of intermediate length. Those prior studies did not account for the effect that length of contracted channel exerts on the water-surface profile and, thereby, the reported depth of contraction scour. Prior studies assumed water depth to be constant along the contracted channels they considered (e.g., the studies cited above).

7.1. Conclusions

The following main conclusions can be drawn from this study:

1. The description of the hydraulics associated with contractions of open channels (Chapter 2) was needed to explain the results of the flume experiments. Such a description was lacking in all prior studies of contraction scour. This lack indicates that prior studies did not adequately consider the flow field associated with scour along contracted channels and the flow-related complexities involved in contraction scour;
2. For sub-critical flow along a contracted open channel, the control section is located at the downstream end of the contracted channel. Consequently, contraction scour is influenced by the depth of flow at the downstream end of the contraction; rather than the flow depth at the entrance to the contracted channel. The flow approach to a contracted channel is non-uniform and assumes the form of an M1 (backwater) gradually varied flow profile. The water-surface profile along a contracted channel of intermediate length conforms with an M2 (drawdown) gradually varied flow profile. The flow profile at the exit of the contraction is taken to be associated with uniform flow through the initially uncontracted channel;
3. Choking occurs when the approach flow and flow along the contracted channel have insufficient specific energy (energy relative to channel bed) to pass through the contraction without increasing in flow depth so that the flow becomes super-critical as it enters the contracted channel and, thereby, alters the flow-field at the contraction entrance. Flow choking is defined in textbooks on open-channel flow (e.g., Henderson 1964). Previous studies mixed choking and no-choking conditions (e.g., Dey and Raikar 2005, Gill 1981, Webby 1984). A new insight from this study is that choking can occur first at the exit of a

contracted channel of intermediate length, and then at the channel's entrance, the present study was limited to no-choking of flow at the contraction exit or entrance;

4. For the category termed intermediate-length contractions, the measured depth of contraction scour along the contracted channel was not constant. Instead, the bed shear stress varied along the contraction and caused the bed-surface profile to become shaped like a gently curved mound. The deepest zones of scour occurred in the vena contracta region and at the end of the contracted channel (barring corner scour). The form of the mound was complicated by the non-uniform development of bedforms along the contracted channel. The flume experiments showed that the dimensions of the bedforms varied spatially with distance along the contracted channel. This spatial variation occurred due to the variation of bed shear-stress along the contracted channel;
5. Considerations of open-channel hydraulics indicates that depth of scour along the intermediate-length contraction will vary as the length of the contracted channel varies. Lengthening the contracted channel increases the energy dissipation along the channel which decreases the bed shear stress at the contraction entrance. The analyses associated with the contraction-scour equations in HEC-18 (Arneson et al. 2012) do not account for the effect of contraction length;
6. The flow entering a contracted channel forms a vena contracta, whereby the actual width of the contracted flow is less that the width of the contracted channel. To improve the accuracy of scour-depth estimation using HEC-18 equations, the width of flow in the vena-contracta should be used instead of the width of the contracted channel. Additionally, the HEC-18 equations apply only to the vena contracta region because that region best replicates the concepts upon which the equations were formulated, especially clear-water formula;

7. Though it is convenient to define approach flow sediment transport condition, i.e., clear-water or live-bed, in terms of the flow depth measured at near the approach to a contracted channel (say, at a bridge waterway), that flow depth is within the backwater water-surface profile created by the contracted channel. It is more correct to use the normal depth associated with the approach flow, because this depth depends only on the approach-channel characteristics. Consequently, the definition of intensity of bed-sediment transport in the approach flow should be based on a shear-stress estimate using the uniform depth, i.e., normal depth of approach flow. The bed shear stress and consequent intensity of sediment transport would vary along the backwater profile;
8. The overall trends for depth of contraction scour in the vena-contracta region are delineated qualitatively in Figure 6.1. This figure shows that, when the bed shear stress along the approach bed causes bed-sediment transport along the approach bed and into the contracted channel (i.e., the shear-stress ratio exceeds one), the depth of contraction scour does not increase as markedly as when the bed shear-stress increases without an inflow of bed sediment. In other words, the deepening of scour during the so-called live-bed situation condition of scour does not occur as markedly as it does for the so-called in comparison with the clear-water situation. This finding is supported by the data trend obtained from the flume experiments. However, the trend is not reflected in the contraction-scour equations presented in HEC-18 and nor is it expressed in the equations developed by Straub (1934) or Laursen and Alawi (1984). Other prior studies do not even consider general trends for contraction scour (e.g., Dey and Raikar 2005, Webby 1984). Also, complicating the trends for high values of bed shear stress is the fact that greater proportions of bed sediment move in suspension rather than move as bedload. Therefore, the balance assumed for equilibrium

of live-bed scour should only apply to bedload entering the vena-contracta region, because the suspended load passes over the region of contraction scour. This statement requires further investigation, as mentioned below;

9. The widely used equations (HEC-18 or Arneson et al, 2012), for estimating depth of contraction scour can be adjusted to include a coefficient for estimating the minimum width of the vena contracta. The adjustments were made to the equations used for the clear-water and live-bed conditions of contraction scour and are given in Eqs. (6.7) -(6.10) of Chapter 6. The adjusted equations yielded results that agreed well with the measured depths of contraction scour in the vena contracta region;
10. An equation based on dimensional analysis and nonlinear-regression analysis was developed from the measured data obtained from the flume experiments. This equation agreed well with the data, and could be considered for use when estimating contraction scour in channels whose beds are formed of fine sand bed and shear stress ratio is within the range used for this study;
11. The depth-averaged-flow code SRH-2D did not correctly simulate the scour depth along the whole contraction, specially near the entrance corners, due to the 3D structure of the flow near corners. However, the model can be used with some error (depending on the sediment transport method used) to estimate the average scour depth at vena-contracta region. More information regarding the results are given in the Appendices E and F.

7.2. Recommendations for Further Research

The following recommendations come to mind regarding further investigation:

1. The values of vena-contracta coefficient K_v should be determined for different entrance shapes, notably shapes typical of bridge abutments, which form the entrance to bridge waterways. Laboratory experiments are needed to obtain the values, because numerical models presently seem not to handle the flow-separation regions suitably accurately;
2. Values of K_v should be determined for conditions preceding contraction scour, during contraction scour and after contraction scour;
3. Research is needed to determine the characteristics and trends that occur when the flow is choked at the exit or entrance of a contracted channel. This condition is common for short-span, masonry arch bridges, because the flow area decreases as flow depth (or elevation) increases;
4. Extensive experiments need to be run for beds comprising non-uniform sediment. Such beds would exhibit armoring. The present flume experiments indicated how contraction scour (and corner scour) are likely rather sensitive to armoring. Contraction scour occurs principally in the vena-contracta region, which is considerably narrower than the gross width of a contracted channel;
5. Experiments should be run for ranges of shear-stress ratio greater than those used in the present study. These experiments are needed to confirm or modify the conceptual trend shown in Figure 6.32;
6. Experiments should be run for ranges of contraction length. These experiments are needed to confirm the effect of contraction length on scour depth along the contraction channels of intermediate length; and,
7. The influence on contraction scour exerted by pier presence should be investigated. Pier presence modifies the vena contracta region and generates turbulence in the region.

References

Alawi, A. J. (1985). “Some Contributions to The Study of Scour in Long Contractions.” PhD thesis, University of Arizona, Tucson, AZ.

ANSYS Inc. (2018). ANSYS Fluent user’s guide, Canonsburg, PA.

Arneson, L. A., Zevenbergen, L. W., Lagasse, P. F., and Clopper, P. E. (2012). HEC 18: Evaluating Scour at Bridges. Fifth Edition. Hydraulic Engineering Circular, Washington, D.C.

ASCE. (2008). Sedimentation Engineering. Manual of Practice 110. The American Society of Civil Engineers (ASCE), Reston, VA.

Ashida, K. (1963). Study on the stable channel through constrictions. Ann. Rept, Disaster Prevention Center, Kyoto, Japan. (In Japanese).

Benedict, S. T. (2003). Clear-Water Abutment and Contraction Scour in the Coastal Plain and Piedmont Provinces of South Carolina, 1996-99, The U.S. Geological Survey, Rept. 03-4064, Columbia, SC.

Benedict, S. T., and Caldwell, A. W. (2009). Development and Evaluation of Live-Bed Pier- and Contraction-Scour Envelope Curves in the Coastal Plain and Piedmont Provinces of South Carolina. SC.

Bettess, R. (2002). “A Review of Predictive Methods for General Scour.” Proc. First International Conference on Scour of Foundations, ICSF-1, Houston, TX.

Bihs, H., and Olsen, N. R. B. (2007). “Three-Dimensional Numerical Modeling of Contraction Scour.” Proc. 32nd IAHR Congress, Venice, Italy.

Briaud, J.-L., Chen, H.-C., Li, Y., Nurtjahyo, P., and Wang, J. (2005). “SRICOS-EFA Method for Contraction Scour in Fine-Grained Soils.” ASCE Journal of Geotechnical and Geo Environmental Engineering, 131(10), 1283–1294.

Chanson, H. (2004). Environmental Hydraulics of Open Channel Flows. Environmental Hydraulics for Open Channel Flows, Elsevier, Amsterdam, The Netherlands.

Chiew, Y., and Melville, B. (1989). “Local Scour at Bridge Piers with Non-uniform Sediments.” Proceedings of the Institution of Civil Engineers, 87(2), 215–224.

Chow, V. T. (1959). Open-channel hydraulics. McGraw-Hill Civil Engineering Series, McGraw-Hill, New York, NY.

Dey, S., and Raikar, R. V. (2006). “Scour in Long Contractions.” International Journal of Sediment Research, 21(2), 166–170.

Dey, S., and Raikar, R. V. (2005). “Scour in Long Contractions.” ASCE, Journal of Hydraulic Engineering, 131(12), 1036–1049.

Duc, B. M., and Rodi, W. (2008). “Numerical Simulation of Contraction Scour in an Open Laboratory Channel.” ASCE, Journal of Hydraulic Engineering, 134(4), 367–377.

Einstein, H. A. (1950). “The Bedload Function for Sediment Transport in Open Channel Flows.” U.S. Department of Agriculture, Soil Conservation Service, No.1026.

Ettema, R., Nakato, T., and Muste, M. (2010). Estimation of Scour Depth at Bridge Abutments. Online Rept. for NCHRP 24-20, National Cooperative Highway Program, Washington, D.C.

Fakhri, A. (2020). “Applications and Limitations of Large-scale Particle Image Velocimetry.” MS Thesis, Colorado State University, Fort Collins, CO.

Froehlich, D. C. (1995). “Armor-Limited Clear-Water Contraction Scour at Bridges.” ASCE, Journal of Hydraulic Engineering, 121(6), 490–493.

Gill, M. A. (1981). “Bed Erosion in Rectangular Long contraction.” ASCE, Journal of Hydraulics Division, 107(HY3), 273–284.

Grant, G. E. (1997). “Critical Flow Constrains Flow Hydraulics in Mobile-bed Streams: A new Hypothesis.” Water Resources Research, American Geophysical Union.

Guy, H. P., Simons, D. B., and Richardson, E. V. (1966). “Summary of Alluvial Channel Data from Flume Experiments, 1956-61.” U.S. Geological Survey Water Supply Paper, 462–I, 1–96, Reston VA.

Henderson, F. M. (1966). Open Channel Flow. Macmillan Series in Civil Engineering, Macmillan. London, U.K.

Hong, S., Gotvald, A., Sturm, T. W., and Landers, M. (2006). “Laboratory and Field Measurements of Bridge Contraction Scour.” Proc. 3rd Intl. Conf. on Scour and Erosion, Gouda, The Netherlands.

Julien, P. Y. (2010). Erosion and sedimentation, Second edition. Erosion and Sedimentation, 2nd Edition, Cambridge University Press, Cambridge, U.K.

Julien, P. Y. (2018). River Mechanics. Cambridge University Press, Cambridge, U.K.

Keller, R. J. (1977). “General Scour in a Long Contraction.” Min. of Works Dept., Central Laboratories Report No 3-77/1, Lower Hutt, New Zealand.

Keller, R. J. (1983). “General Scour in a Long Contraction.” Proc. XX Congress, Intl. Assoc. of Hydraulic Research, Moscow, USSR, Sept. 5-9.

Koken, M. (2017). “Coherent Structures at Different Contraction Ratios Caused by Two Spill-through Abutments.” Journal of Hydraulic Research, Intl. Assoc. of Hydraulic Research, 56(3), 324–332.

Koken, M., and Constantinescu, G. (2007). “An Investigation of Coherent Structures in the Wake of a Bridge Abutment at Equilibrium Bed Scour Conditions.” Restoring Our Natural Habitat – Proc. World Environmental and Water Resources Congress, Tampa, FL.

Komura, S. (1966). “Equilibrium Depth of Scour in Long Contractions.” ASCE, Journal of Hydraulics Division, 92(HY5).

Lagasse, P. F., Clopper, P. E., Zevenbergen, L. W., Spitz, W. J., and Girard, L. G. (2010). Effects of Debris on Bridge Pier Scour, NCHRP Report 653, National Cooperative, Highway Research Program, Washington, D.C.

Lagasse, P. F., Ghosn, M., Johnson, P. A., Zevenbergen, L. W., and Clopper, P. E. (2013). Reference Guide for Applying Risk and Reliability-Based Approaches for Bridge Scour Prediction- NCHRP Report 761, National Cooperative Highway Research Program, Washington, D.C.

Lai, Y. G., and Greimann, B. P. (2010). “Predicting Contraction Scour with a Two- dimensional Depth-averaged Model.” Journal of Hydraulic Research, Intl. Assoc. of Hydraulic Research, 48(3), 383–387.

Landers, M. N., and Mueller, D. S. (1996). Channel Scour at bridges in the United States. Rept. FHWA-RD-95-184, U.S. Geological Survey, Washington, D.C.

Laursen, E. M. (1958). “The Total Sediment Load of Streams.” ASCE, Journal of the Hydraulics Division, 84(1), 1–36.

Laursen, E. M. (1960). “Scour at Bridge Crossings.” ASCE, Journal of Hydraulics Division, 86(HY2), 39–54.

Laursen, E. M. (1963). “An Analysis of Relief Bridge Scour.” ASCE, Journal of the Hydraulics Division, 89(1), 93–118.

Laursen, E. M. (1988). Scour in Supercritical Flow. Arizona Department of Transportation, Report FHWA-AZ88-208, Phoenix, AZ.

Laursen, E. M., and Alawi, A. J. (1989). “The Effects of Velocity on Scour.” Proc. of Sediment Transport Modeling, International Symposium, 441–455.

Lim, S.Y., and Cheng, N.S. (1998). “Scouring in Long Contractions.” ASCE, Journal of Irrigation and Drainage Engineering, 124(5), 258–261.

Madden, E. B. (1993). Modified Laursen Method for Estimating Bed-Material Sediment Load. Rept. HL-93-3, U.S. Army Corps of Engineers, Washington, DC.

Maddock, T. (1976). “Equations for Resistance to Flow and Sediment Transport in Alluvial Channels.” AGU, Journal of Water Resources Research, 12(1), 11–21.

Marek, M., and Dittrich, A. (2004). “3D Numerical Calculations of the Flow in an Open-channel Consisting of an Expansion and Contraction.” Proc. 6th Intl. Conf. Hydro-Science and Engineering, Brisbane, Australia.

Morales, R., and Ettema, R. (2013). “Insights from Depth-averaged Numerical Simulation of Flow at Bridge Abutments in Compound Channels.” ASCE, Journal of Hydraulic Engineering, 139(5), 470-481.

Mueller, D., and Wagner, C. (2005). Field Observation and Evaluations of Streambed Scour at Bridges. US Department of Transportation, Federal Highway Administration, Louisville, KY.

Raudkivi, A. J., and Ettema, R. (1983). “Clear-Water Scour at Cylindrical Piers.” ASCE, Journal of Hydraulic Engineering, 109(3), 338–350.

Solan, B., Ettema, R., Ryan, D. and Hamill, G. (2020). “Scour Concerns at Short-Span Masonry Arch Bridges.” ASCE, Journal of Hydraulic Engineering, 146(2), doI.ORG/10.1061/(ASCE)HY.1943-7900.0001675.

Straub, L. G. (1934), “Effect of channel-contraction works upon regimen of movable bed-streams.”, Eos Trans. AGU, 15(2), 454– 463, doi:10.1029/TR015i002p00454.

Sturm, T., Abid, I., Melville, B., Xiong, X., Stoesser, T., Bugallo, B. F., Chua, K. V., Abt, S., and Hong, S. (2018). “Combining Individual Scour Components to Determine Total Scour. Transportation Research Board”. Web-Only Doc. 249, NCHRP Project 24-37, National Cooperative Highway Research Program, Washington’, D.C.

Sturm, T. W. (2001). “Open channel hydraulics.” McGraw-Hill, New York, 493 pp.

Trieste, D. J. (1992). “Evaluation of Supercritical/Subcritical Flows in High Gradient Channel.” ASCE, Journal of Hydraulic Engineering, 118(8), 1107–1118.

Wagner, C. R., Mueller, D. S., Parola, A. C., Hagerty, D. J., and Benedict, S. T. (2006). "Scour at Contracted Bridges". Web-Onlty Doc 84, National Cooperative Highway Research Program, Washington D.C.

Webby, M. G. (1984). "General Scour at a Long Contraction." Proc. Bridge Design and Research Seminar, New Zealand, Auckland, 109–118.

Weise, S. (2002). "Verifikation eines Zweidimensionalen Feststofftransportmodells anhand von Hydraulischen Versuchen." Diplomarbeit. Fachhochschule für Technik, Wirtschaft und Kultur, Leipzig, Germany.

Yang, C. T. (1973). "Incipient Motion and Sediment Transport." ASCE, Journal of the Hydraulics Division, 99(10), 1679–1704.

Yang, C. T. (1979). "Unit Stream Power Equations for Total Load." Elsevier Journal of Hydrology, doi: 10.1016/0022-1694(79)90092-1.

Zey, S. S. (2017). "Flow Field at Open-Channel Contractions: Insights from a Two-Dimensional Numerical Model." MS Thesis, Colorado State University, Fort Collins, CO.

Appendix A: Available Clear-water Data

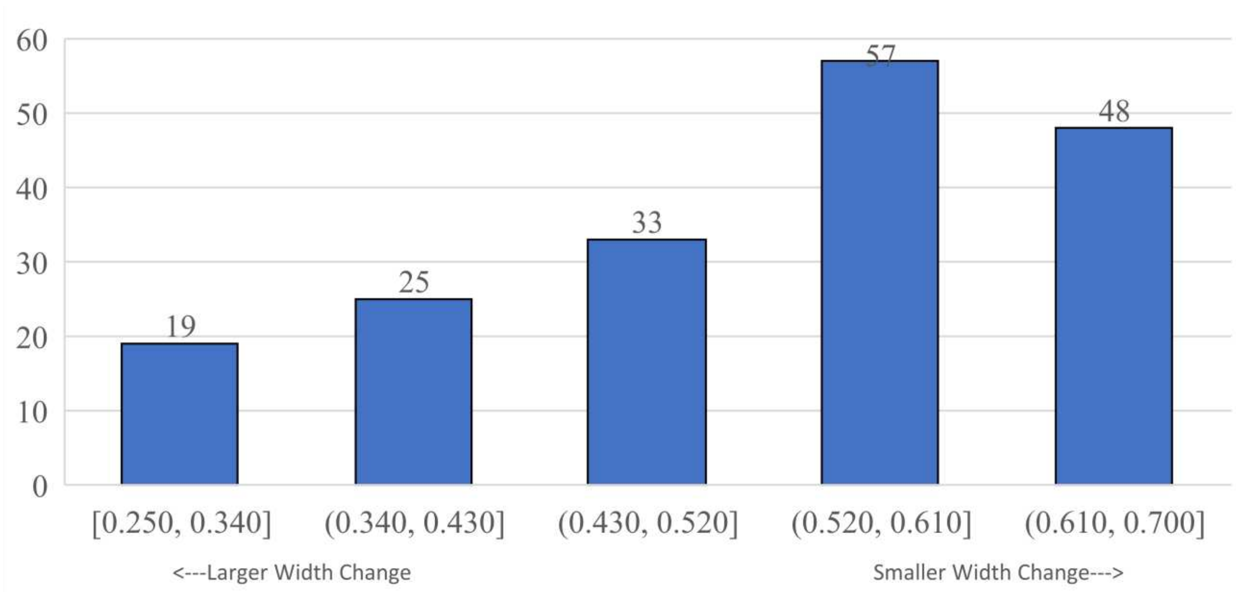

Figure A.1. Clear-water data; Contraction ratio (B_2/B_1)

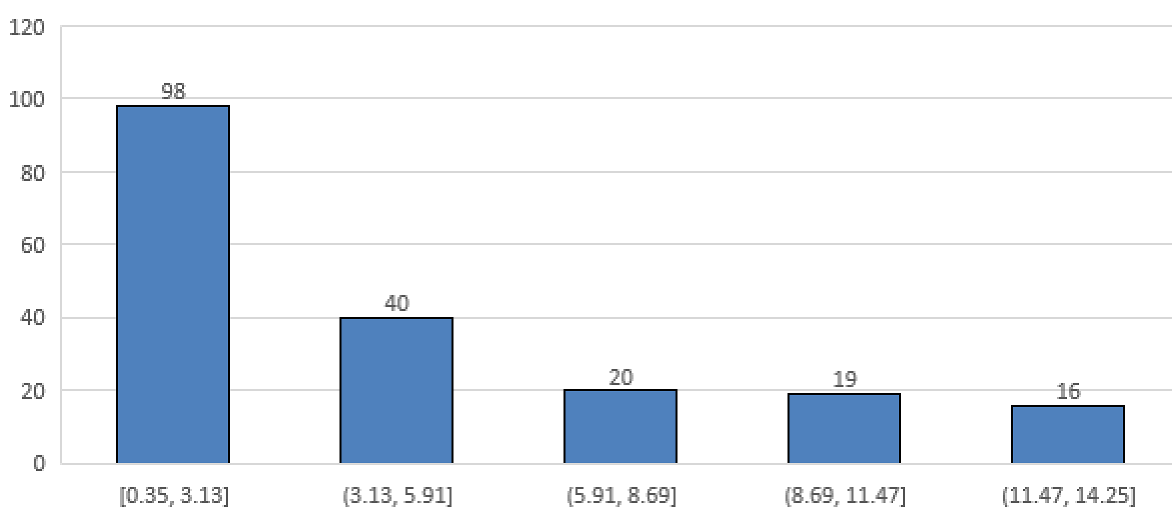

Figure A.2. Mean sediment diameter (D_{50})

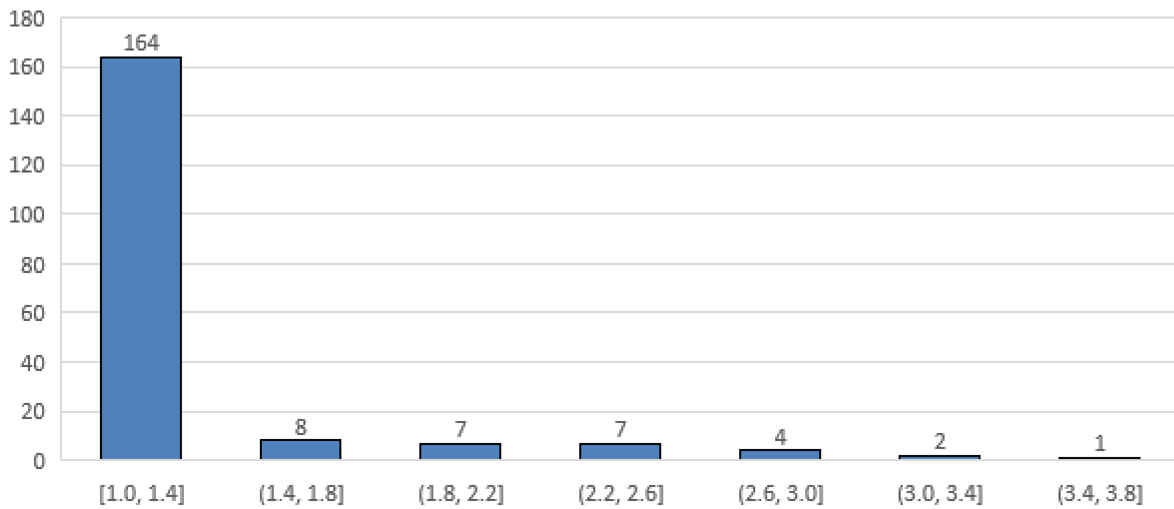

Figure A.3. Geometric standard deviation of grain size.

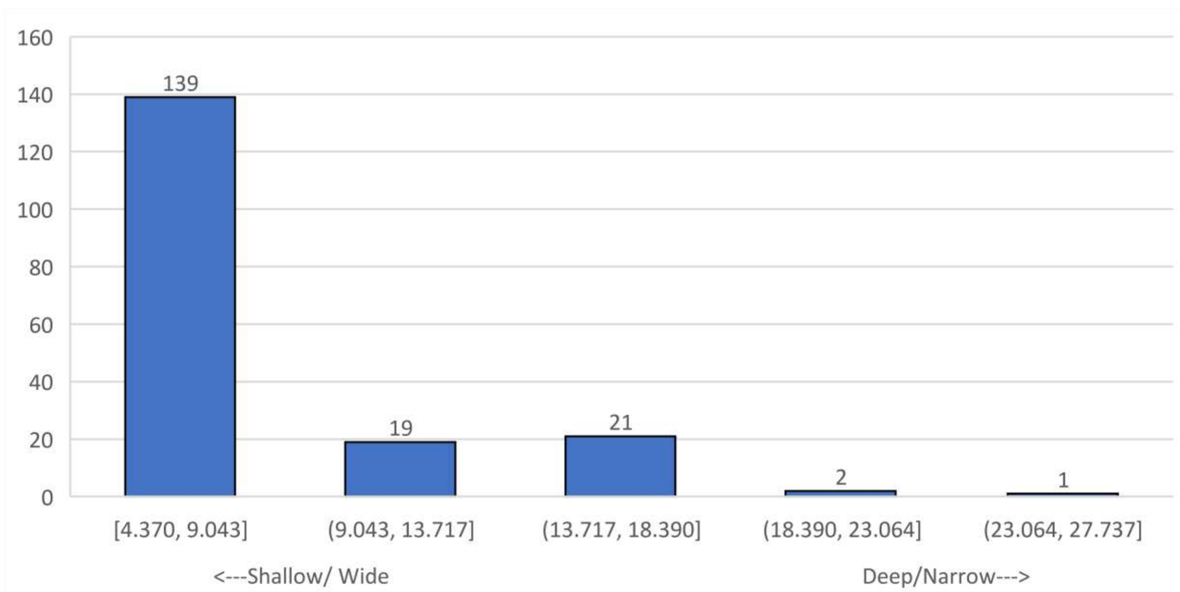

Figure A.4. Clear-water data; relative width (B_1 / Y_1).

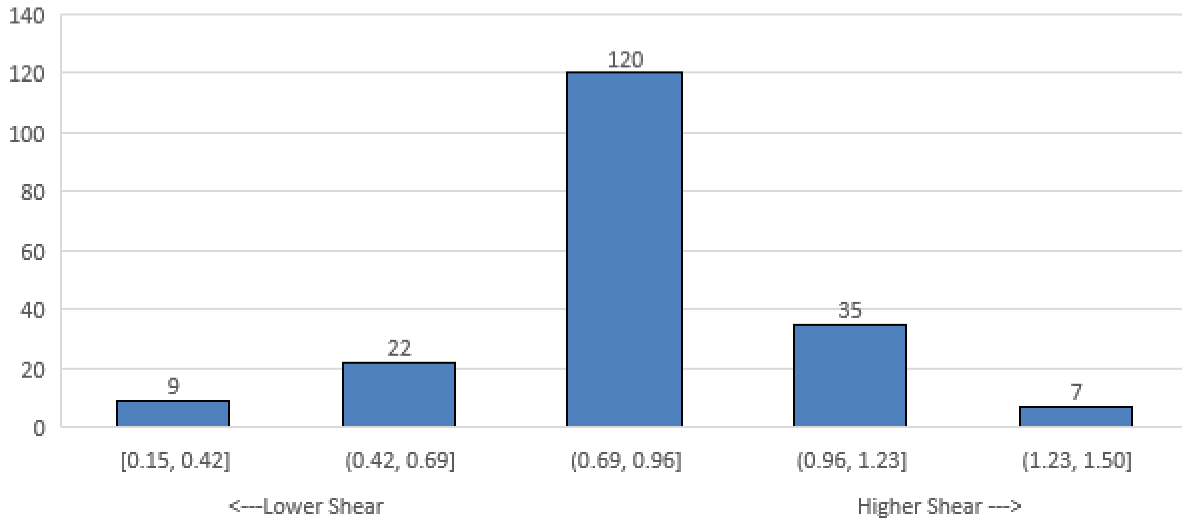

Figure A.5. Clear-water data; shear stress ratio (τ_1 / τ_c).

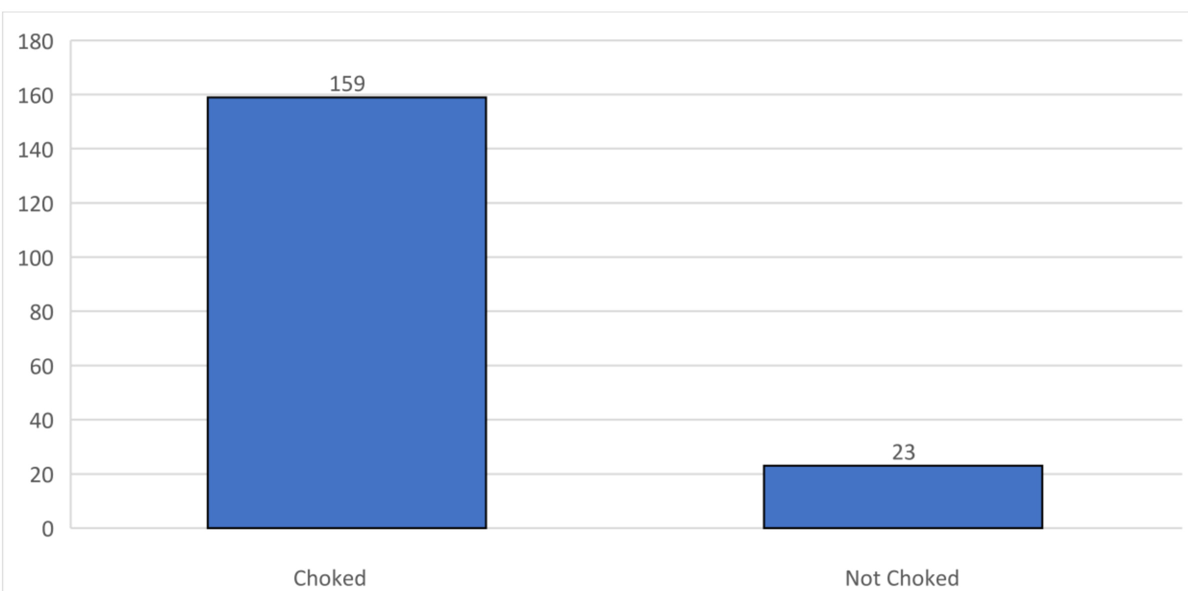

Figure A.6. Clear-water data; choked vs. not choked.

Appendix B: Available Live-bed Data

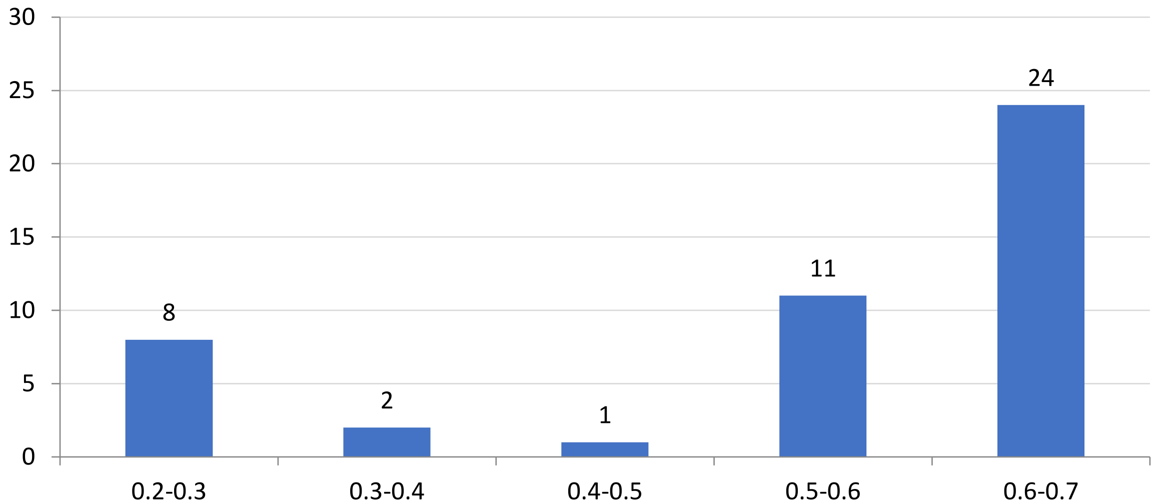

Figure B.1. Live-bed data; Contraction ratio (B_2/B_1)

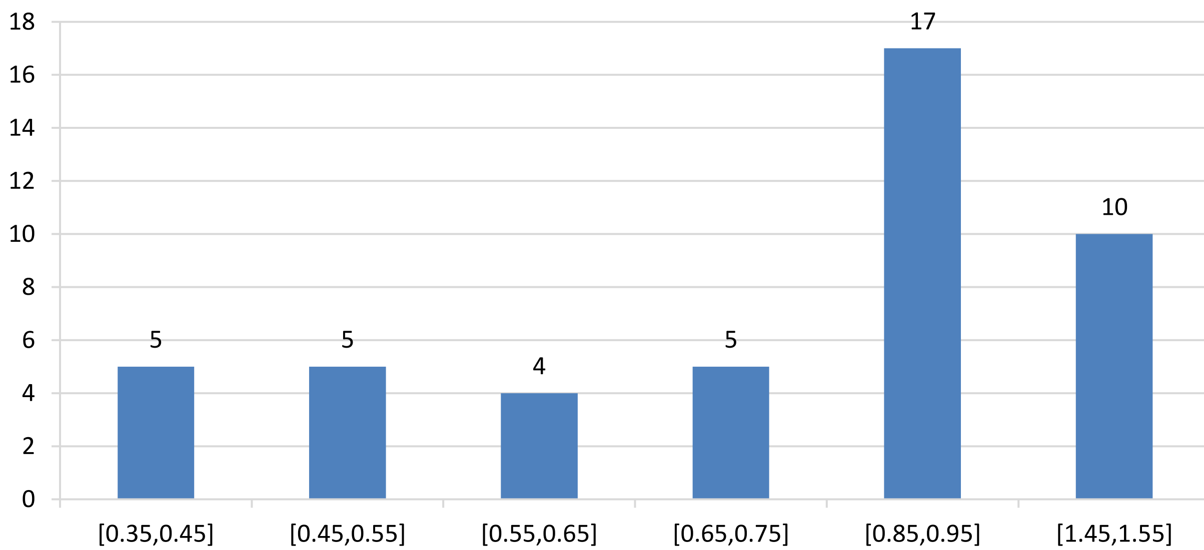

Figure B.2. Live-bed data; Mean sediment diameter (D_{50}).

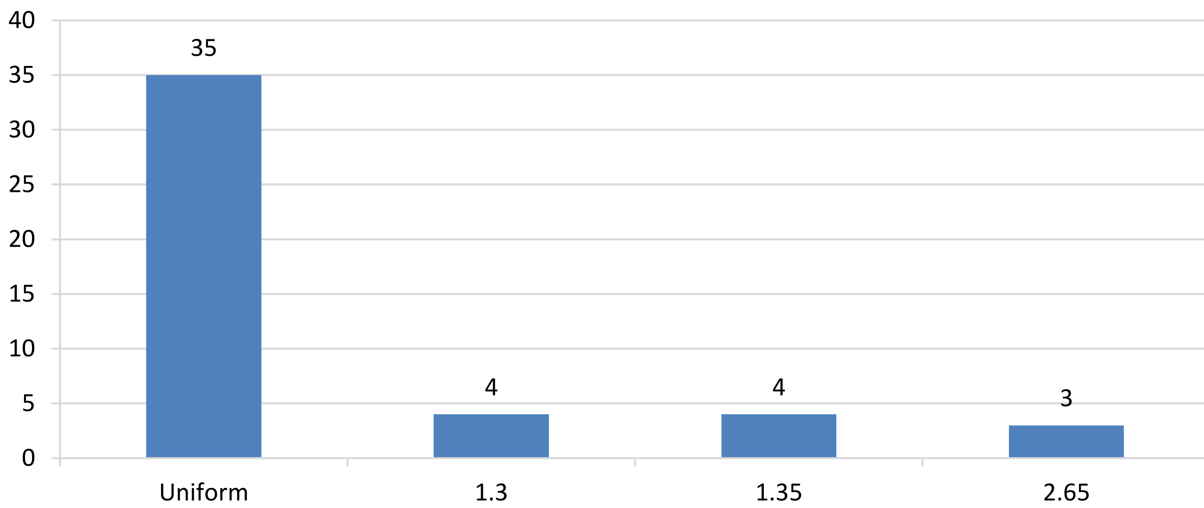

Figure B.3. Geometric standard deviation of grain size.

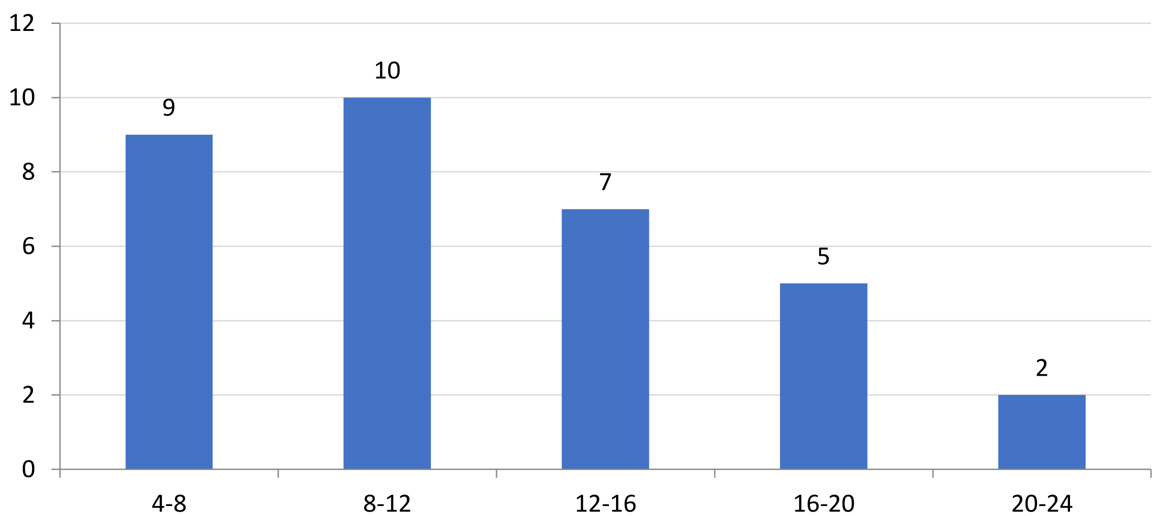

Figure B.4. Live-bed data; relative width (B_1/Y_1).

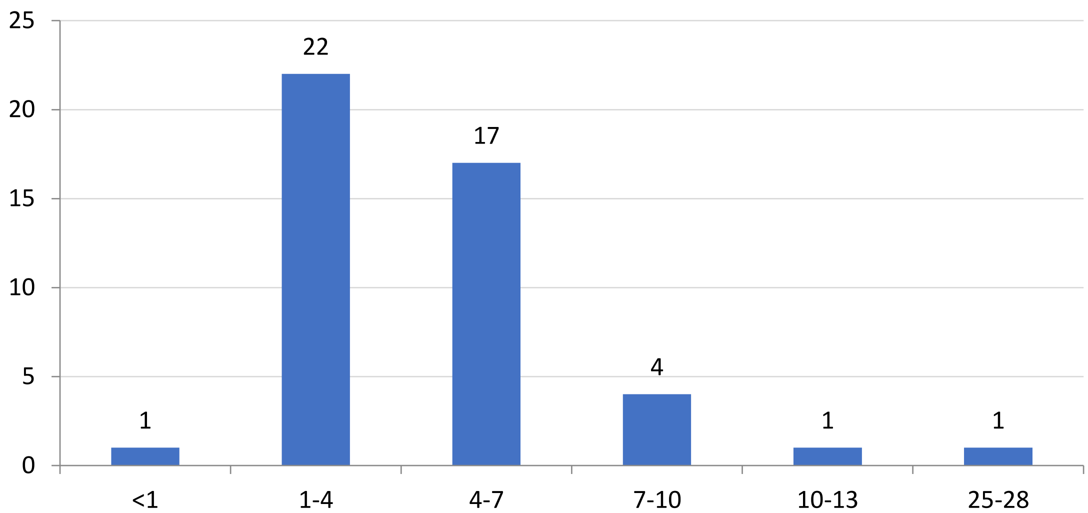

Figure B.5. Live-bed data; shear stress ratio (τ_1 / τ_c).

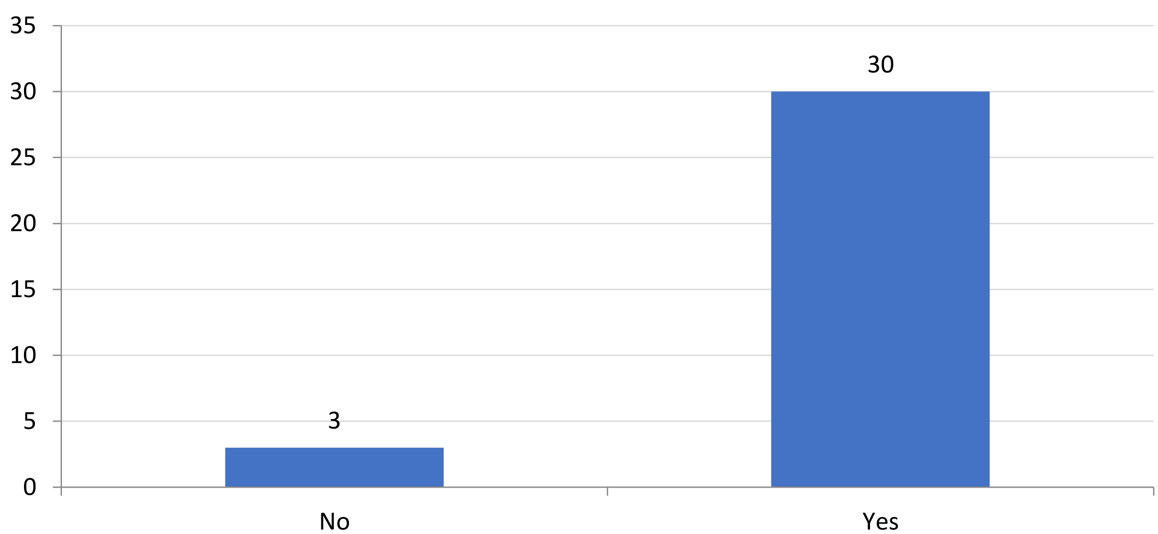

Figure B.6. Live-bed data; choked vs. not choked.

Note, due to the lack of data in Lim and Cheng (1998) about the Ashida (1963) and Rana's (1986) studies; the choked condition was not possible to be defined for these data.

Appendix C: Summary of Prior Studies

C.1. A short review of previous literature

Table C.1.Prior laboratory studies on clear-water contraction scour.

Author(s)	Publication Year	Comment
Laursen and Toch	1956	Curves were fitted to laboratory measurements of scour depth at the piers of a multi-span bridge, comprising a number of circular piers evenly spaced across the flow.
Laursen	1963	Laursen derives a theoretical clear-water scour relationship by using continuity, the energy equation, a critical tractive force approximation, and Strickler's relationship for Manning's *n*. His work appears to be sound until he simplifies the equation by neglecting the difference in the velocity heads and the loss through the contraction. It is this simplified equation that is cited as the basis for the HEC-18 (FHWA 2012) design equation.
Gill	1981	Gill observes that his results are for non-equilibrium conditions. He used two different transitions but could not prevent asymmetrical abutment scour. The abutment scour depth was greater than the long contraction scour. Used Straub (1934) equation.
Webby	1984	Webby assumed that a contraction is long when the length of the counteracted section is at least twice the uncontracted channel width.
Lim	1993	This study provides a useful dimensional analysis. Lim developed an equation for the clear-water situation and stated that it can be used for live-

Author(s)	Publication Year	Comment
		bed scour also. However, the results showed that the equation greatly over-predicts live-bed scour depth. Lim also considered the backwater effect due to choking, which he mentioned was not significant in his experiments.
Lim and Cheng	1998	Applicable for both clear-water and live-bed scour. Lim and Cheng compared Lim's equation with four other equations. Their equation is only related to width ratio. All the equations under-estimated the scour depth.
Laursen	1999	This is a journal Discussion article in which Laursen mentions that clear-water scour and scour by sediment transporting flow are two different phenomena. Theoretically there is no limit for a scour hole to grow under constant clear-water conditions. A research assistant ran a physical model for three weeks and gave up at last. However, a better way to find the scour limit is to reduce the hydrodynamic force, by reducing the velocity and shear stress as the hole develops, until no sediment particles are seen to be leaving the scour hole.
Zevenbergen	2004	Zevenbergen presents a method, built in a spreadsheet, to calculate the depth of the scour hole for either clear-water or live-bed conditions. This method can be used for tidal bridges under storm surge, time-dependent condition. In tidal situations, with periods often less than 3 hours, computing the ultimate scour depth is not reasonable because scour occurs in a very short period of time. It is noted that this method is also applicable for upland streams with flashy flows.
Dey and Raikar	2005	Dey and Raikar conducted 131 laboratory experiments in which they vary a wide variety of parameters. Unfortunately, they do not provide direct measurements of Y_2, and 123 of the 131 data points are under choked flow conditions. They go on to provide a regression analysis and draw

Author(s)	Publication Year	Comment
		comparisons between parameter relationships to the equilibrium scour depth.

Table C.2.Prior laboratory studies on live-bed contraction scour.

Author(s)	Publication Year	Comment
Straub	1934	This is the earliest study regarding live-bed contraction scour. The water surface was used as the datum. The results on scour depth in coarse sand appear not to be in good agreement with the presented equation, but very good for fine sand.
Laursen	1960	Laursen's live-bed equation is used in HEC-18 (FHWA 2012). It is possible to derive another equation with better prediction for high flows, based on Laursen's sediment transport equation.
Komura	1966	Komura developed an equation for bed material with non-uniform grain size ($\sigma_g > 1$) for both clear-water and live-bed conditions.
Gill	1981	Gill's results are for non-equilibrium conditions. He used two different transitions but could not prevent abutment scour. The abutment scour depth was higher than the long contraction scour. He used Straub's (1934) equation.
Lim and Cheng	1998	Applicable for both clear-water and live-bed. They compared Lim's equation with four other equations. Their equation is related only to width ratio. All the equations underestimated the scour depth.

Author(s)	Publication Year	Comment
Dey and Raikar	2006	As with other prior studies, bedforms were not taken into account. Dey and Raikar validated their results by experimental data and compared it with three other equations.
Najafzadeh et al.	2016	The authors developed two predictive models by using neural-network models ANFIS and SVM to predict scour depth in a long contraction. They used a 2004 data set which was gathered from clear-water and live-bed experiments. They showed that ANFIS model and Laursen equation had the best results. However, the equation which they describe as Laursen's equation actually belongs to Lim and Cheng (1998).

Table C.3. Prior Numerical Studies on Contraction Scour.

Author(s)	Publication Year	Comment
Weise	2002	This study investigated the utility of a 2D (depth-averaged) numerical model for modelling contraction scour. It concluded positively.
Marek and Dittrich	2004	This study used a 3D numerical model.
Duc and Rodi	2008	This study used a 3D numerical model; RANS model.
Lai and Greimann	2010	This paper is a useful summary paper indicating the results from prior numerical studies. The study described investigated the utility of a 2D (depth-averaged) numerical model for modelling contraction scour. They compared the results with the 2D model those from 3D models used by prior studies. Additionally, they reviewed the mixed performance of prior attempts.

Table C.4. Prior Field Studies on Contraction Scour.

Author(s)	Publication Year	Comment
Benedict	2003, 2016	In this study Clear-water abutment and contraction scour at 146 bridges in South Carolina is collected. They compared their field date with HEC-18 clear-water prediction method. In General, the HEC-18

Author(s)	Publication Year	Comment
		equation over predicts the scour depth. However, this method also under predict the scour depth in 30 percent of the time by as much as 7.1 ft. Benedict compared the range of the dimensionless variables which is used in experimental studies with field date. He showed the dimensionless experimental variables are outside the range of field data variables; suggesting the current equations may not be applicable in South Carolina.
Mueller and Wagner	2005	They collected the field data from 79 bridges in 17 states. They evaluated 26 different pier-scour equations and suggested a couple of them which are more suitable for design purposes. They added another coefficient, K_4, to the pier scour calculation method by HEC-18. But, their attempt to predict abutment and contraction scour were inconclusive about abutment and contraction scour. Their results showed, the current methodology for computing scour depth has reasonable maximum total scour depth predictions but the individual estimates of contraction and abutment scour did not compare well with the observations.
Hong et al.	2006	Their study was focused on whether or not a laboratory model can correctly model a contraction scour which will happen in reality. They Built a physical model of a bridge on the Ocmulgee River in Macon. The result was promising, and they mentioned some insight related to contraction scour physical modelling

Author(s)	Publication Year	Comment
Wagner et al	2006	Collected data at 15 bridge sites; 4 out of 15 bridges have velocity data.
Benedict and Caldwell	2006, 2016	Clear-water scour at pier and contraction scour envelope curves. Data were gathered from 116 bridges. They compared their field date with HEC-18 clear-water prediction method. In General, the HEC-18 equation over predicts the scour depth. However, this method also under predict the scour depth in 30 percent of the time by as much as 7.1 ft.
Benedict et al.	2007	The collection of the historic scour data is to some extent easy for the clear-water condition, but to find the historic depth of scouring for the live-bed condition is problematic because of the partial or complete refill of the holes. The US Geological Survey utilized ground penetrating radar in South Carolina to address this issue. However, there are uncertainties regarding the results.
Benedict and Caldwell	2009	Live-bed scour at piers and contraction scour envelope curve. Data were gathered from 87 bridges; 89 measurements of live-bed contraction scour depth.

C.2. Analysis of Contraction Scour Formulas

In this section, a selected number of formulas which are brought in the previous section will be discussed more thoroughly. These formulas were chosen based on the frequency of their use and assumptions which were involved in their derivation.

C.2.1. The Analysis of the Clear-water Equations

C.2.1.1. Laursen (1963)

Laursen assumed that this equation can be used for a secondary relief bridge which is placed on floodplain Flow on the flood plain has:

- Low velocity
- Small competence for the movement of sediment.
- Floodplains usually are covered, e.g. grass, bushes, and etc.

Note, one example of a clear-water scour is when there is a riprap structure underneath the bridge. Due to the huge difference between the size of the riverbed sediment in comparison with the riprap this case is also, Clear-water contraction scour. (Laursen 1963)

Assumptions:

- Non-uniform flow in transition is ignored.
- No dunes or ripples, $\tau = \tau'$.
- Assume the scour has already happened,
- The contracted and uncontracted sections would have the same bed slope after the scour ($S_{0-1} = S_{0-2}$),

- $n_1 = n_2$,
- Uniform flow,
- $\tau_2 = \tau_c$,

The procedure is as follow:

Flow continuity:

$$Q_1 = Q_2 \tag{C.1}$$

Energy equation by assuming the same bed slope $\left(S_{0_1} = S_{0_2}\right)$

$$D_s = Y_2 - Y_1 + (1+k)\left(\frac{V_2^2}{2g} - \frac{V_1^2}{2g}\right) \tag{C.2}$$

with a slight change the energy equation will become,

$$\frac{D_s}{Y_1} = \frac{Y_2}{Y_1} - 1 + \frac{1+k}{2} Fr_1^2 \left[\left(\frac{B_1}{B_2}\right)^2 \left(\frac{Y_1}{Y_2}\right)^2 - 1\right] \tag{C.3}$$

Boundary shear stress related to grain size (Manning-Strickler)

$$n = 0.034 {d_{50}}^{\frac{1}{6}} \tag{C.4}$$

$$V = \frac{1.486}{n}\, h^{\frac{2}{3}} S^{\frac{1}{2}} \tag{C.5}$$

$$\tau = \gamma h S \tag{C.6}$$

By combining these three equations we will reach to the equation below:

$$\tau' = \frac{V_1^2 \, d_{50}^{\frac{1}{3}}}{30 \, Y_1^{\frac{1}{3}}} \tag{C.7}$$

τ': Boundary shear stress related to grain size or tractive force.

Equation (C.7) is based on U.S. customary Units. The shear stress ratio between contracted and uncontracted section will be:

$$\frac{\tau_1'}{\tau_2'} = \left(\frac{V_1}{V_2}\right)^2 \left(\frac{Y_2}{Y_1}\right)^{\frac{1}{3}} \rightarrow \text{ which by assuming } \tau_2 = \tau_c \rightarrow \frac{\tau_1'}{\tau_c} = \left(\frac{V_1}{V_2}\right)^2 \left(\frac{Y_2}{Y_1}\right)^{\frac{1}{3}} \tag{C.8}$$

By combining the above-mentioned equation with continuity,

$$\frac{Y_2}{Y_1} = \left(\frac{\tau_1'}{\tau_c}\right)^{\frac{3}{7}} \left(\frac{B_1}{B_2}\right)^{\frac{6}{7}} \tag{C.9}$$

By estimating $\tau_c = 4d_{50}$ or $\tau_c^* = 0.039$, where d_{50} is in feet, and combining that with equations (C.9) and (C.3), by assuming no energy loss, the following equations would be attained for predicting the scour depth:

$$\frac{D_s}{Y_1} = \left(\frac{\tau_1'}{\tau_c}\right)^{\frac{3}{7}} \left(\frac{B_1}{B_2}\right)^{\frac{6}{7}} - 1 \tag{C.10}$$

and

$$\frac{D_s}{Y_1} = 0.13\left(\frac{Q}{d_{50}^{\frac{1}{3}} \, Y_1^{\frac{7}{6}} \, B_2}\right)^{\frac{6}{7}} - 1 \tag{C.11}$$

C.2.1.2 Komura (1966)

Komura (1966) introduced two sets of equations one for clear-water and another one for live-bed cases based on analytical and experimental approaches. He combined flow resistance, flow continuity, and a shear stress ratio assumption to derive his analytical equations for contraction scour.

Flow resistance

$$\frac{V}{u^*} = m\left(\frac{R}{k_s}\right)^p \tag{C.12}$$

Where *m* is constant and equal to 7.66, *p*, is constant and equal to $\frac{1}{6}$, k_s, is equivalent roughness; to calculate k_s, $\frac{k_s}{d_{50}} = k\left(\frac{u_*}{(G-1)gd_{50}}\right)^i$, in which *k* is Constant, *i*, is a constant equal to 1, and $\frac{u_*}{(G-1)gd_{50}}$ is the dimensionless tractive force.

Flow continuity

$$Q_1 = Q_2 \tag{C.13}$$

By combining equations (3.16) and (3.17),

$$\frac{Y_2}{Y_1} = \left(\frac{\tau_1}{\tau_2}\right)^{\frac{1-2mi}{2(i+1)}}\left(\frac{B_1}{B_2}\right)^{\frac{1}{i+1}}\frac{d_1}{d_2}^{\frac{mi-i}{1+i}} \tag{C.14}$$

Komura assumed that the ratio between shear stress in the contracted and uncontracted section is equal to the shear stress ratio at incipient motion.

Shear stress ration assumption

$$\frac{\tau_1}{\tau_2} = \frac{\tau_{c1}}{\tau_{c2}} \tag{C.15}$$

He used Yuichi Iwagaki's formula to estimate the critical shear stress,

$$\frac{\tau_c}{\rho} = a_c(G-1)gd \tag{C.16}$$

Where a_c is constant and a function of grains shear Reynolds number ($a_c = f(\frac{u_{*c}d_{65}}{\vartheta})$).

Note, to the best of author's knowledge this shear stress ratio assumption may not be quite right for different flow scenarios. Consequently, the analytical form of clear water contraction scour equation was derived by combining equations (C.14), (C.15), (C.16), (C.3) and assuming negligible energy loss between contracted and uncontracted section.

$$\frac{Y_2}{Y_1} = \frac{d_s}{Y_1} + 1 = \left(\frac{\tau_{c1}}{\tau_{c2}}\right)^{\frac{2}{7}} \left(\frac{B_1}{B_2}\right)^{\frac{6}{7}} \tag{C.17}$$

Komura also has reached to the following equation for clear water contraction based on his experimental study.

$$\frac{Y_2}{Y_1} = 1.60\, Fr_1^{\frac{1}{5}} \left(\frac{B_1}{B_2}\right)^{\frac{2}{3}} \sigma_{g_1}^{-\frac{1}{2}} \tag{C.18}$$

Where $Fr_1$and σ_{g_1} are Froude number and standard deviation of the particle size distribution of sediment at uncontracted section, respectively.

C.2.1.3. HEC-18 clear-water equation

Arneson et al. (2012) developed an equation based on Laursen (1963) by simply assuming that the shear stress at the contracted section after scour would be equal to the critical shear stress ($\tau_2 = \tau_c = 4d_{50}$) and combined that with equation (C.4).

$$Y_2 = \left[\frac{K_u Q^2}{d_m^{2/3} B_2^2}\right]^{3/7} \tag{C.19}$$

And

$$D_s = Y_2 - Y_0 \tag{C.20}$$

Where,

Y_2=Average equilibrium depth in the contracted section after contraction scour, ft (m)

Q=Discharge through the bridge or on the set-back overbank area at the bridge associated with the width W, ft3/s (m3/s)

d_m=Diameter of the smallest non-transportable particle in the bed material (1.25 d_{50}) in the contracted section, ft (m)

d_{50}=Median diameter of bed material, ft (m)

B_2=Bottom width of the contracted section less pier widths, ft (m)

Y_0=Average existing depth in the contracted section, ft (m)

K_u=0.0077 in English units and 0.025 in SI units

This equation is the one which suggested to engineers to use to estimate the contraction scour depth at this date.

C.2.2. The analysis of the live-bed equations

C.2.2.1. Straub (1934)

Straub (1934) is the first attempt to estimate the contraction scour depth. The equations or particular assumptions which were taken into account to reach the final form of Straub's equation are brought in the following.

The same roughness for the walls and bottom

- Flow Continuity
- Sediment transport equation
- This equation is based on Duboy's principles:

$$q_w = \psi \left(\frac{S^{1.4}}{C^{1.2}}\right) q_c^{\frac{3}{5}} \left(q_c^{\frac{3}{5}} - q_0^{\frac{3}{5}}\right) \qquad \text{(C.21)}$$

Where,

q_w: Sediment load (pound / ft),

S: Bed slope,

q_c: Flow discharge per unit width of chthe annel for slope S which sediment transport begins.

C: $\frac{1.49}{n}$

ψ, q_0, n will be found based on the experiment.

- Rectangular section

The final form of Straub's equation is as follow:

$$Y_2 = \frac{\frac{Y_1}{(1-\alpha)^{\frac{3}{7}}}\left\{-\frac{\tau_c}{\gamma_m S_{f1}} + \left[\left(\frac{\tau_c}{\gamma S_{f1}}\right)^2 + \frac{4Y_1\left(Y_1 - \frac{\tau_c}{\gamma S_{f1}}\right)}{1-\alpha}\right]^{\frac{1}{2}}\right\}^{\frac{3}{7}}}{\left[2\left(Y_1 - \frac{\tau_c}{\gamma S_{f1}}\right)\right]^{\frac{3}{7}}} \tag{C.22}$$

Here,

$(1-\alpha)$: $\frac{B_2}{B_1}$

Y_1: Water depth at uncontracted section,

Y_2: Water depth at contracted section,

S_f: Energy gradient,

γ_m: Specific weight of water and sediment mixture,

τ_c: Critical shear stress,

B_2: Contraction width,

B_1: Approach flow width

C.2.2.2. Laursen (1960)

The equations or particular assumptions which were taken into account to reach to the final form of Laursen's equation are brought in the following:

- Manning formula $Q = \frac{1.49}{n} A\, R^{\frac{2}{3}} S^{\frac{1}{2}}$
- Total Sediment load by Laursen (1958)

$$\bar{C} = \left(\frac{D_s}{Y}\right)^{\frac{7}{6}} \left(\frac{\tau'_0}{\tau_c} - 1\right) b \left(\frac{u_*}{\omega}\right)^{a} \tag{C.23}$$

d_s: Sediment median grain size diameter

Y: Water depth

τ'_0= Bed shear stress related to the grain size

b: Constant

u_*: Shear velocity

ω: Fall velocity of sediment

a: Constant

Table 3.7. Different values for Constant 'a'

a	$\frac{u_*}{\omega}$
1/4	<1/2
1	1
9/4	>2

Critical shear stress τ_c: $\tau_c = 4d_s$

- Shear stress in combination with Manning and Strickler equations would reach to the equation (C.4) and combine that with critical shear stress ($\tau_c = 4d_s$) would lead to the following equation:

$$\frac{\tau'_0}{\tau_c} = \frac{{V_1}^2}{120\, Y_1^{\frac{1}{3}} d_s^{\frac{2}{3}}} \tag{C.24}$$

- Sediment Continuity $C_1 Q_1 = C_2 Q_2$
- During floods, it is assumed that $\frac{\tau'_0}{\tau_c} - 1 = \frac{\tau'_0}{\tau_c}$

The final equation is:

$$\frac{Y_2}{Y_1} = \left(\frac{Q_2}{Q_1}\right)^{\frac{6}{7}} \left(\frac{B_1}{B_2}\right)^{\frac{6}{7}\frac{2+a}{3+a}} \left(\frac{n_2}{n_1}\right)^{\frac{6}{7}\frac{a}{3+a}} \tag{C.25}$$

Note, $\frac{n_2}{n_1} \sim 1$ and the maximum number for its exponent is 0.35. Accordingly, $\left(\frac{n_2}{n_1}\right)^{\frac{6}{7}\frac{a}{3+a}} \approx 1$.

C.2.2.3. Komura (1966)

Komura (1966) introduced two sets of equations one for clear-water and another one for live-bed cases based on analytical and experimental approaches. He combined flow resistance, flow continuity, sediment continuity, and *Kalinske & Brown* sediment transport equations to derive his analytical equations for live-bed contraction scour.

- Sediment continuity

By assuming the same porosity in contracted and uncontracted sections then

$$q_{s1}B_1 = q_{s2}B_2 \tag{C.26}$$

- Laursen (1963) expression of the Energy equation

$$\frac{d_s}{Y_1} = \frac{Y_2}{Y_1} - 1 + \frac{1+k}{2}F_{r1}^2\left[\left(\frac{B_1}{B_2}\right)^2\left(\frac{Y_1}{Y_2}\right)^2 - 1\right] \tag{C.27}$$

k: Minor loss coefficient

Fr_1: Froude number in uncontracted section

- Kalinske and Brown's sediment transport equation of motion

$$\frac{q_s}{u_* d_{50}} = a_s\left(\frac{u_*^2}{(G-1)gd_{50}}\right)^p \tag{C.28}$$

Where, q_s is sediment transport per unit weight (L^2/T), a_s is constant and equal to 10, and p is constant and about 2.

By combining equations (C.26) and (C.28),

$$\frac{D_1}{D_2} = \left(\frac{\tau_1}{\tau_2}\right)^{\frac{1+2p}{2(p-1)}} \left(\frac{B_1}{B_2}\right)^{\frac{1}{p-1}} \tag{C.29}$$

Where D_1 and D_2 are mean sediment particles diameter at uncontracted and contracted sections, respectively.

The final form of analytical Live-bed equation would be derived by combining equations (C.7), (C.27), and (3.29) by neglecting energy loss between two sections:

$$\frac{Y_2}{Y_1} = \frac{d_s}{Y_1} + 1 = \left(\frac{\tau_1}{\tau_2}\right)^{\frac{3m+1}{14}} \left(\frac{B_1}{B_2}\right)^{\frac{m+5}{7}} \tag{C.30}$$

Komura also reached to the following equation for clear water contraction based on his experimental study.

$$\frac{Y_2}{Y_1} = \frac{D_s}{Y_1} + 1 = 1.45\, Fr_1^{1/5} \left(\frac{B_1}{B_2}\right)^{2/3} \sigma_g^{-1/5} \tag{C.31}$$

Where $Fr_1$and σ_{g_1} are Froude number and standard deviation of the particle size distribution of sediment at uncontracted section, respectively.

C.2.2.4. The live-bed equation of HEC-18

This equation is used by engineers at this date to estimate the scour depth and is exactly the same as Laursen (1960) equation. However, instead of using the approach flow depth (*Y_1*), existing depth in the contracted section before scour (*Y_0*) is used to calculate the final scour depth. This slight change made this equation more reliable.

$$\frac{Y_2}{Y_1} = \left(\frac{Q_2}{Q_1}\right)^{\frac{6}{7}} \left(\frac{B_1}{B_2}\right)^{p} \tag{C.32}$$

$$D_s = Y_2 - Y_0 \tag{C.33}$$

Where,

Y_1: Average depth in the upstream main channel, ft (m)

Y_2: Average depth in the contracted section, ft (m)

Y_0: Existing depth in the contracted section before scour, ft (m)

Q_1: Flow in the upstream channel transporting sediment, ft3/s (m3/s)

Q_2: Flow in the contracted channel, ft3/s (m3/s)

B_1: Bottom width of the upstream main channel that is transporting bed material, ft (m)

B_2: Bottom width of the main channel in contracted section less pier width(s), ft (m)

p: Exponent determined in the following

Table 3.8. Different values for the exponent 'p'

u_*/ω	p	**Mode of bed material transport**
<0.50	0.59	Mostly contact bed material discharge
0.50 to 2.0	0.64	Some suspended bed material discharge
>2.0	0.69	Mostly suspended bed material discharge

u_*: $(gY_1S_1)^{0.5}$, Shear velocity in the upstream section, ft/s (m/s)

ω: Fall velocity of bed material based on the D50, m/s

g: Acceleration of gravity (32.2 ft/s2) (9.81 m/s2)

S_1: Slope of energy grade line of the main channel, ft/ft (m/m)

Appendix D: Experimental data

D.1. Clear-water experiments:

I. CW-0.25-0.64

- LiDAR-scanned data:

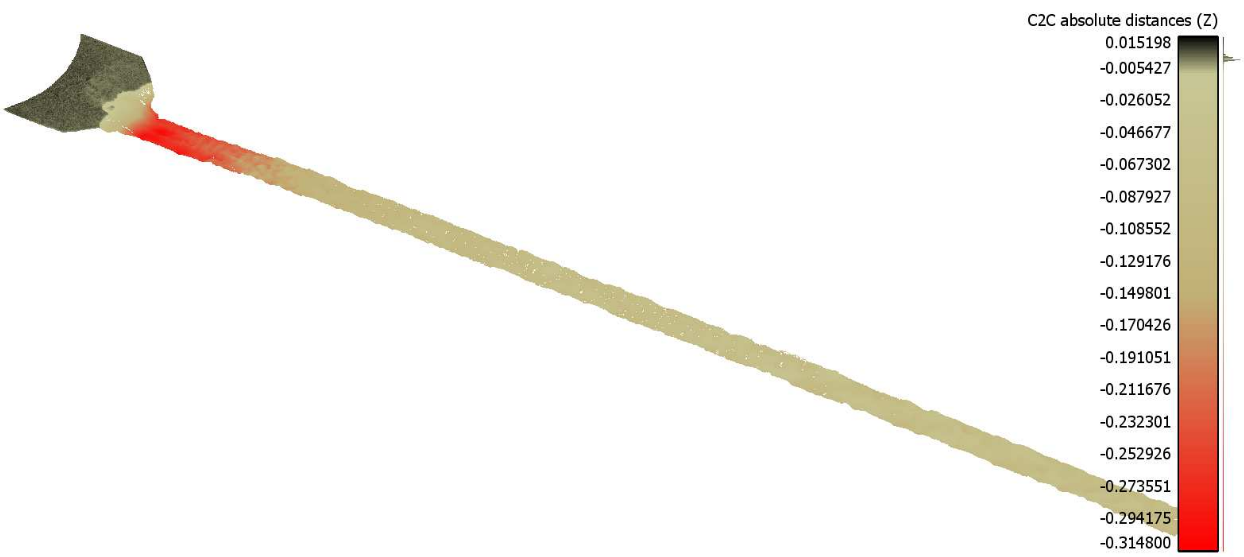

Figure D.1. Bed elevation difference between time zero and after 18-hour of experiments. (CW-0.25-0.64)

- Temporal bed and water surface elevation

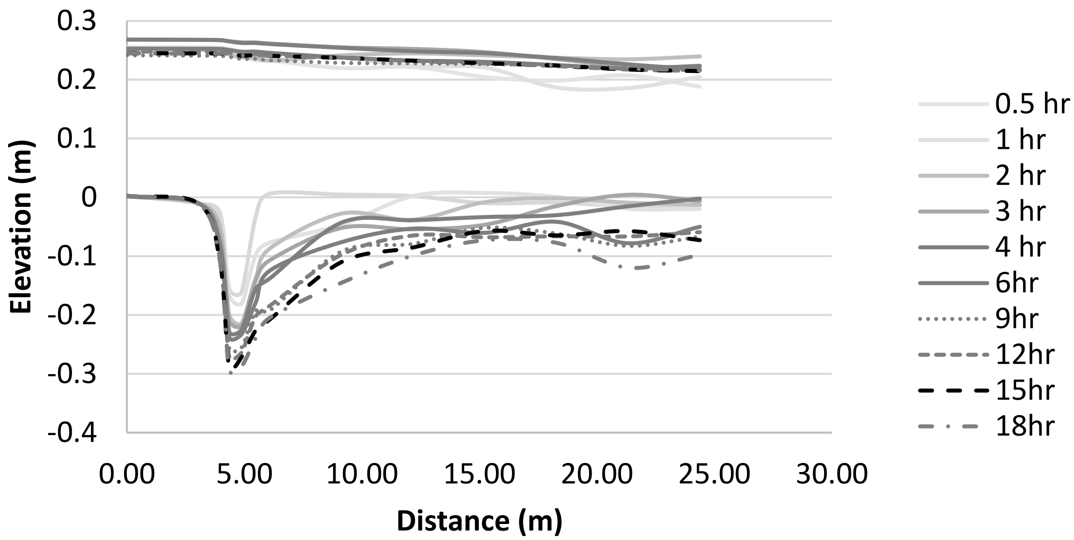

Figure D.2. Water surface and bed elevation at centerline for different time-steps. (CW-0.25-0.64)

II. CW-0.25-0.56

- LiDAR-scanned data:

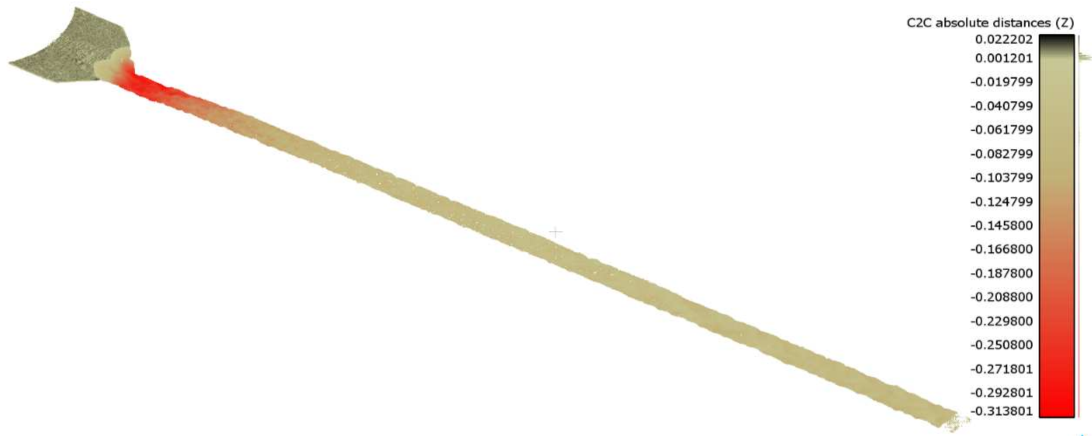

(a)

(b)

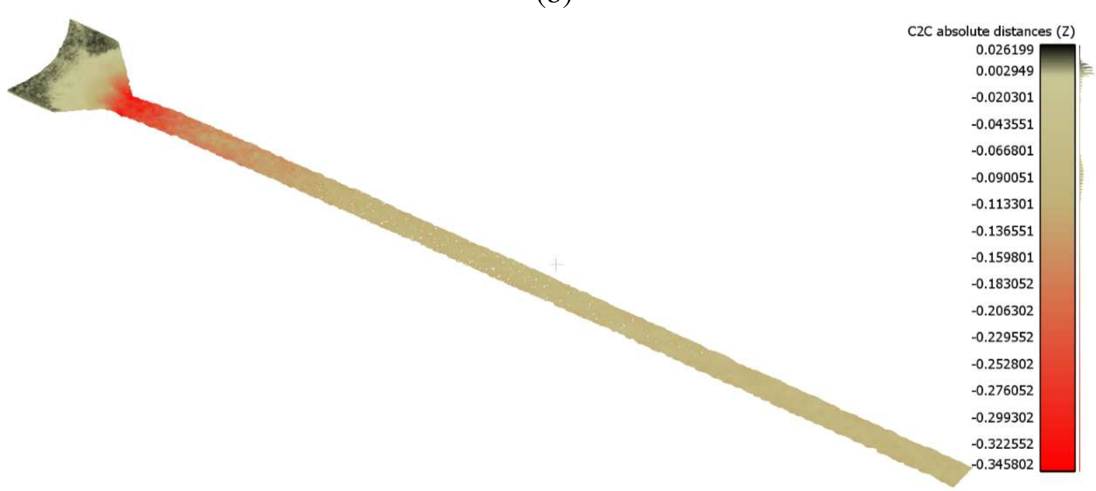

(c)

Figure D.3. LiDAR data at different time steps; (a) 12th hour, (b) 24th hour, (c)30th hour.

- Temporal bed and water surface elevation

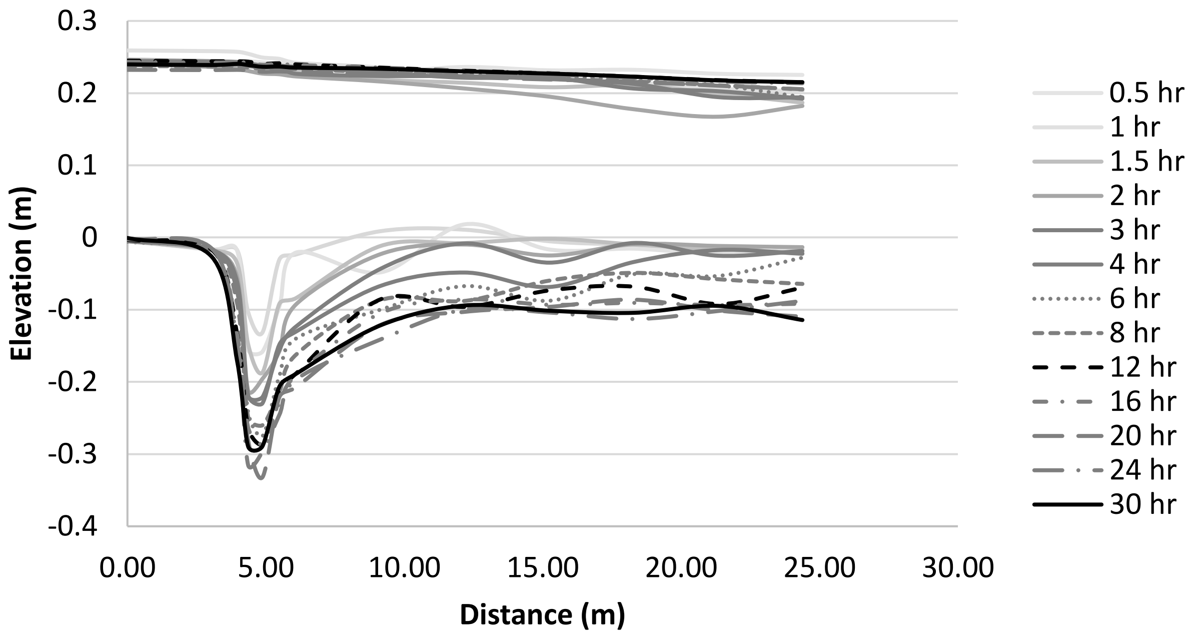

Figure D.4. Water surface and bed elevation at centerline for different time-steps. (CW-0.25-0.56)

III. CW-0.25-0.30

- LiDAR-scanned data:

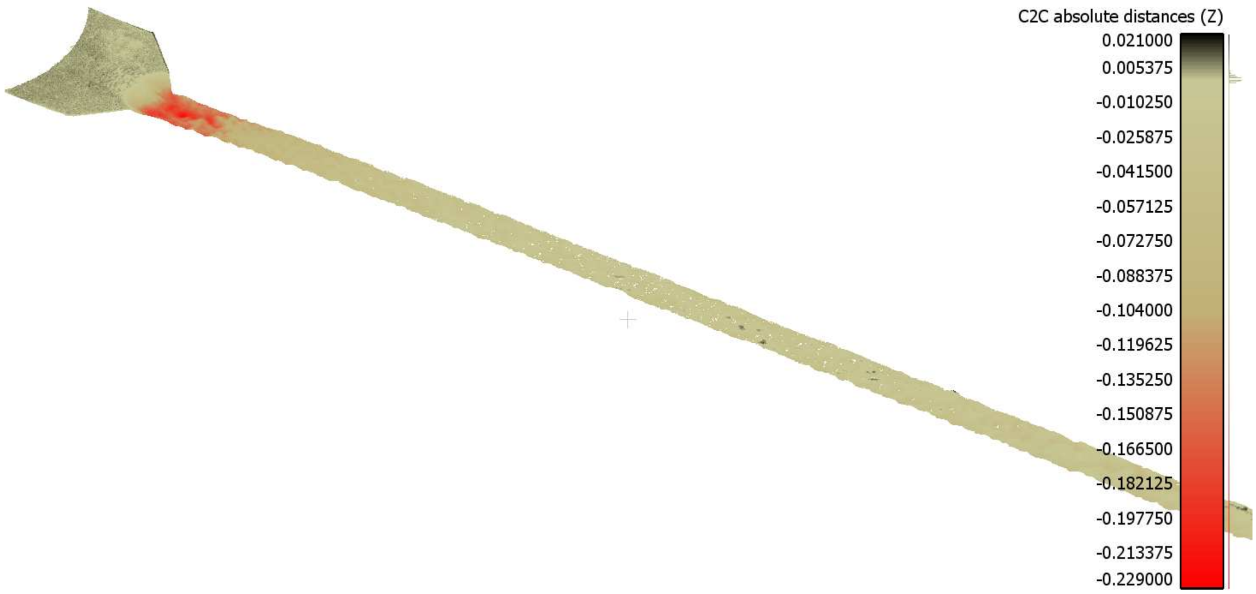

Figure D.5. Bed elevation difference between time zero and after 18-hour of experiments.

(CW-0.25-0.30)

- Temporal bed and water surface elevation

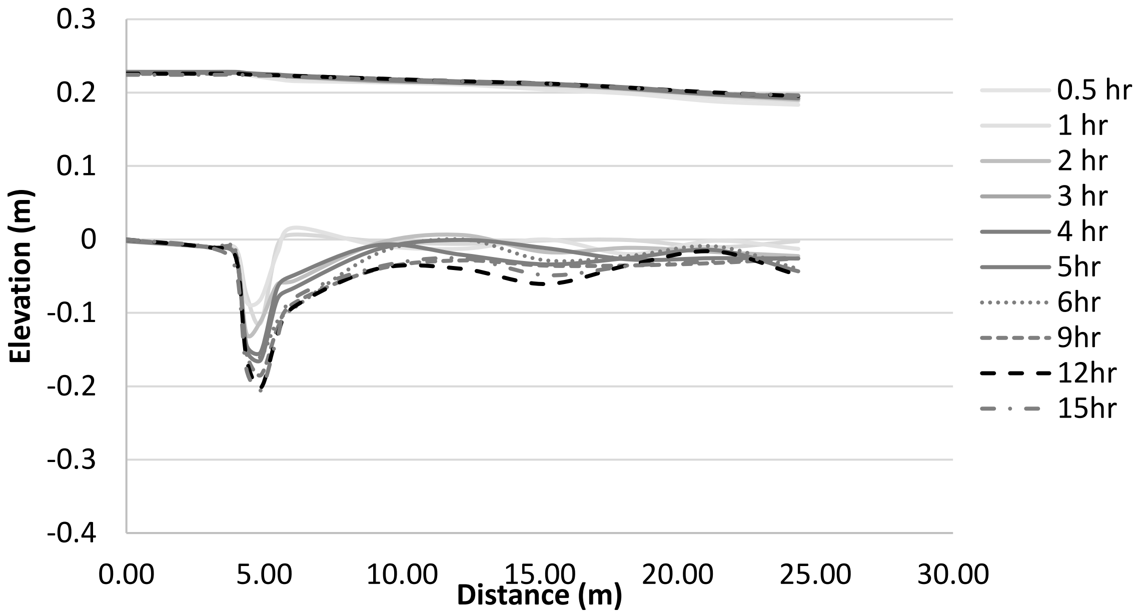

Figure D.6. Water surface and bed elevation at centerline for different time-steps. (CW-0.25-0.30)

IV. CW-0.25-0.42

- LiDAR-scanned data:

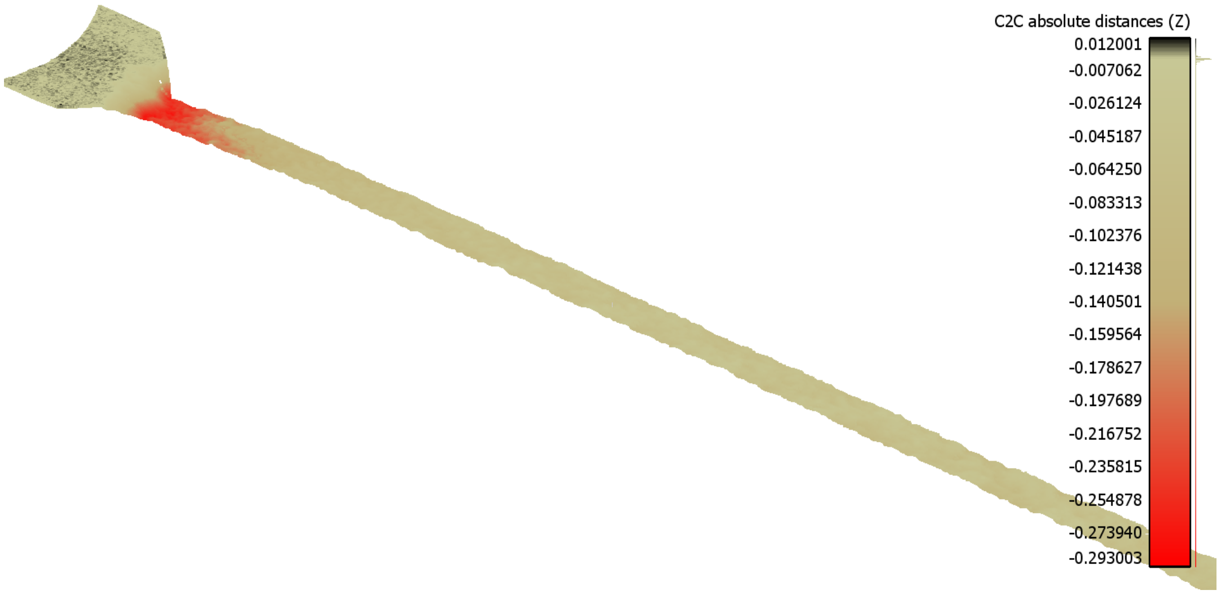

Figure D.7. Bed elevation difference between time zero and after 18-hour of experiments. (CW-0.25-0.42)

- Temporal bed and water surface elevation

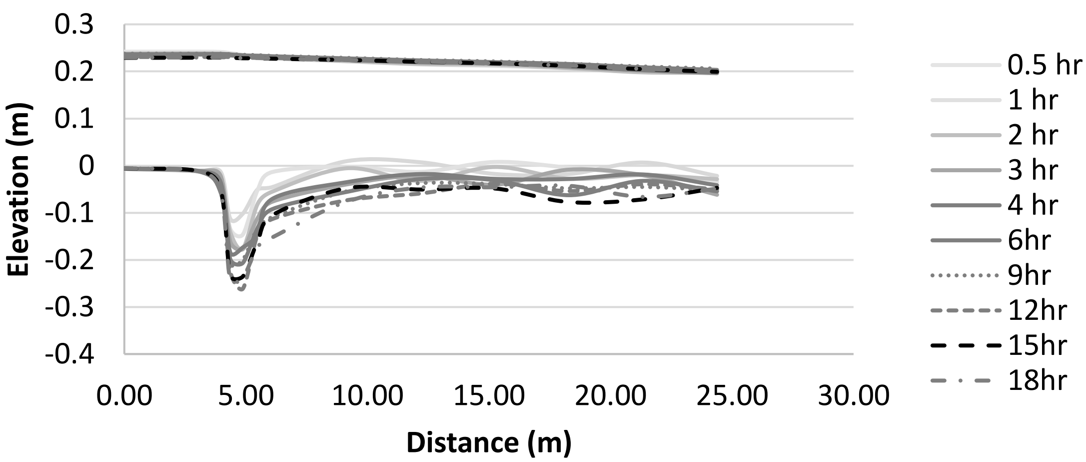

Figure D.8. Water surface and bed elevation at centerline for different time-steps. (CW-0.25-0.42)

V. CW-0.5-0.30

- LiDAR-scanned data:

Figure D.9. Bed elevation difference between time zero and after 18-hour of experiments. (CW-0.50-0.30)

- Temporal bed and water surface elevation

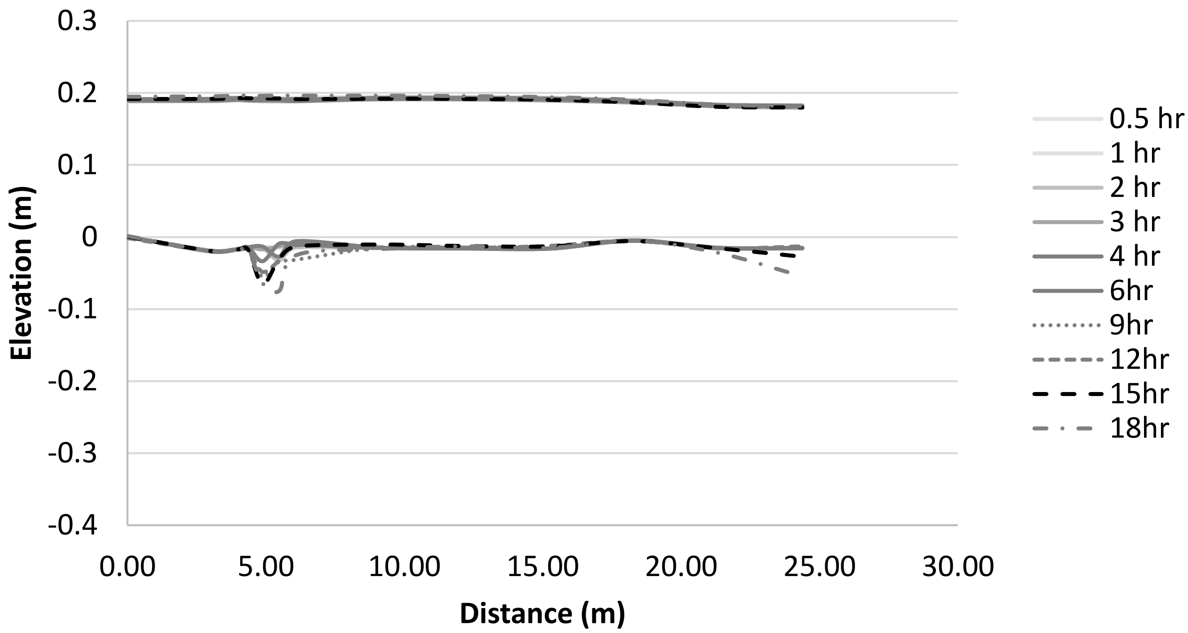

Figure D.10. Water surface and bed elevation at centerline for different time-steps. (CW-0.50-0.30)

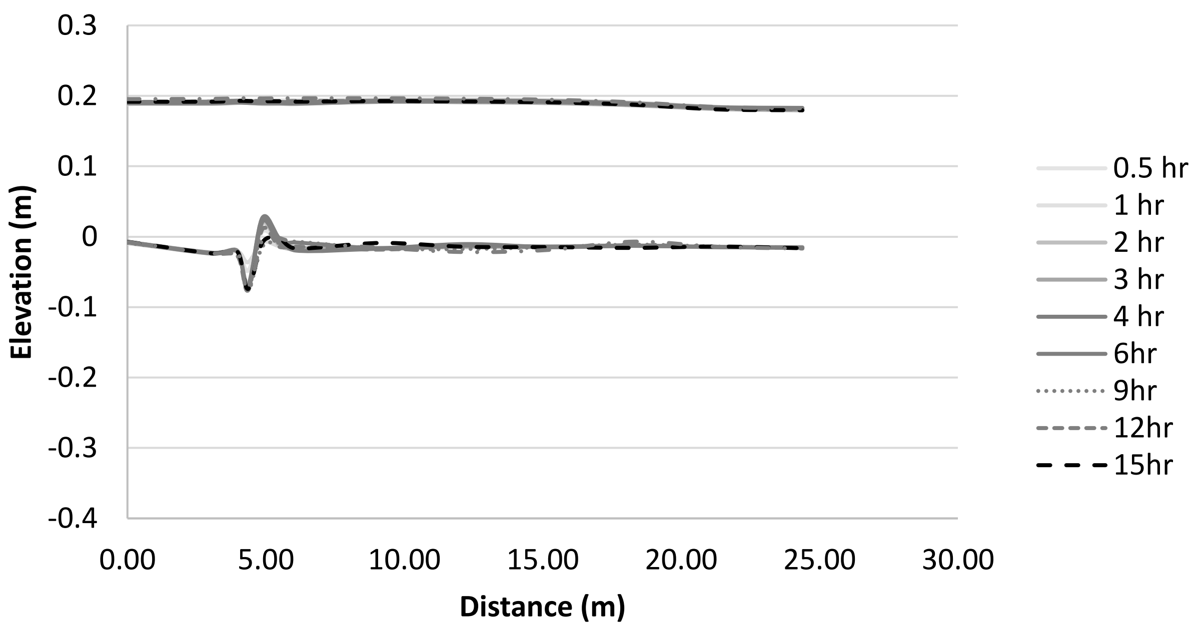

Figure D.11. Water surface and bed elevation near the right-side wall for different time-steps. (CW-0.50-0.30)

VI. CW-0.5-0.42

- LiDAR-scanned data:

Figure D.12. Bed elevation difference between time zero and after 18-hour of experiments. (CW-0.50-0.42)

- Temporal bed and water surface elevation

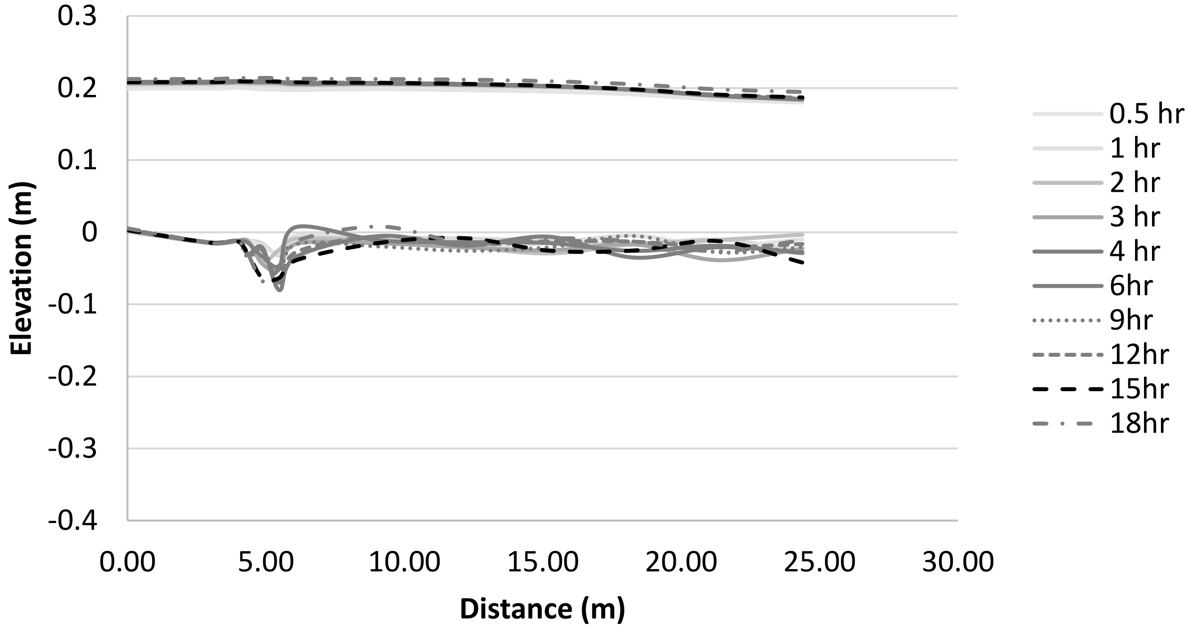

Figure D.13. Water surface and bed elevation at centerline for different time-steps. (CW-0.50-0.42)

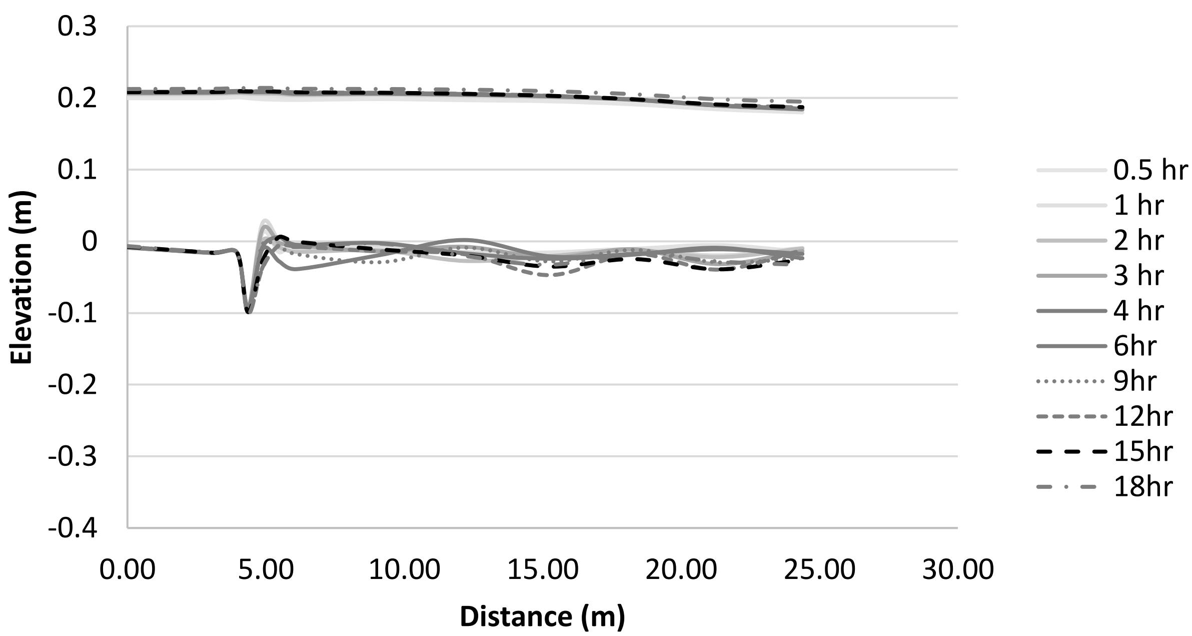

Figure D.14. Water surface and bed elevation near the right-side wall for different time-steps. (CW-0.50-0.42)

VII. CW-0.5-0.56

- LiDAR-scanned data:

Figure D.15. Bed elevation difference between time zero and after 18-hour of experiments. (CW-0.5-0.56)

- Temporal bed and water surface elevation

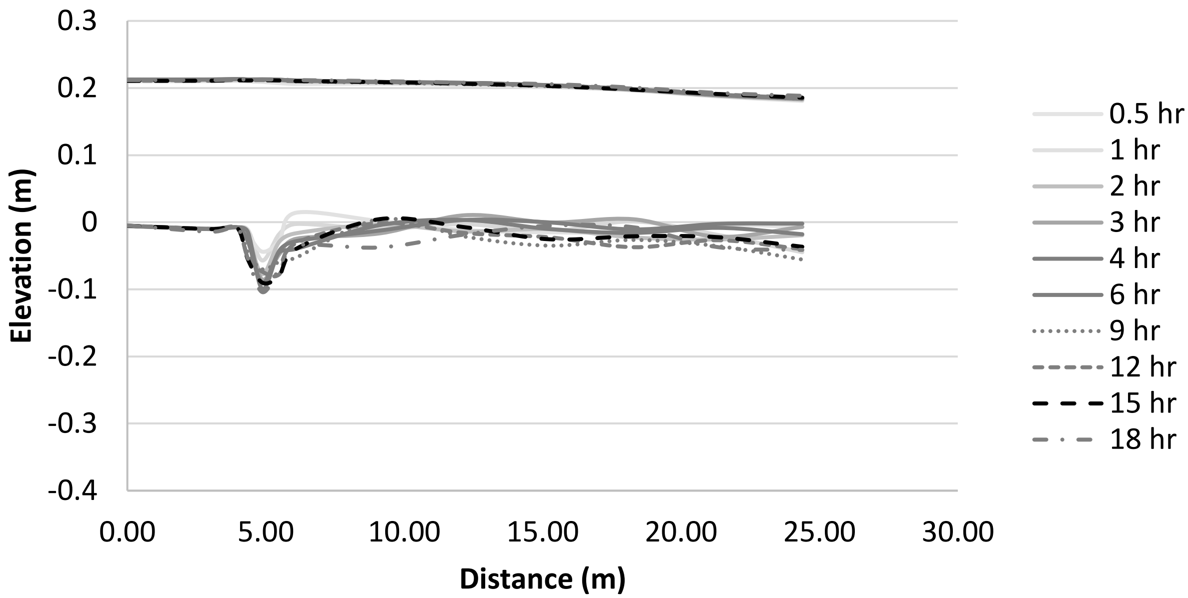

Figure D.16. Water surface and bed elevation at centerline for different time-steps. (CW-0.5-0.56)

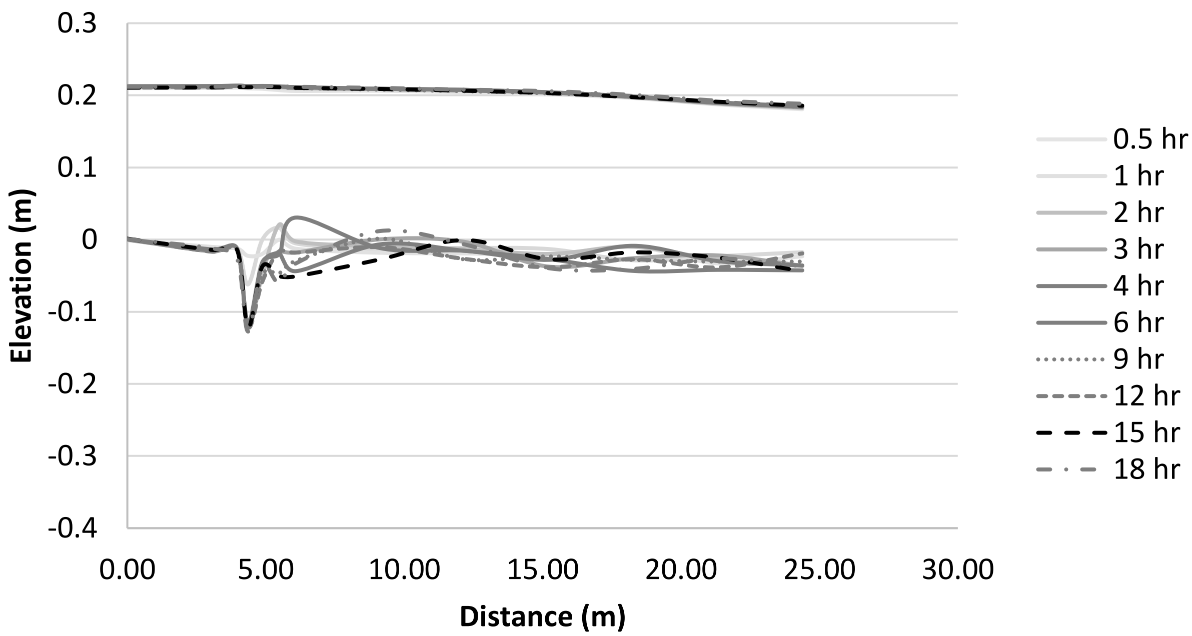

Figure D.17. Water surface and bed elevation near the right-side wall for different time-steps. (CW-0.5-0.56)

VIII. CW-0.75-0.56

- LiDAR scanned data:

Figure D.18. Bed elevation difference between time zero and after 18-hour of experiments. (CW-0.75-0.56)

- Temporal bed and water surface elevation

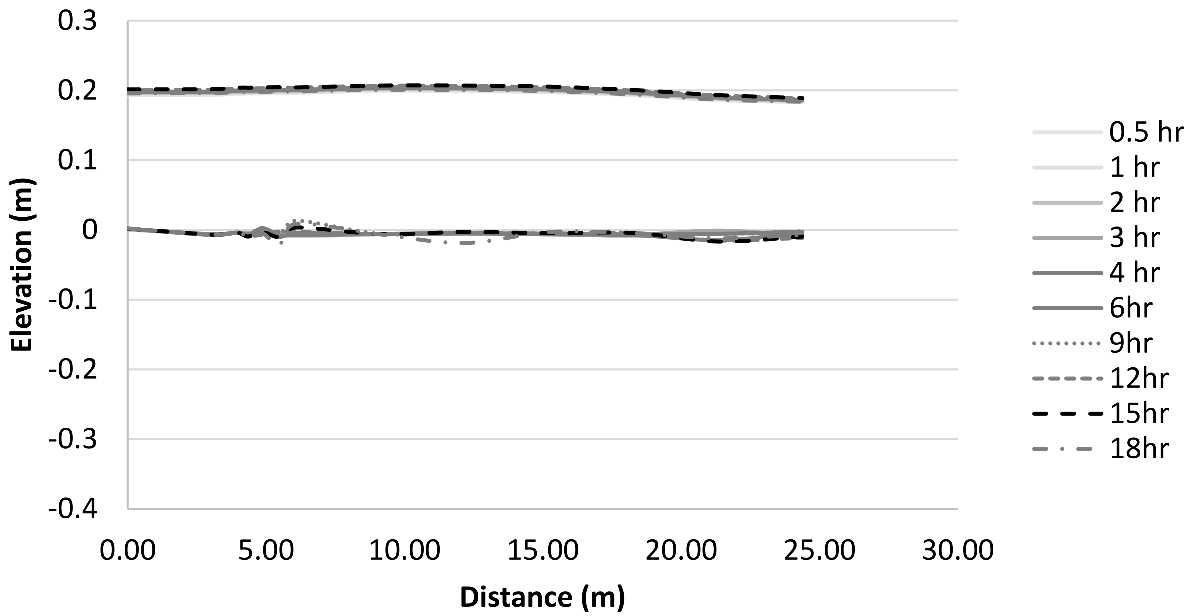

Figure D.19. Water surface and bed elevation at centerline for different time-steps. (CW-0.75-0.56)

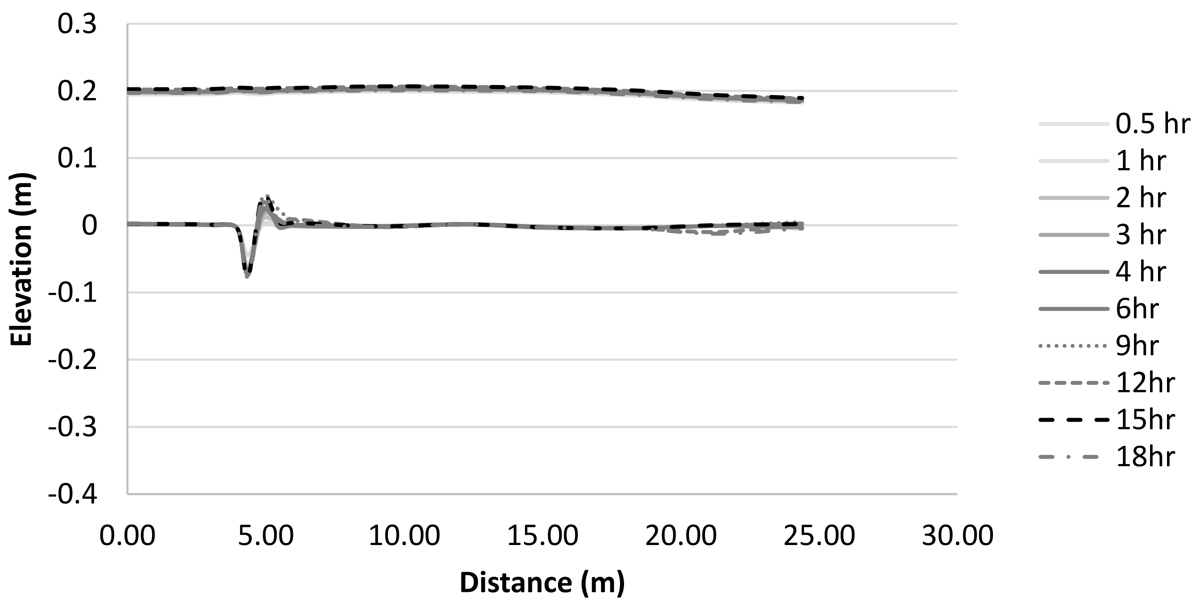

Figure D.20. Water surface and bed elevation near the right-side wall for different time-steps. (CW-0.75-0.56)

IX. CW-0.75-0.72

- LiDAR scanned data:

Figure D.21. Bed elevation difference between time zero and after 18-hour of experiments. (CW-0.75-0.72)

- Temporal bed and water surface elevation

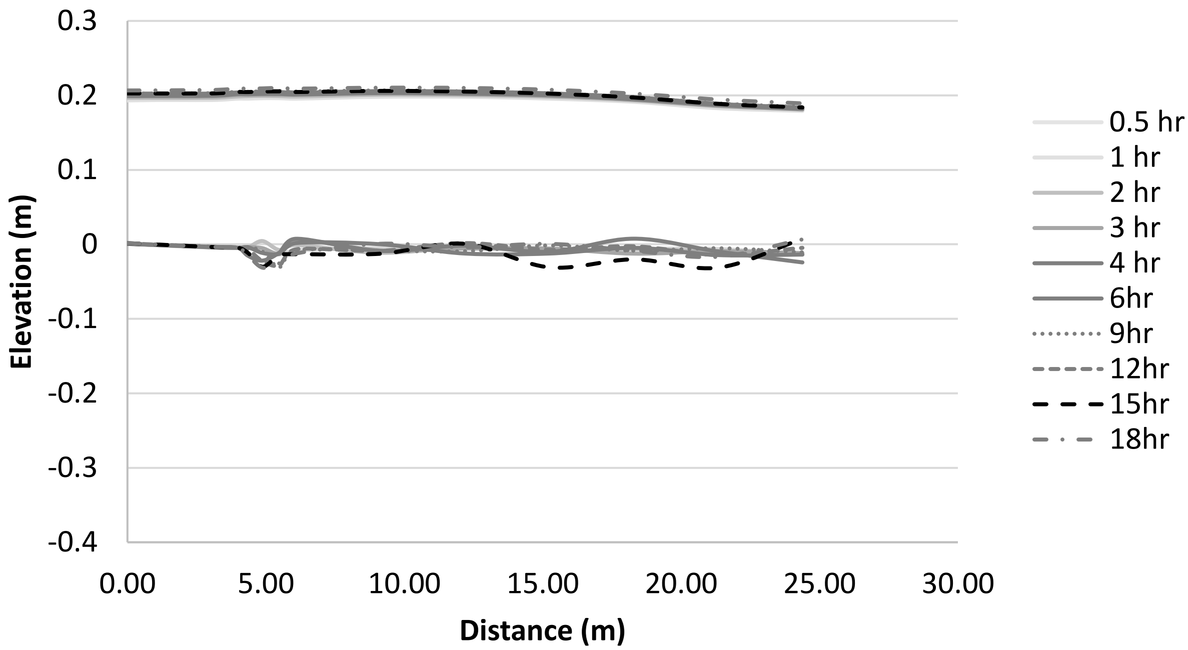

Figure D.22. Water surface and bed elevation at centerline for different time-steps. (CW-0.75-0.72)

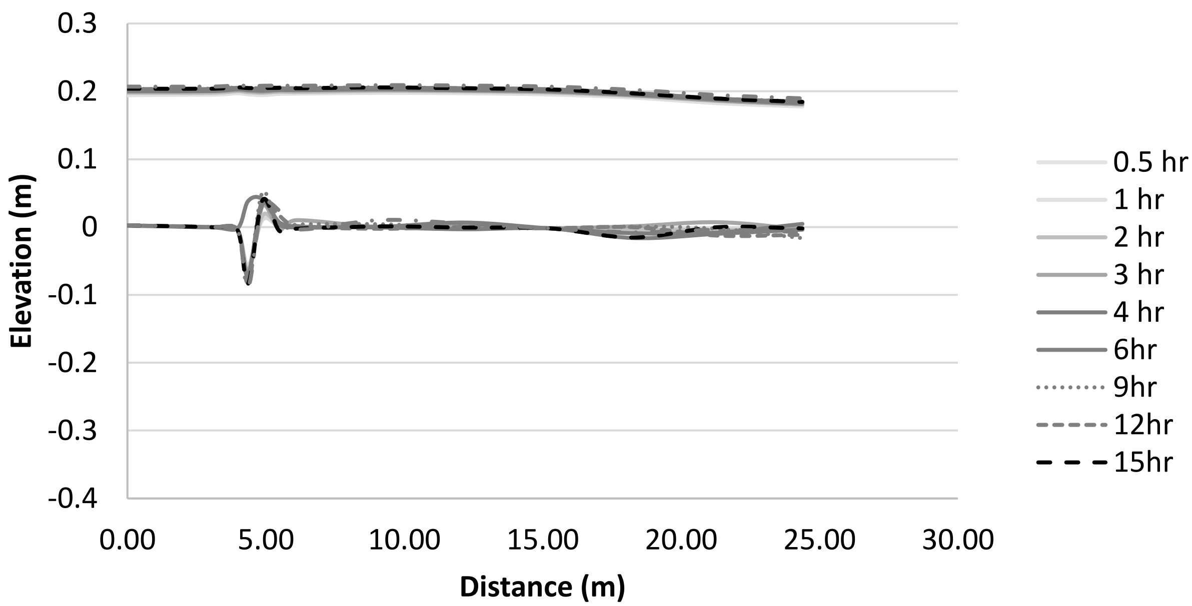

Figure D.23. Water surface and bed elevation near the right-side wall for different time-steps. (CW-0.75-0.72)

X. CW-0.75-0.90

- LiDAR scanned data:

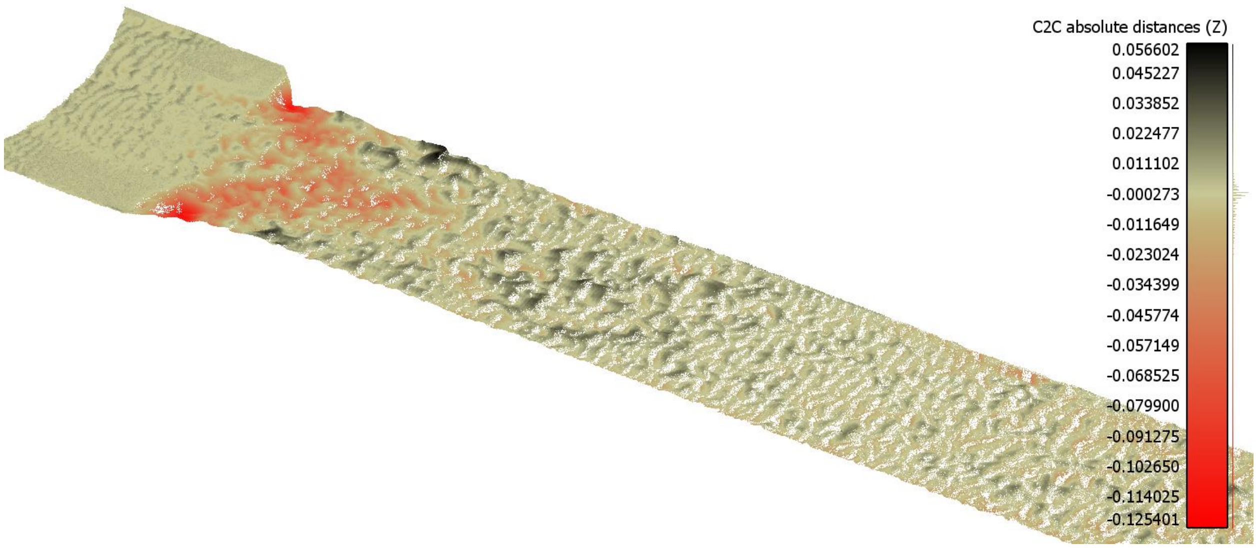

Figure D.24. Bed elevation difference between time zero and after 18-hour of experiments. (CW-0.75-0.90)

- Temporal bed and water surface elevation

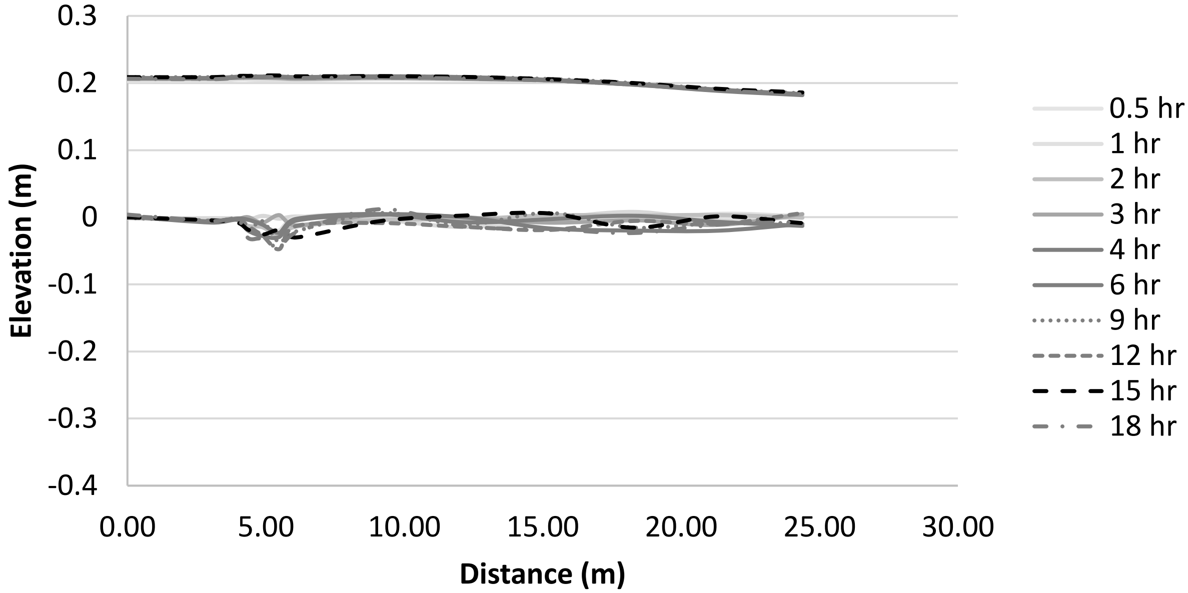

Figure D.25. Water surface and bed elevation at centerline for different time-steps. (CW-0.75-0.90)

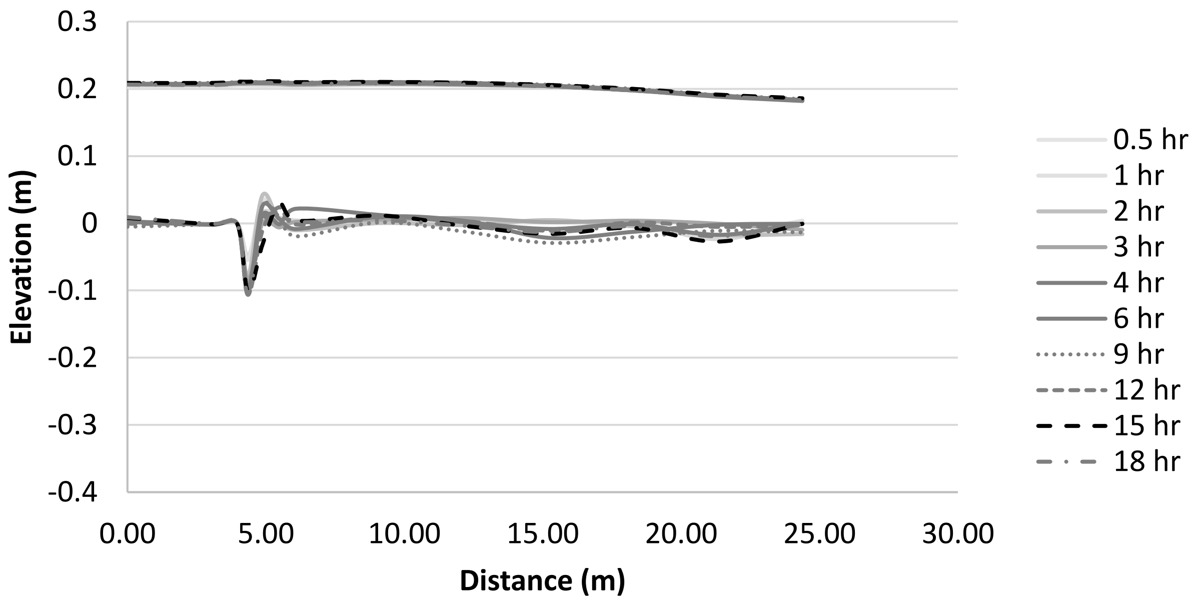

Figure D.26. Water surface and bed elevation near the right-side wall for different time-steps. (CW-0.75-0.90)

XI. CW-0.25-0.81

- LiDAR scanned data:

Figure D.27. Bed elevation difference between time zero and after 18-hour of long-contraction experiments. (CW-0.25-0.81)

XII. CW-0.25-0.98*

- LiDAR scanned data:

(a)

(b)

(c)

Figure D.28. LiDAR data at different time steps regarding long-contraction experiment; (a) 12th hour, (b) 24th hour, (c)30th hour.

D.2. Live-bed experiments:

I. LB-0.5-1.44

- LiDAR-scanned data:

Figure D.29. Bed elevation difference between time zero and after 7-hour of experiments. (LB-0.50-1.44)

- Temporal bed and water surface elevation

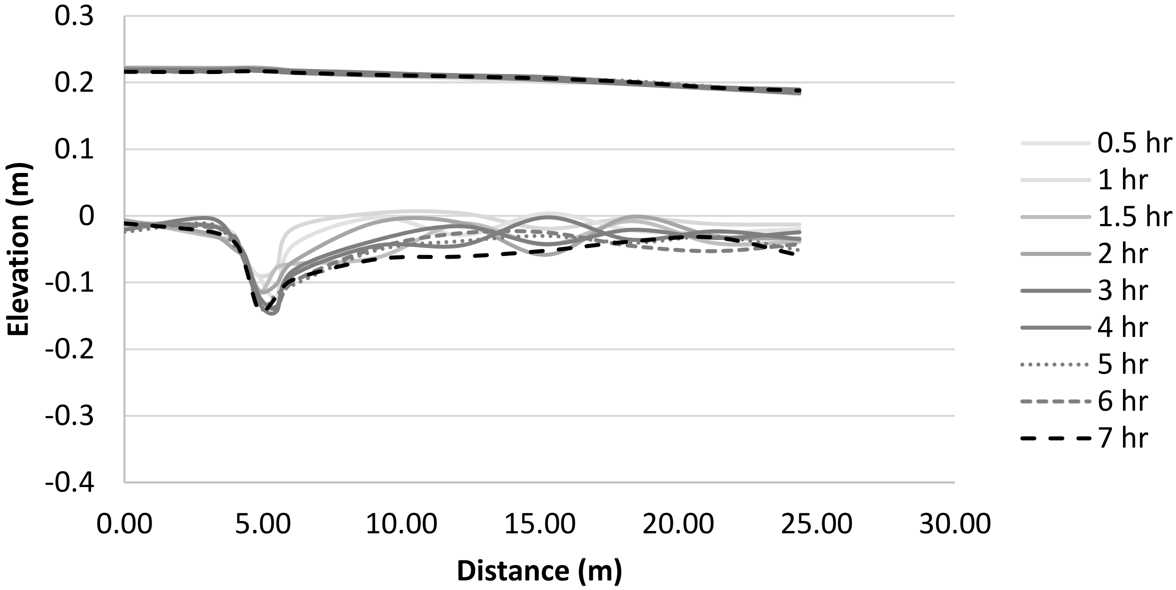

Figure D.30. Water surface and bed elevation at centerline for different time-steps. (LB-0.50-1.44)

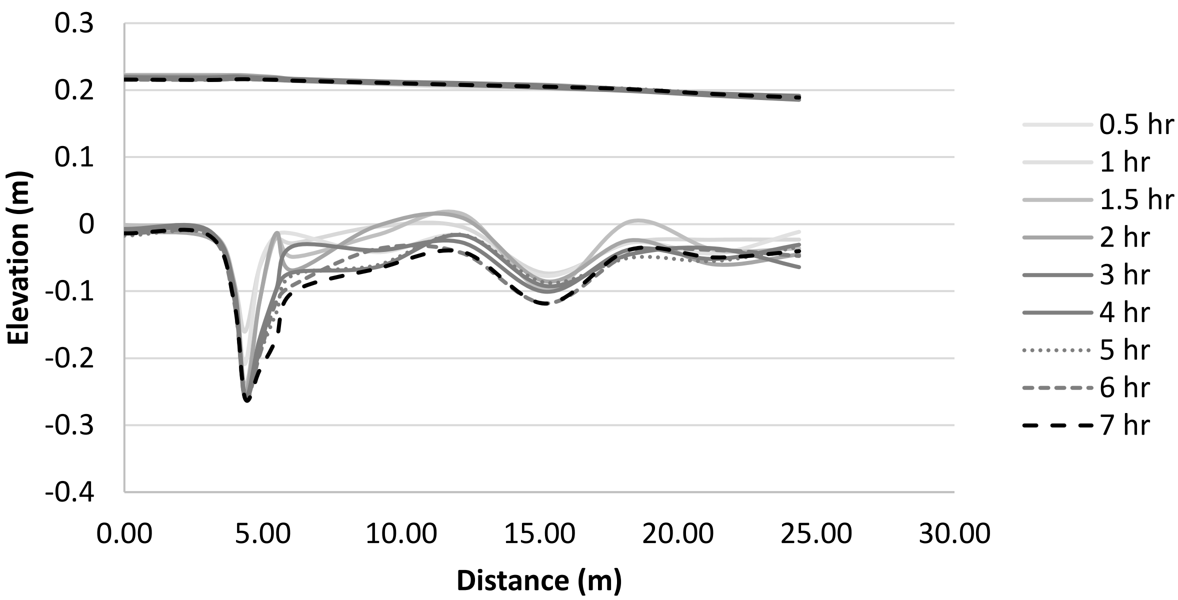

Figure D.31. Water surface and bed elevation near the right-side wall for different time-steps. (LB-0.50-1.44)

II. LB-0.5-1.96

- LiDAR-scanned data:

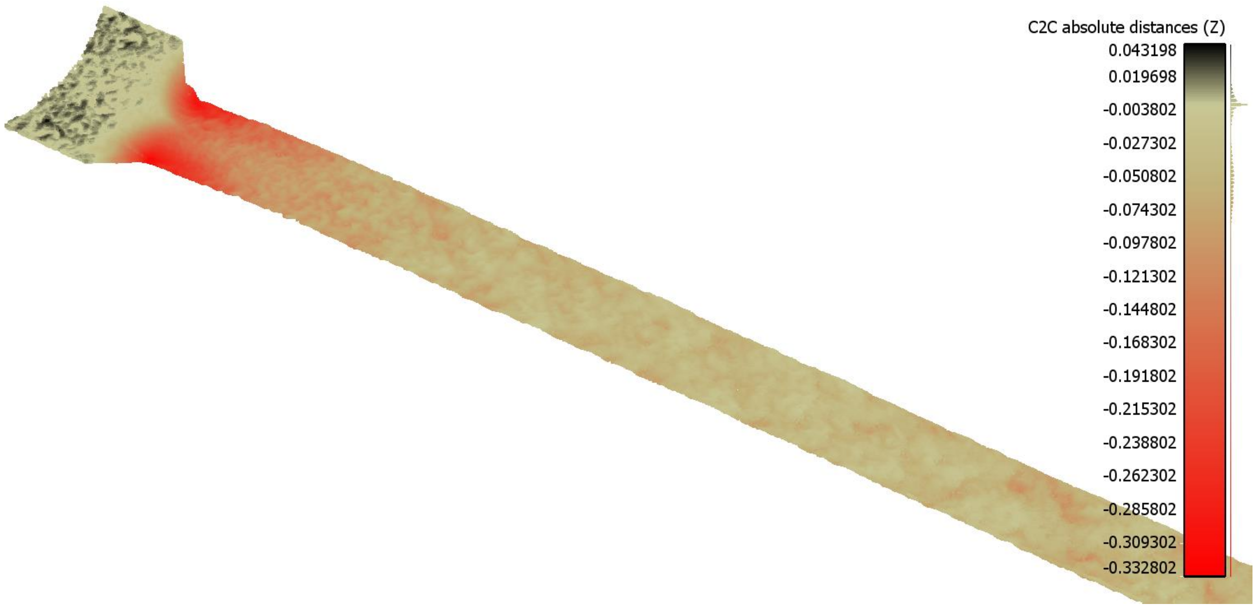

Figure D.32. Bed elevation difference between time zero and after 7-hour of experiments. (LB-0.50-1.96)

- Temporal bed and water surface elevation

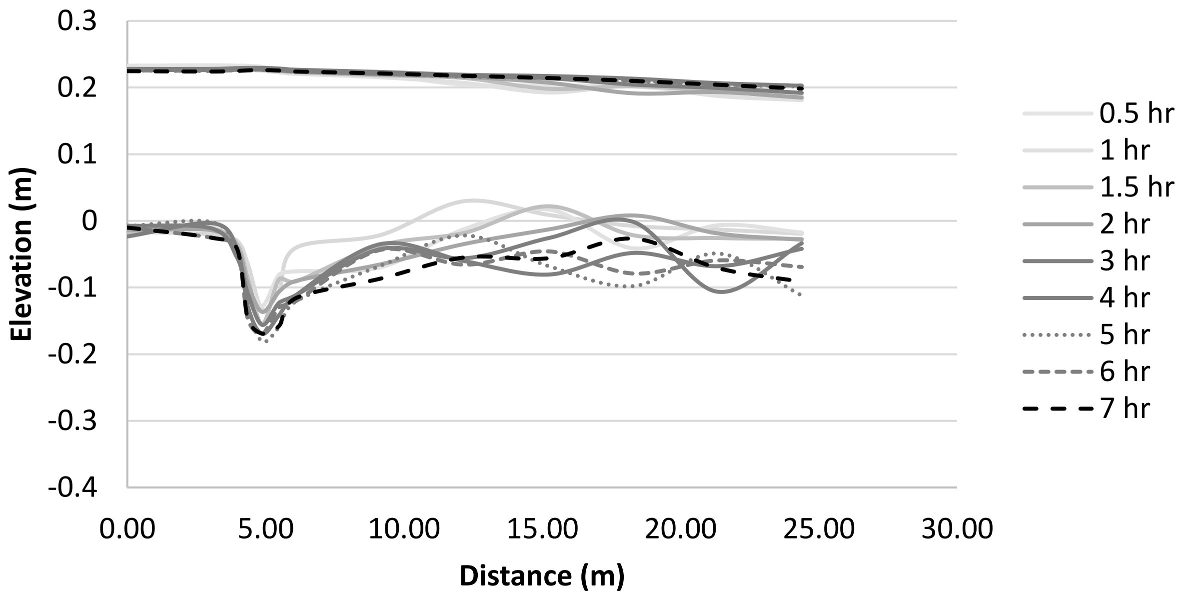

Figure D.33. Water surface and bed elevation at centerline for different time-steps. (LB-0.50-1.96)

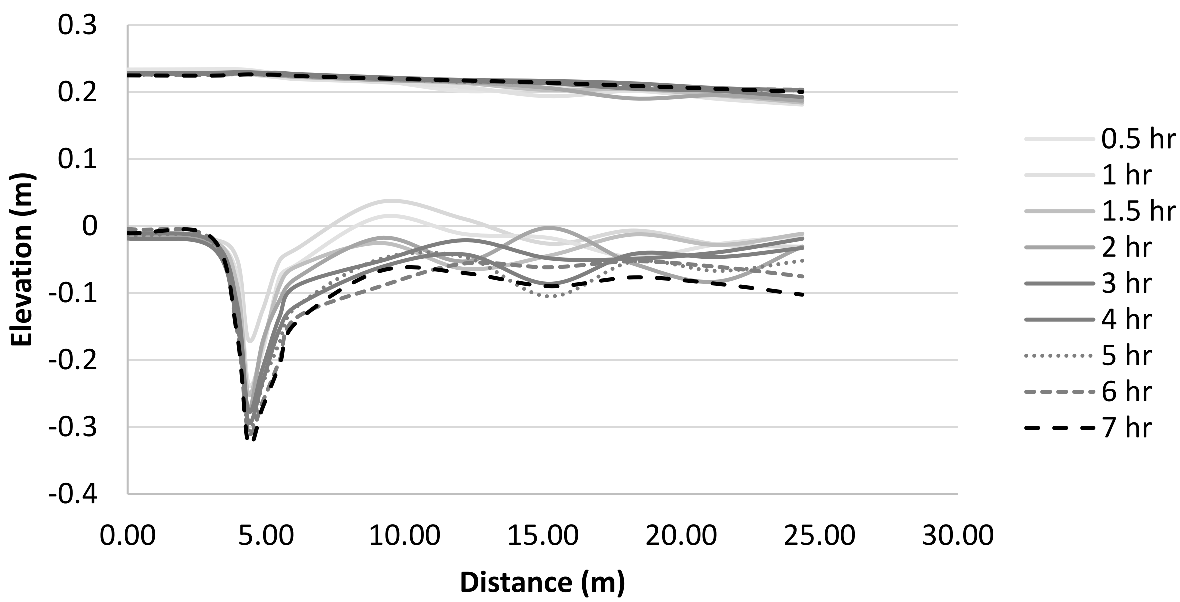

Figure D.34. Water surface and bed elevation near the right-side wall for different time-steps. (LB-0.50-1.96)

III. LB-0.5-2.72

- LiDAR-scanned data:

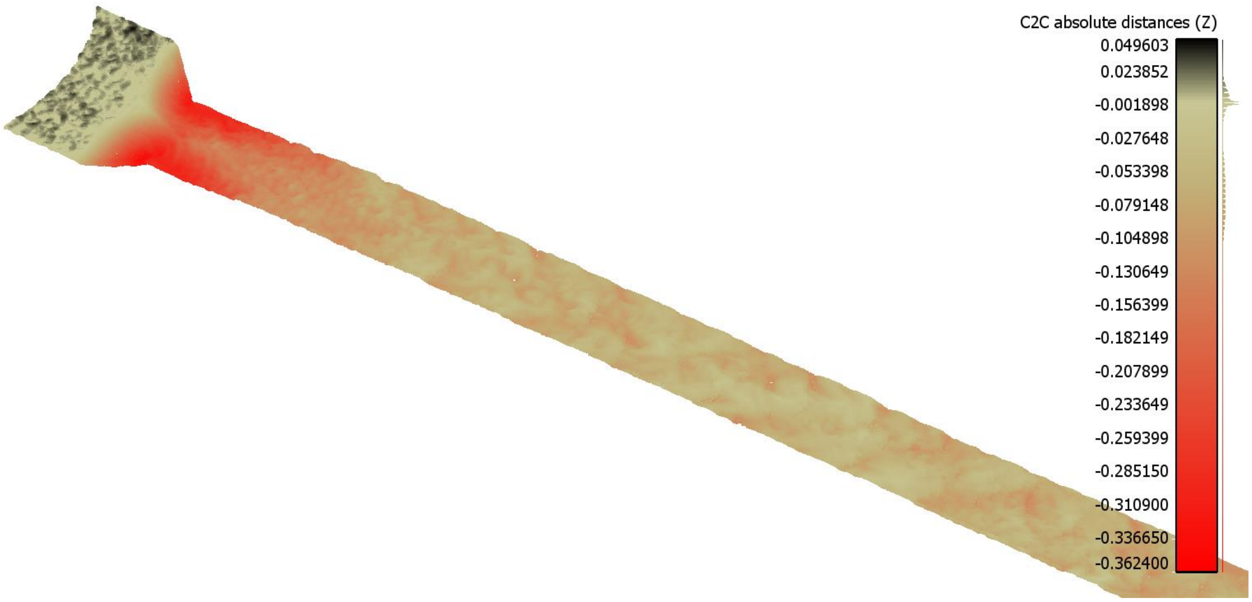

Figure D.35. Bed elevation difference between time zero and after 7-hour of experiments. (LB-0.50-2.72)

- Temporal bed and water surface elevation

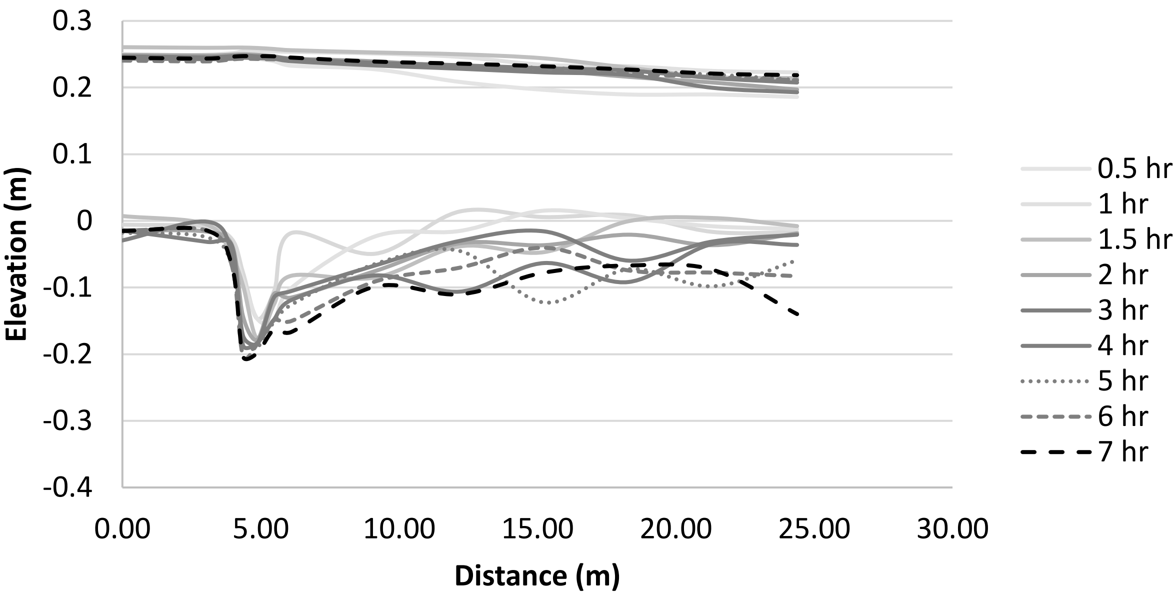

Figure D.36. Water surface and bed elevation at centerline for different time-steps. (LB-0.50-2.72)

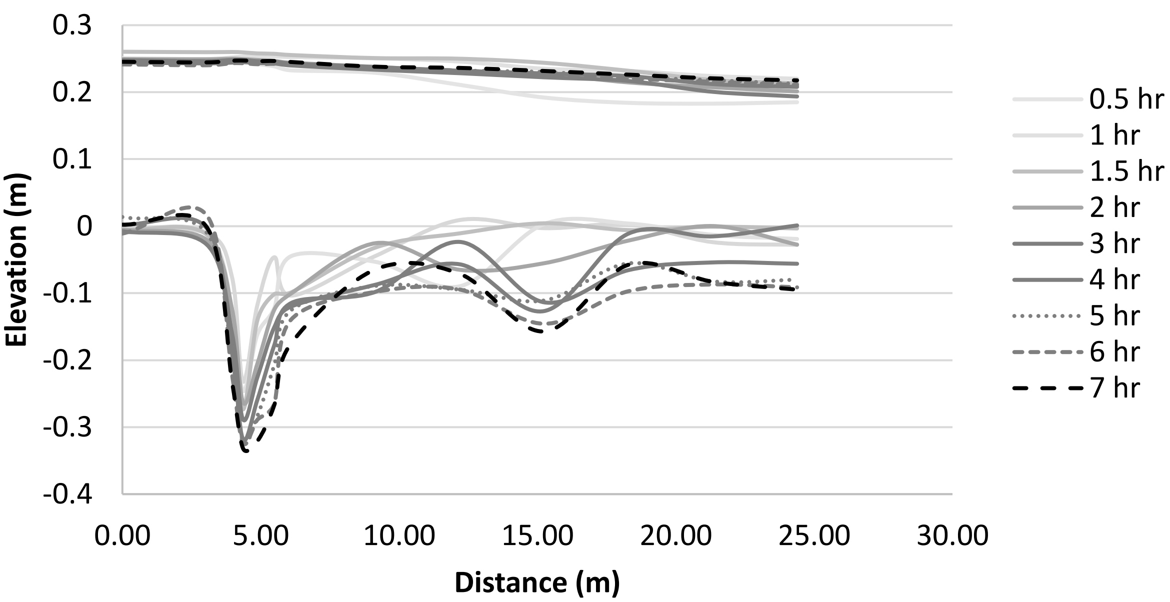

Figure D.37. Water surface and bed elevation near the right-side wall for different time-steps. (LB-0.50-2.72)

IV. LB0-0.5-4.00

- LiDAR-scanned data:

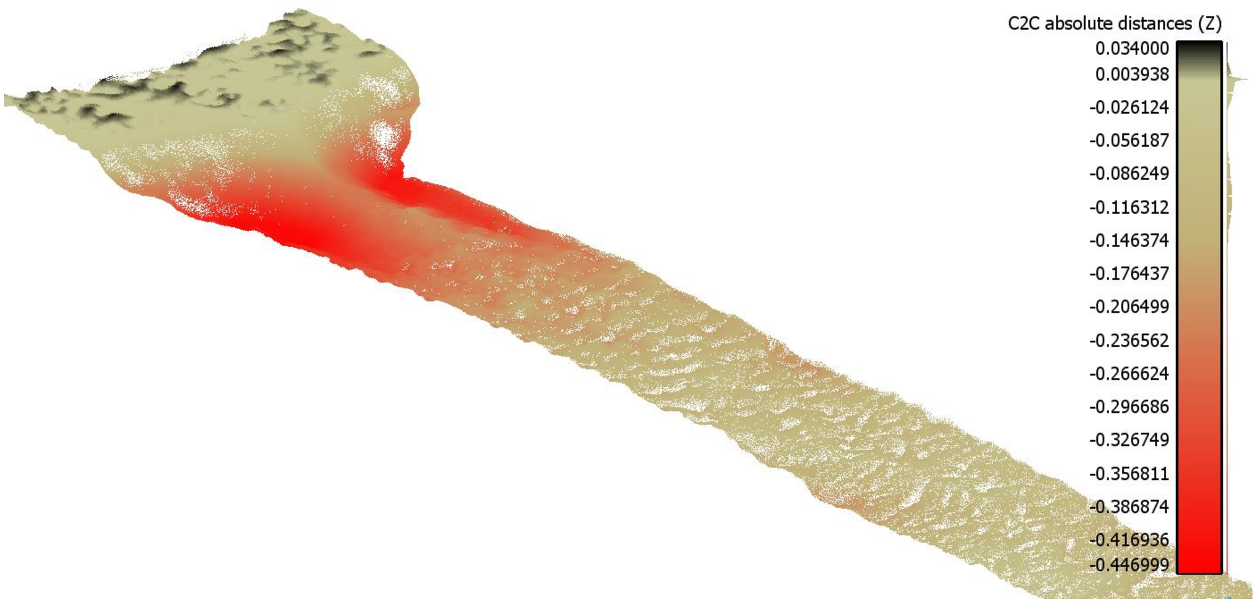

Figure D.38. Bed elevation difference between time zero and after 7-hour of experiments. (LB-0.5-4.0)

- Temporal bed and water surface elevation

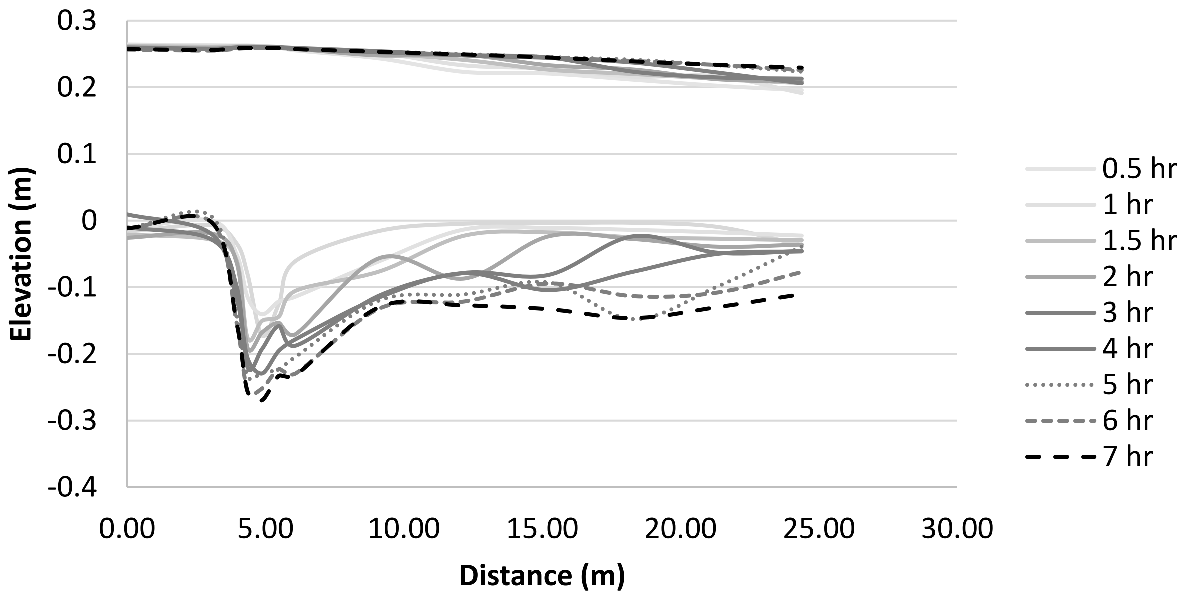

Figure D.39. Water surface and bed elevation at centerline for different time-steps. (LB-0.5-4.0)

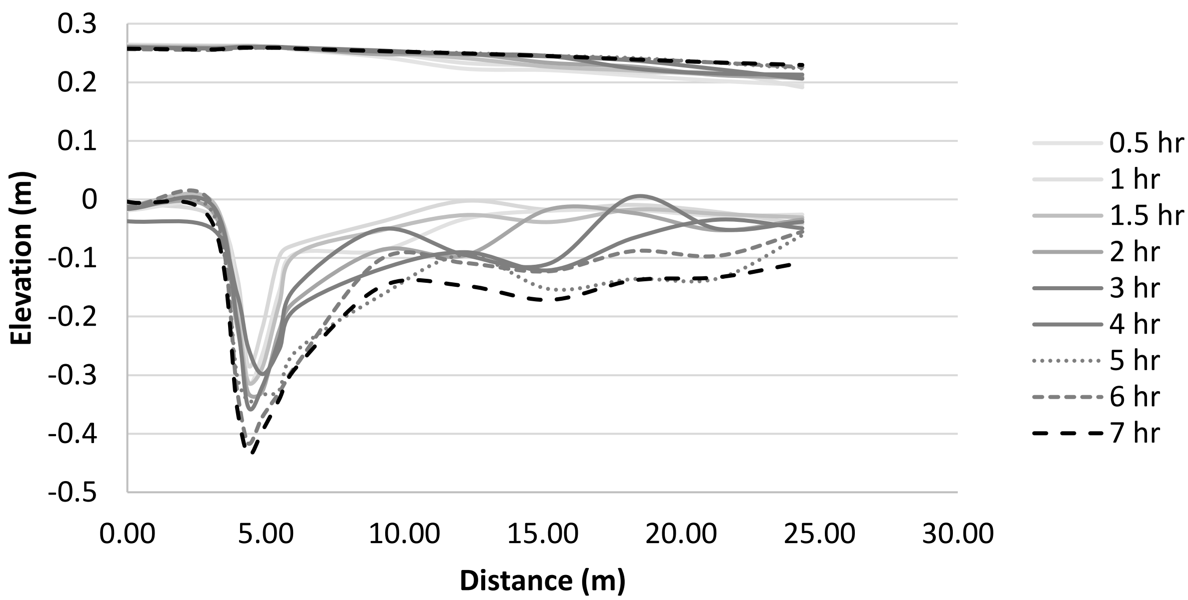

Figure D.40. Water surface and bed elevation near the right-side wall for different time-steps. (LB-0.5-4.0)

V. LB-0.75-1.44

- LiDAR-scanned data:

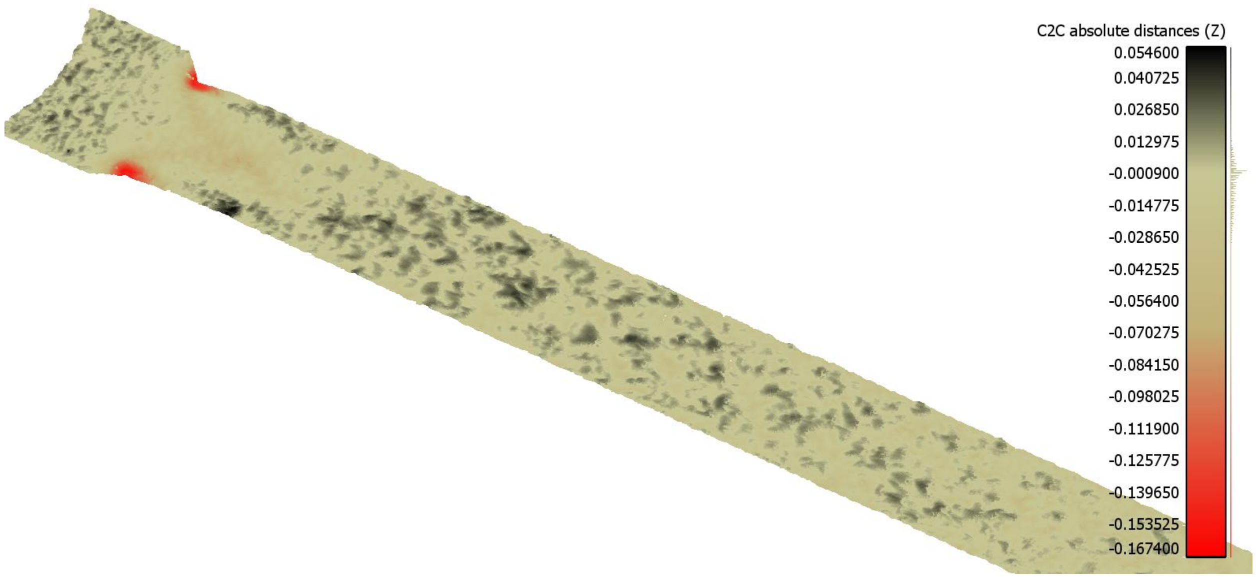

Figure D.41. Bed elevation difference between time zero and after 7-hour of experiments. (LB-0.75-1.44)

- Temporal bed and water surface elevation

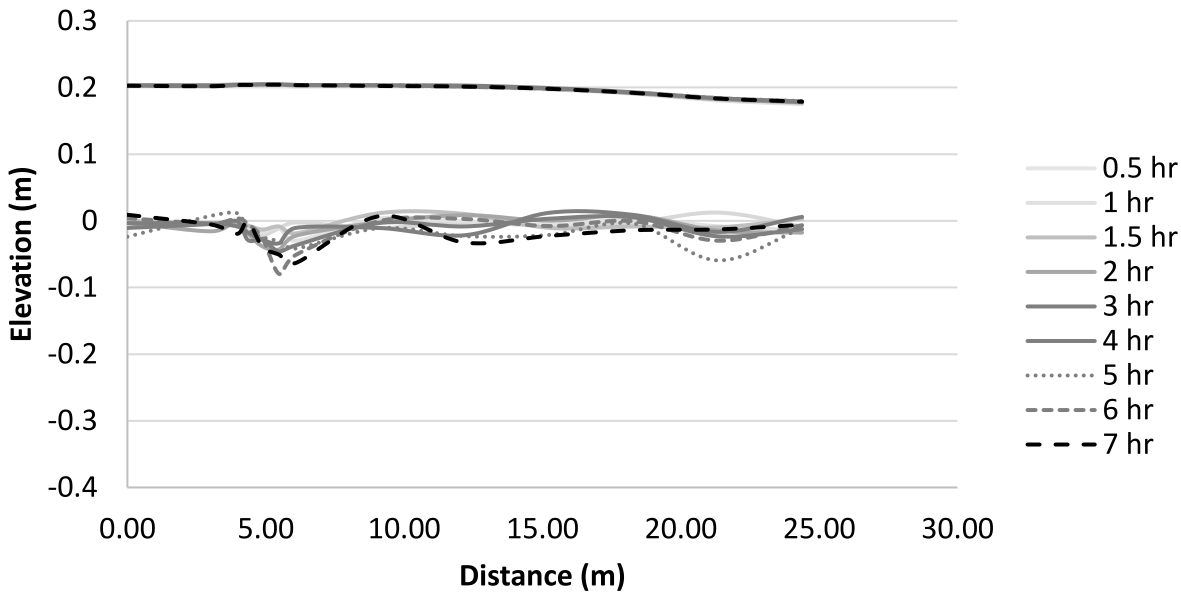

Figure D.42. Water surface and bed elevation at centerline for different time-steps. (LB-0.75-1.44)

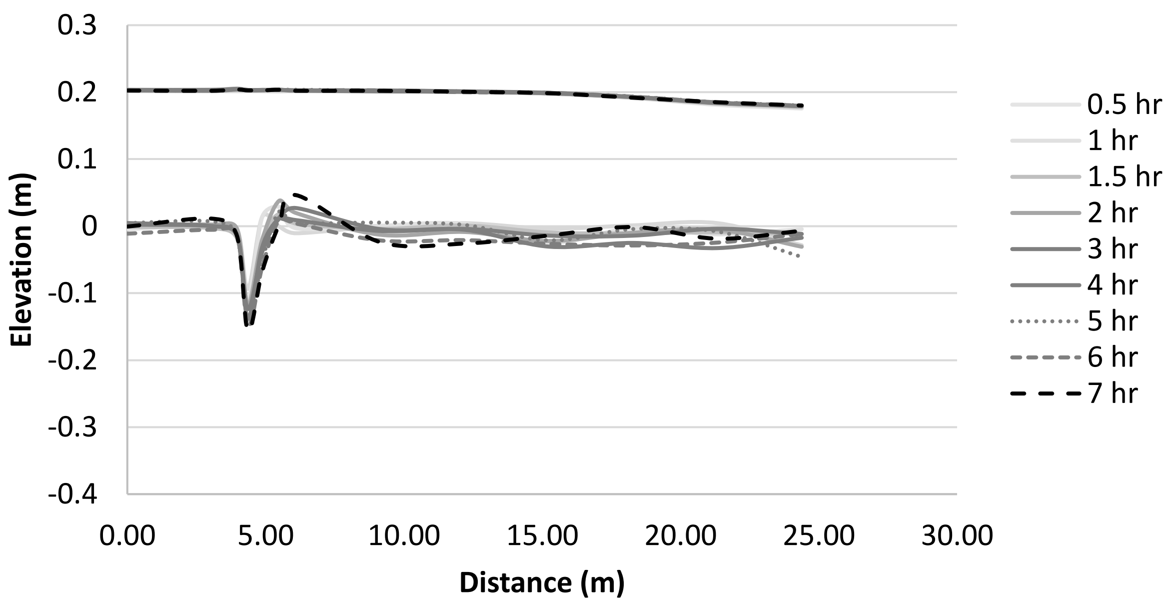

Figure D.43. Water surface and bed elevation near the right-side wall for different time-steps. (LB-0.75-1.44)

VI. LB-0.75-1.96

- LiDAR-scanned data:

Figure D.44. Bed elevation difference between time zero and after 7-hour of experiments. (LB-0.75-1.96)

- Temporal bed and water surface elevation

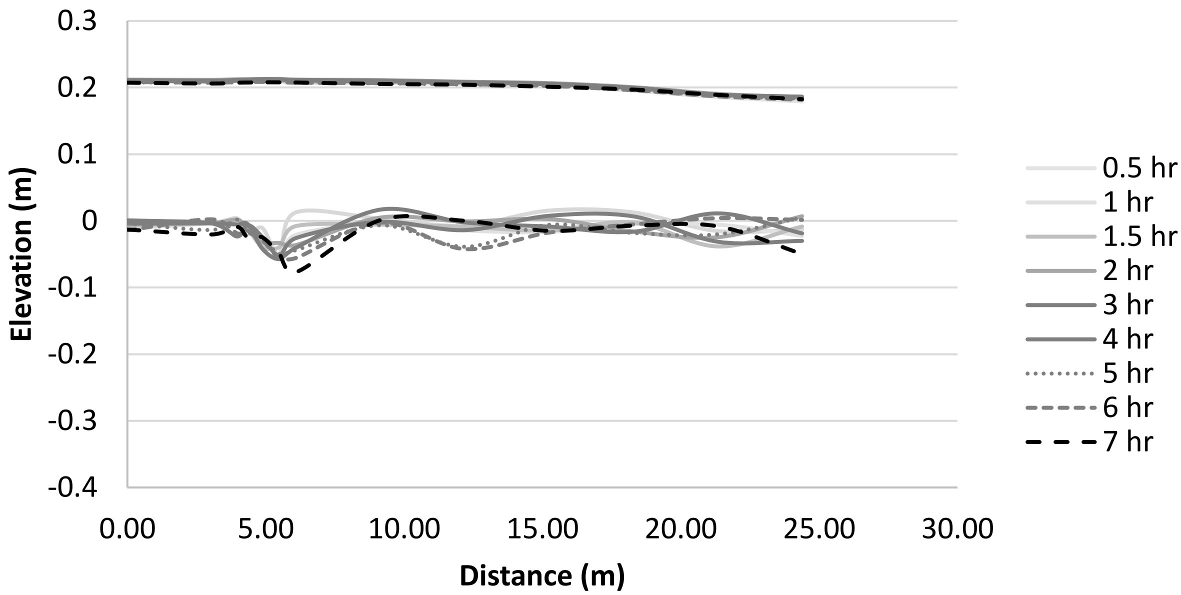

Figure D.45. Water surface and bed elevation at centerline for different time-steps. (LB-0.75-1.96)

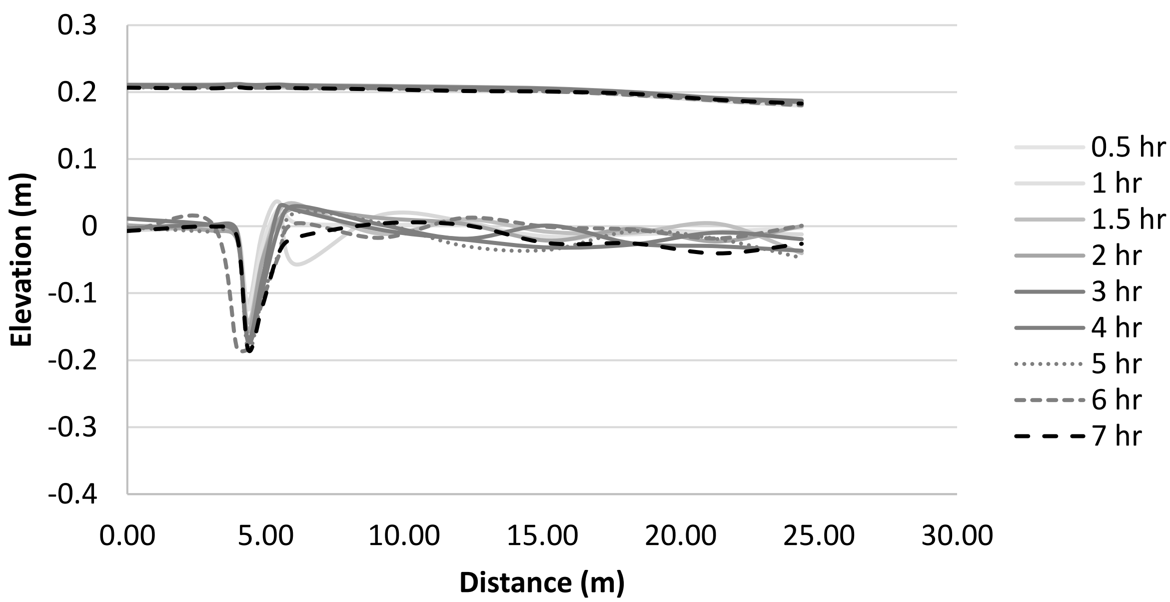

Figure D.46. Water surface and bed elevation near the right-side wall for different time-steps. (LB-0.75-1.96)

VII. LB-0.75-2.72

- LiDAR-scanned data:

Figure D.47. Bed elevation difference between time zero and after 9-hour of experiments. (CW-0.75-2.72)

- Temporal bed and water surface elevation

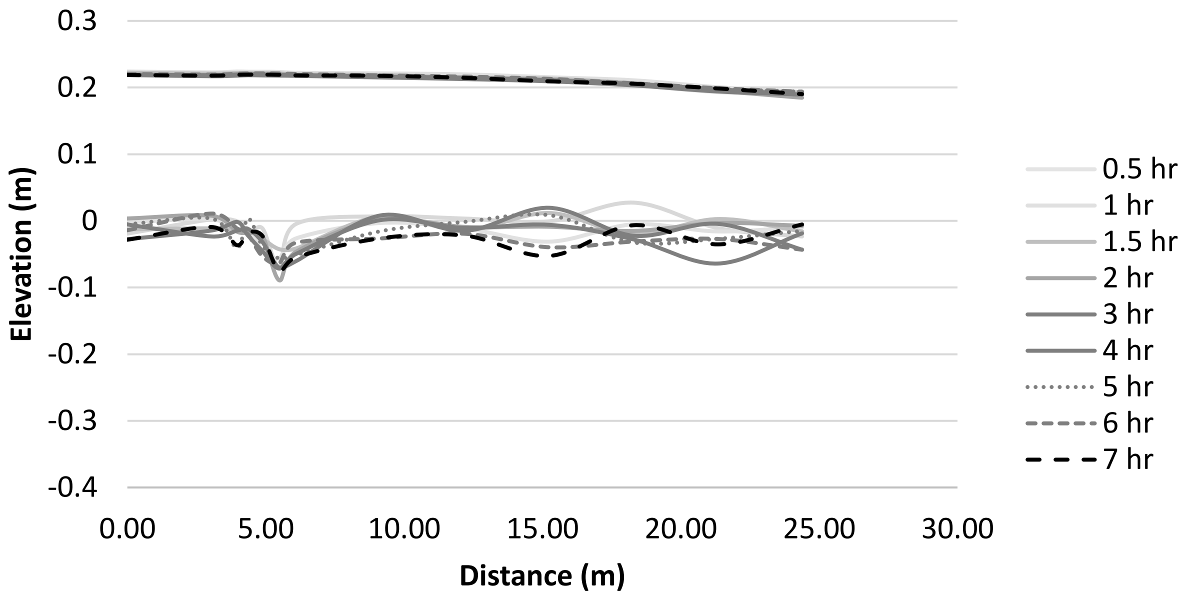

Figure D.48. Water surface and bed elevation at centerline for different time-steps. (LB-0.75-2.72)

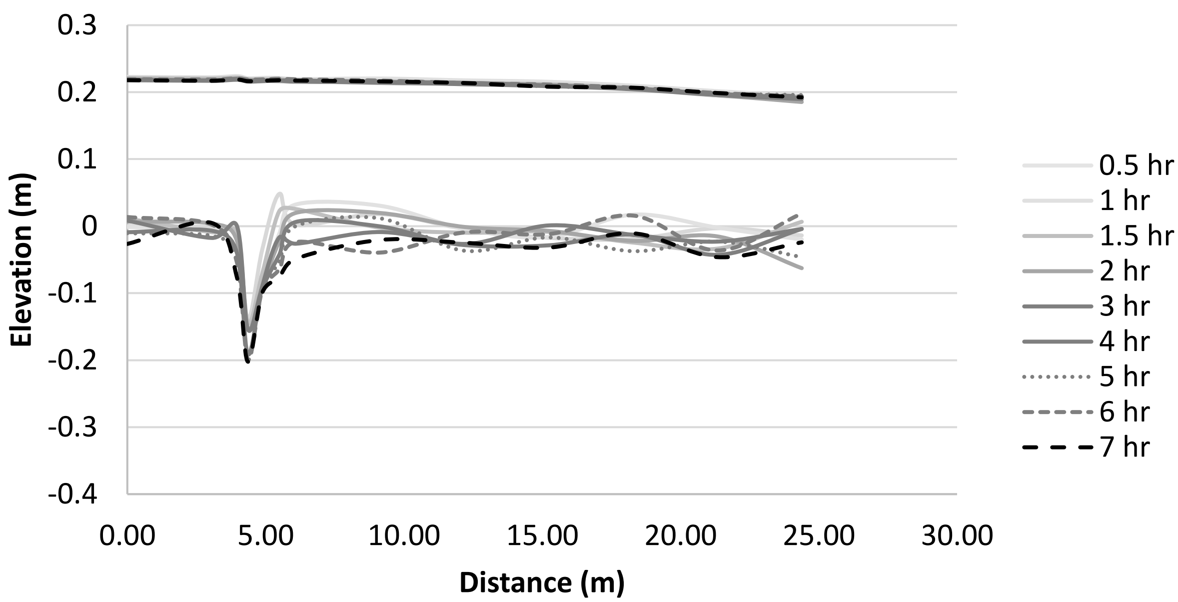

Figure D.49. Water surface and bed elevation near the right-side wall for different time-steps. (LB-0.75-2.72)

VIII. LB-0.75-4.00

- LiDAR-scanned data:

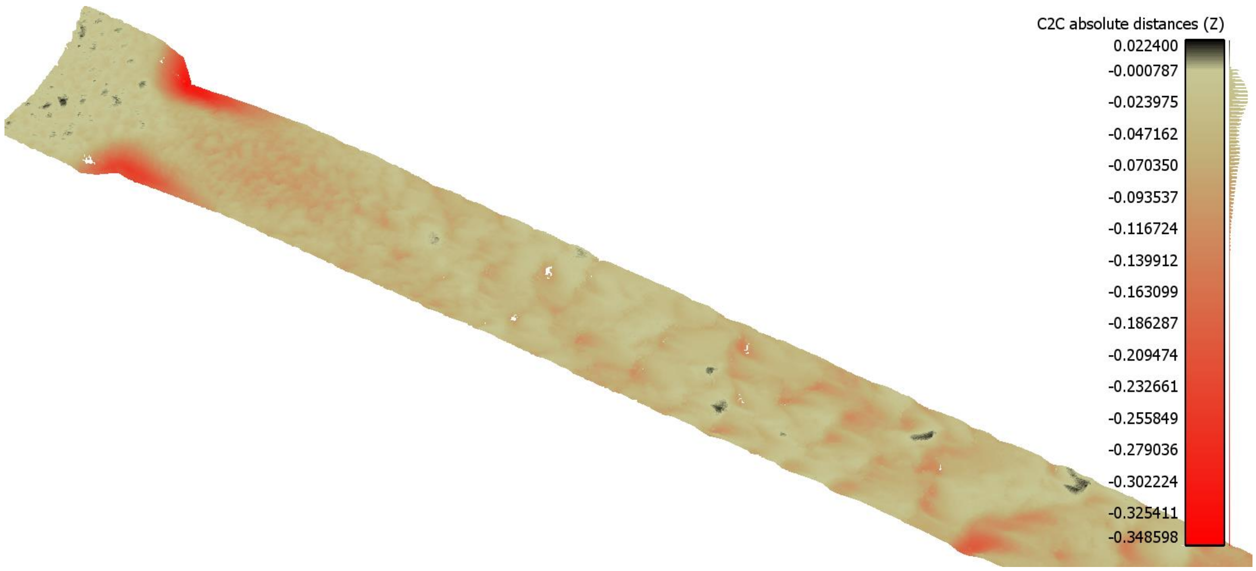

Figure D.50. Bed elevation difference between time zero and after 7-hour of experiments. (LB-0.75-4.0)

- Temporal bed and water surface elevation

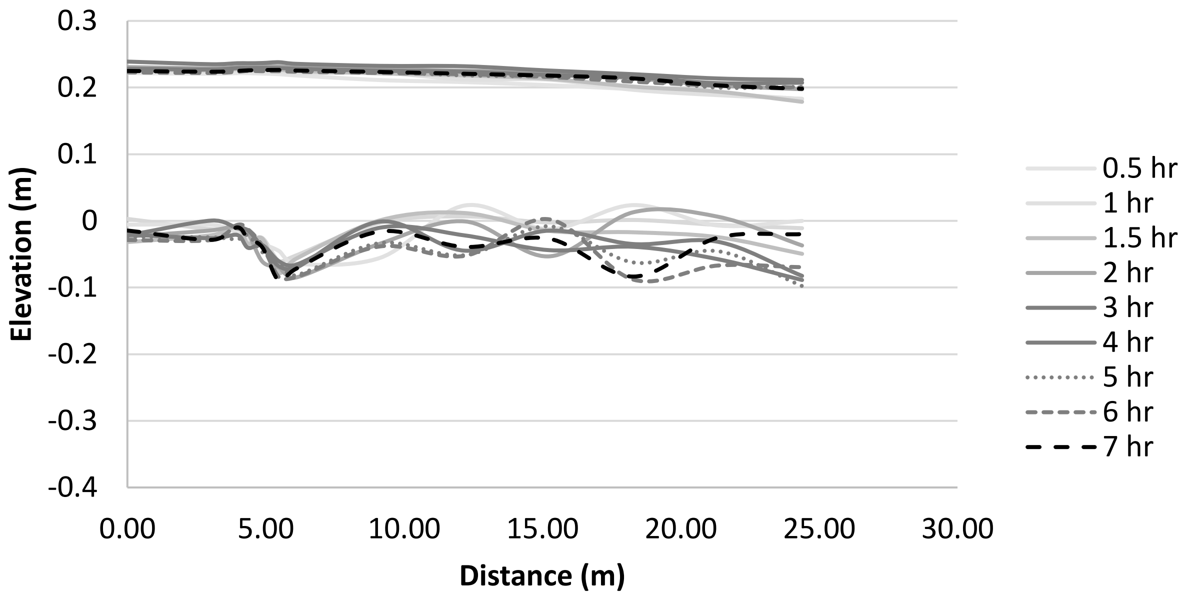

Figure D.51. Water surface and bed elevation at centerline for different time-steps. (LB-0.75-4.0)

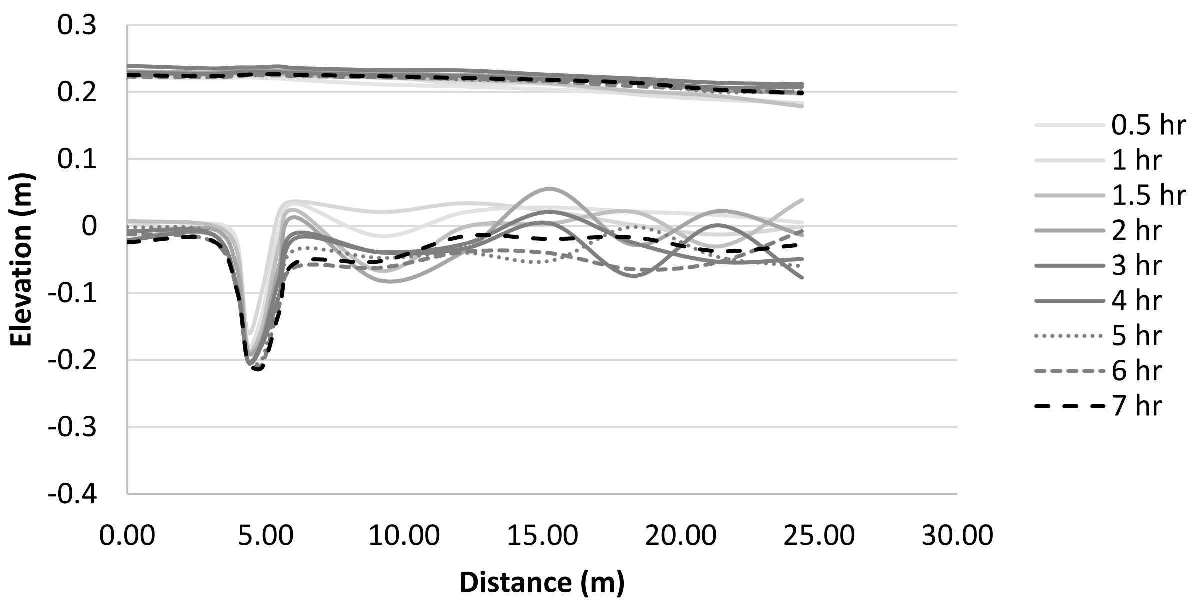

Figure D.52. Water surface and bed elevation near the right-side wall for different time-steps. (LB-0.75-4.0)

IX. LB-0.75-6.25

- LiDAR-scanned data:

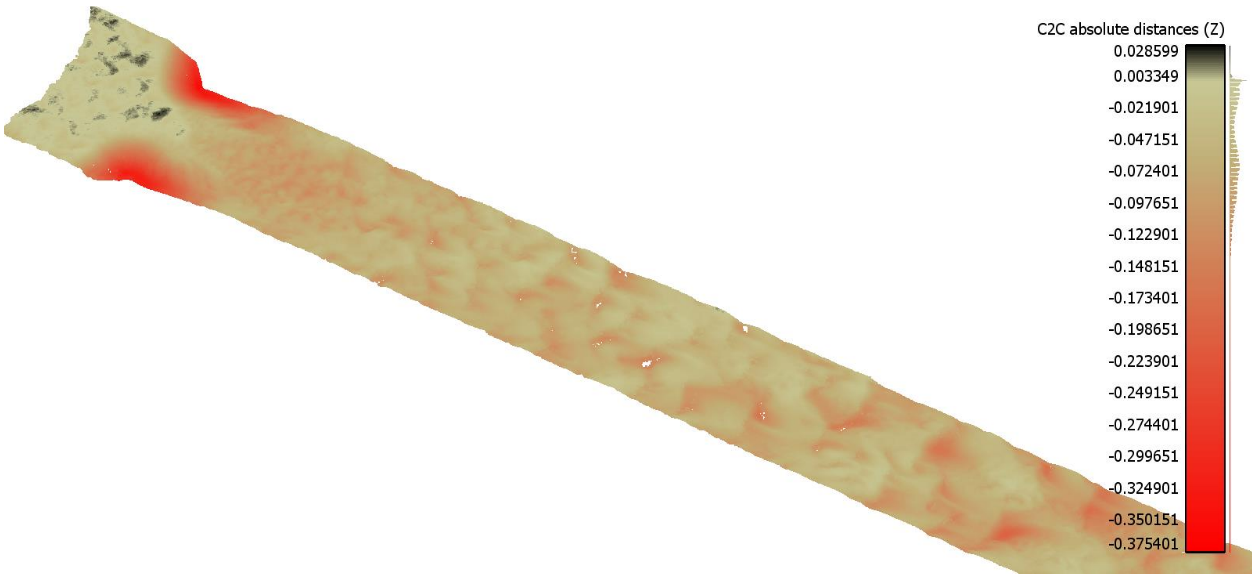

Figure D.53. Bed elevation difference between time zero and after 7-hour of experiments. (LB-0.75-6.25)

- Temporal bed and water surface elevation

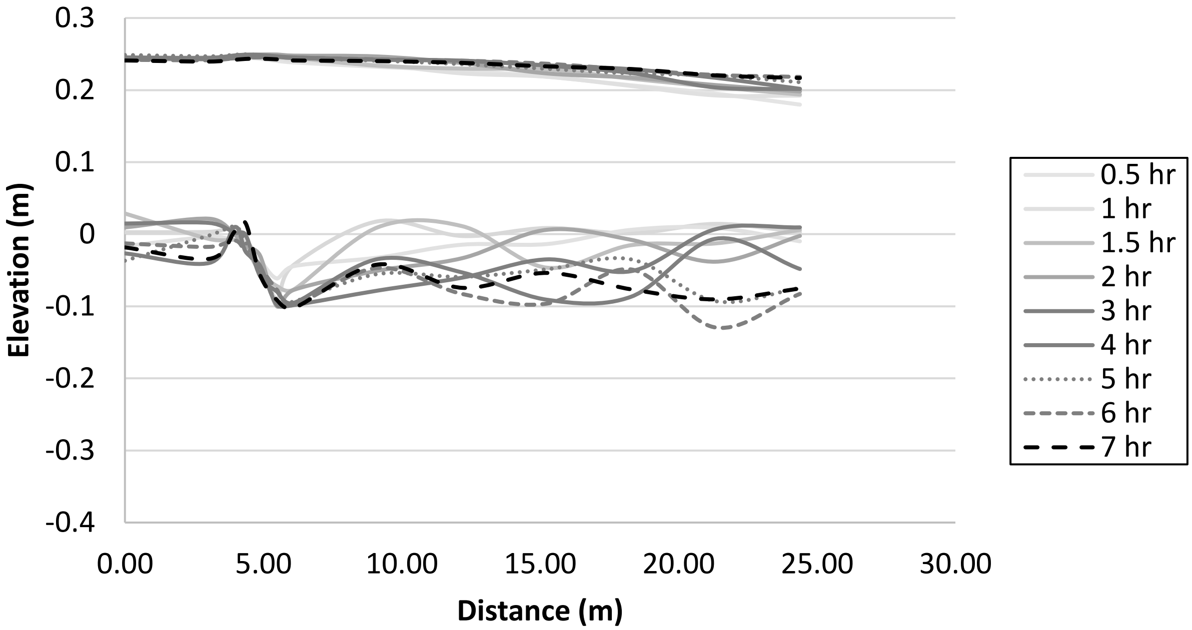

Figure D.54. Water surface and bed elevation at centerline for different time-steps. (LB-0.75-6.25)

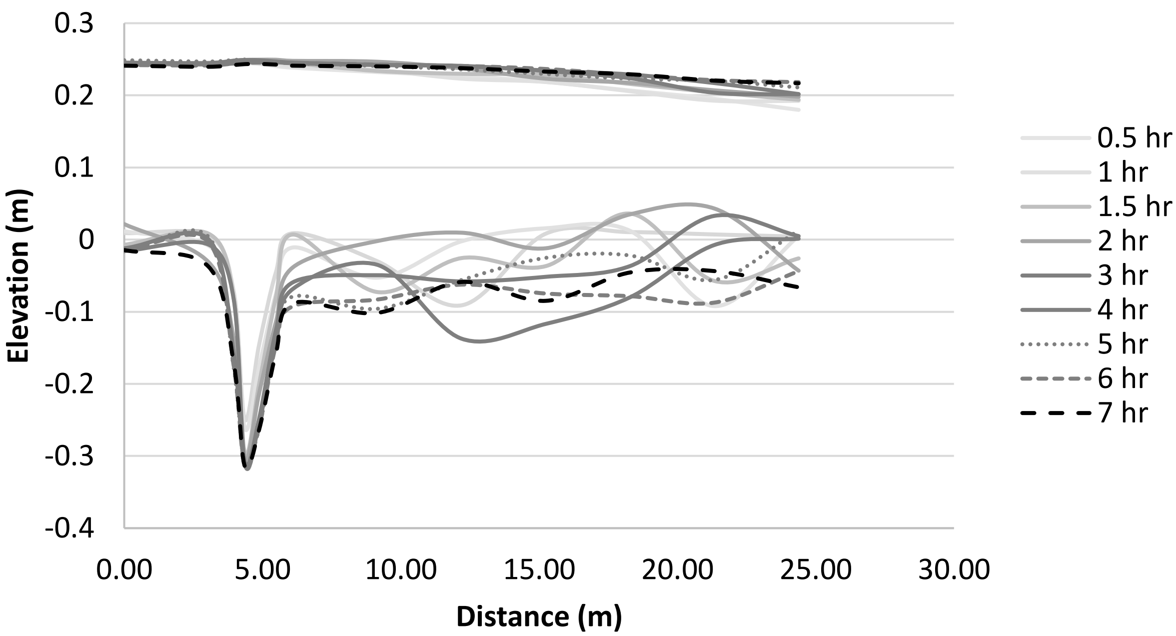

Figure D.55. Water surface and bed elevation near the right-side wall for different time-steps. (LB-0.75-6.25)

Table D.1. Summary of the measurements

Clear-water test #	**B_2/B_1**	**Y_{n1} (m)**	**Q (cms)**	**Measured Y_1 (Backwater)**		**Avg. vena-contracta scour depth (m)**	**Max. corner scour depth (m)**	**Reattachment region scour depth (m)**
				Pre-scour	**Post-scour**			
CW-0.25-0.81*	0.25	0.152	0.087	0.604	0.613	-	0.147	0
CW-0.25-0.98*	0.25	0.152	0.096	0.610	0.622	-	0.166	0
CW-0.25-0.64	0.25	0.178	0.092	0.254	0.245	-	0.315	0.153
CW-0.25-0.56	0.25	0.178	0.087	0.257	0.24	-	0.346	0.150
CW-0.25-0.30	0.25	0.178	0.064	0.227	0.225	-	0.293	0.095
CW-0.25-0.42	0.25	0.178	0.076	0.241	0.23	-	0.229	0.058
CW-0.5-0.30	0.50	0.178	0.064	0.194	0.193	0.036	0.058	0
CW-0.5-0.42	0.50	0.178	0.076	0.205	0.21	0.048	0.076	0
CW-0.5-0.56	0.50	0.178	0.087	0.211	0.211	0.055	0.103	0.011
CW-0.75-0.56	0.75	0.178	0.087	0.197	0.198	0.011	0.055	0
CW-0.75-0.72	0.75	0.178	0.099	0.196	0.204	0.026	0.077	0
CW-0.75-0.90	0.75	0.178	0.111	0.205	0.207	0.029	0.075	0
Live-bed test #	**B_2/B_1**	**Y_{n1} (m)**	**Q (cms)**	**Measured Y1 (Backwater depth)**		**Avg. vena-contracta scour depth (m)**	**Max. corner scour depth (m)**	**Reattachment region scour depth (m)**
				Pre-scour	**Post-scour**			
LB-0.5-1.44	0.50	0.178	0.138	0.222	0.216	0.108	0.157	0.059
LB-0.5-1.96	0.50	0.178	0.161	0.23	0.225	0.145	0.177	0.090
LB-0.5-2.72	0.50	0.178	0.190	0.252	0.246	0.165	0.247	0.126
LB0-0.5-4.0	0.50	0.178	0.231	0.263	0.259	0.232	0.267	0.174
LB-0.75-1.44	0.75	0.178	0.138	0.204	0.204	0.042	0.091	0.006
LB-0.75-1.96	0.75	0.178	0.161	0.211	0.207	0.044	0.092	0.017
LB-0.75-2.72	0.75	0.178	0.190	0.224	0.219	0.050	0.092	0.034
LB-0.75-4.0	0.75	0.178	0.231	0.222	0.225	0.067	0.116	0.067
LB-0.75-6.25	0.75	0.178	0.288	0.244	0.242	0.081	0.141	0.088

Appendix E: Numerical modeling using SRH-2D

The numerical code SRH-2D enables development of two-dimensional models that can be used to investigate water flow, loose boundary and sediment-transport processes at particular reaches of rivers. The software was developed by the U.S.'s Bureau of Reclamation and Federal Highway Administration in the U.S. in collaboration with Taiwan's Water Resources Agency. The code's main features were pertinent to the present study; Accordingly, the code was used in the present study to produce further insight into the flow field within the entrance region of open-channel contractions.

SRH-2D solves the depth-averaged St.Venant equations, also known as the i.e., the dynamic wave equations. The model uses a flexible mesh (a hybrid mesh containing quadrilateral and triangular cells) that can include computational cells of arbitrary shape. Additionally, the model purports to use a robust and stable numerical with a wetting-drying algorithm.

The major capabilities of the SRH-2D flow solver are as follow:

- The depth-averaged dynamic wave equations are solved using a finite-volume numerical method;
- The model can simulate steady state (with constant discharge) or unsteady flows (with flow hydrograph);
- Time integration is based on an implicit scheme to achieve solution robustness and efficiency;

- An unstructured polyhedron mesh is used, which includes the structured quadrilateral mesh, the purely triangular mesh, or a combination of the two. Further, SRH-2D can use both cartesian or raster meshes. In most applications, a combination of quadrilateral and triangular meshes produces greater efficiency and accuracy;
- All flow regimes (subcritical, transitional critical, and supercritical flows) may be simulated simultaneously without the need for a special (user) intervention;
- Modules are available to simulate in-stream structures, such as weirs, spillway gates, culverts, bridges, obstructions of various form, internal boundaries, and pressurized zones;
- A robust wetting-drying algorithm is used; and,
- SRH-2D can be used to solve variables including water surface-elevations, water depths, and depth averaged velocities. Output variables include these variables plus Froude number (Fr) and bed shear stress(τ_b).

The major features of SRH-2D's module for loose-boundary sediment transport include the following sub-modules:

- Multi-Size Sediment Transport (Non-uniform Sediment): Bed sediment can be grouped in different size classes and each class is tracked and transported separately;
- Total-Load (or Variable-Load) Formulation: Enables the simultaneous modeling of suspended-, bed-, and mixed-load transport;
- Non-Equilibrium Transport (vs. Exner Eq): This sub-module can simulate sediment transport for a wide range of flow speeds;
- Multiple-Layer Bed Dynamics: This sub-module takes bed stratigraphy into account and includes simulation of bed-particle sorting and armoring processes;

- Cohesive or Non-Cohesive Sediments: This submodule enables both sizes (and types) of sediment to be present at the same time and as a mixture;
- Sediment Capacity Equations: Various selections are available for choice of sediment transport method; and,
- Secondary Flow and Gravity: Flow along curved paths can be simulated, such as along a channel bend.

SRH-2D is widely used by designers of bridge waterways to simulate flow and mobile-bed conditions. The medium-contraction ($B_2/B_1=0.5$) and three shear stress ratios (τ_1/τ_c), 0.3, 1.44, and 4.0, were chosen to evaluate the capabilities of SRH-2D.

First, the shear stress ratio $\tau_1/\tau_c=1.44$ was chosen and used to calibrate Manning's *n,* which was found to be about 0.016, based on SRH-2D and the use of Van-Rijn method for estimating Manning's *n* in alluvial channels. The comparison of the simulated water surface elevation at the centerline and measurements is shown in Figure E.1, which shows that the simulation agreed well with the measurments. This value n = 0.016 was used for two othe simulations.

Different mesh sizes and cell types, the structured quadrilateral mesh, the purely triangular mesh, or a combination of the two, were all used to study the flow-field effects of B_2/B_1 and τ_1/τ_c. The overall results of different mesh cells differed little, however the quadrilateral mesh had better time efficiency. The 2D mesh with about 2,774 elements is illustrated in Figure E.2.

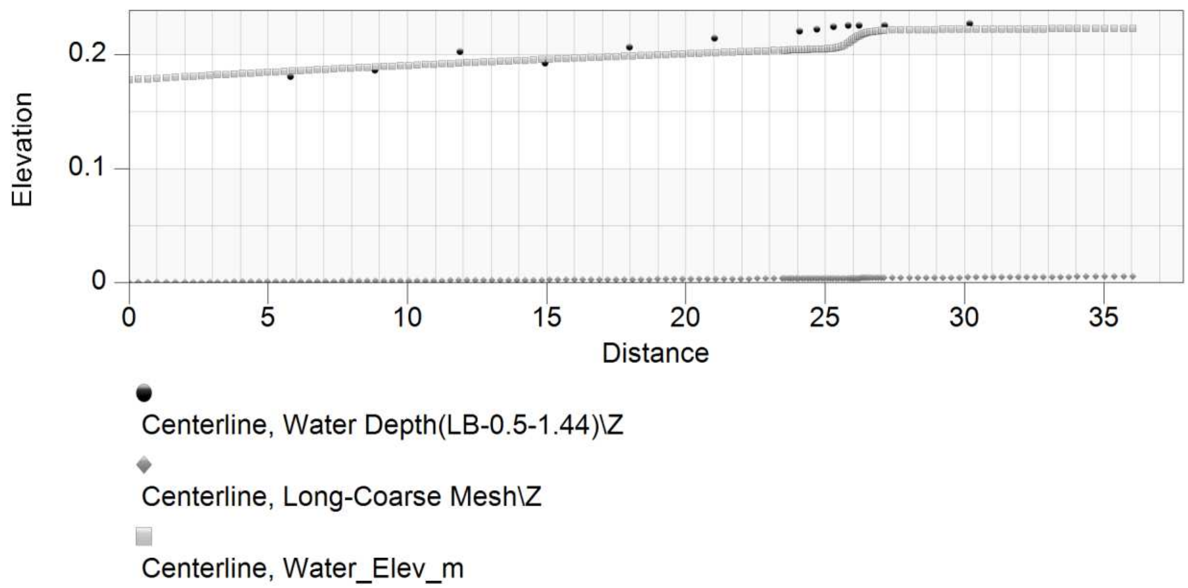

Figure E.1. Comparing model water surface elevation with measurements.

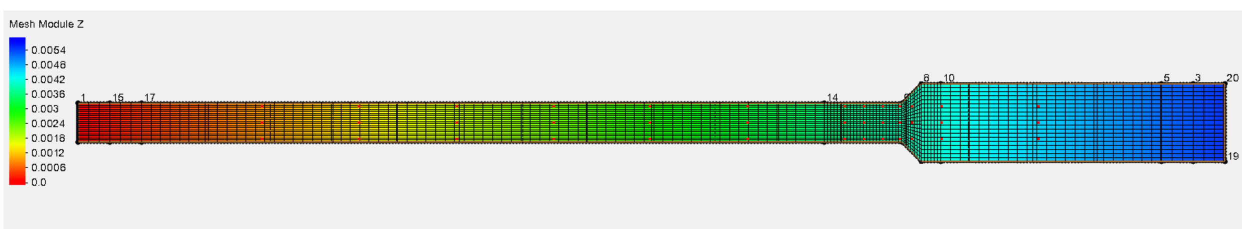

Figure E.2. The 2D numerical domain of the 0.5 contraction ratio.

To compare the influences of the two parameters, various sediment transport and turbulence model were used. However, the use of different turbulence models (e.g., k-ε or parabolic) did not substantially changed the results. Therefore, the parabolic model was used due to its time efficiency. Two sediment transport equations Yang (1973) and Engelund-Hansen had comparable results to the measurements. The results of these two equations are discussed and compared below.

The duration of each run was in accordance with the actual duration of each flume experiment. Therefore, the duration of each run was about 18 and 7 hours for clear-water and live-bed cases, respectively.

An overall finding was that SRH-2D did not yield accurate results for the flow field at the contraction entrance, especially near the entrance corners. This shortcoming is attributed to the highly three-dimensional nature of the flow field at this location and the inability of SRH-2D to simulate such flow fields.

D.1. Model results using Yang (1973) sediment transport method

The plan view of the channel, centerline and near the right sidewall profiles for three shear stress ratios (τ_1/τ_c = 0.3, 1.44, and 4.0) are shown in Figure E.3.

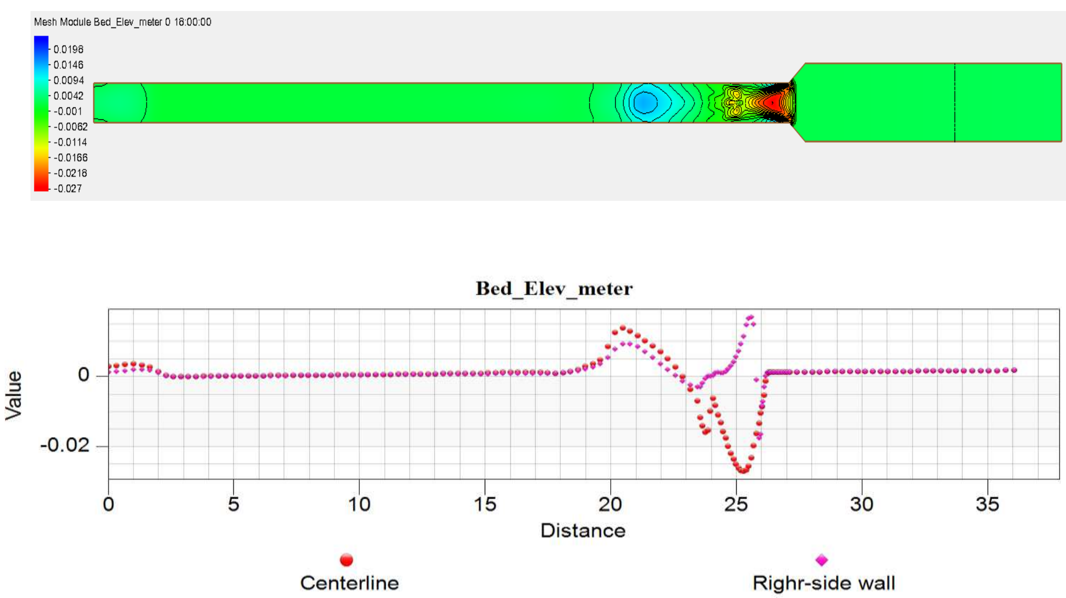

(a)

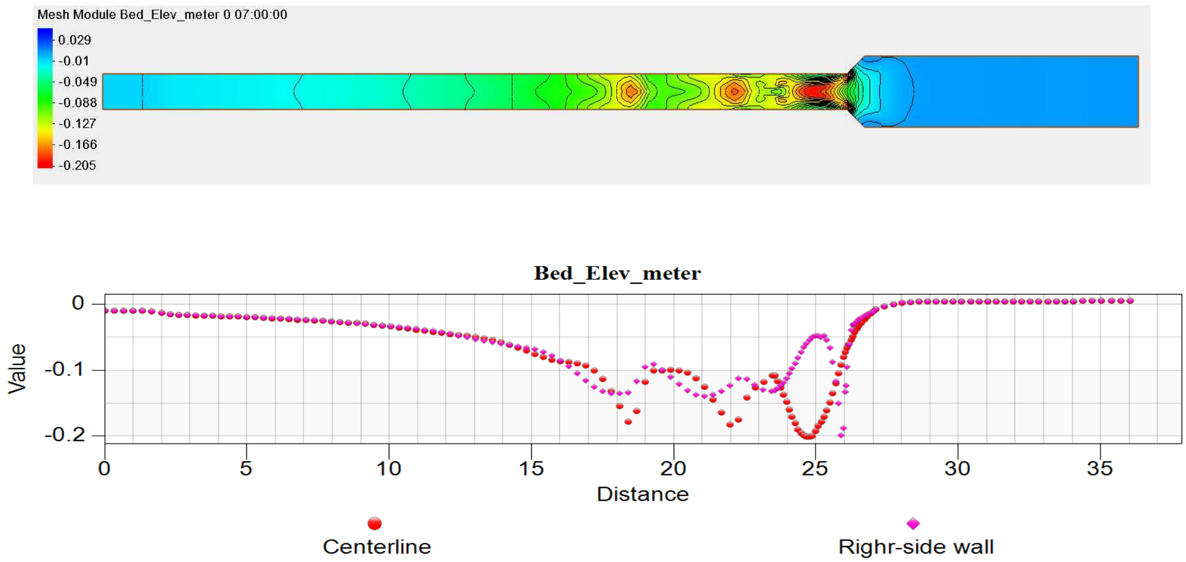

(b)

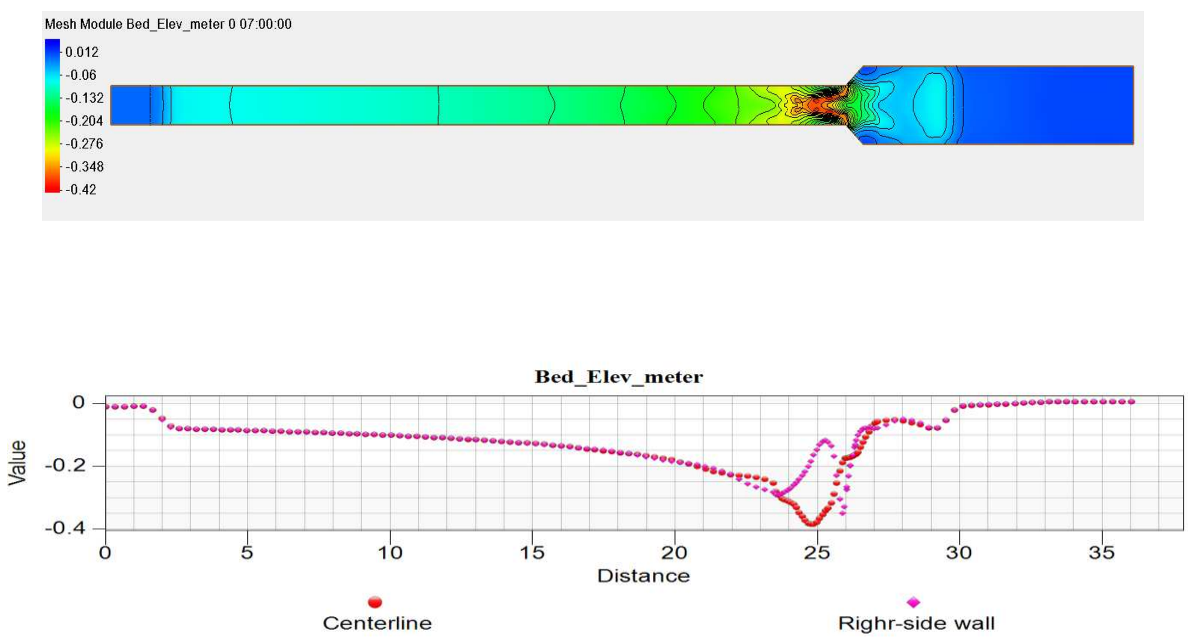

(c)

Figure E.3. The bed elevation plan view, centerline and near the wall profiles along the bed; (a) CW-0.5-0.3 (τ_1/τ_c =0.3), (b) LB-0.5-1.44 (τ_1/τ_c =1.44), (c) LB-0.5-4.9 (τ_1/τ_c =4.0)

As figure E.3 shows, by increasing the shear stress, the scour depth increases. However, for near the incipient of motion case (τ_1/τ_c =1.44) the scour pattern along the bed is not similar to that observed in the flume experiment (Figure E.3b). Also, for high shear ratio (τ_1/τ_c = 4.0) the approach channel started to scour, which was not observed in the flume experiments.

D.2. Model results using Engelund-Hansen sediment transport method

The plan view of the channel, centerline and near the right sidewall profiles for three shear stress ratios (τ_1/τ_c), 0.3, 1.44, and 4.0 are brought in the following.

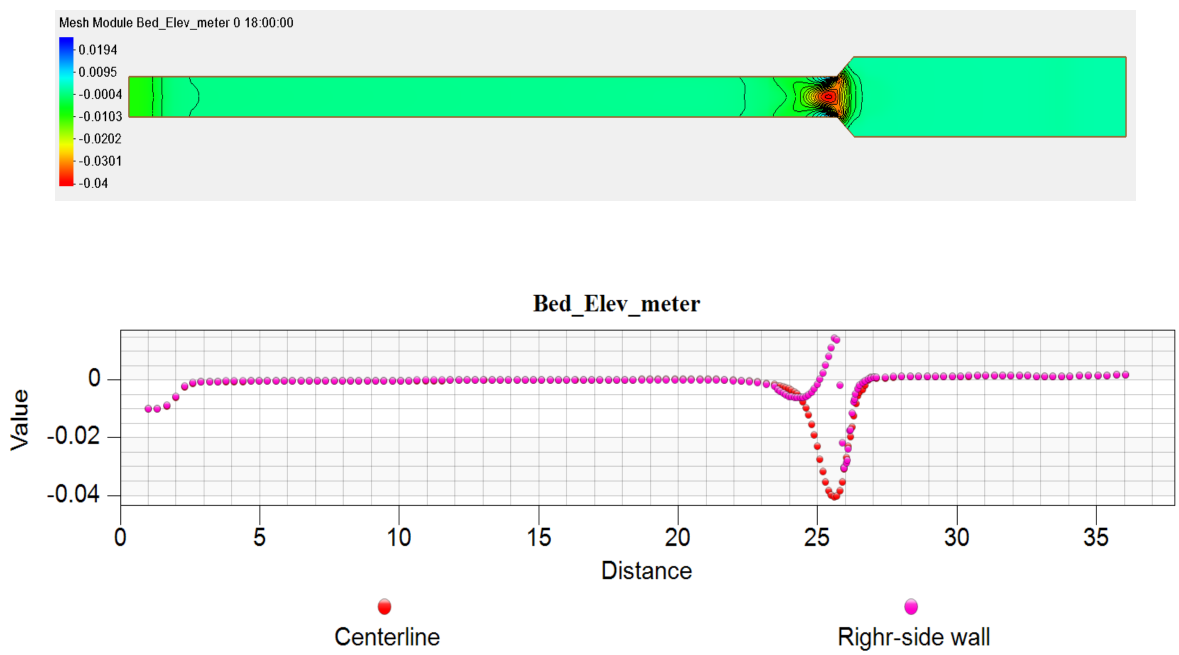

(a)

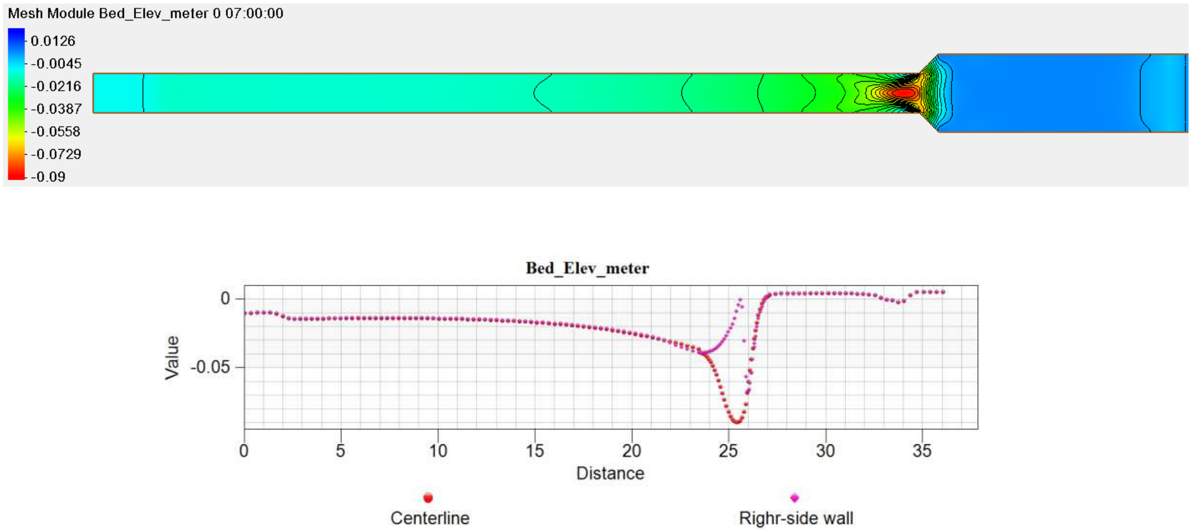

(b)

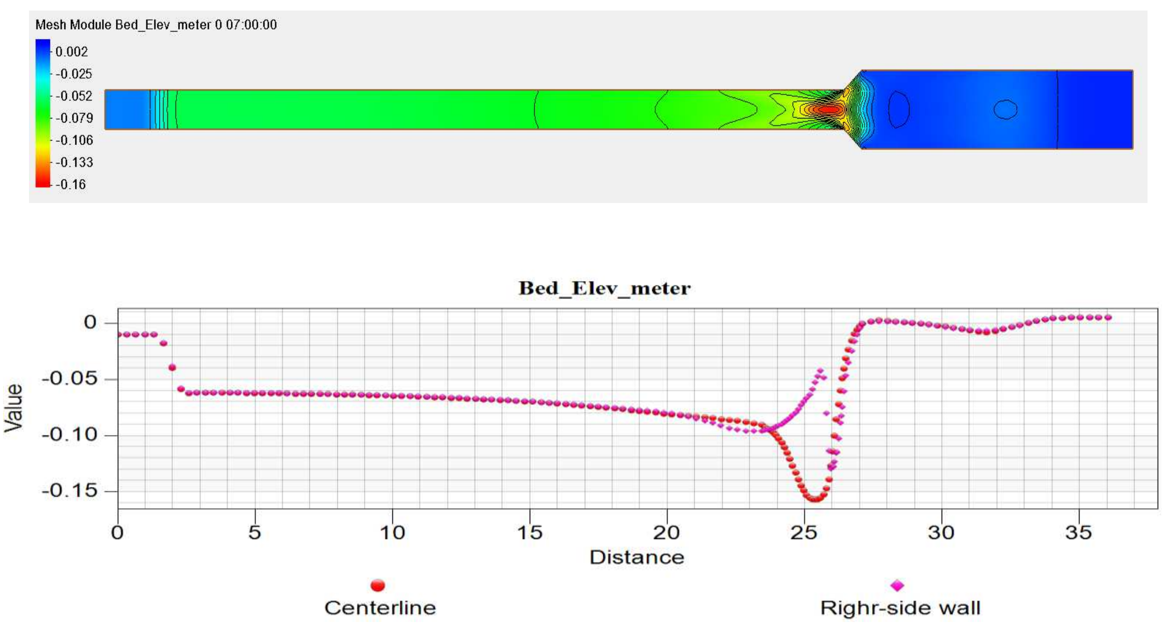

(c)

Figure E.4. The bed elevation plan view, centerline and near the wall profiles along the bed;

(a) CW-0.5-0.3 (τ_1/τ_c =0.3), (b) LB-0.5-1.44 (τ_1/τ_c =1.44), (c) LB-0.5-4.9 (τ_1/τ_c =4.0)

As figure E.4 shows, by increasing the shear stress, the scour depth increases. In contrast with the results of the Yang (1973), the Engelund -Hansen has more stable results for the range of shear stress ratio. However, the inaccurate scour depth estimation near the corners is evident in both cases. Moreover, sediment deposited near the sidewalls.

.

D.3. Conclusion and Results

As shown in the preceding sections, in all cases the predicted depth of the corner-scour was lower than the predicted depth of the scour at vena-contracta region. This is in contrast with findings from the flume measurements. This error arose from the 3D nature of the flow near the contraction entrance and inability of the 2D code to correctly simulate the recirculation zones near the corners. Consequently, the excess shear stress exerted on the corners by turbulent structures was not taken into account and the scour depth near the corners are smaller than vena-contra region.

Moreover, the measurements depicted that the final bed elevation along the contracted section had a curved shape which was not the case for numerical simulations. The simulated scoured bed started from minimum depth at vena-contracta region and reached to a flat-bed at the downstream end of the contraction.

However, it is possible to compare the results of the model at vena-contracta region with the flume data and check the accuracy of the model at this region. Figure E.5 compares of the measurements and simulations.

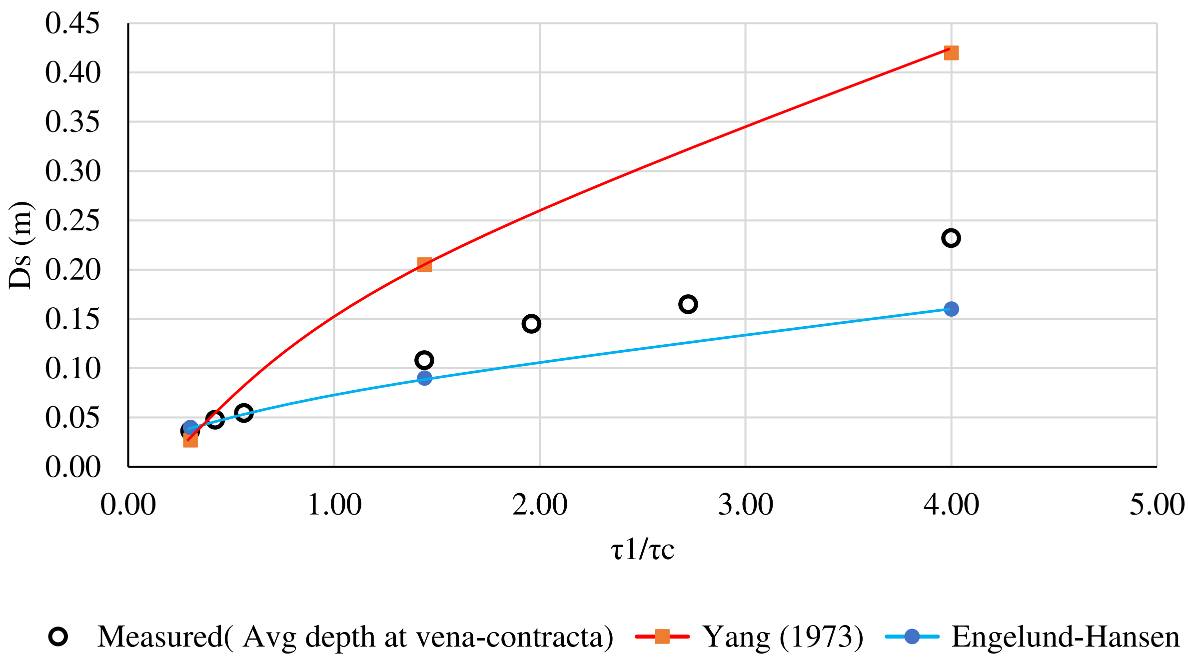

Figure E.5. Comparison between the scour depth at vena-contracta region obtained from the numerical simulations and the measurements.

As the results shown, simulations using Engelund-Hansen sediment transport equation underestimated the scour depth and Yang (1973) greatly overestimates the scour depth, see Figure E.5. However, the scour pattern resulted from utilizing Engelund-Hansen equation has a closer trend to the flume data and scour pattern along the bed is more realistic than the Scour depth resulted from Yang (9173).

Overall, SRH-2D is not able to correctly simulate the scour depth along the whole contraction, specially near the entrance corners. However, the model can be used with some error (depending on sediment transport method used) to estimate the average scour depth at vena-contracta region.

Appendix F: Use of SRH-2D to Extend Flume Experiments

To investigate further the contraction scour trend with increasing shear stress, the flume setup (mild contraction, B_2/B_1=0.75) was numerically extended to have a 45-degree transition exit at the downstream end of the contraction and having a subcritical uniform flow depth at the downstream boundary. Six different discharges (i.e., shear stress ratios τ_{n1}/τ_c= 0.72, 0.9, 2.72, 6.25, 7.84 and 9.0) with their correspondent bed slope used to find the scour depth at the vena contracta region. Values of shear stress ratio higher than 9.0 would cause choking, which was avoided herein. Figures F.1 and F.2 show the plan view of the extended contraction and the final bed profile along the centerline for shear stress ratios, τ_{n1}/τ_c, 6.25 and 9.0, respectively.

(a)

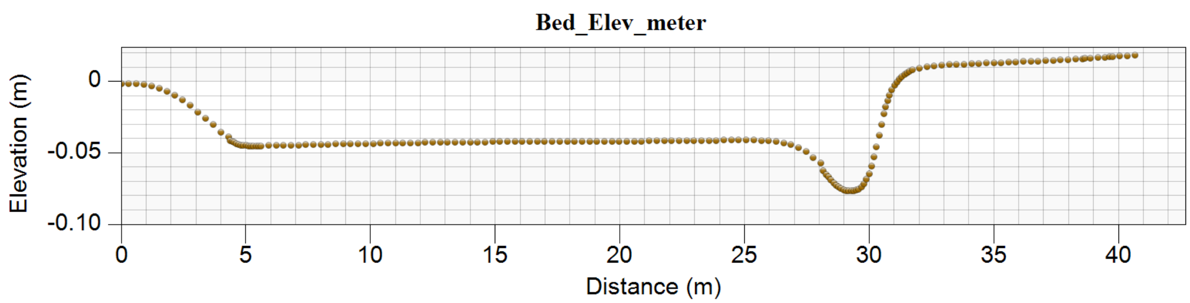

(b)

Figure F.1. The bed elevation plan view and centerline profiles along the bed (τ_{n1}/τ_c= 6.25).

The shear stress ratio, τ_{n1}/τ_c, of 6.25 is the maximum shear which is tested and measured during the experiments. Figure F.2 shows the simulation results of τ_{n1}/τ_c=9.0 which is almost the choking limit, i.e., higher shear stresses would choke the flow.

(a)

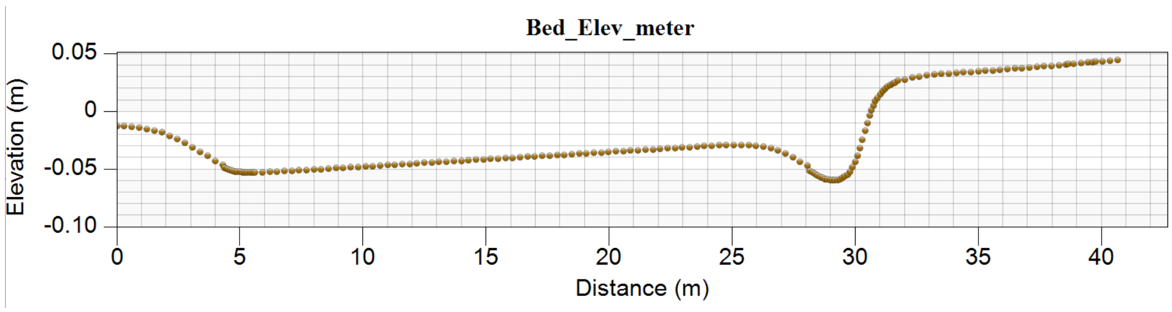

(b)

Figure F.2. The bed elevation plan view and centerline profiles along the bed (τ_{n1}/τ_c= 9.0)

Comparing Figures F.1 and F.2 depicts that by further increase of shear stress ratio the scour depth decreased. The scour depth variation with shear stress ratio is shown in the following figure.

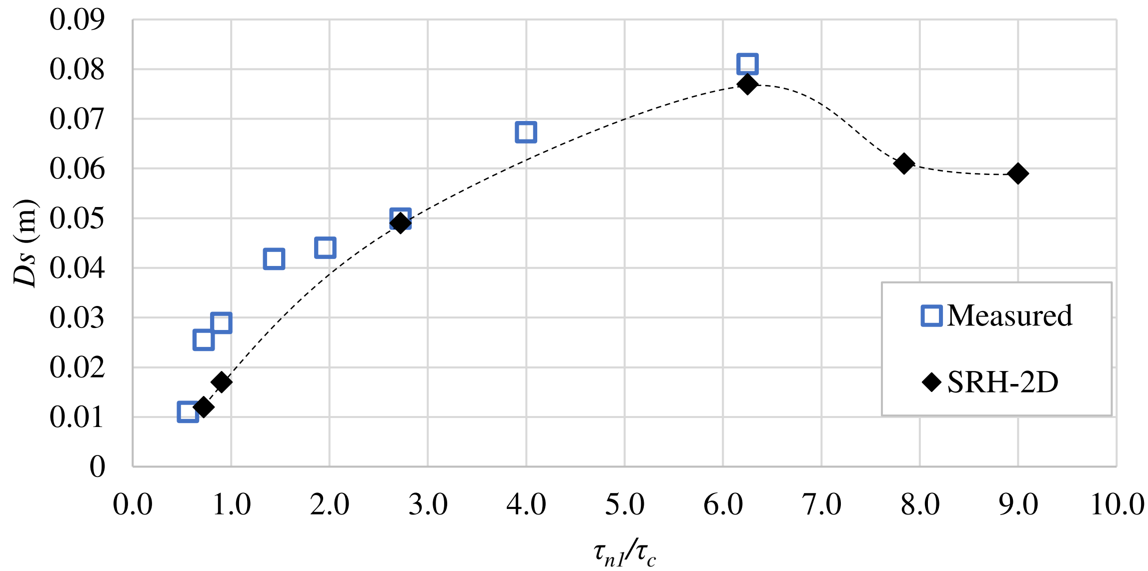

Figure F.3. Comparison between the scour depth at the vena-contracta region obtained from the numerical simulations and the measurements.

Figure F.3 shows the comparison of numerical results and measurements. Also, the numerical results extended to higher shear stress ratios and, as the results show, the scour depth started to decrease as the shear stress ratio increases almost after shear stress ratio of seven. This decrease was anticipated due to exponential increase of sediment transport rate and is in accordance with Straub (1934) and Laursen and Alawi (1989). Figure F.3 confirms the uniform flow at the downstream end (the uniform depth of the flow along the reach before contraction) and using backwater depth to estimate the scour depth would over-estimates the contraction scour depth, especially for high shear stress ratios.